AN ABSTRACT OF THE THESIS OF

Jenda A. Johnson for the degree of Master of Science in Geology presented on June 9, 1995. Title: Geologic Evolution of the Duck Creek Butte Eruptive Center, High Lava Plains, southeastern Oregon.

Redacted for Privacy

Abstract approved: _____

Anita L. Grunder

Mixing during synextensional magmatism of a layered magma chamber, followed by prolonged fractionation during tectonic quiescence, is recorded in the stratigraphy, geochemistry, geochronology, and structural history of the Duck Creek Butte eruptive center (DBEC). DBEC, located in the Basin and Range province of southeastern Oregon is the easternmost center in a west-northwest-trending, northwest-younging sequence of silicic vents. DBEC was studied by a combination of detailed geologic mapping (400 $km^2$), 37 chemical analyses, mineral chemistry, three new $^{40}Ar/^{39}Ar$ ages, and Sr and Nd isotope data.

The DBEC sequence is dominated by rhyodacite and rhyolite but includes andesite, basaltic andesite, and basalt. Effusive volume decreases with time, and the compositional range becomes more restricted and more mafic. The earliest volcanic activity is recorded in more than 6 $km^3$ of pyroclastic and effusive lava flows of porphyritic rhyodacite (10.38±0.04 Ma; $^{40}Ar/^{39}Ar$, biotite) during movement along the faults related to uplift of the Steens Mountain fault block. The lava flowed over existing fault escarpments and was later truncated by these same faults. Late flows of rhyodacite contain quenched andesite inclusions that were entrained during evacuation of the magma chamber. Eruption of dacite

with up to 30 percent quenched basaltic andesite inclusions ensued, possibly as the result of synmagmatic faulting. Andesite with mixing textures, associated with basaltic andesite and basalt, marks the end of DBEC activity along the fault system. Silicic magmatism migrated 2 to 4 km northwest to Indian Creek Buttes, where high-silica rhyolitic magma fractionated during tectonic quiescence, and then erupted (10.32±0.01 Ma; $^{40}Ar/^{39}Ar$, sanidine).

The oldest rock in the area is the 16.2 Ma Steens Basalt. It is conformably overlain by tuffaceous sedimentary strata and 12-11 Ma basalt, basaltic andesite, and andesite. The older strata are overlain conformably to slightly unconformably by the DBEC sequence.

Post-DBEC rocks were deposited chiefly in drainages and west-northwest-trending fault-bounded valleys. The 9.7-Ma Devine Canyon Ash-flow Tuff and underlying tuffaceous sedimentary strata are found throughout southeastern Oregon. Following a protracted hiatus, a primitive high-alumina olivine tholeiite erupted adjacent to DBEC (1.38±0.01 Ma; $^{40}Ar/^{39}Ar$, whole rock). No further volcanic activity is recorded. Quaternary sediment covers much of the area.

Movement along north-northeast- and west-northwest-striking normal faults and synchronous volcanic activity at DBEC near the northern terminus of the Steens Mountain escarpment is constrained between 10.4 and 1.4 Ma. Contemporaneous lavas are affected by at least three periods of faulting. Regionally extensive east-west-directed extension was active prior to and during eruption of the 10.4-Ma rhyodacite, indicated by truncated plunging flow folds. West-northwest-striking faults, which are parallel to the Brothers fault zone, were active in the period between emplacement of the 10.32-Ma rhyolite and the 9.7-Ma Devine Canyon Ash-flow Tuff. The 1.4-Ma olivine basalt filled a northwest-trending valley and subsequently was offset by north-striking normal faults. No further movement is recorded by Quaternary sedimentary units.

Compositional and textural evidence suggests that DBEC rocks result from several mechanisms including crustal melting, fractionation, magma mixing, and filter pressing.

Rhyolite and rhyodacite apparently were derived by crustal melting and fractionation, respectively, during tectonic quiescence. Successive tapping during tectonism caused mixing with underlying, more-mafic magma at a rate faster than silicic magma could be regenerated. Textural evidence and linear element-element arrays indicate that the dacite and andesite were derived mainly by magma mixing. Basalt and basaltic andesite of DBEC resulted from fractional crystallization of a primitive basalt.

# Geologic Evolution of the Duck Creek Butte Eruptive Center, High Lava Plains, Southeastern Oregon

by

Jenda A. Johnson

A THESIS

submitted to

Oregon State University

in partial fulfillment of
the requirements for the
degree of

Master of Science

Completed June 9, 1995

Commencement June 1996

Master of Science thesis of Jenda A. Johnson presented on June 9, 1995

APPROVED:

Redacted for Privacy

Major Professor, representing Geology

Redacted for Privacy

Chair of Department of Geosciences

Redacted for Privacy

Dean of Graduate School

I understand that my thesis will become part of the permanent collection of Oregon State University libraries. My signature below authorizes release of my thesis to any reader upon request.

Redacted for Privacy

Jenda A. Johnson, Author

This thesis is dedicated to
David R. Sherrod,
husband, friend, mentor, critic

## Acknowledgments

Primary funding for this thesis and continuing field work was provided by a graduate student internship with the U.S. Geological Survey (USGS). Additional funding included an award from the Oregon Laurel scholarship fund, a fellowship from Arco Corporation, and a graduate student research position under a grant awarded to A.L. Grunder from the National Science Foundation.

I am grateful to my main thesis advisor, Anita Grunder, for proposing and supporting the project and for her critical analysis during the initial and final stages of the process. John Dilles provided valuable criticism of the map as well as review of the text. Roger Nielsen, Dave Christie, and Marty Fisk spent many hours attempting to help me understand my petrologic mysteries.

The company of my fellow students, especially Lisa Seter, Mike Reed, Jim MacLean, Martin Streck, David Still, Lihua Zhang, Hiroyuki Tsutsumi, Paul Crenna, Peter Powers and Christian Braudrick kept me smiling through most of the process.

Special thanks are due to my friends at Washington State University: Rick Conrey, petrologist extraordinaire, shared many hours expounding on the virtues of magma mixing and shared his petrologic computer programs when I was floundering in a sea of data; Peter Hooper provided XRF analyses of miscellaneous basalts as well as fine companionship in the field; Diane Johnson, GeoAnalytical Lab, cheerfully processed every rock chip I sent her...and asked for more. Chris Hawkesworth , Open University, United Kingdom, provided valuable strontium and neodymium isotope analyses as well as photographic and rock cleaning skills on Steens Mountain.

I would like to thank Jim Evans, USGS, Spokane WA, for sponsoring my USGS internship; Terri Geisler, BLM in Burns OR for providing the comfort of a radio for moral support during my first seasons alone in the field, as well occasional shelter from the

elements; Dwight Hammond for flying me over my field area to take photographs, and especially for teaching me how to steer the craft.

My mother, Anne Johnson, has given much encouragement and wise advice for over 46 years, and never questioned my ceaseless and incurable drive to stay in school. She and my brother, Jeffrey, traveled 1000 miles to cheer me on during my thesis defense. My seven brothers and sisters provided a fine cheerleading squad. And to my daughter, Leya Nicolait....I made it!..Just when you thought I would never learn that school *can* get in the way of an education.

I owe my husband, David, much gratitude for his patience, interest, moral support, geologic input, and field support during all stages of my late-blooming geologic career, and for his critical review of all parts of the final manuscript when I had thrown up my hands in desperation.

## TABLE OF CONTENTS


| | Page |
|---|---|
| CHAPTER 1. INTRODUCTION | 1 |
| 1.1 Geologic Setting | 1 |
| 1.2 Methods of Study | 6 |
| CHAPTER 2. STRATIGRAPHY | 8 |
| 2.1. Introduction | 8 |
| 2.2 Rocks that predate the Duck Creek Butte eruptive center | 8 |
| 2.2.1 Steens Basalt (Ts) | 8 |
| 2.2.2 Older tuff and tuffaceous sedimentary rocks (Tots) | 13 |
| 2.2.3 Porphyritic basalt (Tb) | 14 |
| 2.2.4 Basalt and andesite (Tba) | 15 |
| 2.2.5 Basalt of Stockade Creek (Tbs) | 16 |
| 2.2.6 Lithic tuff of Soldier Creek (Tlt) | 17 |
| 2.2.7 Andesite breccia dikes of Dick Creek (Tad) | 17 |
| 2.2.8 Rhyolite of Dowell Butte (Tr) | 17 |
| 2.3 Duck Creek Butte eruptive center seies | 18 |
| 2.3.1 Rhyodacite of Duck Creek Butte (Tdrd and Tdrdp) | 18 |
| 2.3.2 Inclusion-rich dacite (Tdid) | 24 |
| 2.3.3 Olivine-bearing basaltic andesite ($Tdba_1$) | 27 |
| 2.3.4 Basaltic andesite dike ($Tdba_2$) | 27 |
| 2.3.5 Basalt of Duck Pond Ridge ($Tdb_1$) | 28 |
| 2.3.6 Fine-grained basalt ($Tdb_2$) | 28 |
| 2.3.7 Andesite of Duck Creek Spring ($Tda_1$) | 29 |
| 2.3.8 Andesite of Duck Creek ($Tda_2$) | 29 |
| 2.3.9 Basaltic andesite Brokendown Waterhole ($Tdba_3$) | 30 |
| 2.3.10 Rhyolite of Indian Creek Buttes ($Tdr_1$) | 30 |
| 2.3.11 Rhyolite of Big Gulch ($Tdr_2$) | 32 |
| 2.4 Younger units | 32 |
| 2.4.1 Younger tuffaceous sedimentary strata (Tyts) | 32 |
| 2.4.2 Devine Canyon Ash-flow Tuff (Ttd) | 33 |
| 2.4.3 Quaternary Basalt | 34 |
| 2.4.3.1 Glomerophyric basalt ($Qb_1$) | 34 |
| 2.4.3.2 Basalt of Duck Creek Flat ($Qb_2$) | 35 |
| 2.4.3.3 Basalt of Cord ($Qb_3$) | 35 |
| 2.4.3.4 The basalt of Barren Valley ($Qb_4$) | 37 |
| 2.4.4 Landslide deposits (Qls) | 37 |
| 2.4.5 Lake deposits (Ql) | 37 |
| 2.4.6 Alluvium (Qa) | 38 |

TABLE OF CONTENTS (Continued)


| | Page |
|---|---|
| CHAPTER 3. STRUCTURE | 39 |
| 3.1 Introduction | 39 |
| 3.2 Terminology | 41 |
| 3.3 Pre-eruptive and syneruptive faults | 42 |
| 3.4 Post-DBEC structural history | 43 |
| CHAPTER 4. GEOCHEMISTRY | 46 |
| 4.1 Mineral Chemistry | 46 |
| 4.1.1 Introduction | 46 |
| 4.1.2 Feldspar | 47 |
| 4.1.3 Pyroxene | 47 |
| 4.1.4 Olivine | 54 |
| 4.1.5 Biotite | 54 |
| 4.1.6 Amphibole | 54 |
| 4.1.7 Ilmenite | 54 |
| 4.1.8 Chrome spinel | 54 |
| 4.2 Whole-Rock Chemistry | 57 |
| 4.2.1 Classification | 57 |
| 4.2.2 Older basalts and andesites and Quaternary Basalt | 57 |
| 4.2.3 DBEC series | 72 |
| 4.2.4 Miscellaneous rhyolites | 75 |
| 4.2.5 Discussion | 75 |
| 4.3 Strontium and Neodymium Isotopes | 76 |
| CHAPTER 5. PETROGENESIS | 77 |
| 5.1 Introduction | 77 |
| 5.2 Terminology | 78 |
| 5.3 Basalt Petrogenesis | 78 |
| 5.3.1 Steens and Steens-like basalt | 79 |
| 5.3.2 DBEC basalt | 80 |
| 5.3.3 Quaternary high-alumina olivine tholeiite | 82 |
| 5.4 Petrogenesis of basaltic andesite, andesite, and dacite | 88 |
| 5.4.1 Introduction | 88 |
| 5.4.2 Basaltic Andesites | 89 |

TABLE OF CONTENTS (Continued)


| | Page |
|---|---|
| 5.4.2.1 Olivine-bearing basaltic andesite | 90 |
| 5.4.2.2 Basaltic-andesite dike | 90 |
| 5.4.2.3 Basaltic andesite of Brokendown Reservoir | 91 |
| 5.4.2.4 Basaltic-andesite inclusion | 92 |
| 5.4.3 Andesites | 93 |
| 5.4.4 Dacite | 95 |
| 5.5 Petrogenesis of rhyodacite and rhyolite | 99 |
| 5.5.1 Introduction | 99 |
| 5.5.2 Rhyodacite of Duck Creek Butte | 98 |
| 5.5.3 Rhyolite of Indian Creek Buttes | 103 |
| CHAPTER 6. DISCUSSION AND CONCLUSIONS | 106 |
| 6.1 Tectonomagmatic summary of Duck Creek Butte eruptive center | 106 |
| 6.2 Age Progression | 112 |
| 6.3 Conclusion | 119 |
| REFERENCES CITED | 120 |
| APPENDICES | 130 |

## LIST OF FIGURES


| Figure | | Page |
|---|---|---|
| 1-1 | Location of map and geographic names | 2 |
| 1-2 | Map showing isochrons separating silicic domes in 1-m.y. increments along the High Lava Plains and Snake River Plain | 3 |
| 1-3 | Physiographic provinces of Oregon | 4 |
| 2-1 | Correlation chart for rock units described in text | 9 |
| 2-2 | Simplified geologic map of the Duck Creek Butte study area | 10 |
| 2-3 | Correlation of map units on the south and northeast margins of flows of the rhyodacite of Duck Creek Butte | 11 |
| 2-4 | Map showing approximate extent of Steens Basalt and Columbia River Basalt group | 11 |
| 2-5 | Schematic drawing of a hypothetical cross section through the DBEC study area | 20 |
| 2-6 | Histogram showing volume of lavas at DBEC, grouped by composition | 21 |
| 2-7 | Photograph of basaltic andesite inclusions weathering out of inclusion rich dacite | 25 |
| 2-8 | Petrographic thin section of contact between dacite host and quenched basaltic andesite inclusion in the inclusion-rich dacite | 26 |
| 2-9 | Map showing approximate original extent of Devine Canyon Ash-flow Tuff | 33 |
| 2-10 | Aerial oblique photograph of basalt flows over escarpment | 36 |
| 3-1 | Generalized fault map showing amount of stratigraphic relief on prominent faults in the study area | 40 |
| 3-2 | Photographs of flow lobe of the rhyodacite of Duck Creek Butte and plunging flow lobes in the rhyodacite | 44 |
| 4-1 | Feldspar compositions plotted on the feldspar ternary | 48 |
| 4-2 | Pyroxene and olivine compositions | 51 |
| 4-3 | Chemical analyses of rocks in the DBEC study area plotted on total alkali-silica classification diagram modified from Le Bas and others | 58 |
| 4-4 | Silica versus major element variation diagrams | 64 |

## LIST OF FIGURES (Continued)


| Figure | | Page |
|---|---|---|
| 4-5 | Silica versus trace element variation diagrams | 65 |
| 4-6 | AFM ternary of Irvine and Baragar with DBEC study area rocks plotted | 67 |
| 4-7 | $MgO$-$TiO_2$-$K_2O$ ternary plot showing the fields for basalts and andesites at DBEC | 69 |
| 4-8 | Major-element ratios showing the change in composition from base to top of the Steens Basalt sequence near the type section at Steens Mountain | 70 |
| 4-9 | Rare-earth element diagrams for rocks of DBEC | 71 |
| 4-10 | Spider diagrams of DBEC trace elements | 73 |
| 5-1 | Trace-element variation diagrams | 81 |
| 5-2 | Projection on olivine-diopside-quartz ternary from plagioclase | 83 |
| 5-3 | Variation diagrams showing the fractionation paths of the basalt of Duck Creek Flat using Rayleigh and boundary-layer fractionation models | 84 |
| 5-4 | Map showing distribution of Pliocene and Pleistocene high-alumina olivine tholeiites in High Lava Plains | 85 |
| 5-5 | Spider diagram showing comparison between the basalt of Duck Creek Flat and Devils Garden basalts | 87 |
| 5-6 | La/Sc vs SiO2/Rb ratio-ratio diagram with companion plots for the DBEC series rocks | 94 |
| 5-7 | Trace element concentrations in Tdid compared to a 3:1 mix of Tdrd plus $Tdba_1$ | 96 |
| 5-8 | Cartoon illustrating "wet" magma system | 98 |
| 5-9 | Trace-element spider diagram using hypothetical protolith to create the element concentrations in the rhyodacite of Duck Creek Butte | 102 |
| 6-1 | Cartoon of the tectonomagmatic evolution of the Duck Creek Butte eruptive center | 107 |
| 6-2 | Graph of time versus $SiO_2$. | 108 |
| 6-3 | Evolution of the age progression | 114 |
| 6-4 | Characteristics of a propagating oceanic rift | 118 |

## LIST OF TABLES


| Table | | Page |
|---|---|---|
| 2-1 | Chemical analyses of Tertiary ash deposit (Tots) and the Tuff of Oregon Canyon | 13 |
| 2-2 | $^{40}Ar/^{39}Ar$ ages from DBEC | 19 |
| 4-1 | Samples for microprobe analysis | 46 |
| 4-2 | Representative microprobe analyses of feldspar | 49 |
| 4-3 | Representative microprobe analyses of pyroxene | 52 |
| 4-4 | Representative microprobe analyses of olivine | 55 |
| 4-5 | Microprobe analyses of ilmenite and chrome spinel | 55 |
| 4-6 | Representative microprobe analyses of biotite and amphibole | 56 |
| 4-7 | Whole-rock compositions of DBEC samples | 59 |
| 4-8 | Whole-rock compositions of pre-DBEC basalt and andesite | 62 |
| 4-9 | Miscellaneous rhyolite and tuff | 63 |

## LIST OF APPENDICES


| Appendix | | Page |
|---|---|---|
| Appendix 1 | Map locations and additional procedures performed on rocks that were analyzed by XRF | 131 |
| Appendix 2 | Petrography and mineralogy | 133 |
| Appendix 3 | Microprobe analyses performed for this study | 140 |
| Appendix 4 | XRF analyses of Steens Basalt collected near the type section at Steens Mountain | 145 |
| Appendix 5 | Strontium and neodymium isotope data | 146 |
| Appendix 6 | Unnormalized XRF data for samples in Tables 4-7 through 4-9 | 148 |
| Appendix 7 | CIPW normative minerals for rocks in study area | 149 |
| Appendix 8 | Complete $^{40}Ar/^{39}Ar$ analytical data. | 150 |

## LIST OF APPENDIX FIGURES


| Figure | | Page |
|---|---|---|
| A1-1 | Sample locations for chemical analyses listed in Tables 4-7 through 4-9 | 132 |
| A5-1 | Strontium and neodymium isotopes for DBEC samples listed in Appendix 5 | 147 |

## LIST OF PLATES

Plate 1. Geologic Map of the Duck Creek Butte eruptive Center

Plate 2. Description of map units and cross section of the Duck Creek Butte eruptive center.

(plates are in rear pocket)

# GEOLOGIC EVOLUTION OF THE DUCK CREEK BUTTE ERUPTIVE CENTER, HIGH LAVA PLAINS, SOUTHEASTERN OREGON

## CHAPTER 1: INTRODUCTION

### 1.1 Geologic Setting

Silicic centers in southeastern Oregon have been recognized for more than 30 years (Walker and Repenning, 1965; Greene and others, 1972; Walker and others, 1974; Walker, 1977), and yet the geology and petrology of individual centers are poorly known. Late Tertiary magmatism has been described as a bimodal association of basalt and rhyolite, wherein intermediate rocks are virtually absent (for example, Christiansen and McKee, 1978; Draper, 1991). Although the northern Basin and Range province is bimodal, individual eruptive centers possess a variety of compositions from basalt to rhyolite (for example, Juniper Ridge, MacLean, 1994; Duck Creek Butte, this study; Frederick Butte, J.A. Johnson, unpub. mapping). Duck Creek Butte eruptive center (DBEC; Figure 11) is composed of a sequence of locally erupted lava flows, dikes, and pyroclastic-flow deposits that vary from basalt to rhyolite in composition. Duck Creek Butte and adjacent Indian Creek Buttes are among the easternmost vents in a west-northwest-trending sequence of silicic vents in southeastern Oregon that are progressively younger to the west (Figure 1-2) (MacLeod and others, 1976). DBEC flows were emplaced between 10.5 and 10.3 Ma. A 1.4-Ma primitive olivine basalt vented adjacent to DBEC following a 9-m.y. hiatus in volcanic activity.

The purpose of this study is to understand the geologic evolution of the Duck Creek Butte eruptive center and its relation to the regional geologic setting. This work contributes to a larger project that is examining the 10- to 5-Ma segment of westward-younging silicic volcanism along the High Lava Plains (Figure 1-2) (A.L. Grunder, Oregon State

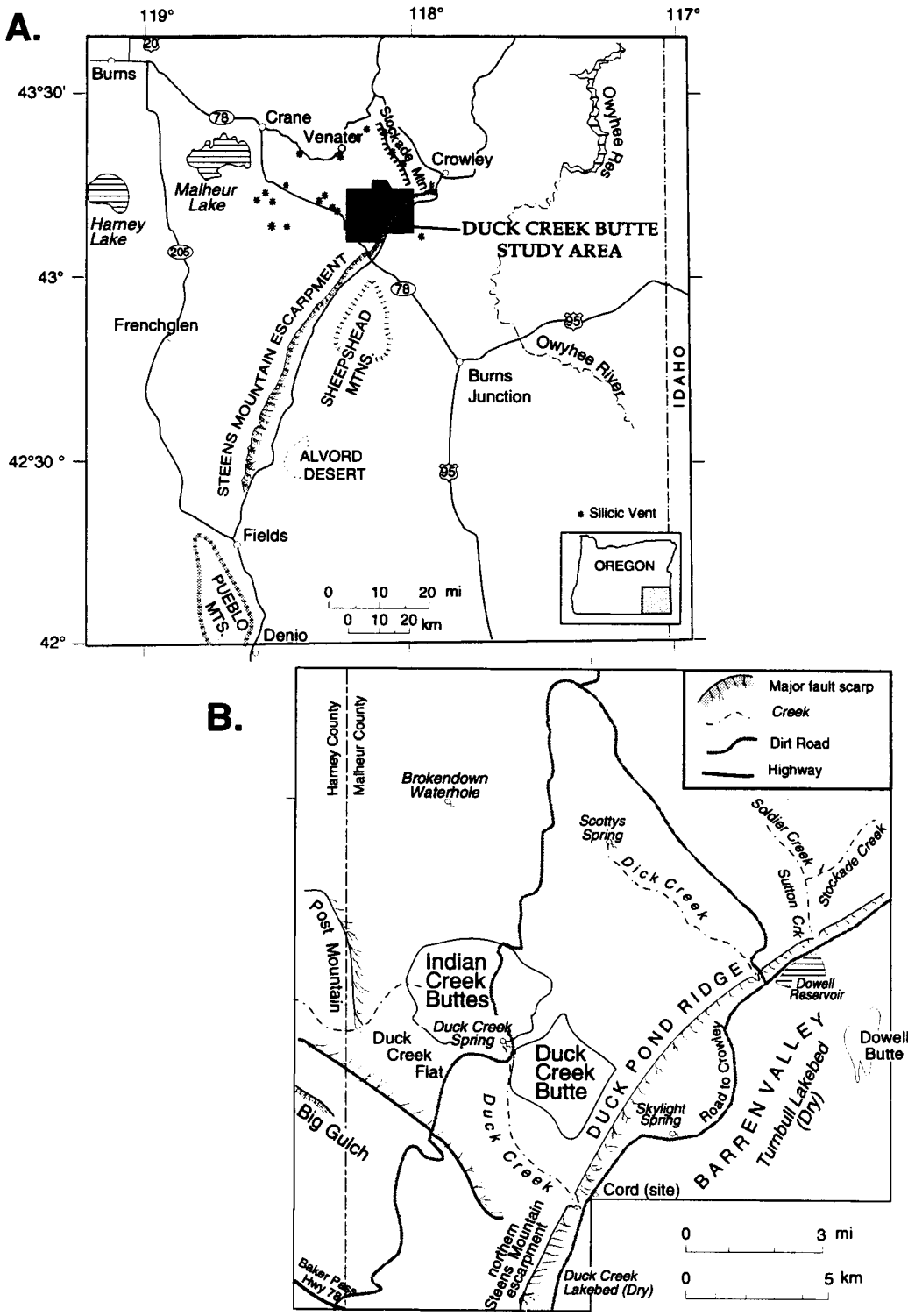


**Figure 1-1**: Location map and geographic names. (A) Southeastern Oregon, (B) Duck Creek Butte study area.

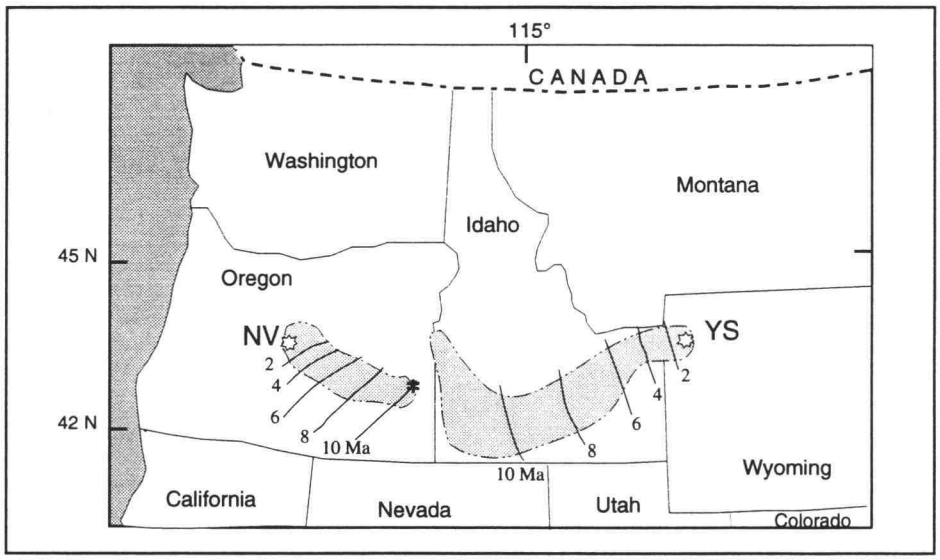


**Figure 1-2:** Map showing isochrons separating silicic domes in 1-m.y. increments along the High Lava Plains of Oregon and Snake River Plain of Idaho indicating opposing age progressions (MacLeod and others, 1976; Anderson and others, 1975).
NV = Newberry volcano; YS = Yellowstone; * = study area.

University, and students M.J. Streck, 1994; J.W. MacLean, 1994; B.T. Jordan, in progress). The broader goal is to develop a petrogenetic model for the region and to determine, in part, if the High Lava Plains trend is a mirror image to the eastward-younging Snake River Plain-Yellowstone hotspot trend. In order to understand the mechanisms that might create the diverging trends, more must be known about the age, distribution, origin, and structural setting of magmatism in the region.

The Duck Creek Butte eruptive center is situated approximately at the junction of three physiographic provinces: the High Lava Plains, the northern Basin and Range, and the Owyhee Upland (Dicken, 1950) (Figure 1-3). The High Lava Plains province encompasses Miocene to Quaternary volcanic rocks. Volcanism changed from dominantly basaltic to mainly silicic about 11 Ma. Basalt again became dominant after 5 Ma and does not appear to have an age progression.

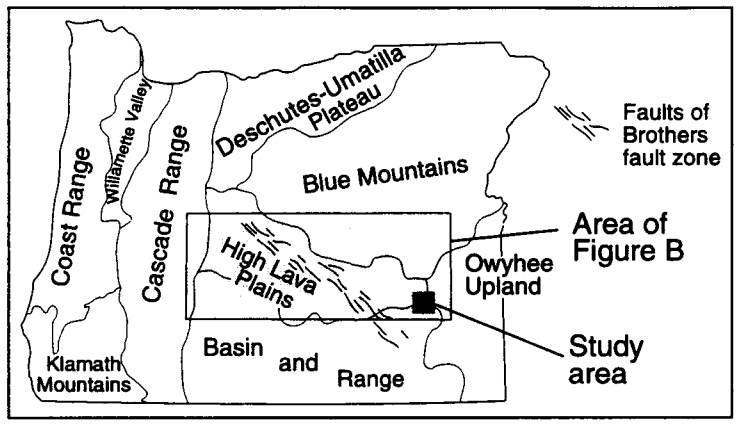


**A.**

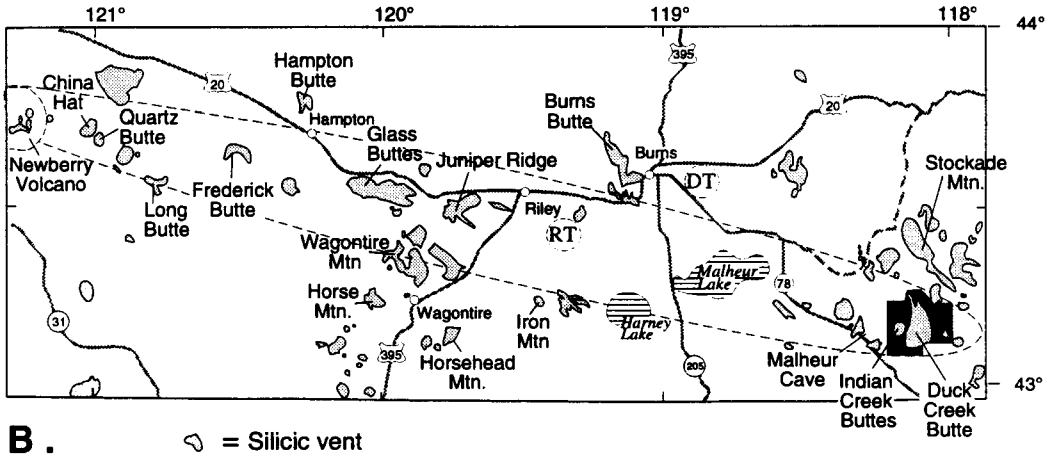


**B.**

= Silicic vent

RT Inferred vent for Rattlesnake Ash-flow Tuff (age 7.2 Ma)

DT Inferred vent for Devine Canyon Ash-flow Tuff (age 9.7 Ma)

**Figure 1-3**: (A.) Physiographic provinces of Oregon. ( B) Enlargement of High Lava Plains. Long-dashed oblong indicates approximate track of northwest-trending age progression of silicic vents.

The High Lava Plains province is bounded on the north by the Blue Mountains province, which is composed of Mesozoic and Paleozoic marine strata, volcanic island-arc sequences, ophiolite assemblages, and granitic plutons, as well as Tertiary volcanic and sedimentary rocks. The Blue Mountains province is characterized by regional uplift and is bounded on the south by the linear structures of the Brothers fault zone that at least locally exhibit transcurrent movement and may represent transform zones (Walker and Robinson, 1990). The High Lava Plains province is bounded on the west by the Cascade Range, a Cenozoic volcanic arc related to subduction of the Juan de Fuca plate beneath the North American plate. To the south, the High Lava Plains province borders the Basin and Range province, which includes most of south Oregon east of the Cascades. The northwestern Basin and Range is characterized by a series of north-trending horsts and grabens that form the major mountain ranges such as Steens Mountain. The Owyhee Upland, which lies to the east of the High Lava Plains, comprises lava flows and sedimentary rocks that are more deeply dissected than the High Lava Plains. Quaternary basalt in the southern part of the Owyhee Upland lacks the north-striking faults that characterize the Basin and Range (Walker and MacLeod, 1991).

The DBEC study area is located in Malheur and Harney Counties, southeastern Oregon. It encompasses over 300 $km^2$ within all or part of five $7^1/_2$-minute quadrangles: Duck Creek Butte, Dowell Butte, Venator Reservoir, Stockade Mountain, and Folly Farm (Plate 1). The closest settlement is Burns Junction, 55 km southeast. Elevation ranges from 1,220 m in the Barren Valley to 1,879 m atop Duck Creek Butte. The study area is located in the high desert and receives an average of 15 cm precipitation yearly, chiefly during the winter. Vegetation includes juniper, sage, and grasses.

Most land in the area is under the jurisdiction of the Bureau of Land Management. It is leased to cattle and sheep ranchers and is fenced for grazing. Private holdings include several farms in the Barren Valley and land adjacent to springs. The area is accessible by dirt roads from Highway 78 and from the Crowley road (Figure 1-1).

## 1.2 Methods of Study

Field work at the Duck Creek Butte eruptive center was begun during the summer of 1992 and completed during the summer of 1994. Geology was mapped on 1:24,000-scale topographic maps. Aerial photographs were used to interpret the extent of faults. Petrographic examination of 76 thin sections was performed to determine modes and textures of the volcanic rocks.

Major and some trace element chemical analyses were obtained using X-ray fluorescence spectroscopy (XRF) on fused glass beads. Fourteen samples were analyzed by X-RAL Laboratories, Vancouver, British Columbia. An additional 23 analyses were obtained using an automated Rigaku 3370 spectrometer at the GeoAnalytical Laboratory, Washington State University, Pullman, Washington. Correction factors for data from X-RAL, based on comparative replicate analyses from Stanford University, were applied for minor systematic differences in MnO (-0.015 weight percent), MgO (-0.07 for MgO <0.2 percent), $P_2O_5$ (-0.02 for $P_2O_5$ <0.1 percent), and Rb (-7 ppm). $Na_2O$ and Cr concentrations from instrumental neutron activation analysis, where available, are used in place of XRF results. Trace element analyses for 20 samples were determined by instrumental neutron activation analysis (INAA) using the 1-MW Triga reactor at the Oregon State University Radiation Center following the procedure outlined in Laul (1979).

Prior to analysis, rock samples were cleaned of all weathered surfaces. Wherever possible glass was collected. All other samples were selected on the basis of both least amount of phenocrysts and least evidence for magmatic inclusions and mixing. All samples were broken in a standard alumina ceramic jaw crusher. Samples to be analyzed by XRF were ground to a fine powder in a tungsten-carbide shatterbox; INAA samples were ground in an alumina ceramic shatterbox. Three age determinations were done by Alan Deino at the Berkeley Geochronology Laboratory, Berkeley (CA) using the single-crystal and whole-rock laser-fusion $^{40}Ar/^{39}Ar$ method.

Microprobe analyses of feldspar, olivine, pyroxene, biotite, and hornblende were done at Oregon State University using a fully automated Cameca SX-50 microprobe with wavelength-dispersive spectrometers. Strontium and neodymium isotope ratios for whole rock samples were obtained using a Finigan 261 mass spectrometer in the laboratory of Chris Hawkesworth at the Open University, Milton Keynes, Great Britain.

# CHAPTER 2: STRATIGRAPHY

## 2.1 Introduction

Rocks exposed at the Duck Creek Butte eruptive center can be divided roughly into three stratigraphic groups: (1) basalt, andesite, and ash-fall tuff that predate DBEC, (2) DBEC series rocks, and (3) overlying ash-flow tuff, basalt, and sedimentary deposits (Figures 2-1 and 2-2, Plate 1). Detailed petrographic descriptions are in Appendix 2. Rock nomenclature is modified from LeBas and others (1986) (see Figure 4-3).

## 2.2 Rocks that predate the Duck Creek Butte eruptive center

Volcanic and volcaniclastic rocks older than DBEC are found throughout the study area. Correlation between rocks northeast of DBEC and south and west of DBEC is not always clear, and not all of the flow units found in the unit of basalt and andesite (Tba) were separated. Figure 2-3, however, indicates correlations defined by this study.

### 2.2.1 Steens Basalt (Ts)

Lava flows of aphanitic to coarsely porphyritic Steens Basalt form the oldest stratigraphic unit in the map area. The Steens Basalt is exposed extensively throughout much of southeastern Oregon (Fuller, 1931; Walker, 1960; Walker and Repenning, 1965; Greene and others, 1972; Carlson and Hart, 1983a; Hart and Carlson, 1985). It underlies an area estimated between 25,000 and 35,000 $km^2$ (Fig. 2-4). Flows extend from DBEC southward 120 km to the Pueblo Mountains (Avent, 1965; Minor, 1986) and 190 km southwest to Abert Rim (Carlson and Hart, 1983b); the southern and eastern extents are poorly defined. The northernmost exposure is west of Dowell Reservoir, on the basis of

## CORRELATION OF MAP UNITS

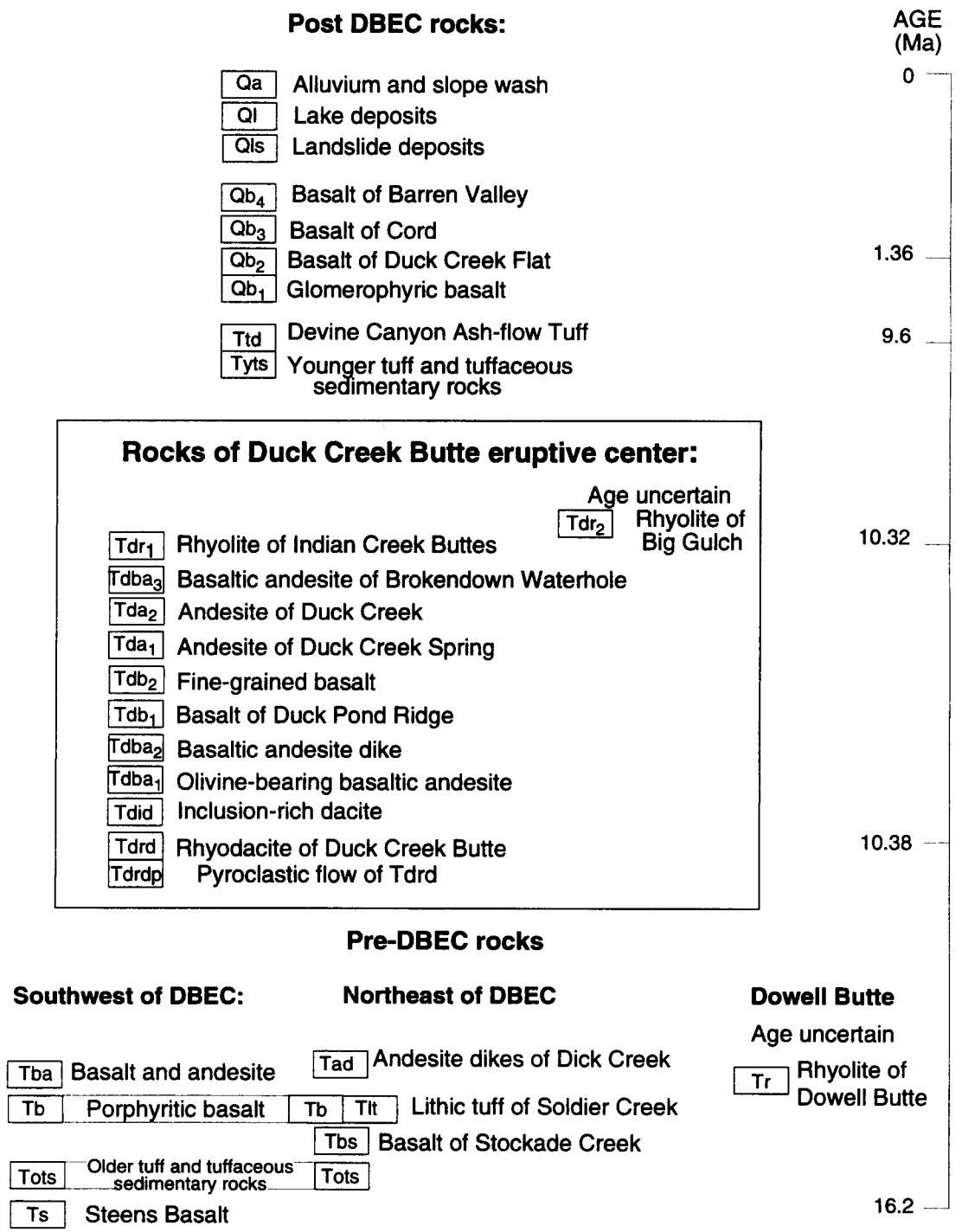


**Figure 2-1**: Correlation chart for rock units described in text.

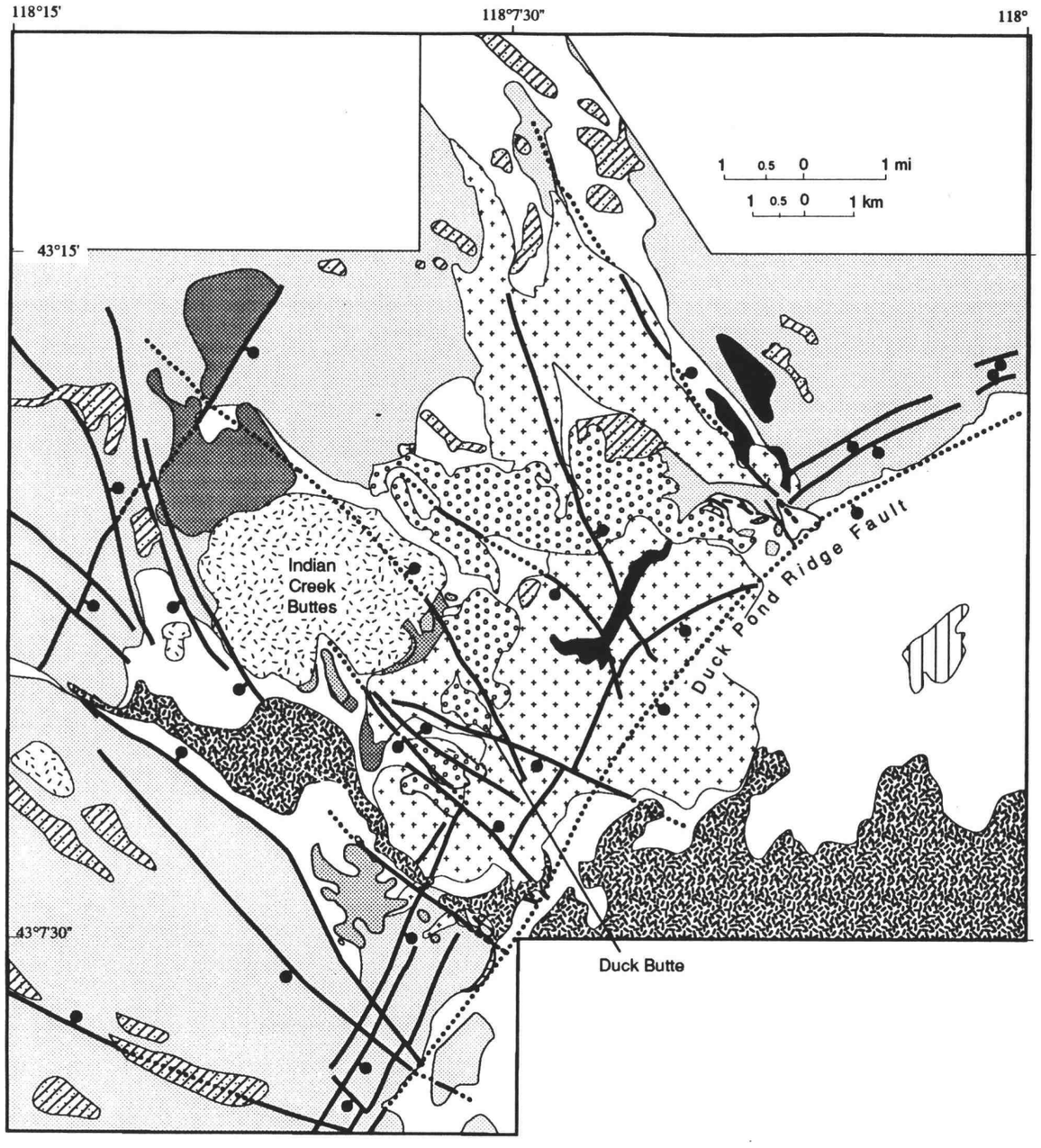


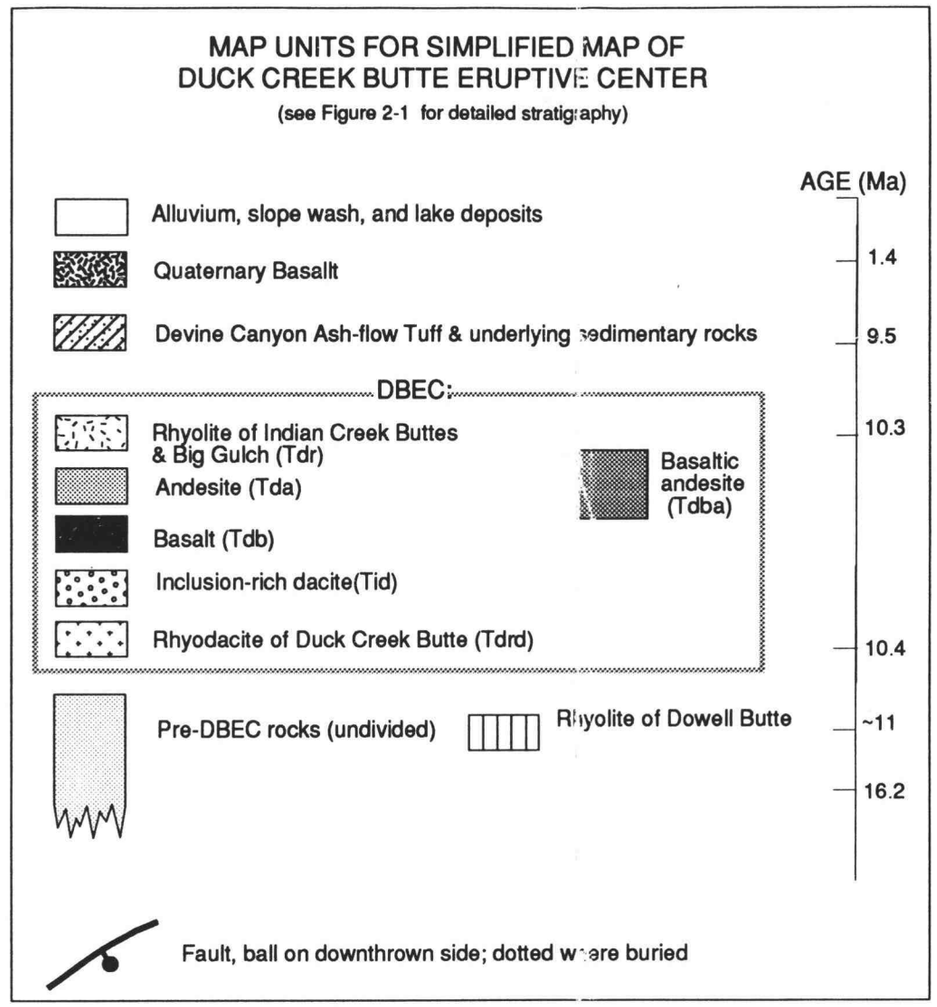


**Figure 2-2**: Simplified geologic map of the Duck Creek Butte Study Area

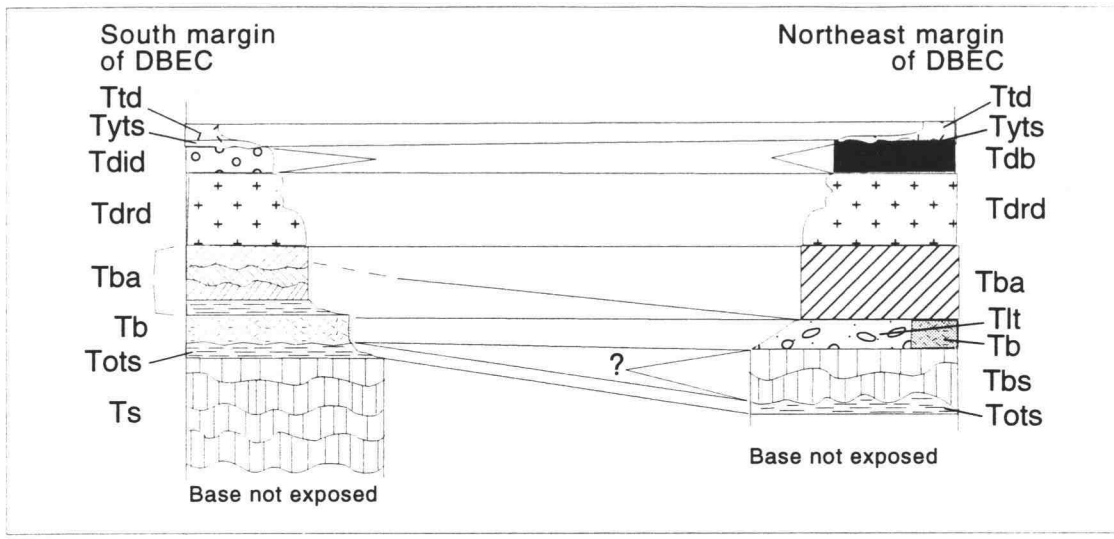


**Figure 2-3**: Correlation of map units on the south and northeast margins of flows of the rhyodacite of Duck Creek Butte.


**Figure 2-4**: Map showing approximate extent of Steens Basalt and Columbia River Basalt group (from Carlson and Hart, 1983 and Mankinen and others, 1985). Diagonal pattern in field of Steens Basalt denotes inferred range of Steens Basalt based on lithologic and/or chemical similarity to Steens Basalt.

basalt detritus in a landslide deposit. Beyond that the basalt is buried beneath younger strata to the north.

The Steens Basalt comprises medium- to dark-gray, diktytaxitic olivine basalt and basaltic andesite. It varies from aphanitic to coarsely porphyritic. Flows in the Duck Creek Butte study area range in thickness from 1 to 10 m and average 2 m thick. Total thickness is unknown because the base is unexposed; the unit is at least 200 m thick where exposed in a fault scarp near the south edge of the map area and at least 150 m thick along the Post Mountain escarpment at the northwest margin of the map area.

Maximum thickness of the unit is approximately 920 m where it is exposed in the Steens Mountain escarpment, 60 km south of the study area (measurement by me near the type section, and determined from geologic map of Minor and others, 1987b). There, the base is exposed and the top is capped by basaltic andesite (Appendix 4). At least 80, and possibly more than 100, individual flows form the Steens Basalt. Vents for the Steens Basalt are found in vertical dikes spectacularly exposed in the Steens Mountain escarpment (Fuller, 1931; Minor and others, 1987b and c). Steens Mountain represents the remains of a shield volcano that may have been 160-200 km in diameter with a total volume of about 12,000 $km^3$ (Mankinen and others, 1985). No vents were found in the map area.

The Steens Basalt is middle Miocene in age. Recent work by Swisher and others (1990) yielded ages of 16.58±0.05 Ma and 16.59±0.02 Ma, determined using $^{40}Ar/^{39}Ar$ laser fusion of coarse plagioclase crystals from flows 1 and 31, respectively, at the type section (flows numbered consecutively upsection). Previously determined K-Ar ages from flows near DBEC range from 17.2 to 14.8 Ma (Hart and Carlson, 1985) but may include younger, petrographically similar basalt that is isotopically distinct from the Steens Basalt. The Steens Basalt is contemporaneous with much of the Columbia River Basalt Group of northeastern Oregon and eastern Washington (Walker, 1969; Hart and others, 1989).

### 2.2.2 Older tuff and tuffaceous sedimentary rocks (Tots)

A 1-m-thick, very fine-grained, well-sorted ash deposit is exposed in a road cut and on a hilltop near the southeast margin of the study area, E$^1/_2$ sec. 23, T. 28 S., R. 37 E. The rock has a white chalk-like appearance except where baked by an overlying basaltic andesite flow. Owing to limited exposure, it is generally included with the sedimentary rock and lava that form the basalt and andesite unit (Tba), but it is shown separately in two locations where it is well exposed.

This ash may be the distal air-fall equivalent of the tuff of Oregon Canyon (Rytuba and McKee, 1984) on the basis of its position directly above the Steens Basalt. It is difficult to correlate chemically owing to interlaboratory variation, differing analytical methods, and the tendency of all rhyolite in the province to be mildly peralkaline (Table 2-1). The tuff of

**Table 2-1**: Chemical analyses of Tertiary ash deposit (Tots) and the Tuff of Oregon Canyon (Rytuba and McKee, 1984).

| Map unit | Tots | Tots | Tuff of Oregon Canyon |
|---|---|---|---|
| Analytical method | XRF | INAA | Emission spectrography |
| **Major-element analyses (wt. percent) normalized to 100 percent volatile free** | | | |
| $SiO_2$ | 75.4 | | 77.50 |
| $Al_2O_3$ | 10.15 | | 11.50 |
| $TiO_2$ | 0.23 | | 0.18 |
| FeO* | 4.45 | 4.39 | 1.90 |
| MnO | 0.07 | | 0.02 |
| CaO | 0.21 | | 0.06 |
| MgO | 0.00 | | 0.10 |
| $K_2O$ | 4.61 | | 4.75 |
| $Na_2O$ | 4.87 | 4.71 | 4.00 |
| $P_2O_5$ | 0.01 | | 0.01 |
| prenormalization total | 100.51 | | 99.88 |
| **Trace-element analyses (parts per million)** | | | |
| Ba | 45 | 182 | 29 |
| Rb | 212 | 209 | 310 |
| Sr | 8 | | 13 |
| Zr | †813 | | 1100 |
| Y | †156 | | 130 |
| Nb | †42 | | 23 |
| Pb | 21 | | 28 |

† denotes values >120 percent above calibrated range

Oregon Canyon is an ash-flow tuff erupted ~16.1 Ma from the McDermitt caldera complex, located about 100 km to the south (Rytuba and McKee, 1984), and is interbedded with basaltic andesite lava flows near the top of the Steens Basalt (Sherrod and others, 1989; Turrin and others, 1989).

In the northeast corner of the map area (sec. 15, T. 27 S., R. 38 E.), a well-bedded sedimentary deposit is the oldest unit exposed in the stream beds of Sutton, Soldier, and Stockade Creeks. Where best exposed the unit consists (from base upward) of 0.5 m of conglomeratic sandstone, 2 m of well-sorted sandstone, a 3-cm lens of crystal-rich sandstone, and at least 2 m of tan and white fallout tuff. The fallout tuff is even thicker, at least 9 m thick, where exposed in a steep stream bank at the confluence of the three creeks. The tuff may be a thicker exposure of the older tuff and tuffaceous sedimentary rocks (Tots) described in paragraphs 1 and 2 of this section, but no analysis was obtained.

### 2.2.3 Porphyritic basalt (Tb)

Fine-grained porphyritic diktytaxitic basalt, which resembles some lava flows of the Steens Basalt, is exposed discontinuously in the map area. I separate it from the Steens Basalt because it is distinctly fresher looking than any of the Steens Basalt and, in one location, float of the older tuff and tuffaceous sedimentary rocks (Tots) weathers out beneath it. The two basalts are commonly separated by a slope-forming unit with no outcrop, interpreted to represent intervening poorly indurated sedimentary strata. Although the porphyritic basalt represents a single flow that is generally less than 3 meters thick, the unit appears thicker in Plate 1 where it includes the slope-forming sedimentary unit. The basalt is medium gray and contains small phenocrysts of plagioclase (5 to 10 percent, to 4 mm in length) and microphenocrysts of olivine (1 percent, to 0.5 mm in diameter).

Similar basalt found 15 km to the west-northwest and 15-20 km southeast of the map area was termed "Steens-like" basalt by Carlson and Hart (1985), who noted that it is chemically similar but isotopically more evolved than Steens Basalt. The so-called Steens-

like samples yielded ages ranging from 11.2 to 11.7 Ma (Hart and Mertzman, 1982) and thus clearly are significantly younger than Steens Basalt. Hart and Carlson (1985) suggested that this pulse of volcanism represented continued, but much diminished, magmatism of the Steens Basalt magmatic episode. I interpret this basalt to have resulted from a separate magmatic event on the basis of its substantially younger age and isotopic differences (see Sec. 5.3.1).

### 2.2.4 Basalt and andesite (Tba)

Very fine grained, aphyric to finely porphyritic basalt, basaltic andesite, and andesite form the youngest unit emplaced throughout the region prior to the growth of the Duck Creek Butte eruptive center. Although the unit varies from basalt to andesite in composition (51-60 percent $SiO_2$), the rocks are typically similar in appearance and are difficult to distinguish from one another and from fine-grained flows of the Steens Basalt. The basalt and andesite were not divided by composition as part of my mapping. Chemical analyses, however, indicate basalt is more abundant in the southern part of the map area and basaltic andesite and andesite are dominant north of DBEC.

On the northern margin of DBEC, a widespread thick sequence of basaltic andesite consists of multiple flows in excess of 100 m thick. There the basaltic andesite overlies the porphyritic basalt (Tb) and is overlain by the rhyodacite of Duck Pond Ridge (Tdrd). Outcrop extends from south of the map area where the unit of basalt and andesite (Tba) occurs as flows less than 15 m thick to beyond the northeast corner of the map area where the unit thickens and becomes more abundant.

The basaltic andesite lava typically varies from fine-grained and sparsely porphyritic to very fine grained and aphyric with abundant clay alteration. Fine-grained rocks contain plagioclase, clinopyroxene, Fe-Ti oxides, ±olivine, ±sideromelane. No petrographic thin-section analysis was performed on the basalts or andesites. The unit varies from medium gray with yellow streaks to medium dark gray. Although most of the unit is composed of

laterally continuous thin flows, near-vent accumulations of moderate reddish-orange to very-dark-red contorted flows and scoria are found where exposed by erosion in drainages.

I correlate these flows stratigraphically with basaltic andesite and andesite that are commonly found overlying the Steens Basalt elsewhere in the region (for example, Fuller, 1931; Minor, 1986; Sherrod and others, 1989; Turrin and others, 1989). South of Steens Mountain thick sequences of andesite flows appear to be contemporaneous with eruption of late flows of Steens Basalt (Mankinen and others, 1985). The map unit includes poorly exposed slope-forming deposits composed of unconsolidated to poorly consolidated sedimentary strata that include the tuff of Oregon Canyon.

### 2.2.5 Basalt of Stockade Creek (Tbs)

A distinctive basalt is exposed in the stream beds of Soldier, Stockade, and Sutton Creeks. Weathered outcrops have a distinctive black mottled snakeskin-like appearance that is attributed to ophitic pyroxene grains confined to areas separated by an intersertal or intergranular matrix (ophimottling as described by Avent, 1965, p. 24). Plagioclase, which is commonly up to 1.5 cm in length, varies in abundance from 2 to 25 volume percent but mostly forms about 5 percent of mode. In the less porphyritic samples, plagioclase megacrysts ranging in size from 4 to 9 cm are locally abundant. Although this basalt is similar in appearance to some lava flows of Steens Basalt (for example, flows I have found 350 m above the base of the sequence at its type section), it is distinguished from the Steens Basalt samples by its substantially higher Ba and lower Cu, V, and Ni concentrations. (Compare sample JJ94-163 in Table 4-7 with samples JS94-33, -34, -39 in Appendix 4.) This basalt weathers to buff-colored rounded outcrops with parallel, decimeter-scale partings. A brecciated flow top found in the northwest fork of Sutton Creek is highly vesiculated and weathers to gravel peppered with clear or yellowed plagioclase crystal fragments smaller than 5 mm.

The basalt of Stockade Creek is about 7 m thick where it overlies the unit of older tuff and tuffaceous sedimentary rocks (Tots). Elsewhere the unit is at least 30 m thick, but the base is not exposed.

### 2.2.6 Lithic tuff of Soldier Creek (Tlt)

An unwelded to moderately welded, pumice- and lithic-rich tuff forms gentle slopes above the basalt of Sutton Creek in the Soldier, Stockade, and Sutton Creek drainages. Pumiceous lapilli (or fiamme where welded) range in abundance from 30 to 50 percent. Lithic fragments, including andesite, basalt, and gabbro, form 3-20 percent of the rock. The tuff also contains 3 to 5 percent clear crystals. The tuff is exposed as large flat boulders that vary in color from tan to pale orange to purplish gray. Maximum thickness is approximately 10 m.

### 2.2.7 Andesite breccia dikes of Dick Creek (Tad)

Brecciated andesite dikes stand out in bold relief on the canyon walls of Dick Creek. They are found only in this location and extend discontinuously for 1 km to the northwest. The dikes weather boldly, forming ribs as high as 6 m, and range from 1 to 4 m in width and 3 to 10 m in length. The dikes are composed of angular blocks of aphanitic to sparsely porphyritic andesite in an altered andesite matrix. The clasts are medium- to dark-gray with grayish-red streaking where fresh and weather grayish- or dark-reddish brown.

### 2.2.8 Rhyolite of Dowell Butte (Tr)

Dowell Butte is a domal mass of heterogeneous high-silica rhyolite flows surrounded by Quaternary sediment in the valley east of Duck Creek Butte. I assign it an age older than the Duck Creek Butte eruptive center on the assumption that it conforms to the trend of westward-younging silicic volcanism, but I lack any stratigraphic relation to support this supposition. Dowell Butte is undated by isotopic methods.

The rhyolite is very light gray to pinkish gray and with 8-10 percent microphenocrysts in a partially devitrified glassy groundmass. Minerals include alkali feldspar, quartz, sericite, and hornblende. This rock is similar in hand sample and composition to the rhyolite of Indian Creek Buttes but is petrographically distinct in that it has bent, strained, and fractured crystals and contains 0.5-1 percent feathery sericite (muscovite?) that is preferentially aligned along flow lines. The strained crystals may have resulted from deformation during flow.

## 2.3 Duck Creek Butte eruptive center series

Duck Creek Butte eruptive center (DBEC) stratigraphic series includes volcanic and volcaniclastic rocks that range in composition from basalt to rhyolite. Eruptive units were emplaced between approximately 10.4 and 10.3 Ma on the basis of $^{40}Ar/^{39}Ar$ ages from the rhyodacite of Duck Creek Butte and the rhyolite of Indian Creek Buttes (Table 2-2). Not all stratigraphic relations can be resolved completely, but generalized stratigraphic relations are depicted in Figure 2-5. The sequence is dominated by rhyodacite and rhyolite (Fig. 2-6) with substantially lesser volumes of intermediate and mafic rocks.

### 2.3.1 Rhyodacite of Duck Creek Butte (Tdrd and Tdrdp)

The rhyodacite of Duck Creek Butte comprises distinctive biotite- and plagioclase-rich lava flows (Tdrd) that were erupted from multiple vents near the Duck Pond Ridge escarpment. Basal pyroclastic deposits (Tdrdp) are rarely exposed. The rhyodacite of Duck Creek Butte forms the most voluminous locally erupted unit in the map area (Fig. 2-6); it extends 18 km north-south and 10 km east-west. The eastern extent is uncertain due to faulting and subsequent burial by Quaternary lake-bed and alluvial deposits and basalt flows. Flows range in thickness from approximately 3 to more than 10 m. Talus obscures most contacts. A 180-m-thick exposure of the unit, found in a northwest-trending fault

**Table 2-2**: $^{40}Ar/^{39}Ar$ analytical data for Duck Creek Butte eruptive center.

| Sample No. | Map Unit | Geologic Unit | Material Dated | $^{40}Ar/^{39}Ar$ Age |
|---|---|---|---|---|
| JJ92-1 | $Tr_1$ | Rhyodacite of Duck Creek Butte | Biotite-1 | 10.37±0.02 |
| | | | Biotite-2 | 10.42±0.02 |
| | | | Plagioclase | 10.93±0.02† |
| JJ92-5 | $Tr_3$ | Rhyolite of Indian Creek Buttes | Sanidine | 10.32±0.01 |
| JJ92-20 | $Qb_2$ | Basalt of Duck Creek Flat | Whole Rock | 1.36±0.04 |

† Note: New plagioclase age for $Tr_1$ was received too late for inclusion in text. Preliminary analytical runs on the plagioclase lacked consistent precision of the biotite ages. See Appendix 8 for detailed $^{40}Ar/^{39}Ar$ data received after thesis was completed. Analytical precision is also reported in Appendix 8.

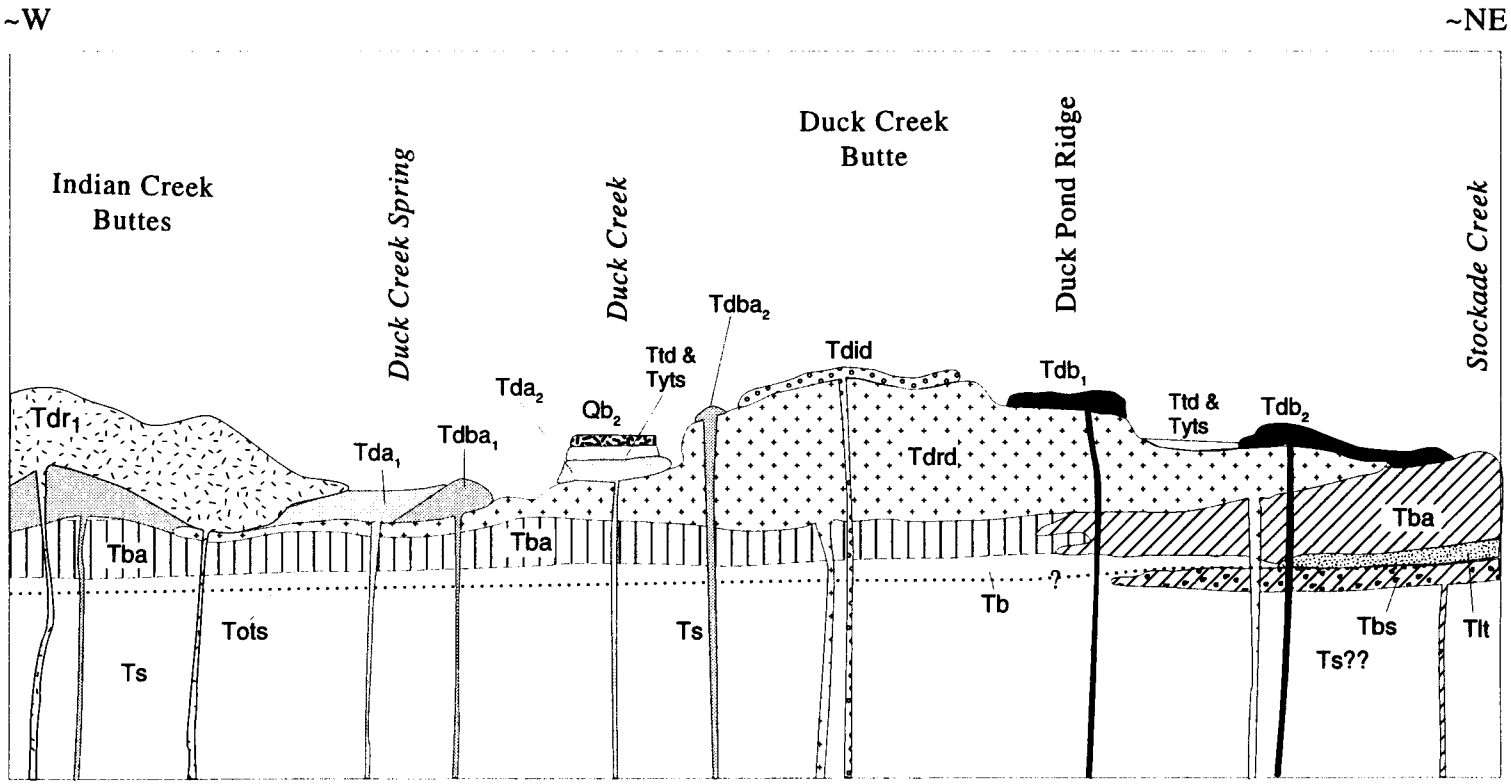


**Figure 2-5**: Schematic drawing of a hypothetical cross section through the DBEC study area. Depicts stratigraphic relations between volcanic and volcaniclastic rocks at separate geographic locations. Does not represent actual cross section, structural relationships, or thicknesses.

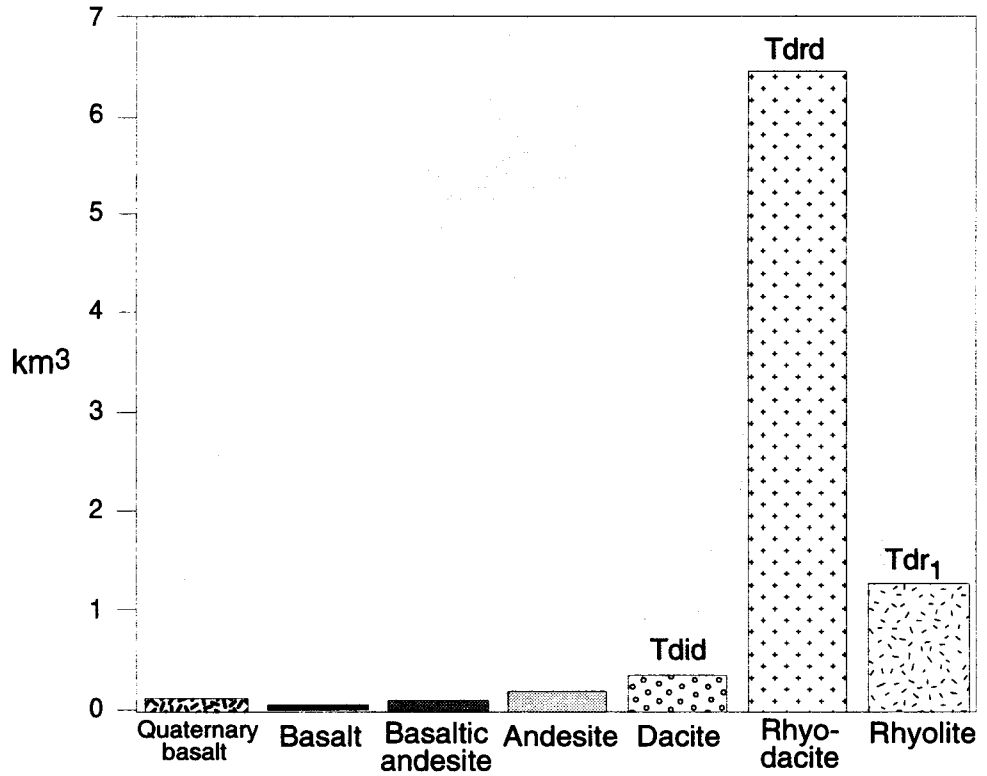


**Figure 2-6**: Histogram showing volume of lavas at DBEC, grouped by composition. Quaternary basalt measured separately from basalt in DBEC series. No pre-DBEC rocks included.

scarp (sec. 7, T. 28 S., R. 38 E.), represents a minimum thickness because the base is not exposed and the upper part has been eroded.

The chief identifying characteristic of the lava is the presence of 7 to 12 percent phenocrysts including plagioclase (5-8 percent, up to 4 mm in length), biotite (1-2 percent, up to 2 mm across), and clinopyroxene (0.5-1 percent, up to 0.7 mm in length). Also found are Fe-Ti oxides, orthopyroxene, and amphibole. Individual flows are distinguished from each other chiefly by textural changes from the vitric, brecciated base, upward through stony, devitrified central zones to an upper vitrophyre. Collective field evidence suggests that an idealized exposure might consist of a pyroclastic surge deposit, a block-and-ash flow, a lower brecciated zone, a lower vitrophyre, an inner stony devitrified zone, an upper vitrophyre, and a capping pumiceous carapace. No more than two zones are exposed in any location, but all elements have been identified. The various lithologic types are described next.

*Pyroclastic deposits (Tdrdp):* Two small outcrops of tuffaceous strata are exposed near the perimeter of Indian Creek Buttes. A 1-m-high ledge is exposed on the southeast flank of Indian Creek Buttes. Bedding planes are defined by well-sorted, clast-free ash and fine lapilli layers alternating with poorly sorted thicker beds containing 1-2 percent black silicic scoria to 3 cm in diameter, 2 percent angular chips of black rhyodacite, and about 1 percent clear crystals. A poorly sorted block-and-ash flow deposit, 3 to 4 m thick, is exposed in a single outcrop interbedded between the basalt and andesite (Tba) and rhyodacite lava flows ($SW^1/_4$ sec. 13, T. 28 S., R. 37 E.). It is composed of matrix-supported angular clasts of the glassy rhyodacite to 25 cm, subangular tan pumice as large as 25 cm in diameter, and subordinate smaller subrounded vesicular basalt clasts as large as 10 cm in diameter that were probably incorporated in the flow during transport across the ground.

*Brecciated lower zones.* Four exposures of the basal brecciated zone were found; elsewhere the basal breccia zone is probably present beneath talus. Three of the

outcrop locations in the eastern part of the map area are composed of clast-supported breccia, with angular rhyodacite clasts as large as 1 m in a compositionally similar, altered matrix. A matrix-supported breccia with angular clasts that range from 2-10 cm across is found in a separate outcrop near the southern margin of the rhyodacite flows.

*Vitrophyre.* The rhyodacite of Duck Creek Butte most commonly occurs as glassy porphyritic lava. Glassy zones have weakly developed perlitic texture owing to incipient hydration. The phenocrysts stand out in sharp contrast to the glass.

*Devitrified zone.* The glassy zone grades abruptly upward to devitrified rhyodacite across a 10-cm interval. The pale-red to medium-light-gray, streaked stony devitrified rock has abundant spherulitic alteration. Devitrified flows above Duck Pond Ridge have finely spaced contorted and parallel flow foliations that are interpreted to be near-vent flows. An unusually spherulite-rich exposure is found 750 m west-northwest of Dowell Reservoir. There, reddish-brown to grayish-red spherulites, 8 mm in diameter, weather out of the gray stony devitrified rock in bold relief mimicking the appearance of lithophysae. Where spherulitic devitrification is pervasive, the biotite and clinopyroxene phenocrysts have been destroyed.

*Pumiceous carapace.* An upper pumiceous zone is only preserved in topographically low areas or where protected by capping flows of the basalt of Duck Pond Ridge. The rock is highly inflated with a web-like texture and weathers to round boulders as large as 40 cm. It is chiefly light tan but varies from light gray to light orange.

Two $^{40}Ar/^{39}Ar$ ages of 10.38±0.04 Ma and 10.42±0.02 were obtained from biotite separated from the glassy part of the rhyodacite lava (Table 2-2). Previously published K-Ar ages of 10.0±0.4 and 9.8±0.6 Ma were obtained from biotite and plagioclase, respectively (Walker, 1974; recalculated by Fiebelkorn and others, 1982). The rhyodacite of Duck Creek Butte concordantly overlies basalt and andesite (Tba). The rhyodacite is overlain by the inclusion-rich dacite (Tdid) in its central part, by undated flows of the

andesite of Duck Creek ($Tda_2$) on the south, by the basalt of Duck Pond Ridge ($Tdb_1$) and by the finely porphyritic basalt ($Tdb_2$).

Eruption of the rhyodacite was coeval with movement along the Duck Pond Ridge fault (see Structure, Sec. 3.3). This finding elucidates timing of faulting along the Steens Mountain fault system (Johnson and Deino, 1994).

### 2.3.2 Inclusion-rich dacite (Tdid)

The sparsely porphyritic inclusion-rich dacite forms lava flows that are easily recognized in the field because they contain 5 to 25 percent by volume of ubiquitous basaltic andesite magmatic inclusions that weather out in bold relief (Fig. 2-7) or, where less abundant, appear as small round dusty-gray spots. The dacite lava flows are distributed across 8 km from south-southwest of Duck Creek Butte to Dick Creek on the north. The elongate shape of the flows suggests that the dacite flowed northward through topographic lows in the rhyodacite of Duck Creek Butte (Tdrd).

The inclusion-rich dacite overlies the rhyodacite of Duck Creek Butte in all locations except on the northeast and the northwest where it overlies the basalt and andesite (Tba). The dacite is overlain by the Devine Canyon Ash-flow Tuff (Ttd) and the Tertiary sediment beneath the tuff (Tyts) near the northern margin of the dacite.

The unit averages 15 m in thickness. Its maximum thickness of 60 m occurs in the eastern cliffs of Duck Creek Butte, where the probable vent site is located. Individual thin flows can be distinguished at the top of Duck Creek Butte. Elsewhere, however, the unit is a single massive homogeneous flow.

The dacite matrix is aphanitic and contains 3-5 percent microphenocrysts of plagioclase, Fe-Ti oxides, orthopyroxene>clinopyroxene. In contrast, the basaltic andesite inclusions, which range from 2 mm to 7 cm in diameter, are fine grained, intersertal, and vesicular. The inclusions are composed of 20-40 percent glass, 40-50 percent plagioclase (up to 0.8 mm in length), 20 percent orthopyroxene and clinopyroxene (up to 0.5 mm in length), 5

**Figure 2-7**: Photograph of basaltic andesite inclusions weathering out of inclusion- rich dacite.

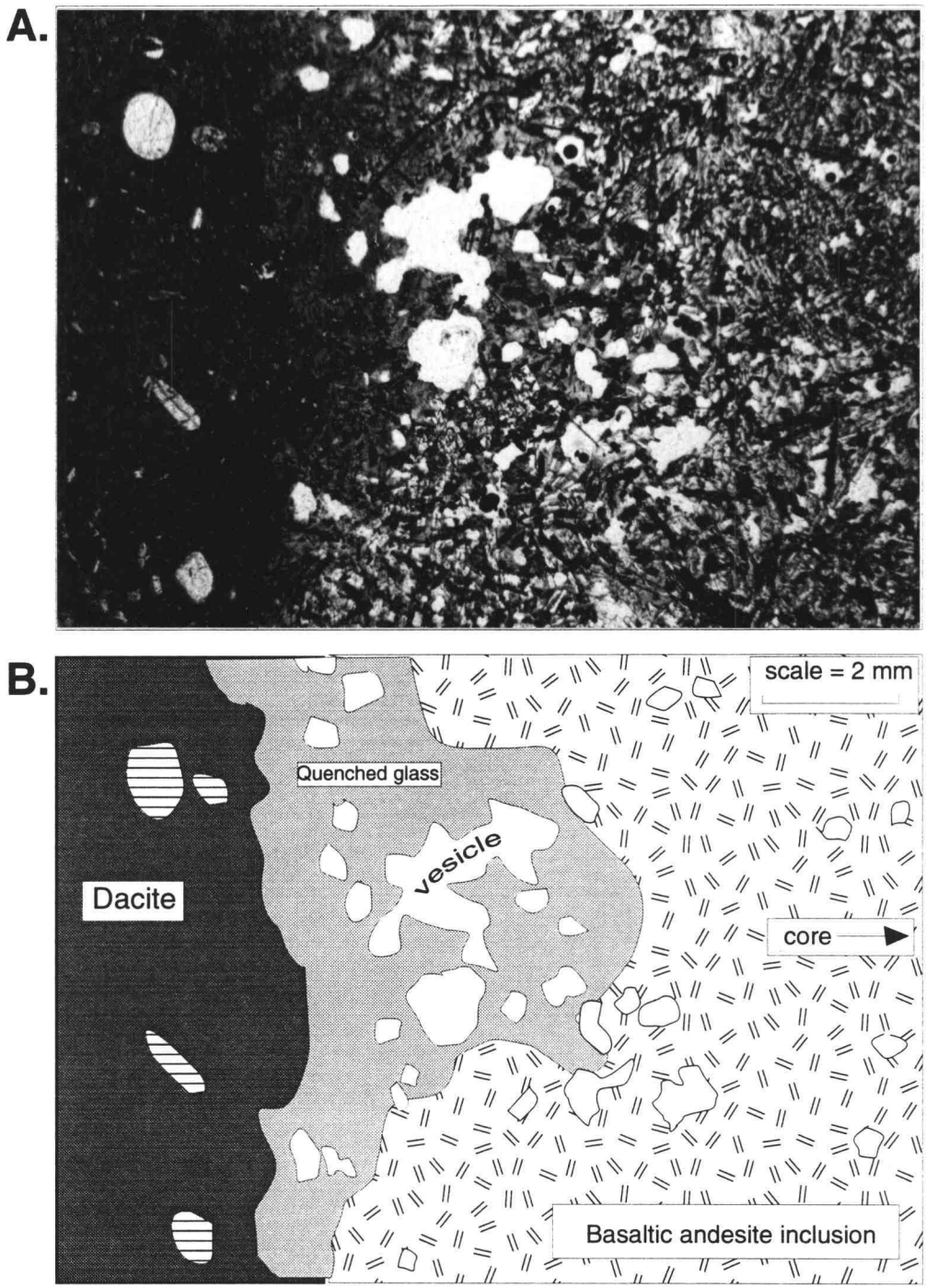


**Figure 2-8:** Petrographic thin section of contact between dacite host and quenched basaltic andesite inclusion in the inclusion-rich dacite (Tdid). (A) photograph of thin section; (B) drawing of quenched contact. White areas are vesicles, which are concentrated in the quenched glassy rim of the inclusion and become smaller and less abundant toward the core of the inclusion. Horizontal-ruled areas are plagioclase and pyroxene phenocrysts in the dacite.

percent Fe-Ti oxides (0.05-1 mm), 3 percent apatite (up to 0.1 mm in diameter), and rare olivine. Vesicles vary from 20 percent irregular-shaped voids as long as 2 mm in the glassy rim, to less than 3 percent chiefly smaller than 0.5 mm in the core. The inclusions have quench textures, indicating that the basaltic andesite was injected into the cooler dacite magma (Fig. 2-8 and Appendix 2).

### 2.3.3 Olivine-bearing basaltic andesite ($Tdba_1$)

A dark-gray, vesicular, sparsely porphyritic basaltic andesite forms a hill southwest of the rhyodacite of Duck Creek Butte. The basaltic andesite has an incipiently altered glassy groundmass and contains 15 percent phenocrysts of plagioclase (10 percent up to 4 mm in length) and microphenocrysts of olivine (3 percent, up to 0.5 mm across) and Fe-Ti oxides (2 percent, up to 0.5 mm). The unit is in contact only with the rhyodacite of Duck Creek Butte. Contacts are concealed by a mantle of talus so the relative ages of the two units may not be determined. Topographic relations on the map might suggest that the rhyodacite of Duck Creek Butte overlies the olivine-bearing basaltic andesite, but I infer that the basaltic andesite vented from the conical hill (spot elevation 5066, sec. 10, T. 28 S., R. 37 E. ), flowed around a lobe of the rhyodacite, and therefore is the younger unit.

### 2.3.4 Basaltic andesite dike ($Tdba_2$)

A dike of glassy basaltic andesite cuts the rhyodacite of Duck Creek Butte (sec. 35, T. 27 S., R. 37 E.). The outcrop is approximately 20 m long, 5 m wide, and 1-3 m high. An upper reddish oxidized carapace looks like spatter, suggesting that the dike vented at its present exposed elevation. In contrast to the compositionally similar olivine-bearing basaltic andesite ($Tdba_1$), it contains a microscopic disequilibrium assemblage of plagioclase ($An_{20}$-$An_{30}$ by Michel-Levy method), clinopyroxene, Fe-Ti oxides, orthopyroxene, biotite, and trace amounts of olivine in a light- and dark-brown banded

glassy matrix. The disequilibrium mineralogy resulted from assimilation of a small amount of melt similar to the rhyodacite of Duck Creek Butte.

### 2.3.5 Basalt of Duck Pond Ridge ($Tdb_1$)

The basalt of Duck Pond Ridge is a coarsely plagioclase-phyric intergranular olivine basalt. It lies directly upon the rhyodacite of Duck Creek Butte. Small cobbles of baked, fine-grained sedimentary rock were found as float from an animal burrow beneath the basalt but could not be found in outcrop. On the basis of field relations between the basalt and the rhyodacite, an intervening sedimentary unit would be either very thin or discontinuous. The 3-km-long flow generally ranges from 2 to 7 m thick. The inferred vent is near the topographically highest location on the unit where it forms a massive, fault-truncated 18-m-high cliff. The basalt is similar in hand specimen to the coarsely porphyritic flows of the Steens Basalt. Phenocrysts include plagioclase (20-25 percent as large as 3 cm) and olivine (7-10 percent, up to 0.6 mm in diameter).

### 2.3.6 Fine-grained basalt ($Tdb_2$)

Platy to massive flows of dark-gray, fine-grained, ophitic, porphyritic basalt cap a prominent hill approximately 0.5 km northwest of Dowell Reservoir and extend for 2.5 km to the northeast. Phenocrysts include plagioclase (8-9 percent, 5 mm) and olivine (1-2 percent, 3 mm). In contrast, the basalt of Duck Pond Ridge, $Tdb_1$, contains numerous blocky coarse plagioclase phenocrysts and differs compositionally (see Sec. 5.3.2). The fine-grained basalt directly overlies the rhyodacite of Duck Creek Butte (Tdrd) and the unit of basalt and andesite (Tba). It is difficult to determine the number or thickness of individual flows, but the maximum thickness of the unit is 60-65 m where it may have accumulated in a topographic depression.

### 2.3.7 Andesite of Duck Creek Spring ($Tda_1$)

An elongate flat-topped sequence of two or three flows of dark-gray, very fine grained andesite is exposed beneath the rhyolite of Indian Creek Buttes at its south, southeast, and northwest margins. Where fully exposed on the south, the andesite exhibits a glassy base, a horizontally to vertically flow-jointed cliff-forming face, and an upper spheroidally weathered zone. Maximum thickness is 20 m. Phenocrysts (2-3 percent) of plagioclase, olivine, and clinopyroxene are 1 to 2 mm in diameter. On the southeast of Indian Creek Buttes, a single flow of pilotaxitic andesite overlies the pyroclastic surge deposit of the rhyodacite of Duck Creek Butte (Tdrdp).

### 2.3.8 Andesite of Duck Creek ($Tda_2$)

Porphyritic andesite is exposed as dikes, near-vent accumulations of scoriaceous lapilli and bombs, and small-volume flows adjacent to and south of Duck Creek. The unit was presumably vented from hill 5052 (NE $^1/_4$ sec. 22, T. 28 S., R. 37 E. ) on the basis of vertical flow jointing observed there. This hill also is the topographically highest point on the flow. The maximum thickness of the unit is 30 m at this location. The andesite flowed both northwest and southeast.

The southeastern lobe of lava flowed down a preexisting drainage in the approximate location of Duck Creek to its terminus near the mouth of Duck Creek. A prominent exposure farther up the canyon (NE $^1/_4$ sec. 23, T. 28 S., R. 37 E. ) has vertical flow foliations and platy contacts with the older rocks suggesting that it is a thick dike. The relationship with other flows in the creek, however, indicate that it instead represents thicker deposition of lava confined in a steep drainage that has been subsequently exposed by erosion.

The rock is distinguished from the andesite of Duck Creek Spring by having 5-9 percent phenocrysts of subhedral to anhedral fresh plagioclase commonly 1 cm (rarely to 3

cm) in diameter, and 1 percent rusty speckles of iddingsitized olivine from 0.5 to 1 mm in diameter in a charcoal-gray aphanitic groundmass.

### 2.3.9 Basaltic andesite of Brokendown Waterhole ($Tdba_3$)

The basaltic andesite of Brokendown Waterhole is an extensive series of lava flows located at the north margin of the rhyolite of Indian Creek Buttes. The basaltic andesite is dark gray, fine grained, and vesicular. Single 2- to 4-m-thick lava flows extend north where they ramped onto and around the south-southeast-dipping strata of the Steens Basalt (Ts) and the unit of basalt and andesite (Tba). These lavas also flowed over a northwest-trending escarpment. Minimum areal coverage is 7 $km^2$ with an average thickness of 20 m. The groundmass comprises plagioclase (50-55 percent, up to 1 mm in length), clinopyroxene (12-15 percent, up to 0.2 mm in length), olivine (4-6 percent, up to 0.3 mm in diameter), Fe-Ti oxides (4 percent, up to 0.5 mm), and clay-altered glass (20-25 percent).

### 2.3.10 Rhyolite of Indian Creek Buttes ($Tdr_1$)

Indian Creek Buttes is constructed entirely of sparsely porphyritic to aphyric homogeneous flows of high-silica rhyolite. The rhyolite of Indian Creek Buttes overlies the Steens Basalt with angular unconformity on the west margin of the buttes and conformably overlies the andesite of Duck Creek Spring ($Tda_1$) near Duck Creek Spring at the southeast margin.

The rhyolite of Indian Creek Buttes is the second most voluminous locally erupted unit in the map area (Fig. 2-6). Maximum total thickness is 135 m at the buttes, which form a dome complex roughly 5 km in diameter. Maximum thickness of individual flows is about 60 m. The rhyolite erupted from multiple vents. One probable vent site is located in a canyon 0.5 km northwest of Duck Creek Spring. There the rhyolite forms a 10-m-high contorted knob with abundant kink folds.

Phenocrysts, found chiefly in the capping flows, include gray or pink quartz (≤1 percent, up to 1 mm in diameter), sanidine ($Or_{34}Ab_{65}$ to $Or_{67}Ab_{32}$, ≤1 percent, up to 3 mm in length), and hornblende (rare, up to 3 mm in length). The rhyolite of Indian Creek Buttes has low total phenocryst content (less than 2 percent) and lacks biotite and plagioclase, in contrast to the rhyodacite of Duck Creek Butte (Tdrd).

Contacts between devitrified, glassy, and poorly developed vapor-phase zones are obscured by talus. No basal or upper breccia or pumiceous carapace was found. The lithologic rock types within the unit are as follows:

*Devitrified zone:* Most of the rhyolite exposed at Indian Creek Buttes is devitrified and contains as much as 90 percent spherulitic alteration. Hand samples have a sugary texture and are speckled with pale-pink spherulites. The rock is very light gray to light brownish gray; weathered surfaces range from light brownish gray to dark reddish brown. Rocks with complete spherulitic overgrowth have secondary silica filling the voids.

*Vapor phase zone:* The ridge above the southwest margin of the flows has a 3-m-thick zone characterized by 30 percent round gas pockets from 5 to 8 mm in diameter with flow banding wrapping around the vesicles. The rock is devitrified with spherulitic alteration and has secondary silica in the voids. There is no petrographic evidence for lithophysae.

*Glassy zone*: Subrounded to rounded weathered obsidian as much as 10 cm in diameter is found in the talus slopes at discrete horizons beneath outcrop of devitrified rhyolite and mark probable locations of now-perlitic glassy zones. The rock varies from black obsidian to streaked black and dark-gray incipiently hydrated glass. Light-gray perlitic zones are exposed only in road cuts. Blackish-red glass is found infrequently as bands in devitrified rock.

Sanidine from Indian Creek Buttes lava yielded a $^{40}Ar/^{39}Ar$ age of 10.32±0.01 Ma (Table 2-1). This rhyolite is similar in chemical composition and hand sample lithology to the slightly more evolved rhyolite of Dowell Butte.

### 2.3.11 Rhyolite of Big Gulch ($Tdr_2$)

Two hills and a flattish poorly exposed area of stony, devitrified, aphyric flow-banded rhyolite are found at the west margin of the study area. This rhyolite is similar in composition to the rhyolite of Indian Creek Buttes, $Tdr_1$ (Table 4-7) but is of uncertain correlation and therefore is not mapped separately. Isotopic age constraints are lacking; for the purposes of this study I will assume that the rhyolite of Big Gulch conforms to the westward-younging trend and therefore is slightly younger than the rhyolite of Indian Creek Buttes. Contact relations with the Steens Basalt are confusing, as the rhyolite is topographically lower than the basalt. Three interpretations are possible: (1) the rhyolite of Big Gulch forms a thick dome deposited adjacent to the topographically higher, already-faulted Steens basalt, (2) the rhyolite is faulted down with respect to the Steens Basalt, or (3) the rhyolite is older than the Steens Basalt. Mapping of this unit was completed late in the study, and therefore the unit will not be described in further detail in this study.

## 2.4 Younger units

### 2.4.1 Younger tuffaceous sedimentary strata (Tyts)

Poorly indurated tuffaceous rocks, exposed only in stream-cut walls (SE $^1/_4$ sec. 18, T. 27 S., R. 38 E. and SE $^1/_4$ sec. 12, T. 28 S., R. 37 E.) and road cuts (S$^1/_2$ sec. 16, T. 27 S., R. 38 E.) overlie the inclusion-rich dacite (Tdid) and are overlain by the Devine Canyon Ash-flow Tuff (Ttd). The thickness of the sedimentary rocks ranges from less than 2 m to more than 15 m; variation in thickness over lateral distances of a few hundred meters may

reflect irregular topographic surfaces that existed during deposition. The unit is composed of poorly indurated sedimentary deposits including ash and sandstone.

### 2.4.2 Devine Canyon Ash-flow Tuff (Ttd)

The Devine Canyon Ash-flow Tuff is a distinctive crystal-rich tuff. The unit has a maximum preserved thickness of 30 m near its type locality, 13 km north of Burns (Greene, 1973; Walker, 1979). Maximum thickness in the map area is about 4 m, though actual thickness is difficult to determine because the tuff mantles canyon walls. The nonwelded to poorly welded uppermost part of the unit has been removed by erosion. The Devine Canyon Ash-flow Tuff was formally named by Walker (1979) for its type locality about 13 km north of Burns, Oregon.

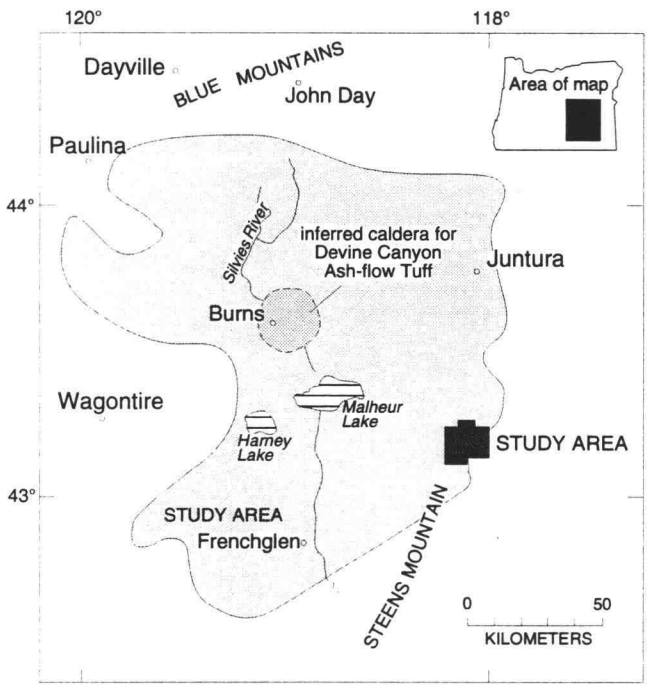


**Figure 2-9**: Map showing approximate original extent and source of Devine Canyon Ash-flow Tuff (from Walker, 1979).

Characteristically, the unit is greenish gray, massive, porphyritic densely welded ash-flow tuff. In a few exposures other parts are exposed, such as basal fallout tephra (as thick as 3 m), poorly welded basal tuff, and rarely, a capping moderately welded zone where not stripped by erosion. The tuff originally covered more than 18,600 $km^2$ of southeastern Oregon (Fig. 2-9) and had a volume of approximately 195 $km^3$ (Greene, 1973). The Devine Canyon Ash-flow Tuff probably erupted from a vent near the vicinity of Burns, as interpreted from isopachs (Greene, 1973).

Potassium-argon ages on sanidine range from 8.7 to 10.3 Ma (Fiebelkorn and others, 1982). A $^{40}Ar/^{39}Ar$ single-crystal age of 9.68±0.03 Ma was obtained from sanidine in the tuff (A.L. Deino and A.L. Grunder, unpub. data, 1993).

The Devine Canyon Ash-flow Tuff probably was largely confined to topographically low areas when emplaced. Most of the movement on northwest-striking faults was completed prior to emplacement of the unit in fault-bounded valleys, such as the Duck Creek drainage, where the tuff is preserved (see discussion in Section 3-4). The tuff conformably overlies the younger tuffaceous sedimentary strata (Tyts) in most locations in the study area. It directly overlies the inclusion-rich dacite (Tdid) in Dick Creek where it may have been deposited in a paleochannel.

### 2.4.3 Quaternary basalt.

Three separable basalt units filled the fault-bounded valley of Duck Creek Flat and Duck Creek. A fourth unit covers part of Barren Valley. Each of the basalts is medium dark gray, fine grained, diktytaxitic, and has an ophitic groundmass. Compositionally the basalts are similar (for example, high Mg and Cr and low Ti and K; Table 4-7).

#### 2.4.3.1 Glomerophyric basalt ($Qb_1$)

The oldest of these basalts ($Qb_1$) is characterized by the presence of glomerocrysts composed of olivine and plagioclase and of phenocrysts of about 2 percent each of olivine

and plagioclase. The basalt is exposed in the south half of Duck Creek Flat and extends west for approximately 4 km (Plate 1). Minimum thickness of the unit ranges from 2 to 6 m on the basis of stream-cut exposures and topographic expression; the base of the unit is not exposed.

#### 2.4.3.2 Basalt of Duck Creek Flat ($Qb_2$)

A younger, olivine-phyric basalt ($Qb_2$) probably was erupted from a vent located near the high point where the main access road crosses Duck Creek Flat. There, the vesicular basalt has abundant wavy flow features evident in morphology, color changes, and bands of vesicles. The lava flowed down Duck Creek for 2.5 km. The upper surface of the drainage-filling distal flow has well-preserved pahoehoe features as well as columnar jointing. A natural arch roughly 5 m wide by 4 m high and 1.5 m long near the terminus of this flow suggests the remnant of a lava tube that may have channeled lava farther down stream. The unit covers about 4 $km^2$ with at least two flows that have a combined thickness ranging from 5 to 30 m. It differs from the underlying glomerophyric basalt in that it lacks plagioclase phenocrysts. A whole-rock sample of the basalt of Duck Creek Flat yielded a $^{40}Ar/^{39}Ar$ age of 1.36±0.04 Ma (Table 2-1) (A.L. Deino, unpub. data; Johnson and Deino, 1994). Possesses reverse-polarity thermal remanent magnetization.

#### 2.4.3.3 Basalt of Cord ($Qb_3$)

Flows of the basalt of Cord are distinguished in the field from the basalt of Duck Creek Flat by having coarser groundmass plagioclase. Lava from this unit flowed around kipukas of the Devine Canyon Ash-flow Tuff and over the escarpment formed by the Duck Pond Ridge fault onto the floor of the Barren Valley (Fig. 2-10), where it is buried by alluvium and lake deposits. Possesses reverse-polarity thermal remanent magnetization.

A.

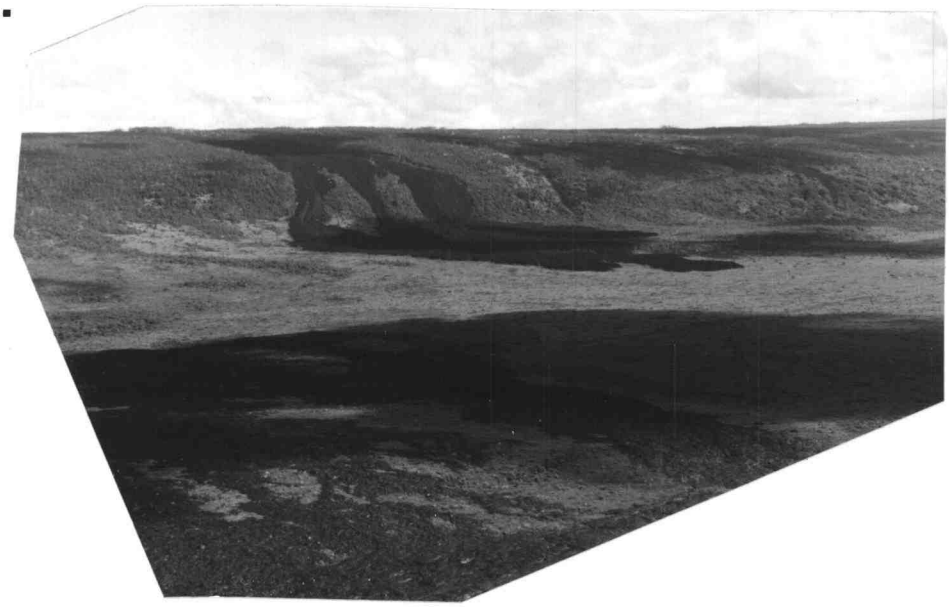

B.

**Figure 2-10:** Photographs of basalt flows over escarpment. A.) Aerial oblique view of basalt flow over the Holei Pali (fault scarp), Hawaii Volcanoes National Park, Hawaii. B.) Photograph of the basalt of Cord that forms dark flat feature where it flowed over the Duck Pond Ridge fault scarp.

#### 2.4.3.4 Basalt of Barren Valley ($Qb_4$)

Much of Barren Valley is floored by medium-gray fine-grained porphyritic basalt. The basalt, which is vesicular and diktytaxitic, entered the valley from the southeast. Chemical analysis of the basalt (sample number CH83-57B, data from W.K. Hart, written commun., 1993) indicates a fairly primitive, high-Mg, high-alumina olivine tholeiite that is chemically similar to the basalt of Duck Creek Flat ($Qb_2$) and the basalt of Cord ($Qb_3$). No age was obtained for this unit. The basalt possesses normal-polarity thermal remanent magnetization, therefore the age is younger than 0.78 Ma. An overlying, compositionally similar basalt analyzed 22 km southeast of DBEC yielded a K-Ar whole-rock age of 0.43±0.09 Ma (Hart and Mertzman, 1982).

### 2.4.4 Landslide deposits (Qls)

Five landslide deposits were mapped. Four are sizable deposits that formed along topographically steep areas of the Duck Pond Ridge escarpment. Unlike many parts of Oregon, where landslides occur where competent rocks overlie incompetent rocks, these landslides appear to be slope collapse entirely in relatively competent lava flows. The fifth is a trifling deposit at the confluence of Sutton, Soldier, and Stockade Creeks.

### 2.4.5 Lake deposits (Ql)

Lacustrine deposits composed of silt, sand, and rounded pebbles were formed by a pluvial lake that occupied the now-dry Turnbull Lakebed in Barren Valley during the Pleistocene (Snyder and others, 1964). Paleolakes were common throughout much of the western United States during the last glaciation between 29 to 11 ka (Freidel and McDowell, 1992). Although several terraces formed by high lake stands are found in the topographic depression that forms most of the south half of the Folly Farm $7^1/_2$ minute quadrangle, no wave-cut terraces were found on the perimeter of Barren Valley. Most of

the area mapped as lake deposits is tilled agricultural land. Thickness of sediment fill in the valley is unknown.

### 2.4.6 Alluvium (Qa)

Deposits mapped as alluvium consist of unconsolidated sediment formed in many environments. Much of the unit is colluvium and talus that blanket the lower slopes of bedrock hills. Moderately to well-sorted sand and gravel are found along stream beds. Much of the alluvium mapped in Barren Valley may be remnants of the Pleistocene lake deposits (Ql) now covered by grasses and wind-blown sand.

Well-indurated white diatomite is found in a 2-m-thick stream-cut exposure 0.5 km west of the west edge of the map area near Big Gulch (sec. 11, T. 28 S., R. 36 E.). Diatomite is found only at this location and probably represents a small impounded body of water adjacent to Big Gulch.

# CHAPTER 3: STRUCTURE

## 3.1 Introduction

The structural history of the map area has three main aspects: (1) the relationship between local and regional patterns of deformation, (2) the timing of faulting episodes, and (3) the relationship between faulting and magmatism at this location.

High-angle normal faults form the dominant structural pattern of DBEC. Faults can be grouped broadly into two sets according to orientation: north- to northeast-striking faults, which parallel the Basin and Range horst and graben fabric, and northwest-striking faults, which parallel the Brothers fault zone pattern (Fig. 3-1).

Basin and Range faulting, which forms the dramatic topography of southeastern Oregon such as Steens Mountain, occurred in response to east-west-directed extension that began in mid-Eocene time (Stewart, 1978; Zoback, 1989; Li and others, 1990). Duck Pond Ridge lies on strike with, and likely is a continuation of the Steens Mountain escarpment. Offset increases along the Steens Mountain escarpment from less than 300 m at Duck Pond Ridge to more than 2 km at Steens Mountain. This northward-diminishing offset is consistent with other Basin-Range faults in southern Oregon, which diminish as they reach the High Lava Plains (my measurements of dip separation on faults mapped by Walker and others, 1967, Greene and others, 1972, and Walker and Repenning, 1965).

East-west-directed extension near the map area was occurring by ~16 Ma as indicated by orientation of approximately north-striking Steens Basalt feeder dikes at Steens Mountain. Indeed, decreasing tilt upward in volcanic strata that underlie the Steens Basalt at Steens Mountain suggests faulting and tilting as early as 18 Ma (Langer, 1991). Relatively uninterrupted extension and tilting between mid-Miocene and Holocene time was proposed by Minor (1986) for the Trout Creek Mountains, 120 km south of DBEC. Evidence that east-west extension may persist to the present includes north-striking faults

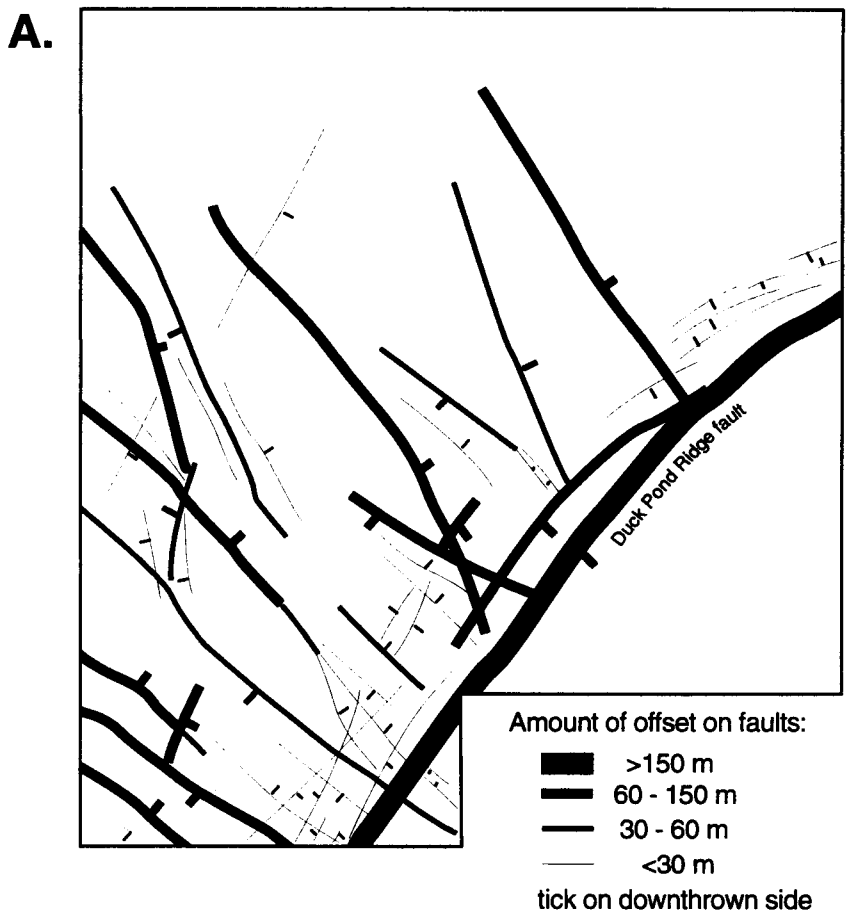


**Figure 3-1:** (A) Generalized fault map showing amount of stratigraphic separation on prominent faults in the study area. Line weight indicates relative amount of offset; (B) Inset of major northeast-striking Basin-Range faults and northwest-striking faults of Brothers fault zone. (C) Heat flow map of northwest United States (Blackwell, 1978). Dark shading indicates areas of high heat flow; gray area of low heat flow in eastern Idaho is caused by the Snake Plain aquifer.

found in the basalt of Barren Valley ($Qb_4$) (Greene and others, 1972; Walker and MacLeod, 1991), as well as in Quaternary alluvium along Steens Mountain (Walker and Repenning, 1965; Hemphill-Haley and Carver, 1988).

The northwest-striking faults that form the Brothers fault zone have been interpreted as a right-lateral strike-slip zone separating more highly extended crust on the south and less-extended crust to the north (Lawrence, 1976). These faults have generally less than 50 m of stratigraphic displacement, and show no clear evidence for strike-slip displacement (MacLean, 1994; Clayton, 1989).

At DBEC the relationship between north-northeast- and northwest-trending fault systems is unclear. The northwest-striking faults appear to be cut by, as well as cut, the north-northeast-striking faults. Both styles of faulting were present from pre-DBEC time into the Pleistocene. Northwest-striking faults are more closely spaced and have less than 120 m of dip separation. In contrast, the broadly spaced northeast-striking faults are dominated by the Duck Pond Ridge fault, which has more than 250 m of displacement.

## 3.2 Terminology

Slip indicates direction of motion or relative displacement of formerly adjacent points on opposite sides of a fault. Separation is the distance, or offset, separating stratigraphic units on both sides of the fault. In the map area, no indicators such as piercing points or slickensides were found to constrain slip. Owing to poor exposure, timing of motion on most faults is poorly constrained. Where the base of a stratigraphic unit is unexposed I estimate the amount of separation on the basis of topographic relief, which is a minimum value because of preferential erosion on the upthrown side and burial of stratigraphic units on the downthrown side.

## 3.3 Pre-eruptive and syneruptive faults

Evidence for timing of faulting along the Duck Pond Ridge-Steens Mountain escarpment can be constrained by lava flows at DBEC. The rhyodacite of Duck Creek Butte (Tdrd) flowed over an escarpment in Steens Basalt and the overlying basalt and andesite; the fault existed by 10.4 Ma when the rhyodacite flowed over the fault and formed the east-sloping flow lobe that protrudes into Barren Valley. I interpret the rhyodacite to have flowed downhill over an escarpment that was at least 30 m high. Although the basal contact is covered by talus, and offset cannot be determined, I think that the lower flows may have been faulted prior to the emplacement of the upper flows for the following reasons. Now-truncated plunging flow folds in the upper flows of the rhyodacite trend S20°E and plunge 15-26° over the edge of the escarpment (Fig. 3-2), indicating the rhyodacite flowed to the southeast over a precipice that may have been a scarp in the lower flows of the rhyodacite. These flow folds were truncated by continued movement along the fault and have ~100 m of additional offset indicating most of the offset occurred after 10.4 Ma. The basalt of Duck Pond Ridge ($Tdb_1$) is also offset by this fault, which indicates later movement.

An exposure of the andesite of Duck Creek ($Tda_2$) at the outlet of Duck Creek appears to be in its original depositional location about 5 m above the Barren Valley floor. I interpret this to indicate that movement along the Duck Pond Ridge fault was largely completed, and evidence for any additional movement is buried beneath Quaternary alluvium and lake-bed deposits. Minimum offset of the Duck Pond Ridge fault is 250 m on the basis of topographic relief.

Another example of faulting that may have preceded or been coeval with the DBEC lava flows is indicated by the unfaulted basaltic andesite of Brokendown Waterhole ($Tdba_3$). Flows of this unit were obstructed by a fault block of Steens Basalt and the older basalt and andesite (Ts and Tba respectively; hill 5425, sections 8 and 17, T. 27 S., R. 37 E.). The

block, formed by two northwest-striking faults, is tilted south-southeast, in contrast to other fault blocks in that area that are untilted or dip to the west, such as Post Mountain. Two other exposures of Steens Basalt 3.5 and 4.2 km due south of hill 5425 dip to the east-southeast beneath the rhyolite of Indian Creek Buttes ($Tdr_1$). Although the lava flows are concordant where the rhyolite ramps onto the dipping basalt strata, the contact is interpreted as an angular unconformity.

The basaltic andesite of Brokendown Waterhole ($Tdba_3$) flowed north, banked onto the lower slopes of hill 5425, and flowed over the northwest-trending escarpment east of the hill to its terminus at Brokendown Waterhole. A northeast-striking fault displaces the basaltic andesite approximately 5-10 m down to the east.

## 3.4 Post-DBEC structural history

Movement along northwest-striking faults continued after deposition of the rhyolite of Indian Creek Buttes. Evidence for this is found in three faults near the west margin of the buttes. The center fault transects the rhyolite west of hill 5766 ($N^1/_4$ sec. 32, T. 27 S., R. 37 E.) and forms the steep slope along the southwest margin of Indian Creek Buttes. The westernmost fault displaced the rhyolite down to the southwest as much as 90 m. These faults may extend down Duck Creek but are buried beneath colluvium and alluvium (Qa) and the basalt of Duck Creek Flat ($Qb_2$). Ramped and contorted flow lobes of the rhyolite and talus-covered contacts make fault traces difficult to locate precisely.

Remnants of the Devine Canyon Ash-flow Tuff (Ttd) are typically preserved as northwest-trending elongate outcrops. These remnants indicate a structural grain highlighted by thicker deposition of the tuff in the topographically lower areas of the northwest-trending fault-bounded valleys. From this evidence I infer that northwest-trending faults existed prior to the emplacement of the Devine Canyon Ash-flow Tuff

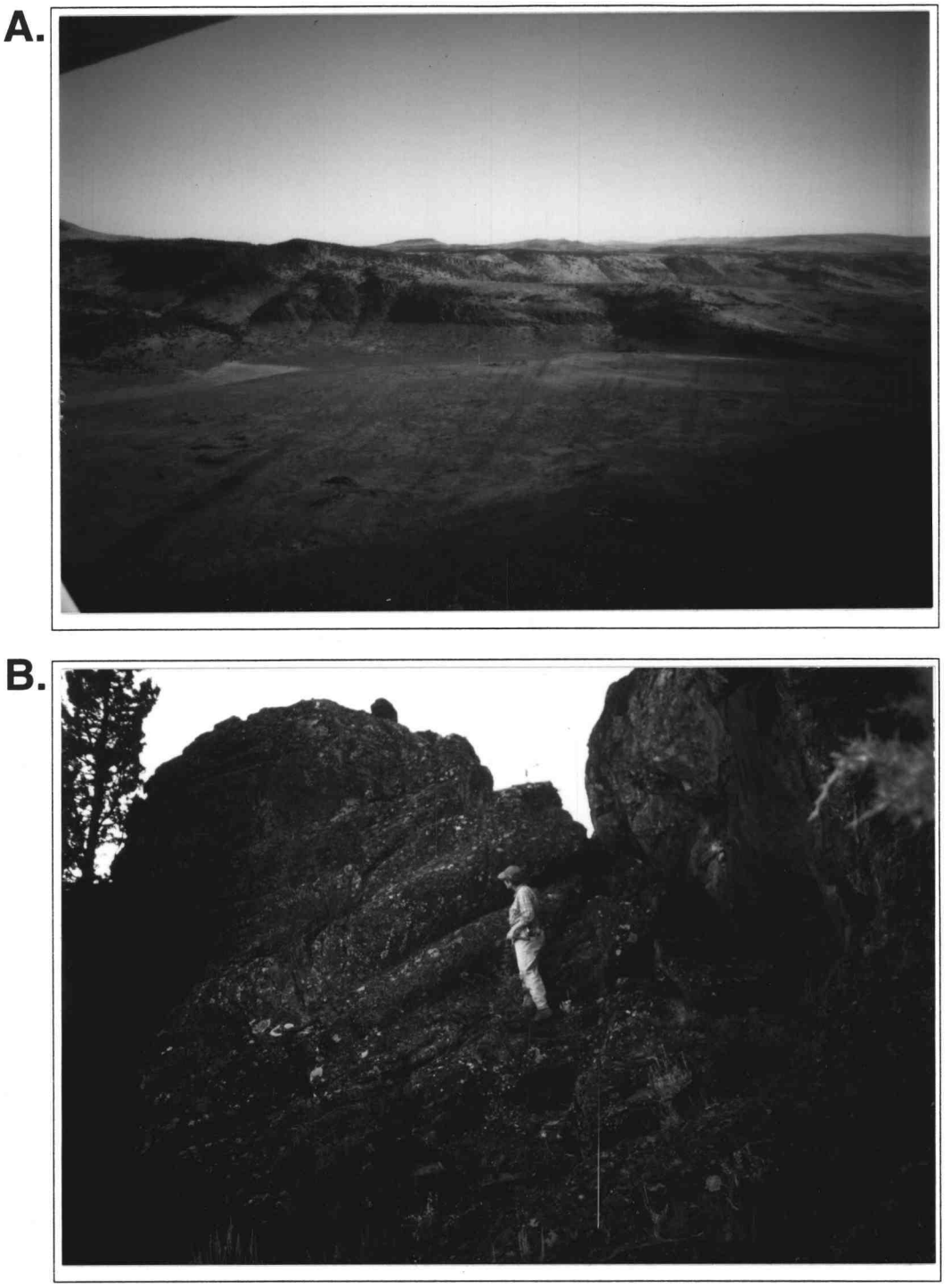


**Figure 3-2**: Photographs of flow lobe of the rhyodacite of Duck Creek Butte and plunging flow lobes in the rhyodacite. A) Aerial oblique view of the flow lobe of rhyodacite that flowed over the Duck Pond Ridge escarpment into Barren Valley. B) Plunging folds in the rhyodacite along Duck Pond Ridge escarpment.

about 9.7 Ma. Alternatively, the present exposures of tuff might represent thicker deposition in stream channels incised in a northwest-dipping fault block. The tuff is found the length of Baker Pass, the southwesternmost drainage in the study area. The Baker Pass trough is a narrow linear graben that drains in opposite directions from its summit near the turnoff to Duck Creek Butte on Highway 78. The Baker Pass exposures, and similar outcrop relations in another west-trending graben south of the map area, suggest that the tuff was entirely constrained along a preexisting graben.

An exposure of the Devine Canyon Ash-flow Tuff at the north end of Post Mountain is undeformed by the northwest-striking fault that formed Post Mountain, indicating that the tuff was deposited after the fault-bounded valley on the east side of Post Mountain had formed. Similarly, an outcrop of Devine Canyon Ash-flow Tuff northwest of the rhyolite of Big Gulch ($Tdr_2$) also blankets a northwest-striking fault.

Quaternary faulting is indicated by deformation of the Quaternary basalt lava flows. A fault offsets the basalt of Duck Creek Flat ($Qb_2$) about 30 m east-side-down at the basalt lava's terminus in Duck Creek. The basalt of Cord ($Qb_3$) is cut by a north-northwest-striking fault with at least 5 m of offset; alluvium mantles the downthrown side. No lineaments are preserved in the tilled Quaternary lake bed deposits of Barren Valley.

# CHAPTER 4: GEOCHEMISTRY

## 4.1 Mineral Chemistry

### 4.1.1 Introduction

The following samples were selected for chemical analysis of phenocrysts by microprobe, on the basis of whole-rock composition, to represent the major petrologic groups of the 10.5- to 10.3Ma DBEC rock series:

**Table 4-1:** Samples for microprobe analysis. Refer to Appendix 2 for detailed petrographic descriptions. pl=plagioclase, san=sanidine, cpx=clinopyroxene, opx=orthopyroxene, ol=olivine, Fe-Ti=Fe-Ti oxides, hb=hornblende, bi=biotite, qtz=quartz, ap=apatite *Italics* = trace phase

| Sample No. | Map Unit | Sample descriptor | Abbreviated phenocryst mineralogy |
|---|---|---|---|
| JJ92-99 | $Tdb_2$ | Fine-grained basalt | pl>>cpx>Fe-Ti>ol |
| JJ93-130 | $Tdb_1$ | Basalt of Duck Pond Ridge | pl>>ol>Fe-Ti>*cpx* |
| JJ92-51 | Tdid | Basaltic-andesite inclusion in dacite | pl>opx>cpx>Fe-Ti>ap |
| JJ92-102 | Tdid | Inclusion-rich dacite | pl>Fe-Ti>opx>cpx>>hb, *bi, qtz, ol* |
| JJ92-1 | Tdrd | Rhyodacite of Duck Creek Butte | pl>bi>cpx>opx>Fe-Ti>am |
| JJ92-5 | $Tdr_1$ | Rhyolite of Indian Creek Buttes | san>pl>qtz>hb |

The bulk of the volcanic rocks at DBEC contain phenocrysts of plagioclase, clinopyroxene, olivine, Fe-Ti oxides, and biotite, with lesser amounts of orthopyroxene, sanidine or alkali feldspar, amphibole, and apatite. Selected feldspars, pyroxenes, olivine, biotite, and amphibole were analyzed by microprobe. Representative analyses for each mineral group are presented in Tables 4-2 through 4-6 (see Appendix 3 for complete analyses).

### 4.1.2 Feldspar

Plagioclase is ubiquitous in DBEC rocks with the exception of the rhyolite of Indian Creek Buttes, $Tdr_1$, which contains only alkali feldspar (Table 4-2, Fig. 4-1). Plagioclase ranges from oligoclase in Tdrd to bytownite in $Tdb_2$. Overall, plagioclase becomes more An rich from rhyodacite to basalt. Variation in core compositions between minerals within the same rock sample result both from slight compositional variation as well as the fact that the polished sections do not necessarily slice through the center of the crystal.

Phenocryst phases in $Tdb_1$ are exclusively normally zoned labradorite ($An_{51}$ to $An_{65}$) (Fig. 4-1). Intergranular groundmass crystals are andesine with a very slight compositional range ($An_{43}$ to $An_{45}$). Plagioclase in $Tdb_2$ exhibits both normal and reverse zoning and ranges between andesine and bytownite ($An_{45}$ to $An_{72}$). Groundmass laths in $Tdb_2$ are labradorite.

Plagioclase in the basaltic-andesite inclusion from unit Tdid has a small compositional range from andesine to labradorite ($An_{37}$ to $An_{54}$) and the single rim-core analysis revealed reverse zonation. Plagioclase phenocrysts in the dacite host are similar to the plagioclase in the inclusion (and may indeed be xenocrysts from the mafic injection) but have a slightly narrower compositional range ($An_{39}$ to $An_{50}$). Plagioclase in Tdrd is chiefly reversely zoned but also exhibits normal zoning. Multiple-point traverses across oscillatory-zoned crystals were not performed. Composition ranges from oligoclase to andesine ($An_{27}$ to $An_{48}$).

Sanidine ($Or_{43}$ to $Or_{67}$) and anorthoclase ($Or_{34}$ to $Or_{37}$) are found only in the rhyolite of Indian Creek Buttes ($Tdr_1$, JJ92-5). All samples showed a slightly more sodic rim relative to core composition.

### 4.1.3 Pyroxene

Clinopyroxene crystals range from $En_{50}$ to $En_{60}$ (enstatite) for basalt to dacite (Table 4–3, Fig. 4-2). In Tdrd, clinopyroxene is slightly more enriched in iron ($En_{32-38}$).

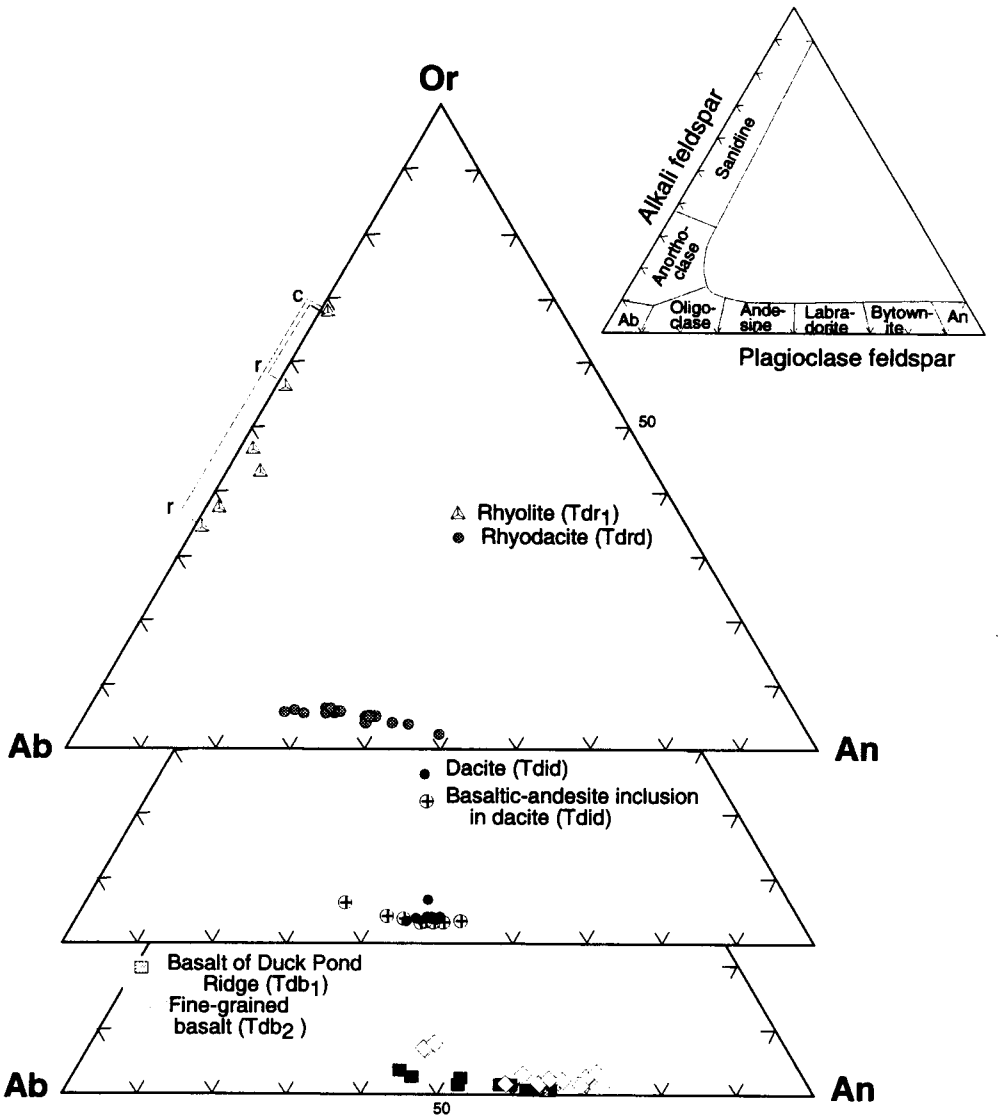


**Figure 4-1**: Feldspar compositions plotted on the feldspar ternary. Inset (upper right) shows fields for alkali feldspar and plagioclase. Or = orthoclase; Ab = albite; An = anorthite. Rim and core compositions for orthoclase feldspar are designated by 'r' and 'c', respectively, and are connected by dashed line.

**TABLE 4-2:** Representative microprobe analyses of feldspar

| | RHYOLITE | | | | | |
|---|---|---|---|---|---|---|
| **Sample No.** | **JJ92-5** | **JJ92-5** | **JJ92-5** | **JJ92-5** | **JJ92-5** | **JJ92-5** |
| **Map unit** | **Tdrl** | **Tdrl** | **Tdrl** | **Tdrl** | **Tdrl** | **Tdrl** |
| | **(c--** | **--r)** | **(c--** | **--r)** | **c** | **c** |
| $SiO_2$ | 65.1 | 65.79 | 64.25 | 65.51 | 65.03 | 65.85 |
| $Al_2O_3$ | 19.17 | 19.19 | 19.18 | 19.53 | 19.27 | 19.47 |
| CaO | 0.17 | 0.2 | 0.19 | 0.29 | 0.36 | 0.32 |
| $Na_2O$ | 3.58 | 4.81 | 3.57 | 7.21 | 5.91 | 6.91 |
| $K_2O$ | 11.35 | 9.42 | 11.36 | 5.65 | 7.94 | 6.18 |
| MgO | 0.01 | 0.01 | 0 | 0.01 | 0 | 0 |
| FeO | 0.06 | 0.09 | 0.05 | 0.09 | 0.15 | 0.13 |
| BaO | 0.24 | 0.23 | 0.22 | 0.16 | 0.4 | 0.42 |
| | 99.68 | 99.74 | 98.82 | 98.45 | 99.06 | 99.28 |
| An | 1 | 1 | 1 | 1 | 2 | 2 |
| Ab | 32 | 43 | 32 | 65 | 52 | 61 |
| Or | 67 | 56 | 67 | 34 | 46 | 37 |
| **plag. comp.** | sanidine | sanidine | sanidine | anorthoclase | sanidine | sanidine |

| | RHYODACITE | | | | |
|---|---|---|---|---|---|
| **Sample No.** | **JJ92-1** | **JJ92-1** | **JJ92-1** | **JJ92-1** | **JJ92-1** |
| **Map unit** | **Tdrd** | **Tdrd** | **Tdrd** | **Tdrd** | **Tdrd** |
| | **c** | **(c--** | **------** | **-------** | **--r)** |
| $SiO_2$ | 61.26 | 58.30 | 59.80 | 56.33 | 57.57 |
| $Al_2O_3$ | 24.17 | 25.83 | 25.27 | 27.92 | 26.39 |
| CaO | 5.42 | 7.63 | 6.59 | 9.82 | 8.84 |
| $Na_2O$ | 7.45 | 6.38 | 6.99 | 5.5 | 5.92 |
| $K_2O$ | 1.18 | 0.79 | 1.02 | 0.47 | 0.61 |
| MgO | 0.01 | 0.01 | 0.00 | 0.04 | 0.02 |
| FeO | 0.1 | 0.20 | 0.18 | 0.32 | 0.44 |
| BaO | 0.02 | 0.02 | 0.04 | 0.08 | 0.09 |
| | 99.61 | 99.16 | 99.89 | 100.48 | 99.88 |
| An | 27 | 38 | 32 | 48 | 43 |
| Ab | 66 | 57 | 62 | 49 | 53 |
| Or | 7 | 5 | 6 | 3 | 4 |
| **plag. comp.** | oligoclase | andesine | andesine | andesine | andesine |

Complete analyses in Appendix 3. c = core; (c----r) = core to rim; gm = groundmass crystal
Beam comditions: beam current, 30 na; accelerating voltage, 15 kv; beam diameter, 5 microns; counting time 10 sec. for all elements except for Ba (20 sec). Analytical precision based on repeat analyses of standards is better than 1 percent for SiO2, Al2O3, K2O (sanidine) and CaO (labradorite), better than 5 percent for Na2O, K2O (oligoclase), CaO (oligoclase), and BaO (sanidine). All others are at or below detection limit.Ternary feldspar compositions: Ab = albite ($NaAlSi_3O_8$); Or = orthoclase ($KAlSi_3O_8O$; An = anorthite ($CaAl_2Si_2O_8$)

TABLE 4-2 (Continued)

BASALT

| Sample No. | JJ92-99 | JJ92-99 | JJ92-99 | JJ92-99 | JJ92-99 | JJ93-130 | JJ93-130 | JJ93-130 |
|---|---|---|---|---|---|---|---|---|
| Map unit | $Tdb_2$ | $Tdb_2$ | $Tdb_2$ | $Tdb_2$ | $Tdb_2$ | $Tdb_1$ | $Tdb_1$ | $Tdb_1$ |
| | (c– | –r) | gm | (c– | –r) | c | c | c |
| $SiO_2$ | 51.35 | 50.37 | 53.01 | 49.96 | 53.43 | 56.33 | 51.67 | 55.02 |
| $Al_2O_3$ | 30.22 | 30.89 | 27.49 | 31.5 | 28.6 | 26.56 | 30.07 | 27.97 |
| CaO | 13.3 | 14.29 | 11.91 | 14.6 | 11.57 | 9.38 | 13.17 | 10.84 |
| $Na_2O$ | 3.82 | 3.17 | 4.3 | 3.14 | 4.65 | 5.81 | 3.87 | 5.26 |
| $K_2O$ | 0.25 | 0.27 | 0.44 | 0.21 | 0.4 | 0.5 | 0.2 | 0.47 |
| MgO | 0.12 | 0.11 | 0.51 | 0.12 | 0.1 | 0.05 | 0.09 | 0.08 |
| FeO | 0.55 | 0.73 | 1.13 | 0.48 | 0.88 | 1.19 | 0.65 | 0.71 |
| BaO | 0.03 | 0.04 | 0.02 | 0.01 | 0.01 | 0.03 | 0.01 | 0.09 |
| | 99.64 | 99.87 | 98.81 | 100.02 | 99.64 | 99.85 | 99.73 | 100.44 |
| An | 65 | 70 | 59 | 71 | 57 | 45 | 65 | 51 |
| Ab | 34 | 28 | 38 | 28 | 41 | 52 | 34 | 46 |
| Or | 1 | 2 | 3 | 1 | 2 | 3 | 1 | 3 |
| plag. comp. | labradorit e | bytownite | labradorit e | bytownite | labradorite | andesine | labradorite | labradorite |

INCLUSION-RICH DACITE (Inclusion and attached dacite from sample JJ92-51)

| Sample No. | JJ92-51 | JJ92-51 | JJ92-51 | JJ92-51 | JJ92-51 |
|---|---|---|---|---|---|
| Map unit | Tdid | Tdid | Tdid | Tdid | Tdid |
| | c | c | c | (c– | –r) |
| $SiO_2$ | 55.66 | 56.93 | 54.76 | 55.85 | 53.42 |
| $Al_2O_3$ | 27.36 | 26.97 | 28.11 | 26.54 | 24.74 |
| CaO | 10.35 | 9.03 | 10.68 | 9.30 | 12.37 |
| $Na_2O$ | 5.28 | 5.68 | 5.23 | 5.71 | 5.16 |
| $K_2O$ | 0.61 | 0.76 | 0.61 | 0.63 | 0.83 |
| MgO | 0.07 | 0.05 | 0.06 | 0.10 | 0.07 |
| FeO | 0.65 | 0.50 | 0.77 | 1.21 | 0.71 |
| BaO | 0.04 | 0.09 | 0.03 | 0.06 | 0.10 |
| | 100.02 | 100.01 | 100.25 | 99.4 | 97.4 |
| An | 50 | 45 | 51 | 45 | 54 |
| Ab | 46 | 51 | 45 | 51 | 41 |
| Or | 4 | 4 | 4 | 4 | 4 |
| plag. comp. | andesine | andesine | labradorite | andesine | labradorite |

Complete analyses in Appendix 3. c = core; (c----r) = core to rim; gm = groundmass crystal
Beam comditions: beam current, 30 na; accelerating voltage, 15 kv; beam diameter, 5 microns; counting time 10 sec. for all elements except for Ba (20 sec). Analytical precision based on repeat analyses of standards is better than 1 percent for SiO2, Al2O3, K2O (sanidine) and CaO (labradorite), better than 5 percent for Na2O, K2O (oligoclase), CaO (oligoclase), and BaO (sanidine). All others are at or below detection limit.Ternary feldspar compositions: Ab = albite ($NaAlSi_3O_8$); Or = orthoclase ($KAlSi_3O_8$); An = anorthite ($CaAl_2Si_2O_8$)

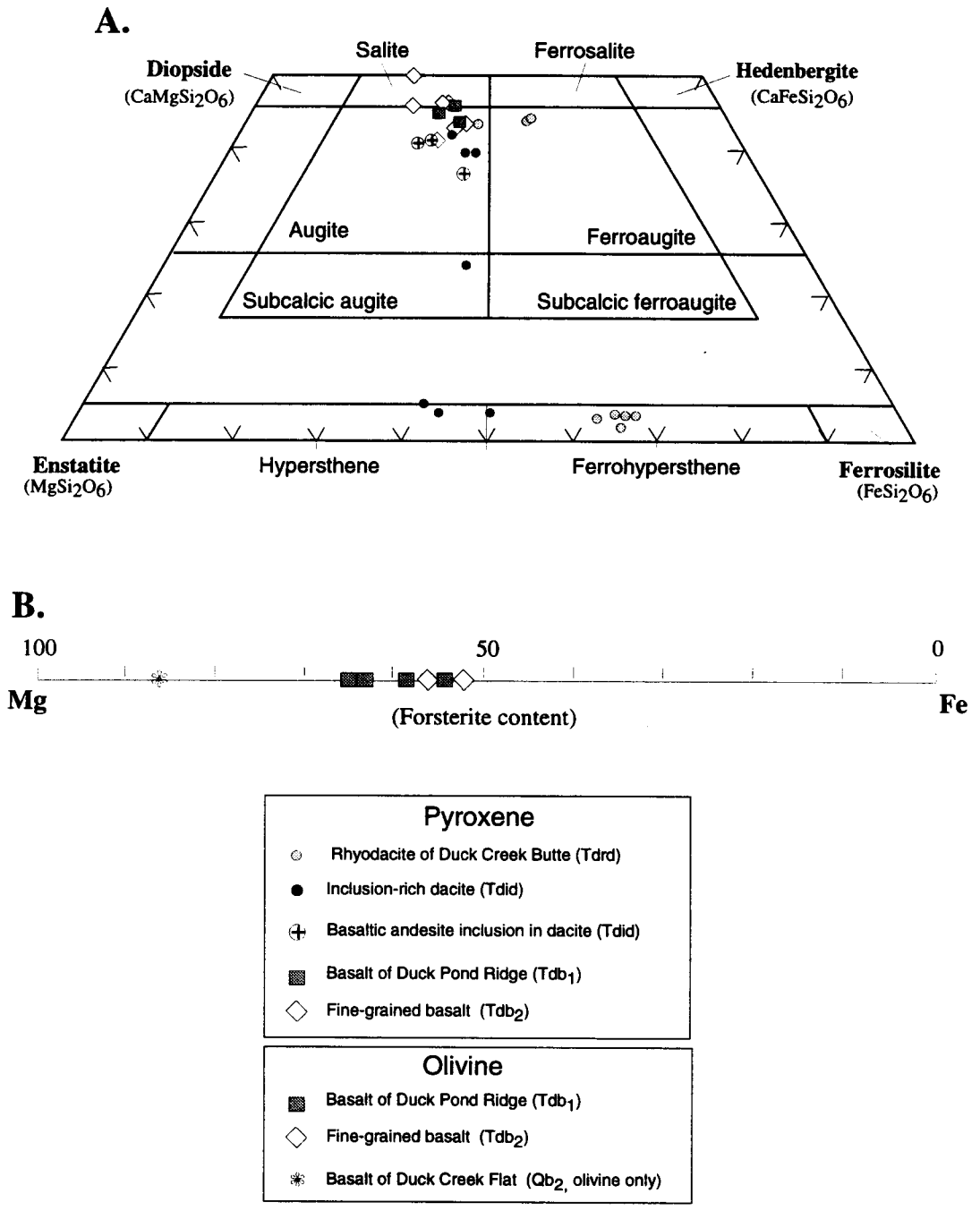


**Figure 4-2:** Pyroxene and olivine compositions. (**A**) Pyroxene quadrilateral. (**B**) Olivine compositions.

**TABLE 4-3:** Representative microprobe analyses of pyroxene.

| Sample No. | JJ92-51 | JJ92-51 | JJ92-51 | JJ92-51 | JJ92-51 | JJ93-130 | JJ93-130 | JJ92-99 | JJ92-99 | JJ92-1 | JJ92-1 | JJ92-1 | JJ92-1 |
|---|---|---|---|---|---|---|---|---|---|---|---|---|---|
| Map unit | Tdid-i | Tdid-i | Tdid-i | Tdid-h | Tdid-h | Tdb1 | Tdb1 | Tdb2 | Tdb2 | Tdrd | Tdrd | Tdrd | Tdrd |
| $SiO_2$ | 50.59 | 50.22 | 49.71 | 50.36 | 51.79 | 51.76 | 49.95 | 50.23 | 52.36 | 50.68 | 51.41 | 51.42 | 51.43 |
| $TiO_2$ | 1.41 | 1.47 | 1.12 | 1.05 | 0.46 | 1.28 | 1.07 | 1.49 | 1.04 | 0.12 | 0.11 | 0.43 | 0.12 |
| $Al_2O_3$ | 4.08 | 4.05 | 3.16 | 3.09 | 1.42 | 2.05 | 1.72 | 3.45 | 1.45 | 0.58 | 0.72 | 1.69 | 0.89 |
| FeO | 12.89 | 11.34 | 12.43 | 10.96 | 22.03 | 10.95 | 10.59 | 9.78 | 11.77 | 30.63 | 27.42 | 11.99 | 15.30 |
| MnO | 0.34 | 0.31 | 0.41 | 0.34 | 0.56 | 0.33 | 0.35 | 0.19 | 0.38 | 1.55 | 0.97 | 0.42 | 0.92 |
| MgO | 15.71 | 14.76 | 14.81 | 14.83 | 21.67 | 14.36 | 14.24 | 14.26 | 14.99 | 14.34 | 16.91 | 13.20 | 10.56 |
| CaO | 15.90 | 17.97 | 17.34 | 18.73 | 2.04 | 20.38 | 19.62 | 20.40 | 18.55 | 1.35 | 1.37 | 19.30 | 20.12 |
| $Na_2O$ | 0.41 | 0.37 | 0.34 | 0.39 | 0.02 | 0.38 | 0.61 | 0.37 | 0.36 | 0.03 | 0.05 | 0.37 | 0.36 |
| $Cr_2O_3$ | 0.00 | 0.00 | 0.00 | 0.00 | 0.04 | 0.00 | 0.04 | 0.15 | 0.00 | 0.00 | 0.02 | 0.00 | 0.00 |
| | 101.33 | 100.49 | 99.32 | 99.75 | 100.03 | 101.49 | 98.19 | 100.32 | 100.90 | 99.28 | 98.98 | 98.82 | 99.70 |
| Wo | 36 | 41 | 39 | 42 | 4 | 45 | 44 | 46 | 41 | 3 | 3 | 43 | 44 |
| En | 35 | 33 | 33 | 33 | 47 | 31 | 32 | 32 | 33 | 31 | 37 | 30 | 23 |
| Fs | 29 | 26 | 28 | 25 | 48 | 24 | 24 | 22 | 26 | 66 | 60 | 27 | 33 |

Complete analyses are found in Appendix 3. Beam conditions: beam current, 50 na; accelerating voltage, 15 kv; beam diameter, 1 micron; than 1 percent for $SiO_2$, $Al_2O_3$, MgO, and CaO; better than 5 percent for $TiO_2$ and $Na_2O$; 5 to 15 percent for FeO, MnO, and $Cr_2O_3$.
Pyroxene compositions: Wo = wollastonite (Ca2Si2O6); En = enstatite (Mg2Si2O6); Fs = ferrosilite (Fe2Si2O6)

Orthopyroxene is found only in the dacite (Tdid) and the rhyodacite (Tdrd) andoccurs as hypersthene and ferrohypersthene, respectively. No pyroxene was found in $Tdr_1$.

$Tdb_1$ has sparse, tiny intergranular augite that averages $Wo_{44}En_{32}Fs_{24}$ with slight variation. The ophitic augite of $Tdb_2$ ranges from $Wo_{41}En_{33}Fs_{26}$ to $Wo_{50}En_{26}Fs_{24}$, with a systematically higher calcium (Wo) component when measured adjacent to plagioclase versus adjacent to olivine or iron oxides. The basaltic-andesite inclusion of Tdid has only clinopyroxene with a small range of compositions in the augite field (Fig. 4-2a), typically about $Wo_{40}En_{32}Fs_{29}$. It is subhedral and unzoned. The dacite host has both clinopyroxene and orthopyroxene, and shows the widest range of calcium content within the augite field ($Wo_{24}$-$Wo_{42}$). In general, the cores of the augite in the dacite are similar to those of the basaltic-andesite inclusion ($Wo_{36}$-$Wo_{42}$) with the exception of a Wo-depleted rim on a crystal in the dacite ($Wo_{24}$). Crystals vary from subhedral to euhedral. Orthopyroxene ranges from hypersthene ($En_{56}$) to low-iron ferrohypersthene ($En_{47}$), and varies from euhedral laths to anhedral subround remnants. If I assume that the two pyroxenes formed in equilibrium with the dacite, then temperatures between 900 and 1,000°C are calculated by using the pyroxene compositions and the projection method of Lindsley (1983); however, mineral relations are not clear owing to uncertainties introduced during magmatic mixing.

Unit Tdrd has both ferrohypersthene and ferrohedenbergite phenocrysts. The crystals are most commonly subhedral to anhedral and are unzoned, though both a normally zoned, subhedral and a reversely zoned, anhedral ferrohypersthene were found. A single anhedral augite phenocryst probably represents a phase in disequilibrium with the melt, because $Wo_{44}En_{23}Fs_{33}$ is the most common clinopyroxene in the rhyodacite. Using the two-pyroxene thermometer of Lindsley (1983), and assuming partial requilibration on cooling, a minimum temperature of formation of ≈700°C is estimated. The estimated temperature may be in error owing to compositional variation reflecting analytical or calibration errors, or due to mixed mineralogy caused by hybridization of magmas.

### 4.1.4 Olivine

Olivine in both basalts ($Tdb_1$, $Tdb_2$) is homogeneous with a range in composition from $Fo_{65}$ to $Fo_{53}$ (Fig. 4-2b; Table 4-4). Phenocryst phases in both lavas are normally zoned. Groundmass crystals in $Tdb_2$ are typically more iron rich ($Fo_{53}$) than the phenocrysts. Groundmass olivine was not found in $Tdb_1$. Although olivine was found in thin-section analysis of the Tdid basaltic-andesite inclusion and in one thin section of the dacite host, none was found in the polished section. An olivine separate from $Qb_2$ was considerably more magnesian, $Fo_{86}$, than the DBEC basalts olivine.

### 4.1.5 Biotite

Biotite was found only in Tdrd and is commonly euhedral (Table 4-6).

### 4.1.6 Amphibole

Amphibole is present in Tdrd, but was not found on the polished section prepared for microprobe analysis. Amphibole in $Tdr_1$ is hornblende. It is remarkably uniform in composition both between and within individual crystals, suggesting equilibrium crystallization (Table 4-6).

### 4.1.7 Ilmenite

A single groundmass phenocryst of ilmenite was microprobed using the pyroxene standard and is presented in Table 4-5.

### 4.1.8 Chrome spinel

A single cryptocrystalline chrome spinel inclusion was found in an olivine separate from the basalt of Duck Creek Flat (Table 4-5)

**Table 4-4:** Representative microprobe analyses of olivine.

| Sample No. | JJ93-130 | JJ93-130 | JJ93-130 | JJ92-99 | JJ92-99 | JJ92-99 | JJ92-20 |
|---|---|---|---|---|---|---|---|
| Map unit | Tdb1 | Tdb1 | Tdb1 | Tdb2 | Tdb2 | Tdb2 | Qb2 |
| | c-- | --r | typ | c-- | --r | typ | typ |
| SiO2 | 36.17 | 34.83 | 35.10 | 36.05 | 35.35 | 34.47 | 40.9 |
| TiO2 | 0.03 | 0.07 | 0.06 | 0.01 | 0.08 | 0.09 | 0.01 |
| Al2O3 | 0.00 | 0.00 | 0.00 | 0.00 | 0.00 | 0.00 | 0.07 |
| FeO | 30.90 | 37.89 | 36.33 | 31.32 | 36.21 | 39.69 | 14.03 |
| MnO | 0.37 | 0.64 | 0.54 | 0.40 | 0.46 | 0.56 | 0.19 |
| MgO | 32.63 | 26.21 | 27.87 | 31.45 | 26.36 | 24.62 | 47.67 |
| CaO | 0.18 | 0.11 | 0.15 | 0.15 | 0.14 | 0.07 | 0.28 |
| NiO | 0.07 | 0.03 | 0.06 | 0.05 | 0.05 | 0.06 | 0.01 |
| ZnO | 0.01 | 0.03 | 0.00 | 0.05 | 0.06 | 0.03 | |
| | 100.36 | 99.81 | 100.11 | 99.48 | 98.71 | 99.59 | 103.16 |
| Fo | 65 | 55 | 58 | 64 | 56 | 53 | 86 |

**Table 4-5: Microprobe analyses of ilmenite and chrome spinel.**

| Ilmenite | | Chrome-spinel inclusion in olivine | |
|---|---|---|---|
| Sample No. | JJ93-130 | | JJ92-20 |
| Map unit | Tdb1 | | Qb2 |
| SiO2 | 0.12 | SiO2 | 0.16 |
| TiO2 | 20.84 | TiO2 | 0.26 |
| Al2O3 | 1.62 | Al2O3 | 47.79 |
| FeO | 70.94 | FeO | 17.52 |
| MnO | 0.61 | MnO | 0.17 |
| MgO | 1.88 | MgO | 17.99 |
| CaO2 | 0.10 | CaO | 0.00 |
| Na2O | 0.03 | Cr | 14.35 |
| Cr2O3 | 0.00 | | |
| | 96.14 | | 98.24 |

Complete analyses are found in Appendix 3. Beam conditions: beam current, 50 na; accelerating voltage, 15 kv; beam diameter, 1 micron; counting time, 10 sec. for all elements. Analytical precision based on repeat analyses of olivine standard is better than 1% for SiO2, MgO (Mg-rich olivine), FeO, and MnO (Fe-rich olivine), and 5 to 15 % for MgO(Fe-rich olivine), and MnO (Mg-rich olivine). Values for Al2O3, CaO, NiO, ZnO, Cr2O5 are at or below detection limits.
Olivine composition: Fo = forsterite (Mg2SiO4).
c = core; r = rim; typ = typical crystal composition.

**Table 4-6: Representative analyses of biotite and amphibole.**

| BIOTITE | | |
|---|---|---|
| **Sample #** | **JJ92-1** | **JJ92-1** |
| **map unit** | **Tdrd** | **Tdrd** |
| SiO2 | 36.50 | 38.02 |
| TiO2 | 5.66 | 5.31 |
| Al2O3 | 13.22 | 12.60 |
| FeO | 19.78 | 20.44 |
| MnO | 0.08 | 0.16 |
| MgO | 11.46 | 10.97 |
| CaO | 0.00 | 0.04 |
| Na2O | 0.56 | 0.56 |
| K2O | 8.81 | 8.44 |
| Cr2O3 | 0.05 | 0.00 |
| Ox%(Zn) | 0.03 | 0.03 |
| | 96.15 | 96.57 |
| | | |
| F | 0.76 | 0.60 |
| Cl | 0.08 | 0.07 |

| AMPHIBOLE | | | |
|---|---|---|---|
| **Sample #** | **JJ92-5** | **JJ92-5** | **JJ92-5** |
| **map unit** | **Tdrl** | **Tdrl** | **Tdrl** |
| SiO2 | 42.63 | 43.68 | 44.24 |
| TiO2 | 2.16 | 1.80 | 1.59 |
| Al2O3 | 8.55 | 8.47 | 8.25 |
| FeO | 27.50 | 23.90 | 23.55 |
| MnO | 0.51 | 0.51 | 0.50 |
| MgO | 5.16 | 7.49 | 7.63 |
| CaO | 9.99 | 10.37 | 10.19 |
| Na2O | 1.83 | 1.76 | 1.80 |
| K2O | 1.06 | 0.95 | 0.91 |
| Cr2O3 | 0.05 | 0.00 | 0.02 |
| | 99.44 | 98.93 | 98.68 |
| | | | |
| Cl | 0.20 | 0.14 | 0.14 |
| F | 0.54 | 0.60 | 0.51 |

Complete analyses are found in Appendix 3. Beam conditions: beam current, 50 na; accelerating voltage, 15 kv; beam diameter, 1 micron; counting time, 10 sec. for all elements except TiO2 (20 sec.). Analytical precision based on repeat analyses.

## 4.2 Whole-Rock Composition

### 4.2.1 Classification

Bulk chemical composition for rocks sampled in the DBEC study area ranges from high-magnesia basalt to high-silica rhyolite (Fig. 4-3; Tables 4-7 through 4-9). Classification for the series of rocks is based on $SiO_2$ concentration: basalt (48-52 weight percent), basaltic andesite (52-57 percent), andesite (57-63 percent), dacite (63-68 percent), rhyodacite (68-72 percent) and rhyolite (>72 percent). On the total alkali versus silica diagram of LeBas and others (1986) the intermediate (>52, <63 percent $SiO_2$) samples of the DBEC series plot on and slightly above the trachybasalt to trachydacite boundary (Fig. 4-3). Although these samples are properly trachytic in composition owing to elevated total alkalies, they shall be referred to without the "trachy" designation herein. Major and trace elements are presented in Figures 4-4 and 4-5. All basaltic andesite and andesite is classified as "potassic" on the basis of $Na_2O - 2 < K_2O$ (Le Maitre, 1989). $K_2O$ and $Na_2O$ vary smoothly with $SiO_2$, indicating that there has been little alteration of the original magmatic composition. All rocks are hypersthene normative and metaluminous (Shand, 1951), with the exception of the slightly peraluminous aphyric obsidian from the rhyolite of Indian Creek Buttes ($Tdr_1$, JJ92-5). CIPW norms are presented in Appendix 7.

### 4.2.2 Older basalts and andesites and Quaternary basalt

Steens Basalt in the map area (Ts, FF94-49: Table 4-8) is classified as a tholeiitic basalt by the system of Irvine and Baragar, (1971; Fig. 4-6A). At the type section, 60 km south of DBEC, the basalt varies from calc-alkaline at the base to tholeiitic near the top of the section (Fig. 4-6B and Appendix 4). Variations in many major and trace elements (for example, Al, Mg, K, Ba) between flows correlate with modal abundance of plagioclase and olivine. Although these variations have long been recognized (Gunn and Watkins, 1970), compositional change from base to top has been largely ignored. Fifty samples from the

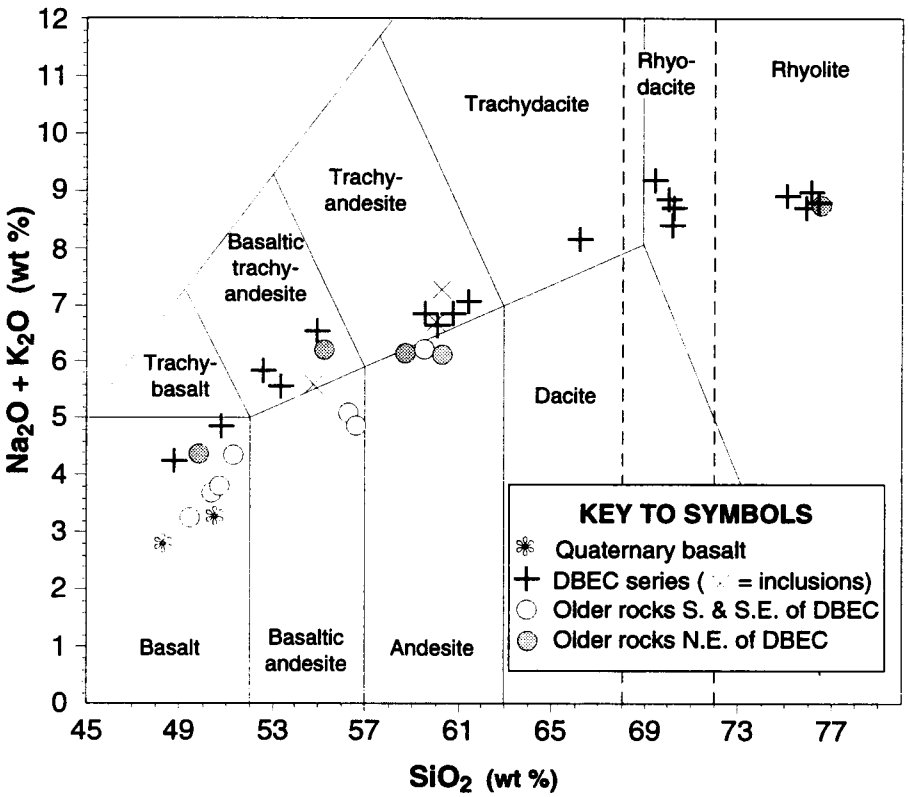


**Figure 4-3:** Chemical analyses of rocks in the Duck Creek Butte study area plotted on total alkali-silica classification diagram, modified from Le Bas and others (1986) to include a field for rhyodacite indicated by dashed lines. Data from Tables 4-6 through 4-8. "Trachy" designation is not used in the text.

**TABLE 4-7:** Whole-rock compositions of DBEC samples (includes Quaternary basalt).

| | Rhyolite | | | | Rhyodacite | | | |
|---|---|---|---|---|---|---|---|---|
| | JJ92-4 | JJ92-5 | JJ94-158 | JN94-16 | JJ92-1 | JJ92-7 | JJ92-88 | JJ92-101 |
| Map Unit | $Tdr_1$ | $Tdr_1$ | $Tdr_2$ | $Tdr_2$ | Tdrd | Tdrd | Tdrd | Tdrd |
| Lithology | O | L | O | O | L | L | L | L |
| $SiO_2$ | 76.35 | 76.00 | 76.04 | 75.03 | 70.19 | 70.26 | 70.08 | 69.47 |
| $TiO_2$ | 0.11 | 0.12 | 0.08 | 13.98 | 0.55 | 0.53 | 0.55 | 0.56 |
| $Al_2O_3$ | 12.79 | 13.03 | 13.00 | 0.06 | 14.51 | 14.61 | 14.53 | 14.99 |
| FeO* | 1.18 | 1.29 | 1.14 | 0.85 | 3.15 | 3.02 | 3.01 | 2.96 |
| MnO | 0.04 | 0.04 | 0.04 | 0.07 | 0.07 | 0.07 | 0.07 | 0.08 |
| MgO | 0.04 | 0.10 | 0.00 | 1.10 | 0.80 | 0.67 | 0.67 | 0.66 |
| CaO | 0.66 | 0.66 | 0.76 | 0.00 | 2.18 | 1.98 | 2.06 | 1.92 |
| $Na_2O$ | 3.74 | 3.57 | 4.00 | 4.55 | 3.59 | 3.76 | 3.75 | 4.06 |
| $K_2O$ | 5.07 | 5.15 | 4.93 | 4.34 | 4.79 | 4.95 | 5.13 | 5.13 |
| $P_2O_5$ | 0.02 | 0.04 | 0.01 | 0.02 | 0.18 | 0.15 | 0.15 | 0.18 |
| | 100 | 100 | 100 | 100 | 100 | 100 | 100 | 100 |
| XRF analyses (ppm) | | | | | | | | |
| Rb | 179 | 166 | 171 | 9 | 115 | 109 | 136 | 127 |
| Ba | 216 | 237 | 183 | 1 | 1630 | 1660 | 1990 | 1550 |
| Sr | 51 | 18 | 29 | 6 | 283 | 259 | 272 | 296 |
| Zr | 156 | 149 | 139 | 4 | 242 | 278 | 273 | 233 |
| Nb | 34 | 49 | 34 | 508 | 22 | 33 | 17 | 26 |
| Y | 67 | 50 | 51 | 141 | 30 | 33 | 36 | 15 |
| Pb | | | 23 | 84 | | | | |
| Zn | | | 49 | 83 | | | | |
| Ga | | | 18 | 27 | | | | |
| V | | | 0 | 17 | | | | |
| Cu | | | 8 | 19 | | | | |
| Ni | | | 14 | 5 | | | | |
| Cr | *4.39* | *4.56* | 0 | 36 | *6.37* | 43 | 41 | 55 |
| Sc | | | 1 | 23 | | | | |
| INAA | | | | | | | | |
| Cs | 4.24 | 4.06 | | | 3.28 | | | |
| U | 5.08 | 6.18 | | | 4.62 | | | |
| Th | 12.92 | 12.62 | | | 10.37 | | | |
| Hf | 4.93 | 4.72 | | | 5.48 | | | |
| Ta | 2.13 | 1.99 | | | 1.20 | | | |
| Sb | nd | 0.70 | | | 0.65 | | | |
| As | 2.50 | 2.74 | | | 1.50 | | | |
| Sc | 2.89 | 2.75 | | | 6.15 | | | |
| Co | 0.34 | 0.42 | | | 4.58 | | | |
| La | 33.35 | 34.03 | | | 34.15 | | | |
| Ce | 68.86 | 73.24 | | | 62.11 | | | |
| Nd | 30.70 | 32.59 | | | 26.46 | | | |
| Sm | 7.06 | 7.24 | | | 5.24 | | | |
| Eu | 0.36 | 0.37 | | | 1.16 | | | |
| Tb | 1.25 | 1.17 | | | 0.77 | | | |
| Yb | 4.71 | 5.31 | | | 3.33 | | | |
| Lu | 0.72 | 0.70 | | | 0.44 | | | |
| W | 1.80 | 2.30 | | | 1.60 | | | |

† = exceeds standard. *italics in XRF = INAA data* Major element data normalized to 100%; prenormalized data is in Appendix 6. FeO* = total iron as FeO. JJ92 XRF data are from XRAL, British Columbia; JJ93, -94, -95 and FF XRF data are from Washington State University, Pullman WA. Key to Lithology: L = lava; O = obsidian; Qi = quenched inclusion; D = dike; UT & WT = unwelded & welded tuff

TABLE 4-7 (Continued)

| | Dacite | Andesite | | | | | |
|---|---|---|---|---|---|---|---|
| | JJ92-102 | JJ92-27 | JJ93-41 | JJ93-126 | JJ93-140 | JJ94-1iA | JJ94-1iB |
| Map Unit | Tdid | $Tda_1$ | $Tda_1$ | $Tda_2$ | $Tda_2$ | Tdrd | Tdrd |
| Lithology | L | L | L | L | L | Qi | Qi |
| $SiO_2$ | 66.27 | 59.61 | 61.42 | 60.76 | 60.13 | 60.28 | 60.02 |
| $TiO_2$ | 0.87 | 1.44 | 1.32 | 1.17 | 1.13 | 1.53 | 1.44 |
| $Al_2O_3$ | 14.78 | 15.08 | 15.81 | 15.74 | 15.80 | 15.78 | 15.62 |
| FeO* | 5.30 | 7.90 | 6.13 | 6.93 | 7.16 | 8.93 | 8.43 |
| MnO | 0.12 | 0.14 | 0.13 | 0.14 | 0.13 | 0.13 | 0.18 |
| MgO | 1.06 | 3.03 | 2.53 | 2.64 | 3.05 | 1.22 | 1.40 |
| CaO | 3.12 | 5.52 | 5.27 | 5.46 | 5.69 | 4.59 | 4.72 |
| $Na_2O$ | 4.06 | 3.71 | 3.83 | 3.91 | 3.76 | 3.97 | 4.35 |
| $K_2O$ | 4.09 | 3.14 | 3.24 | 2.94 | 2.85 | 2.77 | 2.96 |
| $P_2O_5$ | 0.33 | 0.44 | 0.32 | 0.33 | 0.30 | 0.80 | 0.88 |
| | 100 | 100 | 100 | 100 | 100 | 100 | 100 |
| XRF analyses (ppm) | | | | | | | |
| Rb | 100 | 67 | 67 | 68 | 63 | 61 | 63 |
| Ba | 1530 | 1260 | 1727 | 1159 | 1132 | 1931 | 1453 |
| Sr | 287 | 278 | 256 | 259 | 266 | 380 | 353 |
| Zr | 296 | 366 | 367 | 327 | 323 | 316 | 324 |
| Nb | 38 | 38 | 29 | 26 | 26 | 34 | 32 |
| Y | 26 | 54 | †48 | †45 | †47 | 48 | 57 |
| Pb | | | 10 | 9 | 7 | 9 | 9 |
| Zn | | | 105 | 96 | 90 | 128 | 146 |
| Ga | | | 20 | 18 | 21 | 19 | 21 |
| V | | | 123 | 128 | 117 | 39 | 17 |
| Cu | | | 27 | 38 | 23 | 17 | 5 |
| Ni | | | 42 | 34 | 34 | 4 | 2 |
| Cr | *2.97* | *45.362* | *76* | *70* | *75.50* | 3 | 2 |
| Sc | | | 23 | 19 | 24 | 22 | 22 |
| INAA (pm) | | | | | | | |
| Cs | 2.90 | 1.55 | 1.64 | 1.66 | 1.36 | | |
| U | 4.50 | 3.20 | 3.92 | 2.67 | 2.47 | | |
| Th | 9.11 | 5.95 | 6.90 | 5.80 | 5.80 | 4.00 | 7.00 |
| Hf | 6.08 | 7.40 | 10.20 | 8.31 | 8.51 | | |
| Ta | 2.95 | 2.59 | 1.75 | 1.42 | 1.43 | | |
| Sb | 0.56 | 0.54 | 0.18 | 0.23 | 0.19 | | |
| As | 2.20 | 2.10 | 5.10 | 4.20 | 3.90 | | |
| Sc | 9.94 | 18.55 | 20.20 | 19.40 | 20.10 | | |
| Co | 23.98 | 36.21 | 24.90 | 19.80 | 19.70 | | |
| La | 42.74 | 37.12 | 41.00 | 35.90 | 39.00 | 39.00 | 48.00 |
| Ce | 82.62 | 73.48 | 85.30 | 72.20 | 74.90 | 86.00 | 99.00 |
| Nd | 38.33 | 35.54 | 37.70 | 35.70 | 38.20 | | |
| Sm | 7.69 | 7.96 | 8.58 | 7.61 | 8.58 | | |
| Eu | 1.96 | 2.18 | 2.39 | 1.99 | 2.17 | | |
| Tb | 1.11 | 1.35 | 1.36 | 1.18 | 1.30 | | |
| Yb | 4.78 | 4.76 | 4.88 | 4.49 | 4.86 | | |
| Lu | 0.56 | 0.71 | 0.74 | 0.69 | 0.73 | | |
| W | 143.30 | 116.60 | 1.70 | 1.70 | 2.30 | | |

† = exceeds standard. *italics in XRF = INAA data* Major element data normalized to 100 percent; prenormalized data is in Appendix 6. FeO* = total iron as FeO. JJ92 XRF data are from XRAL, British Columbia; JJ93, -94, -95 and FF XRF data are from Washington State University, Pullman WA.
Key to Lithology: L = lava; O = obsidian; Qi = quenched inclusion; D = dike; UT & WT = unwelded & welded tuff

**TABLE 4-7** (DBEC continued)

| | Basaltic Andesite | | | | Basalt | | | |
|---|---|---|---|---|---|---|---|---|
| | JJ92-6 | JJ92-38 | JJ92-51 | JJ92-62 | JJ92-99 | JJ93-130 | JJ93-20 | JJ94-151 |
| Map Unit | $Tdba_1$ | $Tdba_2$ | Tdid | $Tdba_3$ | $Tdb_2$ | $Tdb_1$ | $Qb_2$ | $Qb_3$ |
| Lithology | L | D | Qi | L | L | L | L | L |
| $SiO_2$ | 52.66 | 53.43 | 54.81 | 54.98 | 50.86 | 48.83 | 48.72 | 49.43 |
| $TiO_2$ | 2.11 | 2.09 | 2.49 | 2.11 | 1.74 | 2.56 | 0.92 | 1.13 |
| $Al_2O_3$ | 16.05 | 15.88 | 14.27 | 14.60 | 16.95 | 15.88 | 16.23 | 16.96 |
| FeO* | 10.92 | 10.81 | 10.90 | 10.60 | 10.32 | 13.04 | 9.97 | 9.48 |
| MnO | 0.18 | 0.18 | 0.21 | 0.18 | 0.17 | 0.21 | 0.18 | 0.17 |
| MgO | 4.26 | 4.22 | 3.33 | 4.05 | 5.55 | 5.45 | 10.03 | 8.36 |
| CaO | 7.23 | 7.11 | 7.00 | 6.46 | 8.84 | 9.05 | 11.06 | 11.16 |
| $Na_2O$ | 3.69 | 3.42 | 3.18 | 4.10 | 3.58 | 3.41 | 2.53 | 2.82 |
| $K_2O$ | 2.16 | 2.14 | 2.43 | 2.42 | 1.28 | 0.87 | 0.26 | 0.35 |
| $P_2O_5$ | 0.74 | 0.73 | 1.39 | 0.50 | 0.70 | 0.69 | 0.10 | 0.14 |
| | 100 | 100 | 100 | 100 | 100 | 100 | 100 | 100 |
| XRF analyses (ppm) | | | | | | | | |
| Rb | 37 | 33 | 39 | 50 | 22 | 11 | 4 | 6 |
| Ba | 914 | 904 | *1770* | 1200 | 760 | 548 | 91 | 137 |
| Sr | 596 | 591 | 353 | 255 | 584 | 324 | 207 | 240 |
| Zr | 207 | 208 | 256 | 328 | 151 | 262 | 65 | 78 |
| Nb | 44 | 27 | 53 | 49 | 46 | 24 | 7 | 8 |
| Y | 37 | 29 | 58 | 40 | 19 | †60 | 19 | 20 |
| Pb | | | | | | 4 | 0 | 0 |
| Zn | | *82* | *147* | *124* | *113* | †140 | 67 | 68 |
| Ga | | | | | | 25 | 14 | 17 |
| V | | | | | | 255 | 230 | 254 |
| Cu | | | | | | 64 | 69 | 53 |
| Ni | *54.59* | *17.00* | *21.00* | *65.00* | *112.00* | 48 | 189 | 123 |
| Cr | *20.33* | *4* | *4.9* | *82* | *98.69* | *46* | *399* | 257 |
| Sc | | | | | | 34 | 41 | 36 |
| INAA | | | | | | | | |
| Cs | 0.70 | 2.97 | 1.23 | 1.13 | 0.18 | 0.23 | 0.15 | |
| U | 2.10 | 2.10 | 1.76 | 1.95 | 2.70 | 1.80 | 1.90 | |
| Th | 1.64 | 9.70 | 4.76 | 4.60 | 1.26 | 0.81 | 0.30 | |
| Hf | 3.99 | 8.63 | 6.28 | 8.18 | 3.96 | 6.85 | 1.48 | |
| Ta | 0.86 | 1.61 | 2.41 | 1.64 | 1.87 | 1.19 | 0.24 | |
| Sb | 0.45 | 0.20 | | 0.30 | | 0.15 | 0.26 | |
| As | 2.40 | 1.00 | 0.90 | 2.20 | 3.00 | 1.40 | 3.00 | |
| Sc | 19.48 | 9.82 | 22.30 | 23.50 | 23.30 | 29.80 | 34.20 | |
| Co | 29.31 | 4.12 | 39.70 | 29.70 | 54.40 | 42.30 | 53.30 | |
| La | 27.81 | 45.00 | 49.10 | 39.60 | 31.70 | 30.50 | 4.43 | |
| Ce | 60.28 | 85.20 | 93.20 | 85.40 | 62.00 | 63.60 | 9.20 | |
| Nd | 34.00 | 37.70 | 54.70 | 43.00 | 29.40 | 39.50 | 7.20 | |
| Sm | 7.42 | 7.86 | 12.10 | 9.34 | 6.80 | 9.92 | 2.17 | |
| Eu | 2.09 | 2.03 | 3.57 | 2.80 | 2.12 | 3.06 | 0.87 | |
| Tb | 1.07 | 1.19 | 1.94 | 1.44 | 1.03 | 1.73 | 0.47 | |
| Yb | 3.10 | 4.26 | 5.14 | 4.95 | 2.59 | 5.14 | 2.01 | |
| Lu | 0.49 | 0.63 | 0.81 | 0.73 | 0.39 | 0.73 | 0.30 | |
| W | 2.80 | 3.30 | 72.50 | 1.80 | 71.70 | 5.40 | 1.20 | |

† = exceeds standard. *italics in XRF = INAA data* Major element data normalized to 100 percent; prenormalized data is in Appendix 6. FeO* = total iron as FeO. JJ92 XRF data are from XRAL, British Columbia; JJ93, -94, -95 and FF XRF data are from Washington State University, Pullman WA.
Key to Lithology: L = lava; O = obsidian; Qi = quenched inclusion; D = dike; UT & WT = unwelded & welded tuff

**TABLE 4-8:** Whole-rock composition of pre-DBEC basalt and andesite

| | Pre-DBEC basalt and andesite | | | | | | |
|---|---|---|---|---|---|---|---|
| | JJ93-19 | JJ92-59 | JJ93-133 | JJ93-134 | JJ93-147 | JJ94-161 | JJ94-163 |
| Map Unit | Tba | Ts? | Tba | Tas | Tad | Tba | Tbs |
| Lithology | L | L | L | L | L | L | L |
| $SiO_2$ | 56.16 | 51.28 | 56.52 | 61.86 | 59.28 | 55.05 | 49.93 |
| $TiO_2$ | 2.00 | 2.57 | 2.01 | 1.06 | 2.33 | 2.13 | 2.49 |
| $Al_2O_3$ | 13.85 | 15.25 | 14.58 | 16.56 | 14.11 | 15.49 | 15.53 |
| FeO* | 11.06 | 12.16 | 9.48 | 5.56 | 10.14 | 10.57 | 12.24 |
| MnO | 0.17 | 0.18 | 0.15 | 0.11 | 0.15 | 0.19 | 0.17 |
| MgO | 3.95 | 4.96 | 4.11 | 2.24 | 1.93 | 3.18 | 5.63 |
| CaO | 7.46 | 8.75 | 7.99 | 5.28 | 5.34 | 6.33 | 8.80 |
| $Na_2O$ | 3.25 | 3.21 | 3.41 | 4.00 | 3.91 | 3.81 | 3.22 |
| $K_2O$ | 1.78 | 1.24 | 1.45 | 2.97 | 2.25 | 2.52 | 1.23 |
| $P_2O_5$ | 0.31 | 0.40 | 0.30 | 0.36 | 0.56 | 0.73 | 0.76 |
| | 100 | 100 | 100 | 100 | 100 | 100 | 100 |
| XRF analyses (ppm) | | | | | | | |
| Rb | 49 | 27 | 37 | 49 | 56 | 52 | 17 |
| Ba | 652 | 492 | 608 | 1087 | 757 | 1053 | 769 |
| Sr | 346 | 379 | 371 | 476 | 285 | 417 | 385 |
| Zr | 189 | 190 | 171 | 212 | 274 | 243 | 202 |
| Nb | 15 | 30 | 13 | 15 | 22 | 22 | 17 |
| Y | 35 | 31 | 32 | 26 | †53 | 40 | 37 |
| Pb | 5 | | 4 | 11 | 7 | 10 | 6 |
| Zn | 111 | | 110 | 86 | †132 | 120 | 131 |
| Ga | 24 | | 20 | 17 | 21 | 23 | 20 |
| V | 285 | | 300 | 133 | 180 | 220 | 276 |
| Cu | 62 | | 64 | 27 | 17 | 23 | 20 |
| Ni | 11 | *74.27* | 17 | 6 | 0 | 0 | 42 |
| Cr | *14* | *63.301* | 24 | *3* | 1 | 4 | 69 |
| Sc | 39 | | 32 | 18 | 30 | 24 | 29 |
| INAA | | | | | | | |
| Cs | 1.61 | 1.08 | | 0.85 | | | |
| U | 2.18 | 1.90 | | 1.45 | | | |
| Th | 5.50 | 2.80 | | 3.90 | | | |
| Hf | 5.18 | 4.47 | | 5.22 | | | |
| Ta | 0.98 | 1.50 | | 0.80 | | | |
| Sb | 0.22 | 0.55 | | 0.20 | | | |
| As | 1.80 | 1.70 | | 3.30 | | | |
| Sc | 29.70 | 28.10 | | 15.40 | | | |
| Co | 34.20 | 51.50 | | 17.10 | | | |
| La | 22.50 | *19.78* | | *29.60* | | | |
| Ce | 48.60 | 39.79 | | 58.00 | | | |
| Nd | 26.20 | 24.88 | | 27.10 | | | |
| Sm | 6.43 | 6.60 | | 5.43 | | | |
| Eu | 1.87 | 2.05 | | 1.48 | | | |
| Tb | 1.03 | 1.19 | | 0.74 | | | |
| Yb | 3.15 | 3.37 | | 2.60 | | | |
| Lu | 0.46 | 0.43 | | 0.39 | | | |
| W | 2.10 | 74.01 | | 3.30 | | | |

† = exceeds standard. *italics in XRF = INAA data* .Major element data normalized to 100 percent; prenormalized data is in Appendix 6. FeO* = total iron as FeO. JJ92 XRF data are from XRAL, British Columbia; JJ93, -94, -95 and FF XRF data are from Washington State University, Pullman WA.
Key to Lithology: L = lava; O = obsidian; Qi = quenched inclusion; D = dike; UT & WT = unwelded & welded tuff

**TABLE 4-8** (Continued)

**Basalt and andesite (cont.)**

| | FF94-23 | FF94-36 | FF94-39 | FF94-49 |
|---|---|---|---|---|
| Map Unit | Tb | Tba | Tba | Ts |
| Lithology | L | L | L | L |
| $SiO_2$ | 50.37 | 50.66 | 59.46 | 49.28 |
| $TiO_2$ | 2.05 | 1.94 | 2.01 | 1.95 |
| $Al_2O_3$ | 16.48 | 15.69 | 13.70 | 17.16 |
| FeO* | 11.01 | 12.01 | 10.27 | 12.05 |
| MnO | 0.17 | 0.17 | 0.15 | 0.18 |
| MgO | 5.63 | 6.07 | 2.33 | 5.80 |
| CaO | 10.36 | 9.39 | 5.63 | 8.98 |
| $Na_2O$ | 3.07 | 3.24 | 3.78 | 3.46 |
| $K_2O$ | 0.61 | 0.58 | 2.36 | 0.84 |
| $P_2O_5$ | 0.24 | 0.26 | 0.32 | 0.30 |
| | 100 | 100 | 100 | 100 |
| **XRF analyses (ppm)** | | | | |
| Rb | 12 | 10 | 68 | 14 |
| Ba | 213 | 398 | 892 | 327 |
| Sr | 388 | 447 | 307 | 494 |
| Zr | 140 | 137 | 243 | 136 |
| Nb | 10 | 15 | 17 | 8 |
| Y | 31 | 26 | 41 | 29 |
| Pb | 3 | 2 | 12 | 4 |
| Zn | 96 | 108 | 121 | 104 |
| Ga | 24 | 22 | 20 | 22 |
| V | 319 | 256 | 291 | 291 |
| Cu | 95 | 6 | 14 | 175 |
| Ni | 63 | 11 | 0 | 105 |
| Cr | 177 | 32 | 8 | 61 |
| Sc | 33 | 30 | 28 | 28 |
| **INAA** | | | | |
| Cs | | | | |
| U | | | | |
| Th | | | | |
| Hf | | | | |
| Ta | | | | |
| Sb | | | | |
| As | | | | |
| Sc | | | | |
| Co | | | | |
| La | | | | |
| Ce | | | | |
| Nd | | | | |
| Sm | | | | |
| Eu | | | | |
| Tb | | | | |
| Yb | | | | |
| Lu | | | | |
| W | | | | |

**TABLE 4-9:** Miscellaneous rhyolite and tuff

| | JJ92-90 | JJ93-123 | JJ93-124 |
|---|---|---|---|
| Map Unit | Tr | Tots | Ttd |
| Lithology | L | UT | WT |
| $SiO_2$ | 76.52 | 76.21 | 75.40 |
| $TiO_2$ | 0.06 | 0.20 | 0.23 |
| $Al_2O_3$ | 13.00 | 11.15 | 10.15 |
| FeO* | 0.81 | 2.67 | 4.45 |
| MnO | 0.05 | 0.05 | 0.07 |
| MgO | 0.03 | 0.00 | 0.00 |
| CaO | 0.72 | 0.30 | 0.21 |
| $Na_2O$ | 4.24 | 4.07 | 4.87 |
| $K_2O$ | 4.56 | 5.32 | 4.61 |
| $P_2O_5$ | 0.02 | 0.02 | 0.01 |
| | 100 | 100 | 100 |
| **XRF analyses (ppm)** | | | |
| Rb | 235 | 128 | 212 |
| Ba | 48 | 29 | 45 |
| Sr | 10 | 6 | 8 |
| Zr | 106 | †938 | †813 |
| Nb | 45 | †87 | †42 |
| Y | 70 | †149 | †156 |
| Pb | | 26 | 21 |
| Zn | | †223 | †262 |
| Ga | | †28 | †30 |
| V | | 0 | 0 |
| Cu | | 12 | 5 |
| Ni | | 18 | 21 |
| Cr | *3.906* | 3 | *3* |
| Sc | | 0 | 0 |
| **INAA** | | | |
| Cs | 7.67 | | 5.29 |
| U | 11.09 | | 9.85 |
| Th | 17.85 | | 23.30 |
| Hf | 4.57 | | 25.90 |
| Ta | 4.13 | | 2.72 |
| Sb | 0.94 | | 0.78 |
| As | 4.27 | | 2.90 |
| Sc | 0.95 | | 1.38 |
| Co | 8.51 | | 0.40 |
| La | 11.92 | | 89.40 |
| Ce | 33.25 | | 214.00 |
| Nd | 20.39 | | 102.00 |
| Sm | 6.61 | | 25.00 |
| Eu | | | 2.23 |
| Tb | 1.44 | | 4.41 |
| Yb | 7.34 | | 15.80 |
| Lu | 0.94 | | 2.29 |
| W | 71.53 | | 2.50 |

† = exceeds standard. *italics in XRF = INAA data.* Major element data normalized to 100%; prenormalized data is in Appendix 6. FeO* = total iron as FeO. JJ92 XRF data are from XRAL, British Columbia; JJ93, -94, -95 and FF XRF data are from Washington State University, Pullman WA.
Key to Lithology: L = lava; O = obsidian; Qi = quenched inclusion; D = dike; UT & WT = unwelded & welded tuff

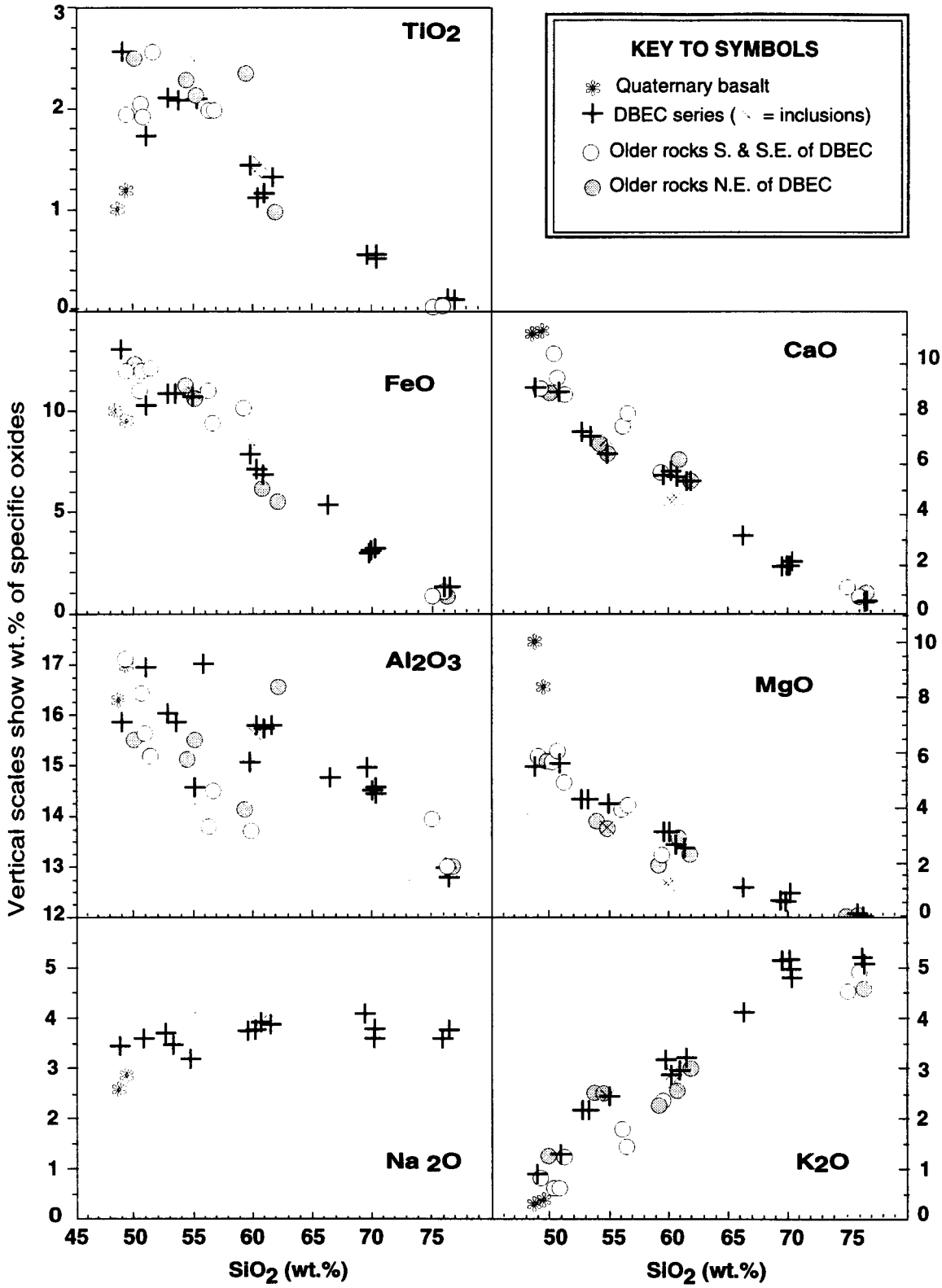


**Figure 4-4**: Silica versus major element variation diagrams. MnO and $P_2O_5$ diagrams are continued on next page. Data from Tables 4-7 through 4-9.

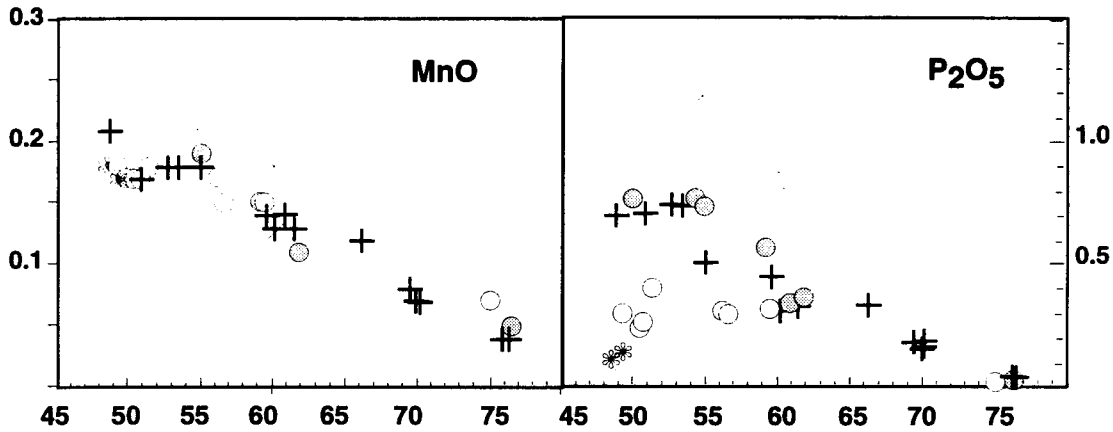


**Figure 4-4** (continued from previous page).

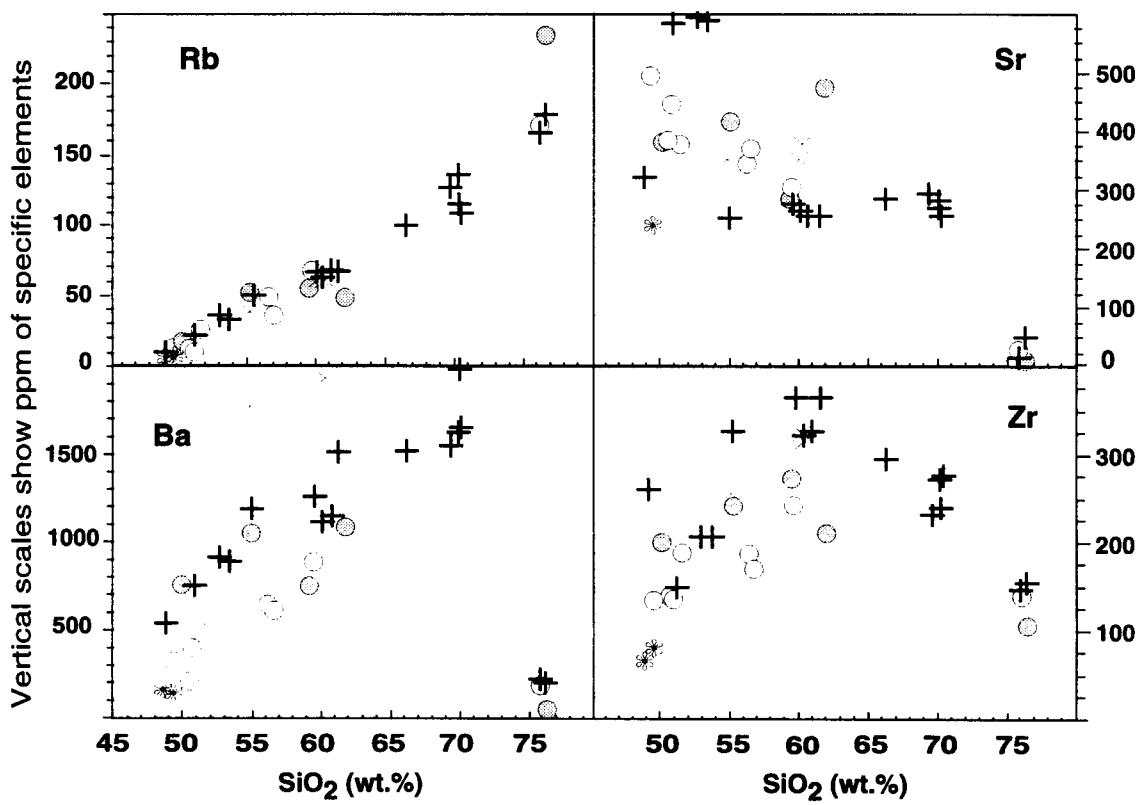


**Figure 4-5**: Silica versus trace element variation diagrams. Symbols as in Figure 4-4.

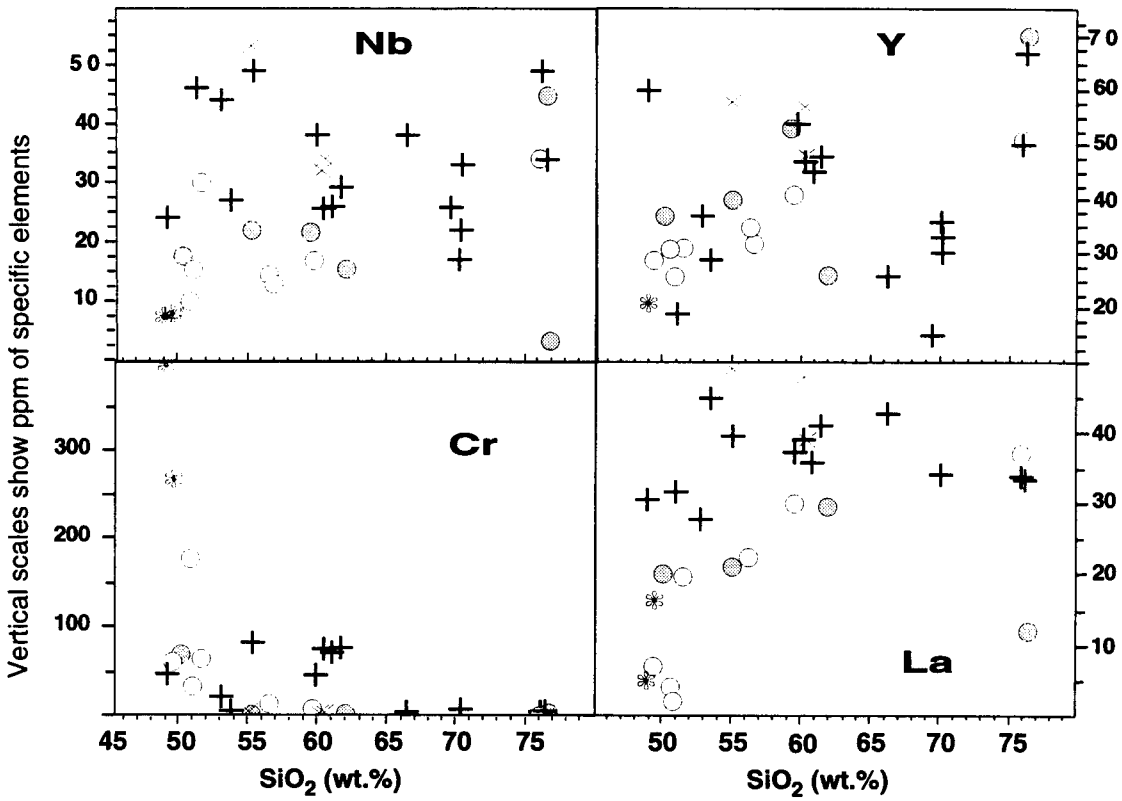


**Figure 4-5** (continued from previous page).

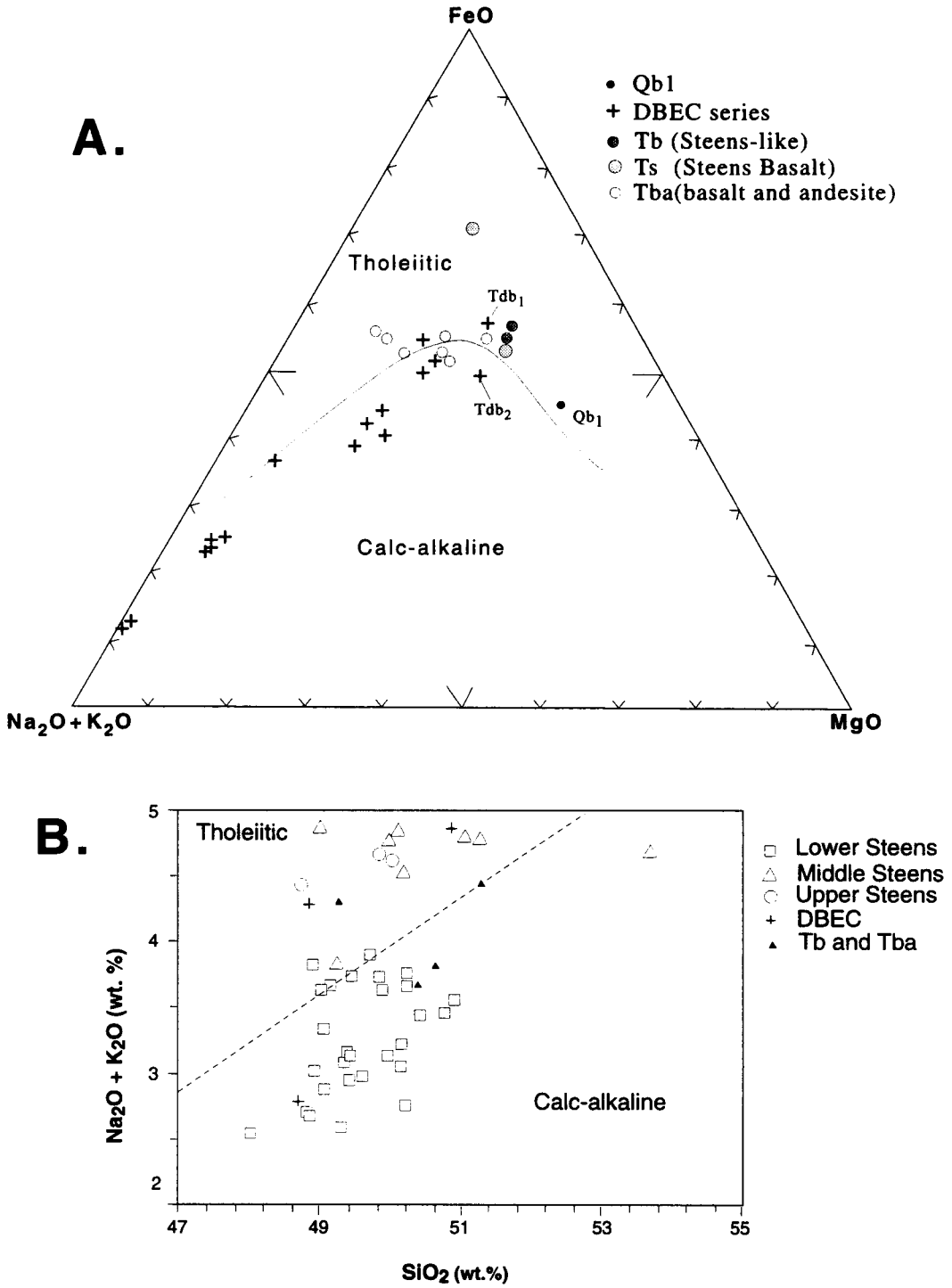


**Figure 4-6**: (A) AFM diagram indicating the fields of tholeiitic and calcalkaline basalts (Irvine and Baragar, 1971). Includes only samples from study area; (B) Alkalies versus silica diagram indicating fields of tholeiitic and calc-alkaline basalts (MacDonald and Katsura, 1964). Most middle- and upper-Steens Basalt samples exceed 5 percent $Na_2O+K_2O$, and therefore are not plotted on this diagram.

lower, middle, and upper parts of the Steens Basalt sequence near the type section (Appendix 4) show a continuum with increasing $K_2O$ and decreasing Mg from base to top (Fig. 4-7). Variation in the sequence is also seen in decreasing Cr and increasing FeO/MgO, $P_2O_5/TiO_2$ and Zr/Nb vs. Zr upsection (Figs. 4-8 and 5-1). The lower flows show a remarkable trace-element homogeneity whereas the upper flows have increasing compositional scatter (Fig. 5-1).

On the basis of major- and trace-element compositions, the porphyritic basalt (Tb, FF94-23) is compositionally similar to the Steens Basalt (Fig. 5-1), which is consistent with its correlation with the "Steens-like" or "Steens Mountain type" basalt southeast of DBEC defined by Carlson and Hart (1987). The basalt of Stockade Creek (Tbs, JJ94-163) is also compositionally similar to some of the Steens Basalt flows (see Appendix 4, samples JS94-33, -34, and -39) but lacks the characteristic Cu, V, and Ni enrichment and has substantially higher Ba than the Steens Basalt. South of DBEC, both the porphyritic basalt (Tb) and the unit of basalt and andesite (Tba) are tholeiitic and have higher Sc and Ca and lower Ba, Rb, Nb, Zr, $K_2O$, and $P_2O_5$ than the DBEC series (Figs. 4-4, 4-5, and 5-1). Northeast of DBEC, however, the pre-DBEC andesite (JJ93-134, JJ94-161) is similar in major- and trace-element composition to the DBEC series.

The basalt of Duck Creek Flat ($Qb_2$, JJ92-20) is an olivine-normative high-alumina tholeiite with a primitive MORB*-type signature. The basalt is characterized by low $SiO_2$, $K_2O$, $Na_2O$, $TiO_2$, Zr, Nb, and Y, and high CaO, MgO, Cr, $CaO/Al_2O_3$, and CaO/FeO. It has a relatively flat REE** pattern (Fig. 4-9D) typical of MORB (Basaltic Volcanism Study Project, 1981). A spider diagram for other elements shows enriched large-ion-lithophile elements and depleted high-field-strength elements relative to MORB (Fig. 4-10). $Qb_2$ has $^{87}Sr/^{86}Sr$ and $^{143}Nd/^{144}Nd$ ratios of 0.70508 and 0.512717, respectively (Appendix 5). The

* Mid-Ocean Ridge Basalt

** REE: Rare-earth elements, include LREE, light rare-earth elements, and HREE, heavy-rare earth elements.

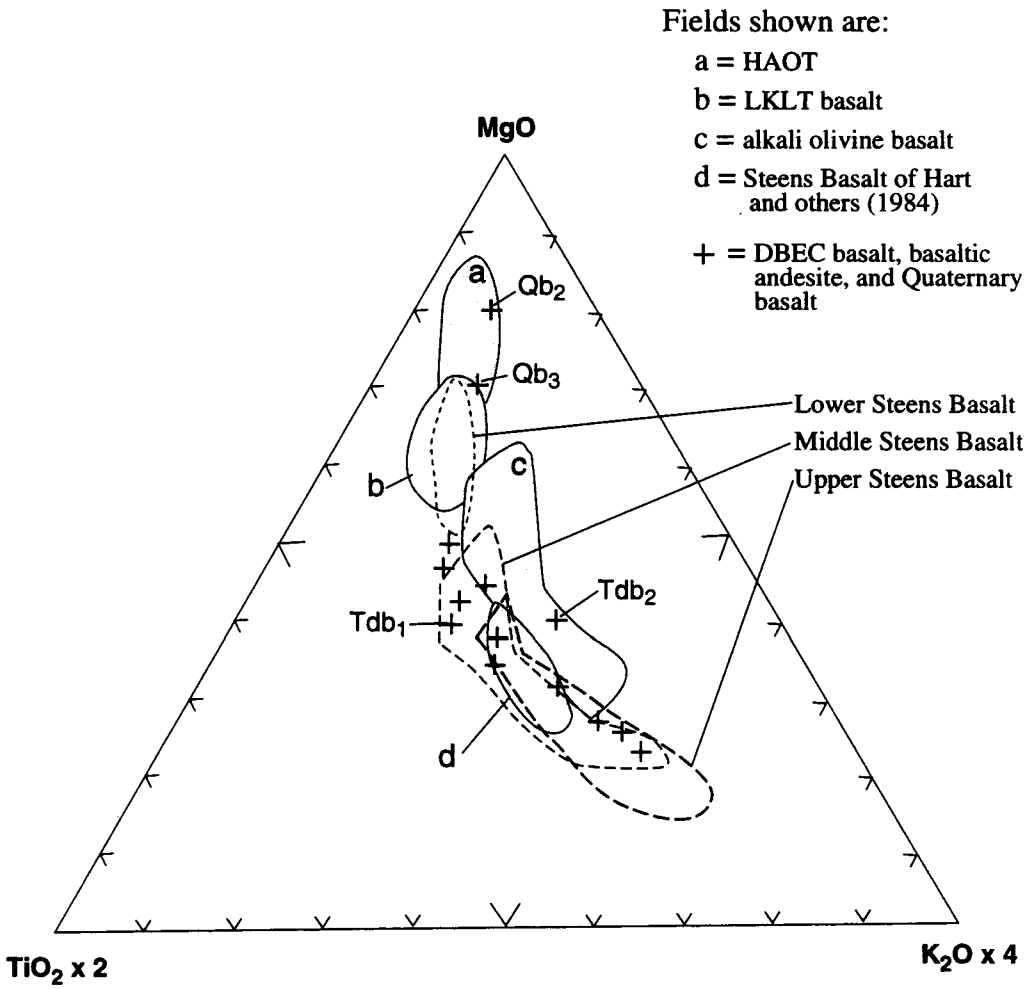


**Figure 4-7**: $MgO$-$TiO_2$-$K_2O$ ternary plot showing the fields for basalt and basaltic andesite at DBEC. Shown shaded are fields of high-alumina olivine tholeiite (HAOT), transitional tholeiite (LKLT = low K, low Ti), alkali olivine basalt, and Steens Basalt (from Hart and others, 1984). Dashed fields of Steens Basalt from this study indicate stratigraphic location, data from Appendix 4.

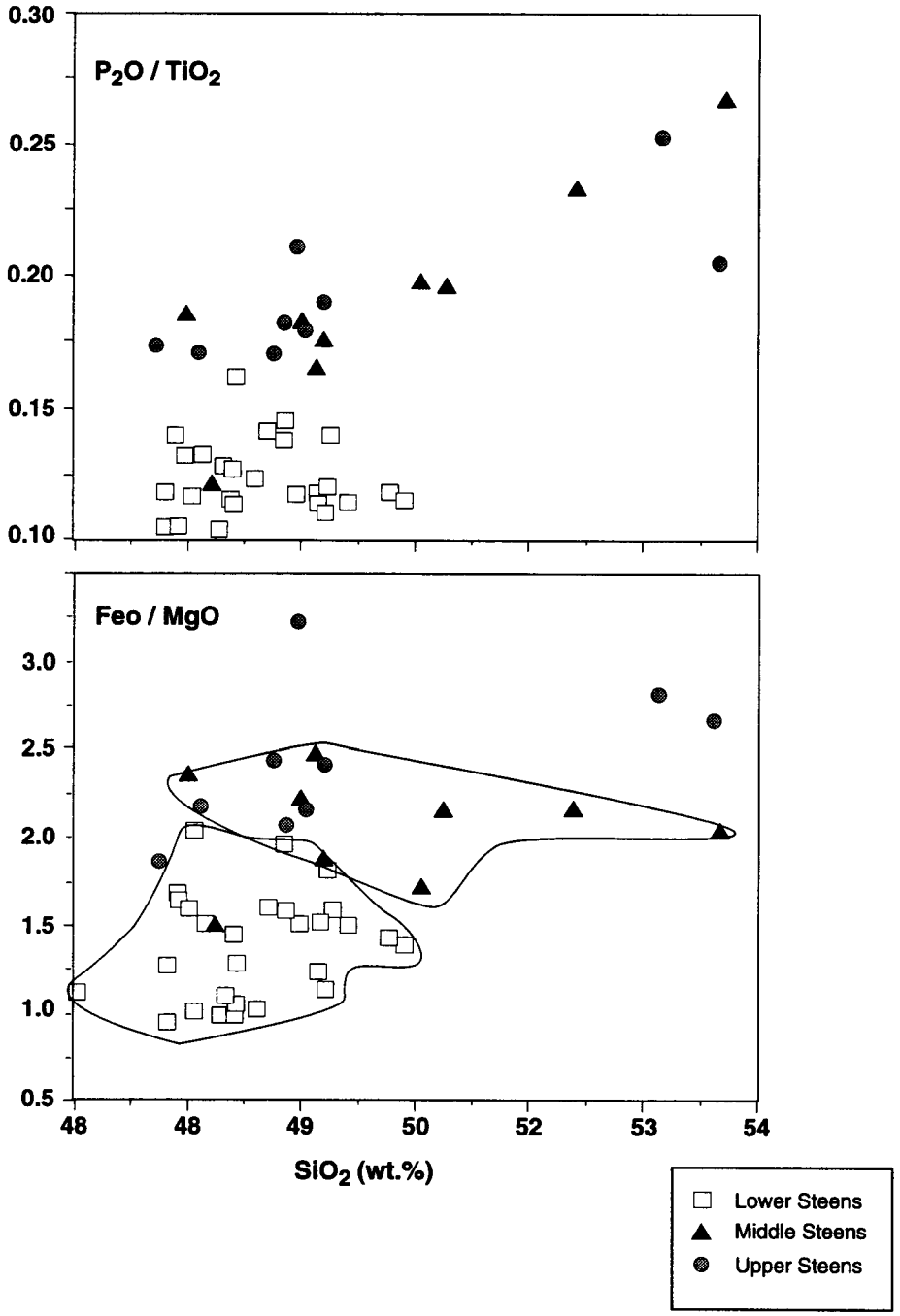


**Figure 4-8**: Major-element ratios showing the change in composition from base to top of the Steens Basalt sequence near the type section at Steens Mountain.

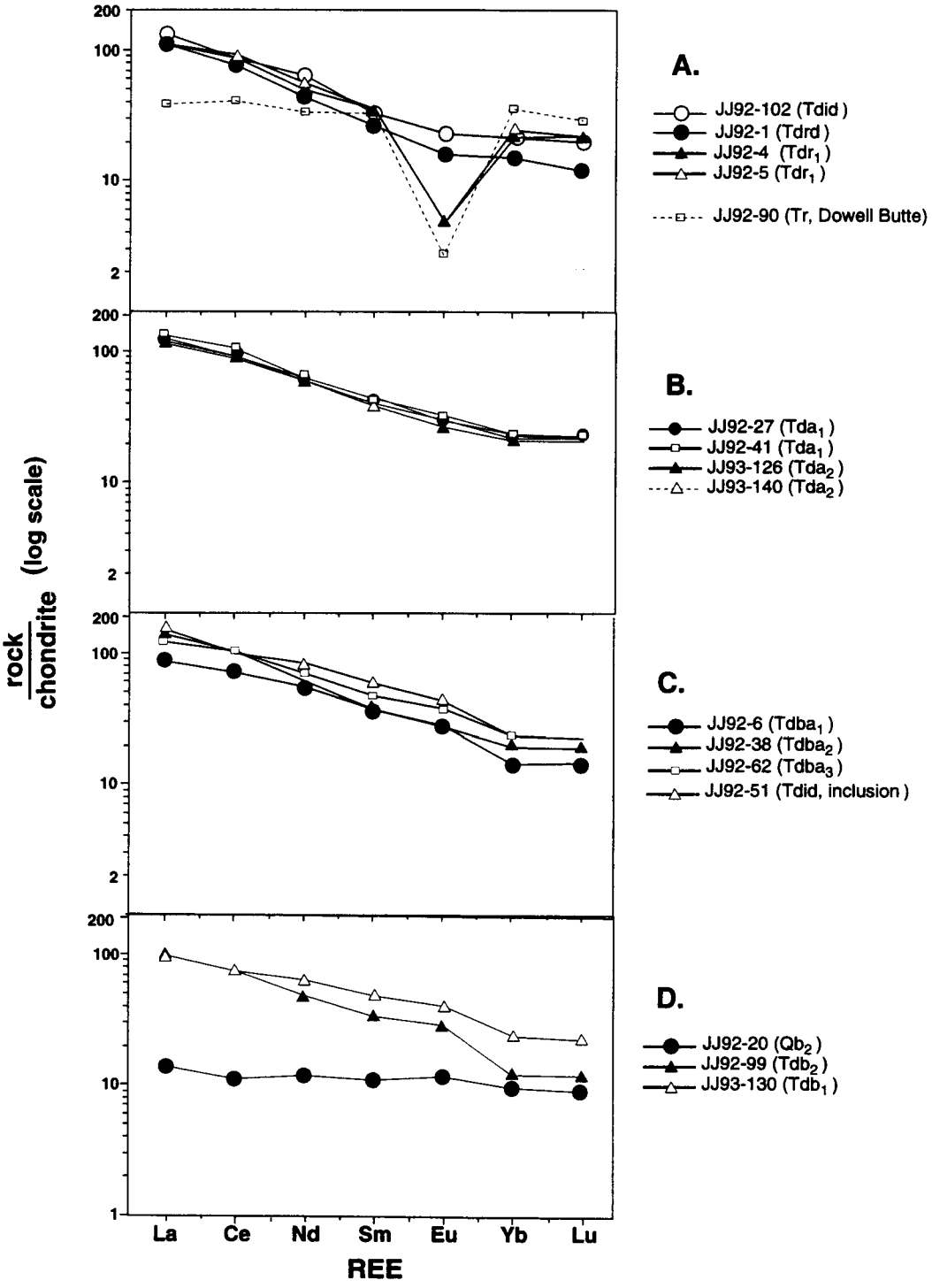


**Figure 4-9**: Rare-earth element diagrams for rocks of DBEC. REE values are normalized to C1 chondrite values (Anders and Ebihara, 1982). (A) Rhyolite and rhyodacite; (B) andesite; (C) basaltic andesite; (D) basalt.

basalt of Cord ($Qb_3$) is more evolved than $Qb_2$, as indicated by having lower Mg and higher alkalis, $Al_2O_3$, Rb, Sr, Ba, and Zr.

### 4.2.3 DBEC series

Magma that erupted between 10.38 and 10.32 Ma from DBEC forms a coherent suite of rocks that ranges from 48.8 to 76.3 percent $SiO_2$ (Table 4-7; Fig. 4-3). Within the DBEC suite, major and minor elements form nearly linear arrays on silica variation diagrams (Figs. 4-4 and 4-5). CaO, MgO, and MnO decrease and $Na_2O$ and $K_2O$ increase systematically with increasing $SiO_2$ content. Intermediate-composition lavas are high in $K_2O$ (Gill, 1981). Rare-earth-element patterns for the DBEC series samples are generally similar to each other (Fig. 4-9). There is no systematic relationship between silica content and REE enrichment. All rocks are depleted in high-field-strength elements and enriched in large-ion-lithophile elements relative to MORB (Fig. 4-10).

*Basalts* : $Tdb_1$ (JJ92-130) and $Tdb_2$ (JJ92-99) can be termed tholeiitic and calc-alkaline, respectively (Fig. 4-6). They can also be described high-potash, high-titania tholeiite (HKHT, $Tdb_1$) and alkali olivine basalt ($Tdb_2$) by the criteria of Hart and others (1984) (Fig. 4-7). $Tdb_1$ has higher Fe, Ti, Zr, Y, and Hf and lower K, Sr, Ba, Rb, Cr, Th, Ta, and LREE/HREE than $Tdb_2$.

*Basaltic andesites* : The basaltic andesites are high-potash (Gill, 1981), calc-alkaline rocks (Irvine and Baragar, 1971). Trace-element enrichments mimic those of the basalts (Fig. 4-10). $Tdba_2$ (JJ92-38) has lower Sc, Co, Nb, and Cr and higher Cs, Th, LREE, and HREE relative to $Tdba_1$ and $Tdba_3$ (Table 4-7). A tholeiitic basaltic-andesite inclusion (JJ92-51) found in Tdid (JJ92-102) is enriched in P, Ti, Mn, Ba, Y, Nb, and REE relative to all other basaltic andesites. Perhaps loss of the outer glassy rim of the inclusions during sample preparation creates an analysis of only the

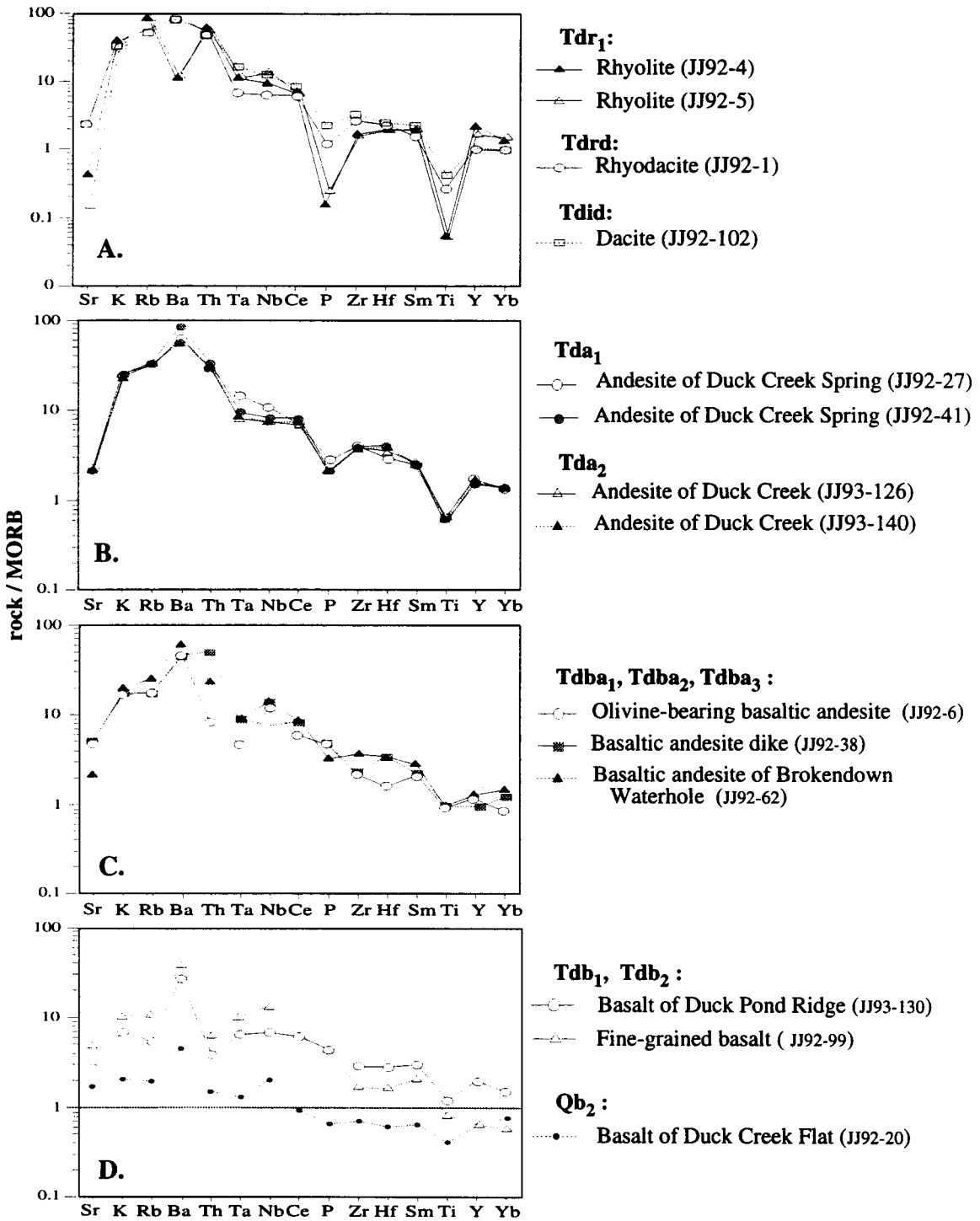


**Figure 4-10:** Spider diagrams of DBEC elements.
(A) rhyolite to dacite; (B) andesite; (C) basaltic andesite; (D) basalt.
Normalization factors from Pearce (1983).

filter-pressed cumulate that forms the core (see Section 5.4.2.4, petrogenesis of the basaltic andesite inclusion).

*Andesite:* The most remarkable feature of the four andesites (JJ92-27, -41, JJ93-126, -140) is their major- and trace-element similarity (Fig. 4-10). With respect to the rest of the suite, they represent a continuum between the evolved basalts and Tdrd, with the exception of possessing higher Zr and Y, lower Sr, and high Cr for their $SiO_2$ content. The andesite inclusions in the rhyodacite (JJ94-1iA, -1iB) have higher $TiO_2$, $Fe_2O_3$, $P_2O_5$, Ba, and Sr, and lower MgO, Cu, and Ni than the andesite flows.

*Dacite:* The composition of the dacite is fairly consistently on a mixing line between the rhyodacite and $Tdba_1$ (JJ92-6) for both major and trace elements (Figs. 4-4, 4-5, 5-2). Although care was taken to remove all inclusions, some undetected mafic inclusions may skew the analysis slightly.

*Rhyodacite:* Analyses from different flow lobes from separate vents of the rhyodacite of Duck Pond Ridge (Tdrd; JJ92-1, -7, -88, -101) show little variation in major-element composition. Trace-element variations and modal abundance of different mineralogic phases vary.

*Rhyolite:* A silica gap between 70.3 and 76 percent $SiO_2$ highlights the difference between the rhyodacite and the relatively aphyric rhyolite ($Tdr_1$; JJ92-4, -5). Samples from the upper and lower flows straddle the dividing line between the peraluminous and metaluminous fields of Shand (1951) and are similar to other high-silica metaluminous rhyolites (for example, Hildreth, 1979; Metz and Mahood, 1991). They are enriched in Rb, Zr, Y, and Nb and depleted in Fe, Ti, Ca, Mg, Ba, Sr, Sc, and La with respect to the less-evolved rhyodacite. They also exhibit a flatter, slightly less

LREE-enriched pattern and strong negative Eu anomaly typical of metaluminous high-silica rhyolite (Fig. 4-9).

### 4.2.4 Miscellaneous rhyolites

Dowell Butte (Tr, JJ92-90) and the rhyolite of Big Gulch ($Tdr_2$, JJ94-158 and JN94-16) have compositions similar to the rhyolite of Indian Creek Buttes. Dowell Butte may be more evolved as inferred from lower Ba, Sr, and Zr and higher Rb. The Devine Canyon Ash-flow Tuff (JJ92-123) is not related to the rest of the suite. These rocks were not used in modeling the evolution of DBEC and therefore are not discussed further.

### 4.2.5 Discussion

Minor silica gaps spanning 55 and 59 percent $SiO_2$ and 62-66 percent $SiO_2$ may be a function of incomplete sampling of multiple flow units. Alternatively, the gaps may represent a real break in the continuum due to hybridization of mafic magmas with smaller amounts of silicic magma. In this case, it is possible for complete mixing of the liquid phases to take place. Petrographic, textural, and mineralogic evidence for disequilibrium is common in the intermediate-composition rocks that otherwise appear homogeneous in hand specimen and within flows. In an opposite case, if a small volume of mafic magma were injected into a silicic magma chamber, the hotter mafic melt would cool before hybridization was complete, forming immiscible blobs (Sparks and Marshall, 1985), such as seen in the inclusion-rich dacite (Tdid) and late flows of the rhyodacite of Duck Pond Ridge (Tdrd).

At high concentrations of $SiO_2$ the leveling off of $K_2O$ may reflect fractionation of potassium feldspar and biotite from the less silicic melts. The scatter in FeO for the basalts may reflect either a component of Fe enrichment during differentiation of a tholeiitic magma or source heterogeneity. The $Al_2O_3$ content, which does not correlate with $SiO_2$, shows a pronounced low between 54 and 59 percent $SiO_2$ but otherwise decreases with increasing $SiO_2$. An inverse relationship for the same samples is reflected in $TiO_2$ and may represent

a Ti-Al substitution. The large scatter in $TiO_2$ may also reflect the appearance of Fe-Ti oxides, which is controlled by oxygen fugacity and/or source heterogeneity.

It is common for MnO, $TiO_2$, and $P_2O_5$ (as well as Zn and Zr) to increase between basalt and basaltic-andesite composition due to fractional crystallization of olivine, plagioclase, and augite. Phosphorous and Zr maxima at intermediate compositions are well documented in the Thingmuli and Skaergaard rocks (Carmichael and others, 1974).

Compatible elements (Sr, Cr, Sc, Co) decrease and incompatible elements (Rb, Ba, Th, Hf, Ta, V, Cs) generally increase with increasing silica content. The scatter in Sr composition reflects plagioclase and apatite accumulation in porphyritic samples. The positive initial slope in Zr is due to incompatibility of the element with minerals fractionating in the mafic liquids. With increasing $SiO_2$ content, zircon becomes a stable phase on the liquidus and can be removed in a fractionating crystalline assemblage. Elevated Nb indicates source enrichment.

## 4.3 Strontium and Neodymium Isotopes

Strontium and neodymium isotopic analyses for five samples from the DBEC series and one Quaternary basalt were received late in the study (Appendix 5). Rocks selected for isotopic analysis include:

(1) the oldest and youngest mafic units, the basalt of Duck Pond Ridge ($Tdb_1$) and the basalt of Duck Creek Flat ($Qb_2$), respectively. These samples were selected to determine isotopic composition within the same eruptive center over time;

(2) the inclusion-rich dacite and the basaltic andesite inclusion. This co-eruptive pair was selected to determine if isotopic ratios reflected similar sources; and

(3) the rhyolite of Indian Creek Buttes and the rhyodacite of Duck Creek Butte. Isotopic composition of these silicic rocks will be used to test the relationship between them and the composition of the crust from which they may have been derived.

# CHAPTER 5: PETROGENESIS

## 5.1 Introduction

Chemical, petrographic, and mineralogic evidence indicates that all of the units at the Duck Creek Butte eruptive center formed under open-system conditions. Although magma mixing appears to be the dominant mechanism, complex models involving more than one source and/or secondary modification are necessary to account for differences in trace-element concentrations. Contributing petrologic processes include Rayleigh fractionation, boundary-layer fractionation, magma mingling, zone melting, and filter pressing.

Numeric modeling of both Rayleigh and boundary-layer fractionation for major and trace elements evolution, as well as phase equilibria of the basalts was accomplished using MIXNFRAC and BLF computer models (Nielsen, 1989; Nielsen and DeLong, 1992). Additional mathematical programs include: mass balance calculations for least-squares fractionation and mixing (XLFRAC, Stormer and Nicholls, 1978); equations for assimilation and fractional crystallization for trace elements (DePaolo, 1981); the general equations for Rayleigh fractional crystallization and batch melting of trace elements (for example, Cox and others, 1979, Chapter 14); and a trace-element-ratio model for magma mixing to qualify end members for intermediate compositions (Langmuir and others, 1978).

The petrogenetic models are based on simplistic assumptions with respect to parental melt and daughter magma composition, crustal composition, pressure, temperature, partition coefficients, oxygen fugacity, and volatile content. They can, however, serve to elucidate basic principles, as well as show which mechanisms are possible and which were most likely operating in the system.

## 5.2 Terminology

*Magma mixing* is the mixing of two or more magmas, regardless of origin, to form a single homogeneous hybrid that may or may not reach equilibrium. I distinguish mixing as a batch process from assimilation. *Assimilation* is the continuous digestion of magma derived from the wall rock during heating. During partial assimilation, low-melting-temperature and incompatible elements are preferentially enriched in the melt. *Magma mingling* is the incorporation of two or more melts of contrasting viscosity or miscibility that form quenched inclusions (Bacon, 1986). *Zone melting* refers to a differentiation process wherein an ascending body of hot magma partially melts and assimilates the overlying crustal material while simultaneously fractionating liquidus minerals (Cox and others, 1979). *Boundary-layer fractionation* of a magma chamber combines crystallization with mixing of the interstitial liquids formed during crystallization at the margin of the magma with the main magma (Nielsen and DeLong, 1992). *Fractional crystallization* is the separation of precipitating crystals from the melt.

## 5.3 Basalt Petrogenesis

Basalt exposed in the study area includes the Steens Basalt (Ts), the porphyritic basalt (Tb), basalt of Duck Creek Butte eruptive center ($Tdb_1$ and $Tdb_2$), and the Quaternary basalt ($Qb_1$, $Qb_2$, and $Qb_3$). The most primitive basalt is the basalt of Duck Creek Flat ($Qb_2$), which therefore was used as a potential parent for DBEC basalt. Despite the large age difference between this basalt and the DBEC basalts, similarity in trace elements (Fig. 4-10) suggests a general similarity of basalt input over time. Although there is some compositional diversity among the basalts in the study area, they probably represent a small

portion of the potential basaltic magmas that were injected during the evolution of the magmatic center.

### 5.3.1 Steens and Steens-like basalt

The Steens Basalt and porphyritic basalt are treated here because they provide insight into mantle and crustal sources near DBEC. An experimental study of plagioclase-hosted melt inclusions in the Steens Basalt suggest that the phenocrysts grew in a fairly shallow (1-3 kbar), well-mixed, evolved magma chamber that could have originated by crustal assimilation and fractionation of plagioclase and olivine from a mantle-derived primary basalt (Johnson and others, 1995). High Fe and incompatible element concentrations with low Mg and compatible element concentrations indicate fractionation and some assimilation, whereas $^{87}Sr/^{86}Sr$ and $\varepsilon_{Nd}$ analyses (Fig. A5-1, Appendix 5) of the Steens Basalt indicate a depleted mantle source (Carlson and Hart, 1983b). Carlson and Hart (1983b) and Hart and Carlson (1987a) propose that the parental Steens Basalt was subjected to extensive crustal contamination by a crustal material that was predominantly Cenozoic in age and consisted only of the extrusive rocks and their reworked products that were produced as a magmatic arc migrated across southern Oregon and northern Nevada. This mafic crustal material was only slightly more isotopically evolved than the primary magmas themselves. Recent sampling of the Steens Basalt at the type section (Appendix 4) indicates a compositional change up section, including higher $P_2O_5$/TiO2, $K_2O$, and Zr/Nb (Fig. 5-1) and lower MgO. It is unclear which basalt Carlson and Hart sampled (that is, whether it was the least evolved or not) and whether there are isotopic differences between the base and the top of the complete Steens Basalt section.

Following a ≈4 m.y. lull, small-volume flows of basalt (Tb) that are compositionally similar to the Steens Basalt flowed disconformably over the surface of the undeformed older basalt along the northern flank of the Steens Basalt shield. It is suggested that these flows represent a younger pulse of magmatism genetically related to the bulk of the Steens

Basalt (Hart and Mertzman, 1982; Hart and others, 1984). Higher $^{87}Sr/^{86}Sr$ and lower $\varepsilon_{Nd}$ values (Appendix 5) obtained for these basalts, however, indicate either derivation from an enriched mantle source (Carlson, 1984) or contamination by a more evolved crustal source (Carlson and Hart, 1983a).

### 5.3.2 DBEC basalt

The basalt of Duck Pond Ridge ($Tdb_1$) and the fine-grained basalt ($Tdb_2$) difer from the bulk of the Steens Basalt lavas in that they contain higher $P_2O_5$ and Nb and lower Cu (Table 4-7 and Appendix 4). They are similar in many major and many trace elements to select flows in the upper part of the Steens Basalt sequence at its type section.

In the study area the $Tdb_1$ and $Tdb_2$ are considerably more evolved than $Qb_2$. The systematic increase in most incompatible elements in $Tdb_1$ and $Tdb_2$ suggests that they were derived by crystal fractionation from a primitive basalt (Fig. 4-5). Elevated Ti, Fe, and V implies fractional crystallization, in contrast to crustal assimilation which would result in a decrease in these elements (Marsh, 1989). In addition, the ternary diagram of Grove and others (1982) indicates a fractionation trend from a primitive parent similar to $Qb_2$ (Fig. 5-2).

The basalt of Duck Creek Flat ($Qb_2$) is the most primitive basalt in the area, therefore was used as a potential parental magma. Simple Rayleigh fractionation, however, cannot produce the DBEC basalts because incompatible trace-element calculations yield widely varying results that require up to 85 percent fractionation of $Qb_2$ to produce the evolved basalts. Low CaO/FeO and Sc depletions in $Tdb_1$ and $Tdb_2$ relative to $Qb_2$ strongly suggests a crystal fractionation process, in particular one that includes the removal of clinopyroxene. High Sr values in $Tdb_2$ also requires the significant removal of clinopyroxene from a basalt similar to $Qb_2$. No clinopyroxene phenocrysts, however, were found in any of the basalts. In addition, the relatively high Cr, Ni, and Co contents would require spinel, or at least orthopyroxene as a liquidus phase, but they also are absent

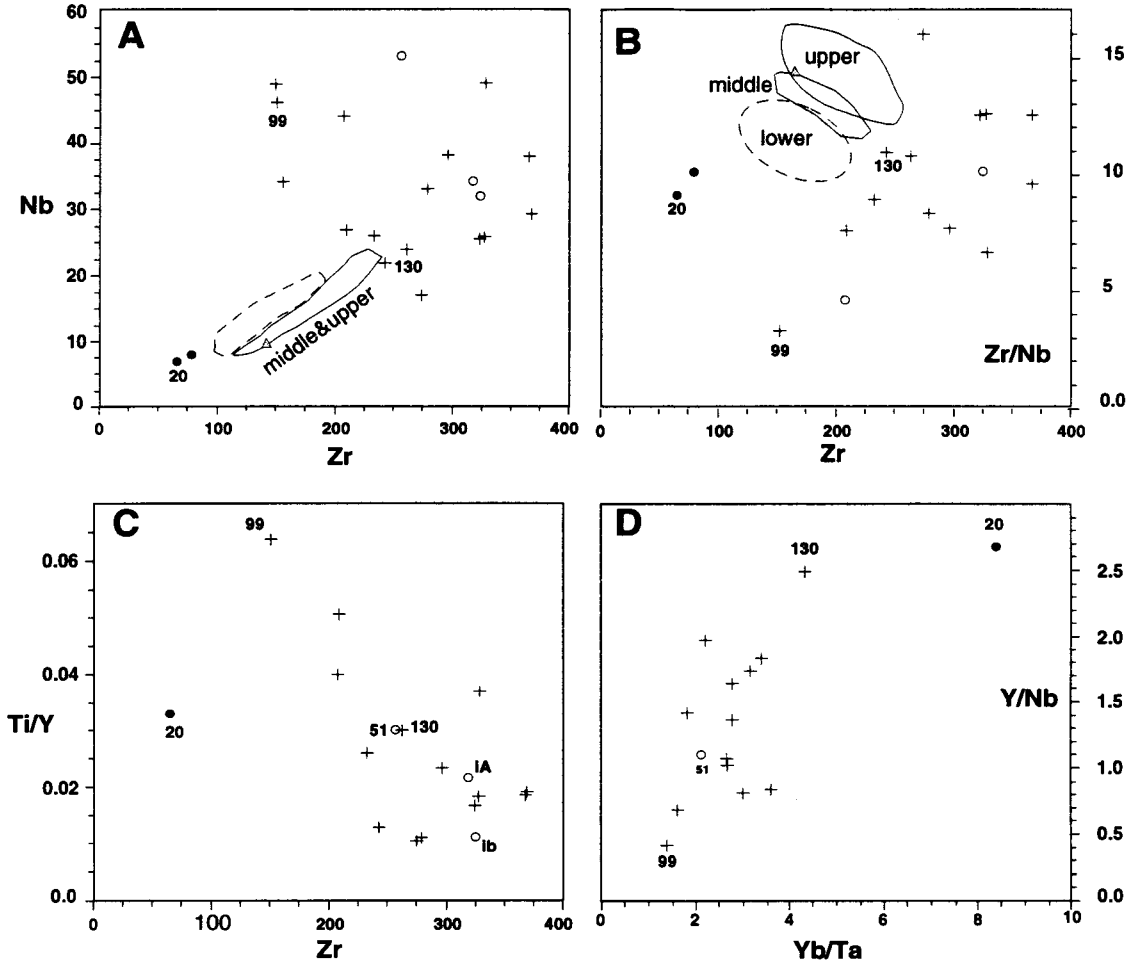


**Figure 5-1**: Trace element variation diagrams.

A. Zr vs. Nb, includes fields for Steens Basalt collected from the type section 60 km south of DBEC (select analyses from lower, middle, and upper sections of the sequence are included in Appendix 4).

B. Zr vs. Zr/Nb. Includes fields for lower, middle, and upper flows of Steens basalt at type section (see A).

C. Zr vs. Ti/Y. DB EC study area only.

D. Yb/Ta vs. Y/Nb. DBEC study area only.

E. Zr/Nb vs. Ce/Y. Indicator of degree of partial melting.

from the modal assemblage. (A single microscopic chrome spinel inclusion in olivine was found in the basalt of Duck Creek Flat.). Hence a boundary-layer fractionation model was tested using BLF (Nielsen and DeLong, 1992). Although boundary-layer fractionation can account for some of the chemical variation between $Qb_2$ and DBEC basalts (Fig. 5-3), it cannot account for the elevated Ti, $P_2O_5$, Sr, Ba, Nb, Hf, and REE characteristic of the basalt of Duck Pond Ridge ($Tdb_1$) or the fine-grained basalt ($Tdb_2$).

$Tdb_1$ and $Qb_2$ are similar in trace-element ratios, such as Ti/Y and Y/Nb (Figs. 5-1), possibly indicating similar mantle sources. $Tdb_2$, on the other hand, has trace element ratios that differ from $Tdb_1$ and $Qb_2$ indicating possible contributions from several processes including derivation from a different source than $Tdb_1$ and $Qb_2$ (for example, Zr/Nb, Fig. 5-1B), smaller degrees of partial melting (Ce/Y, Fig. 5-1E), or lesser amounts of crustal assimilant (indicated by lower K/Rb). Compared to $Tdb_1$, $Tdb_2$ has both higher compatible-element concentrations (Cr, Ni, Co, Table 4-7) with respect to Rb/Sr, indicating a more primitive composition, and higher less-incompatible elements (Sr, Rb, K, Th, Ba, Ta, and Nb) indicating a more evolved composition. These can be resolved by invoking different sources. Alternatively, magma recharge or extensive boundary-layer fractionation could also be reconciled with the observed chemistry. Grove and others (1982) reported a Sr enrichment at Medicine Lake and noted that models that successfully reproduce major and most trace elements cannot account for the elevated Sr content. They attribute the variability in high-alumina basalt Sr contents in part to source region characteristics plus AFC and magma mixing. Strontium is one of the most difficult elements to explain due to variability in both crustal concentration and partition coefficients (Marsh, 1989).

### 5.3.3 Quaternary high-alumina olivine tholeiite

Compositionally similar primitive high-alumina olivine tholeiites (HAOT) are found scattered across the High Lava Plains with no obvious temporal pattern (Fig. 5-4).

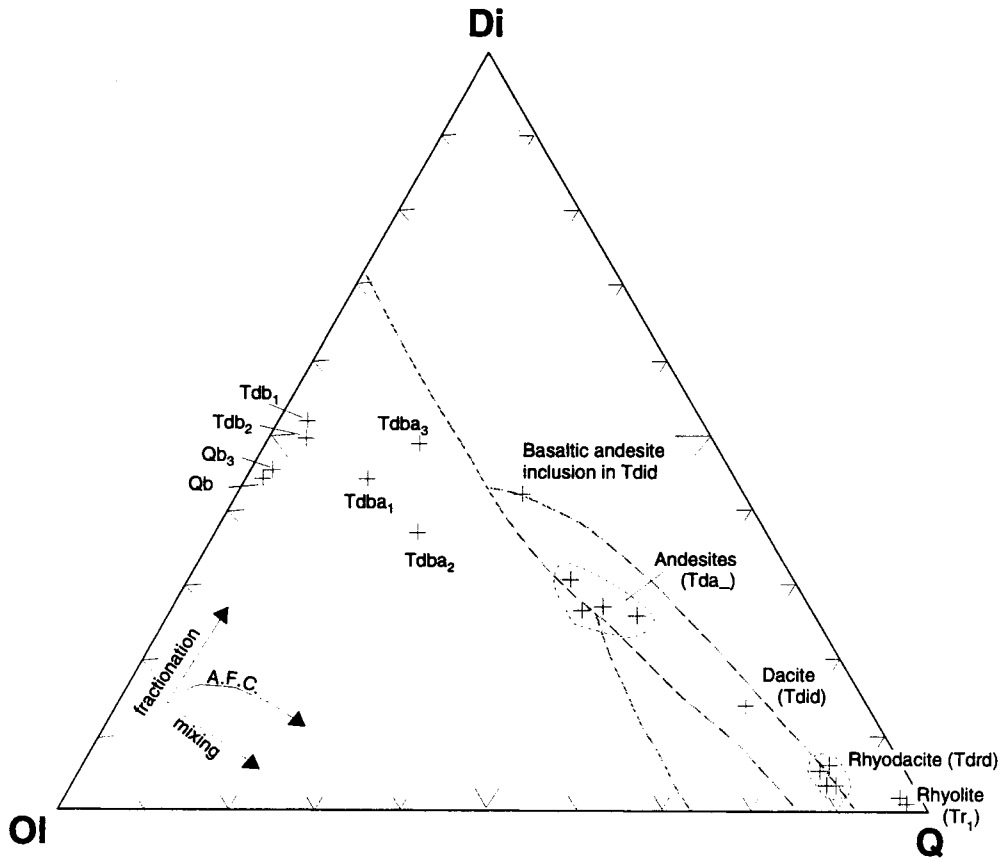


**Figure 5-2**: Projection on olivine-diopside-quartz ternary from plagioclase. Mineral components and projection scheme are defined in Grove and others (1982). $FeO/Fe_2O_3$ ratio reset by method of Sack (1980). Anhydrous low-pressure phase boundaries are shown as dashed lines.

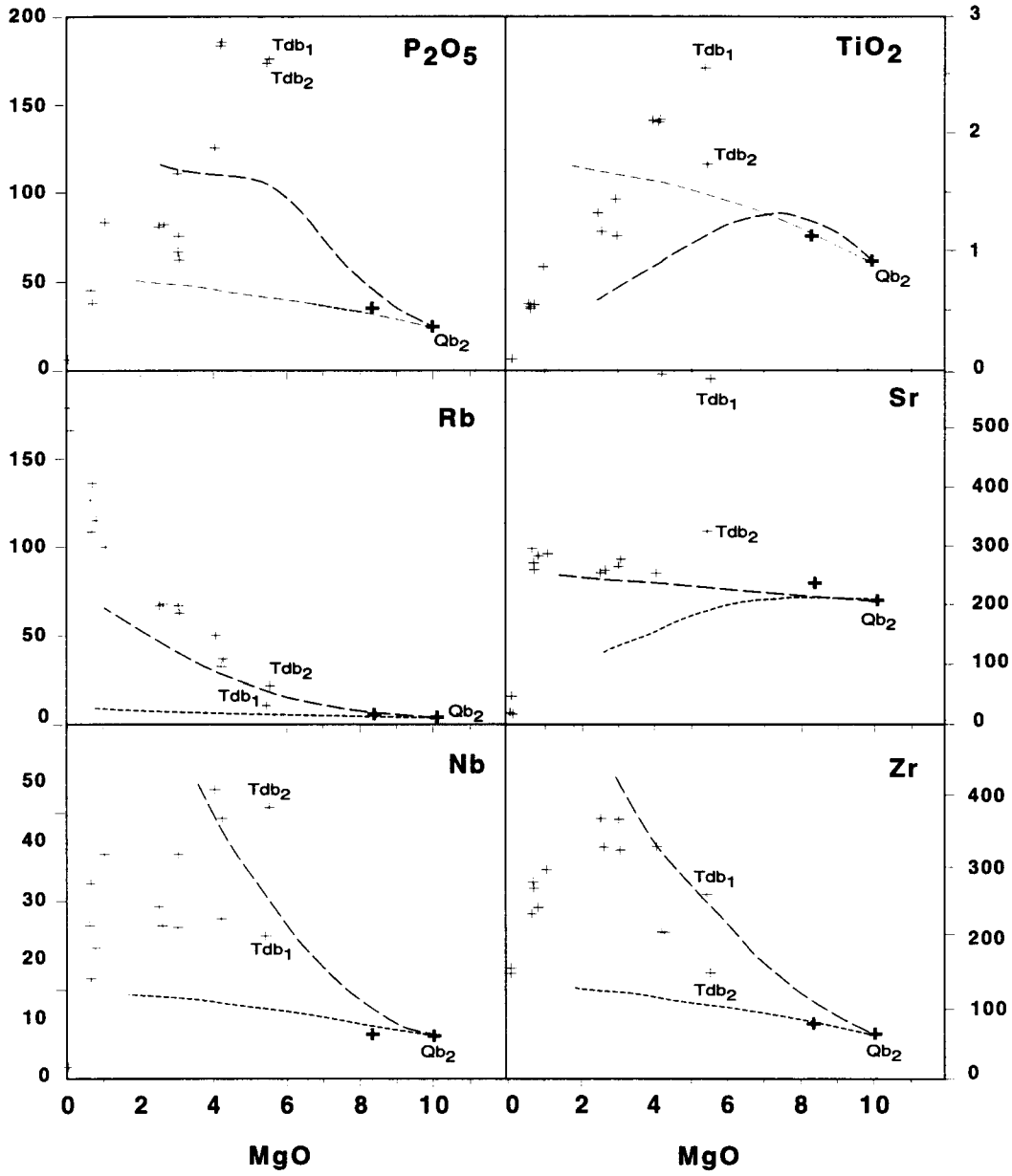


**Figure 5-3:** Variation diagrams showing the fractionation paths of the basalt of Duck Creek Flat using Rayleigh (MIXNFRAC) and boundary-layer fractionation (BLF) models (Nielsen, 1990; Nielsen and DeLong, 1992). Rayleigh trend is short dashed; BLF trend is long dashed.
Bold + = Quaternary basalt; light + = DBEC.

Primitive HAOTs are characterized by $Al_2O_3$>16 weight percent, MgO>8.9 percent, $CaO/Al_2O_3$ ~0.7, $P_2O_5$ ~0.1 percent, $TiO_2$ <1.0 percent, Zr ~50 ppm, Cr ≥ 200 ppm. Although HAOTs in general range in age from 16 Ma in the Steens Basalts to ~6 ka near Newberry volcano (MacLeod and Sherrod, 1992), the primitive tholeiites along the High Lava Plains appear to have erupted exclusively during Pliocene and Pleistocene time.

The basalt of Duck Creek Flat ($Qb_2$) is a primitive HAOT and has a trace-element pattern characteristic of both continental and ocean-island basalt (Pearce, 1983). This pattern is indicated by greatest enrichment in the most incompatible elements, Ba, Th, Ta, and Nb, and no enrichment in the least incompatible elements, Y and Yb, relative to mid-ocean ridge basalt (Fig. 4-10). Trace-element enrichments have been interpreted to reflect minor contamination with a crustal component of oceanic origin ranging from oceanic basalt to pelagic sediments (McKee and others, 1983; Mullen, 1983; Hart and others, 1984; Draper, 1991; Bailey and Conrey, 1992). The back-arc basin signature has contributed to the hypothesis that volcanism in southeastern Oregon may be related to the subduction of

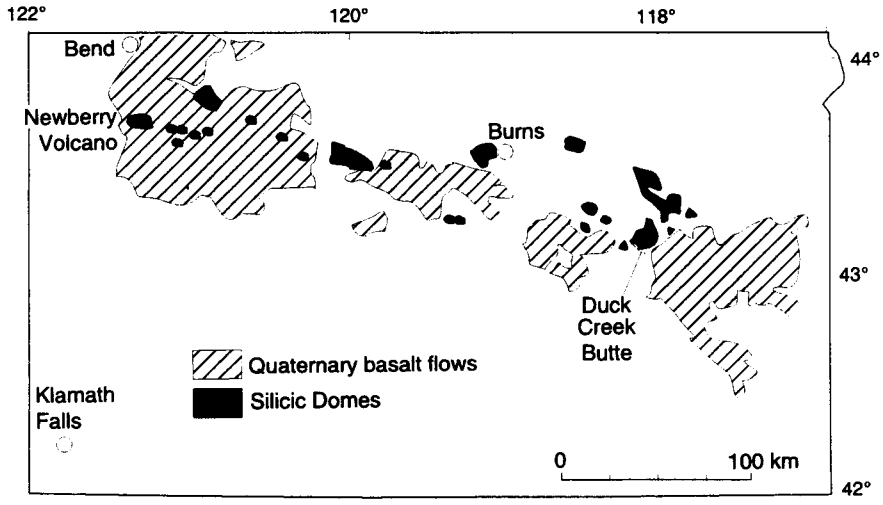


**Figure 5-4**: Map showing distribution of Pliocene and Pleistocene high-alumina olivine tholeiite in High Lava Plains (modified from Walker, 1973).

the Juan de Fuca Plate beneath the North American plate with ensuing arc-related volcanism behind the Cascades arc. Chemical and isotopic similarity of the southeastern Oregon HAOTs, regardless of time and space, suggests that a compositionally monotonous mantle source underlies the area (Bailey and Conrey, 1992). The HAOTs probably resulted from direct mantle melting with little crustal residence time in small widely dispersed magma chambers (Hart and others, 1984; Draper, 1991).

The composition of $Qb_2$ mimics the trends at Devil's Garden, northern California/south-central Oregon (Fig. 5-5) (McKee and others, 1983). It matches, within analytical error, the lowest abundances obtained at Devil's Garden for Sr and Ba, and the highest obtained for K and Rb. Values for major elements, Cr, Ni, and Ba/Sr are similar. McKee and others (1983) argue for a source consistent with origin by 20 percent melting of an anhydrous mantle peridotite. They emphasize that the basalt represents an uncontaminated primary melt of a mantle depleted in K, Rb, and Cs, but not in Ba and Sr. Higher K and Rb at DBEC could be due to source heterogeneity.

In spite of close similarities between the Devils Garden basalts and primitive basalts in the study area, I argue that the lava in the study area represents a primary melt that was contaminated by a small degree of crustal melting. Rb/Sr and Sm/Nd ratios (0.0194 and 0.301, respectively) are similar to the mantle signature (Pearce, 1983). $Qb_2$ is relatively little fractionated, as indicated by high Mg, Cr, Ni, and Ca contents and low K/Zr and K/Ti ratios. The relative enrichment in large-ion lithophile (LIL) elements relative to high-field-strength (HFS) elements (Fig. 4-10D) is best explained by assimilation or mixing with silicic melts that originated through partial melting of a crustal source with a large sedimentary contribution (Bailey and Conrey, 1992). In addition, the slightly elevated $^{87}Sr/^{86}Sr$ value for $Qb_2$ relative to $Tdb_1$ suggests contamination. Digestion of a small increment of an enriched metagraywacke or similar biotite-bearing protolith by dehydration melting would provide the necessary enrichments. The ease of contaminating primitive tholeiites is due to an increased liquidus temperature and decreased incompatible-element

concentration (Bailey and Conrey, 1992). Whole-rock phase relations calculated using MIXNFRAC (Nielsen, 1990) indicate a high liquidus temperature of 1,240°C with the appearance of $Fo_{86.6}$ olivine. Microprobe analysis of olivine yielded values of $Fo_{86}$.

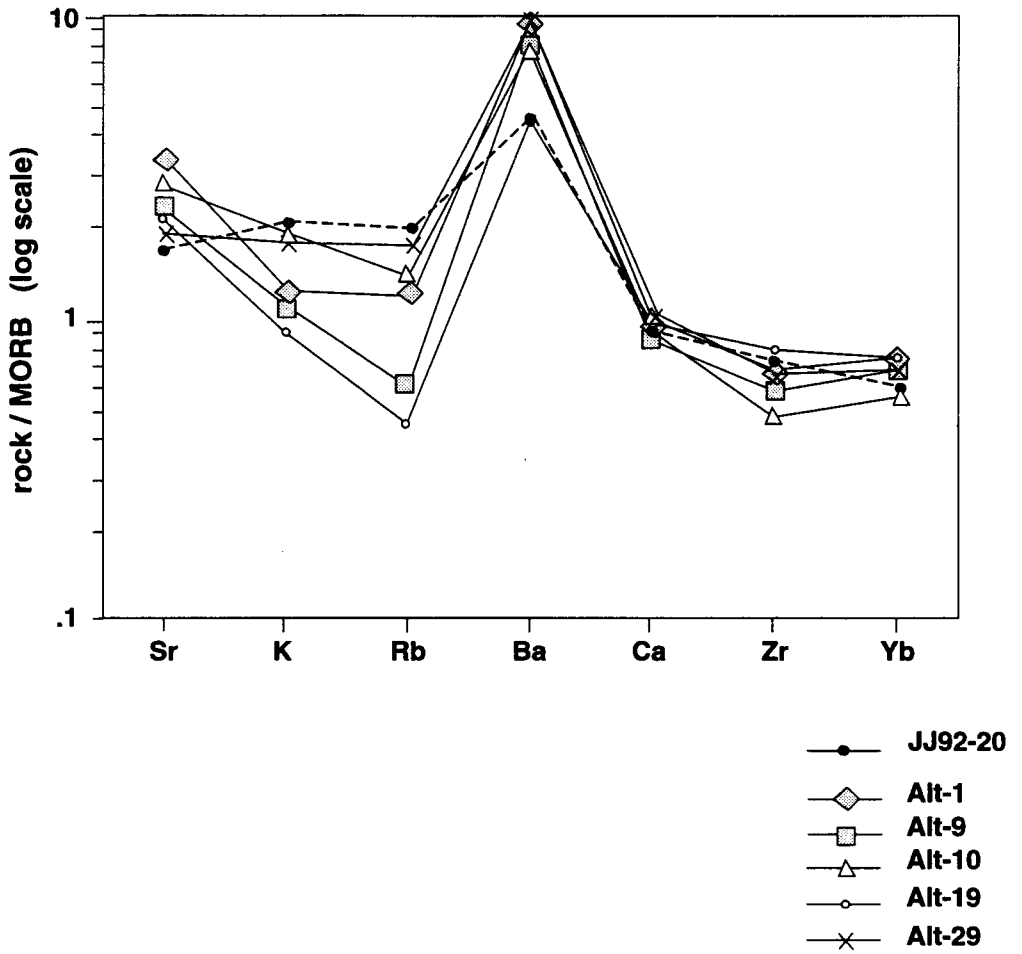


**Figure 5-5**: Spider diagram showing comparison between the basalt of Duck Creek Flat ($Qb_2$, JJ92-20) and Devils Garden basalt. Data from McKee and others (1983) except JJ92-20 (this study).

## 5.4 Petrogenesis of basaltic andesite, andesite, and dacite

### 5.4.1 Introduction

The broad range of compositions from basaltic andesite to dacite is considered together because, in general, they form a continuum. Although they are chemically fairly uniform, most samples contain disequilibrium phenocryst assemblages derived from basaltic and rhyolitic magmas like those in extrusive units in the area.

Intermediate-composition lavas across the Oregon plateau have gone relatively unrecognized, and their importance in the petrologic framework needs to be ascertained. Recent detailed and reconnaissance field work of at least four separate volcanic centers along the High Lava Plains indicates that andesite and dacite are more common than previously recorded. Petrographic and geochemical analyses of intermediate rocks from Duck Creek Butte eruptive center, Frederick Butte (Johnson, unpub. data), Juniper Ridge (MacLean, 1994), Newberry volcano (MacLeod and Sherrod, 1988; Linneman, 1990; Linneman and Myers, 1990; MacLeod and Sherrod, 1992; MacLeod and others, 1995), and the Rattlesnake Ash-flow Tuff (Streck, 1994) indicate that mixing appears to be the dominant process in the formation of intermediate lava, but that other processes, including crustal assimilation, crystal fractionation, magma recharge (MacLean, 1994; Grunder and others, 1994; Grunder and others, 1995), and filter pressing, are required to explain details of variable chemical composition.

With the exception of a small-volume glassy vent and the quenched basaltic andesite inclusions in the dacite, the basaltic andesites and andesites are relegated to the perimeter of DBEC. This "shadow effect" is evidently common in small-volume silicic centers (Wiebe, 1993b). Wiebe (1993b) attributes the spatial correlation to ponding of multiple intrusions of basalt beneath a less dense silicic cap, allowing denser mafic liquids to reach the surface only around the periphery of a central silicic magma reservoir (also, Hildreth and others, 1991).

Andesitic magma began erupting before initiation of silicic volcanism (unit Tba) and continued after emplacement of the inclusion-rich dacite but was inactive during and after emplacement of the rhyolite of Indian Creek Buttes. Andesite inclusions are also present in the rhyodacite of Duck Creek Butte (Tdrd). The mixed-composition lavas appear to be related to active tectonism during which time both movement along faults and coincident influx of fresh basalt provided the magmatic and convective input necessary to produce the hybrids (see Chapter 6).

Petrogenetic models for the origin of intermediate composition magma falls into four categories:

(1) fractionation of basalt to basaltic andesite coupled with assimilation of a trace-element enriched crustal component,
(2) mixing of basalt with rhyodacite,
(3) mixing of basaltic andesite with rhyodacite or dacite,
(4) magma mingling and filter-pressing owing to devolatilization during quenching of basaltic-andesite cumulate blobs within cooler dacite.

### 5.4.2 Basaltic Andesites

The three basaltic andesite flows and the basaltic andesite inclusion have similar major element patterns but show trace-element variability. They are also texturally and mineralogically distinct from each other. Their relationship to the basalt flows is reflected in similar patterns on trace-element spider diagrams (Fig. 4-10). Mass balance calculations using the basalt and mineral analyses suggest that fractionation of reasonable quantities of olivine + plagioclase ± clinopyroxene ± Fe-Ti oxides will account for most of the major element variations. However, discrepancies in calculated versus observed trace-element concentrations require other processes to account for various enrichments and depletions.

#### 5.4.2.1 Olivine-bearing basaltic andesite

The olivine-bearing basaltic andesite ($Tdba_1$) has 15 percent phenocrysts of plagioclase, olivine, and Fe-Ti oxides in an intersertal groundmass with plagioclase and unidentified mafic phases. There is no petrographic evidence for magma mixing, and the phenocrysts appear to be in equilibrium.

Attempts to model fractional crystallization of the basalts ($Qb_2$, $Tdb_1$, and $Tdb_2$) is precluded by poor incompatible element fits. Mixing and fractional-crystallization models are required to enrich Sr, Th, and Nb to levels unattained by simple fractionation.

The best fit is provided by 30 to 40 percent fractionation of plagioclase, clinopyroxene and olivine from $Tdb_2$, but low resultant P, Mn, Sr, Ti, and Sc, and high Rb, K, Ca, and Al suggest less fractionation and some incompatible element-enriching assimilation. High Sr values require a Sr-enriched parental basalt such as the $Tdb_2$ basalt, but other trace elements better fit a model that uses $Tdb_1$ as the mafic end-member. Zone melting by an ascending magma similar to $Tdb_1$ could also produce this melt by partial melting of crustal rocks (for example, metagraywacke), thus enriching the melt in K, Rb, Cs, Ba, Sr, Th, and Nb. Simultaneous fractionation of plagioclase with small amounts of ilmenite (Ti, Ta, Hf, Zr, and Sc) and apatite (P, Y, REE) would produce the necessary trace element depletions.

I prefer a mixing-fractional crystallization model which combines mixing 80 percent basalt, similar to $Tdb_1$, with 20 percent rhyodacite (Tdrd) in concert with about 3-4 percent fractionation of plagioclase + ilmenite ± olivine ± apatite, plus the addition of a crustal component contributing excess Sr, Th, and Nb.

#### 5.4.2.2 Basaltic-andesite dike

A small-volume basaltic-andesite dike ($Tdba_2$) that erupted through flows of the rhyodacite of Duck Creek Butte (Tdrd) is nearly chemically identical, within analytical error, to the olivine-bearing basaltic andesite ($Tdba_1$) for most major and trace elements

with the exception of having lower Sc and Cr, and higher Cs, Th, LREE, and HREE. Petrographic analysis of $Tdba_2$ reveals a distinctly different mineralogy than $Tdba_1$. There are no phenocryst phases present that would be in equilibrium with a basaltic melt. Instead, the observed assemblage of $Tdba_2$ comprises sodic plagioclase, clinopyroxene, Fe-Ti oxides, orthopyroxene, and biotite in a dark- and light-brown swirled glass matrix. Presumably the banding in the glass represents partially mixed mafic and silicic melts. A single fine-grained glomerocryst of olivine and plagioclase was found in thin section. A physical model for this lava suggests an aphyric basaltic magma mixed with low-silica rhyolitic melt and erupted prior to subliquidus cooling of the basalt or resorption of the felsic phenocrysts. Decompression associated with the rapid rise of magma can generate magma that is above its liquidus (Philpotts, 1990). Alternatively, assimilation of K- and $H_2O$-rich contaminant may also contribute by lowering the liquidus as long as the percent of assimilation is low.

Figure 5-2 indicates that a mix of 75 percent basalt of Cord ($Qb_3$) and 25 percent rhyodacite (Tdrd) yields a plausible mix model for $Tdba_2$. Additional fractionation of pyroxene from the basaltic melt would account for the depletions in Sc and Cr.

#### 5.4.2.3 Basaltic andesite of Brokendown Reservoir

$Tdba_3$ has the same general trace-element profile as the other basaltic andesites but doesn't conform well to mixing of any of the flows at DBEC. The aphyric fine-grained flows appear to have had plagioclase, clinopyroxene, olivine, and Fe-Ti oxides on the liquidus just prior to eruption. No petrographic evidence for mixing was found.

Through comparison to Grove and others (1982; Fig. 5-2) assimilation of a rhyolitic melt by $Tdb_1$ or $Tdb_2$ in conjunction with fractionation of plagioclase and olivine is indicated. Simple fractionation from any of the basalts provides poor trace element fits.

#### 5.4.2.4 Basaltic-andesite inclusion

The quenched basaltic andesite inclusions in the inclusion-rich dacite, Tdid, represent classic magma mingling of a rapidly crystallizing quenched basaltic magma in a cooler silicic melt. The inclusions are anomalous because they possess $P_2O_5$, Ba, and trace-element enrichments consistent with plagioclase, apatite, and ilmenite accumulation relative to the other flows of DBEC.

The concentration of vesicles towards the glassy rim (Fig. 2-8) in concert with the observed mineralogy suggests that a cumulate origin could be accomplished by a filter pressing process (Bacon and Metz, 1984; Sisson and Bacon, 1994). During crystallization and devolatilization of the entrained mafic magma, forced expulsion of intercumulate liquid may have resulted in small enclaves that display a textural and compositional cumulate signature. The selective exchange of elements that possess high diffusion rates could selectively enrich the mafic portion of the system. Chemical diffusion between comingled basaltic and silicic melts can produce enrichments in Fe, P, Mn, Rb, and REE and depletion in Na in the mafic melt until equilibrium is reached (Watson, 1982). The inclusions lack evidence for vapor-phase transport from the dacite to the enclave.

Clues to possible magmatic mechanisms can be found in the inferred crystallization sequence. Subhedral to euhedral clinopyroxene and Fe-Ti oxides were the first phases to crystallize, as evidenced by their common presence as inclusions in plagioclase. This reversal in the crystallization order relative to plagioclase may be due to high water content, high $P_2O_5$, and rapid cooling rates, all of which lower the plagioclase crystallization temperature relative to other phases (Eggler and Burnham, 1973; Grove and Bence, 1979).

Prior to eruption, a double-diffusive interface may have formed when a pulse of volatile-rich basaltic magma was injected into the base of the dacitic magma chamber (see Dacite, Section 5.4.4). Heat exchange can drive convection in both layers forming a sharp interface between them (Sparks and others, 1977). Sudden convective overturning of the

volatile-rich mafic layer into the overlying cooler dacite layer may have triggered an eruption due to rapid quenching, crystallization, and exsolution of volatiles.

Alternatively, the ubiquitous presence of small inclusions may have resulted from the forceful injection of a primitive-composition basaltic dike into the dacite. Mechanical and thermal properties of the compositionally contrasting melts may have prevented hybridization, and the predominantly silicic chamber, which was below the solidus of the basalt, rapidly quenched the entrained basalt (Bacon, 1986). Additional convection in the chamber then resulted from superheating and decreased viscosity of the dacite due to heating. Concurrent movement along the fault may have facilitated convection. Textural evidence in the dacite indicates rapid expulsion of the magma before mineral equilibrium could be established.

### 5.4.3 Andesites

In contrast to the compositionally diverse basaltic andesites, the andesites form a chemically cohesive group (Fig. 4-10) that erupted from separate locations around the southern and eastern perimeter of the rhyodacite of Duck Creek Butte. Mineralogy of the andesites is similar; all have sieved and zoned (normal, reverse, and oscillatory) plagioclase, altered olivine, clinopyroxene, and Fe-Ti oxides. $Tda_2$ differs from $Tda_1$ in that it contains 5 to 9 percent equant plagioclase grains as long as 3 cm in length. No microprobe analyses of minerals from the andesites were obtained.

Linear element-element diagrams (Figs. 4-4 and 4-5) and abundant textural evidence support derivation by mixing of two or more magmas. However, some fractionation is consistent with enrichments in Zr, although elevated Cr concentrations imply that fractionation of pyroxene or spinel was not extensive.

Trace-element ratio diagrams based on the calculations of Langmuir and others (1978) (Fig. 5-6), indicate a good fit between rhyodacite (Tdrd) or dacite (Tdid) and basaltic andesite ($Tdba_1$), or rhyodacite and basalt to produce the andesites. However, simple

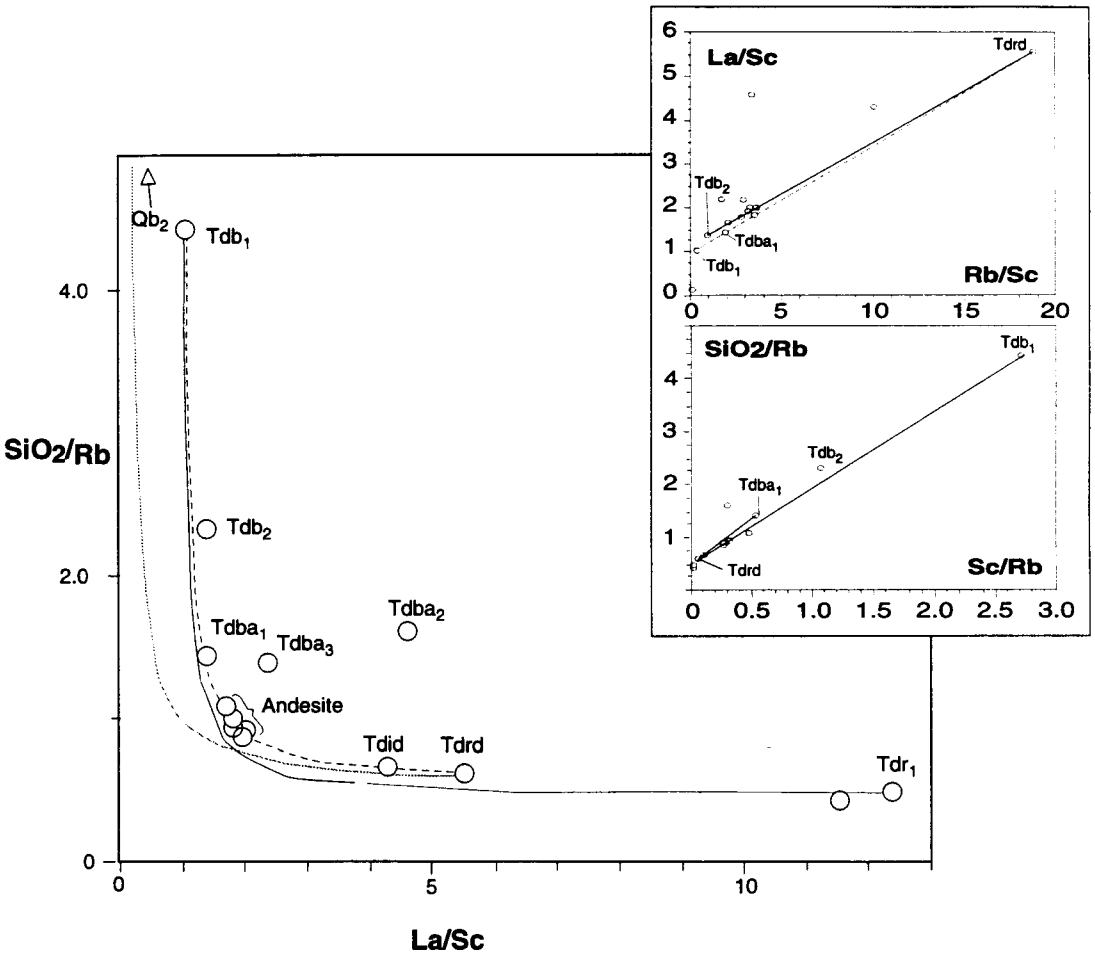


**Figure 5-6**: La/Sc versus $SiO_2$/Rb ratio-ratio diagram with companion plots for the DBEC series rocks. Dashed line indicates mix between the basalt of Duck Pond Ridge ($Tdb_1$) and the rhyodacite of Duck Creek Butte (Tdrd). The same relationship holds for the olivine-bearing basaltic andesite ($Tdba_1$) and the rhyodacite. The upper companion plot does not include the rhyolite of Indian Creek Buttes ($Tdr_1$), and the lower plot does not include the basalt of Duck Creek Flat ($Qb_2$).

mixing of $Tdba_1$ and Tdrd to produce any of the andesites using XLFRAC (Stormer and Nichols, 1978) yielded high $\Sigma r^2$ values in spite of evident linear relationships.

The best sum of the square of the residuals ($\Sigma r^2$) is obtained by mixing Tdrd with two or more basaltic compositions. A simple mix of Tdrd and a single basalt did not satisfy trace element requirements. Mixing a mafic end member with the rhyolite ($Tdr_1$) provided consistently poor fits. The following mixes provide low $\Sigma r^2$ values and calculated trace element abundances (with the exception of Sr, calculated too high, and Zr, too low) within analytical error to produce $Tda_2$ (JJ93-140):

(1) 55 percent Tdrd + 9 percent $Qb_2$+ 36 percent $Tdb_1$: $\Sigma r^2 = 0.43$;
(2) 49 percent Tdrd + 10 percent $Tdb_1$ + 41 percent $Tdb_2$: $\Sigma r^2 = 0.12$.

Similar models performed on $Tda_1$ had the lowest $\Sigma r^2$ value (0.36) when mixing 51 percent $Tdba_1$ (JJ92-6)+ 49 percent Tdid dacite.

This type of end-member mixing between evolved basalt and rhyodacite or basaltic andesite and dacite is common in producing andesites and dacites (Grunder and others, 1995). The occurrence of subequal proportions of mixing end members is commonly modeled (for example, Feeley and Grunder, 1991) and probably reflects the limiting condition that $\geq$50 percent of the mafic end member is required to effect mixing (Sparks and Marshall, 1985).

### 5.4.4 Dacite

The inclusion-rich dacite, Tdid, contains ubiquitous quenched magmatic inclusions (see Section 5.4.2.4) and a complicated phenocryst assemblage which includes anhedral feldspar, Fe-Ti oxides, orthopyroxene, clinopyroxene, ± biotite, ± quartz, ± olivine in varying proportions. Fine-grained clinopyroxene overgrowth on some Fe-Ti oxides and glass-inclusion-rich rims on anhedral feldspar indicate disequilibrium conditions prior to eruption.

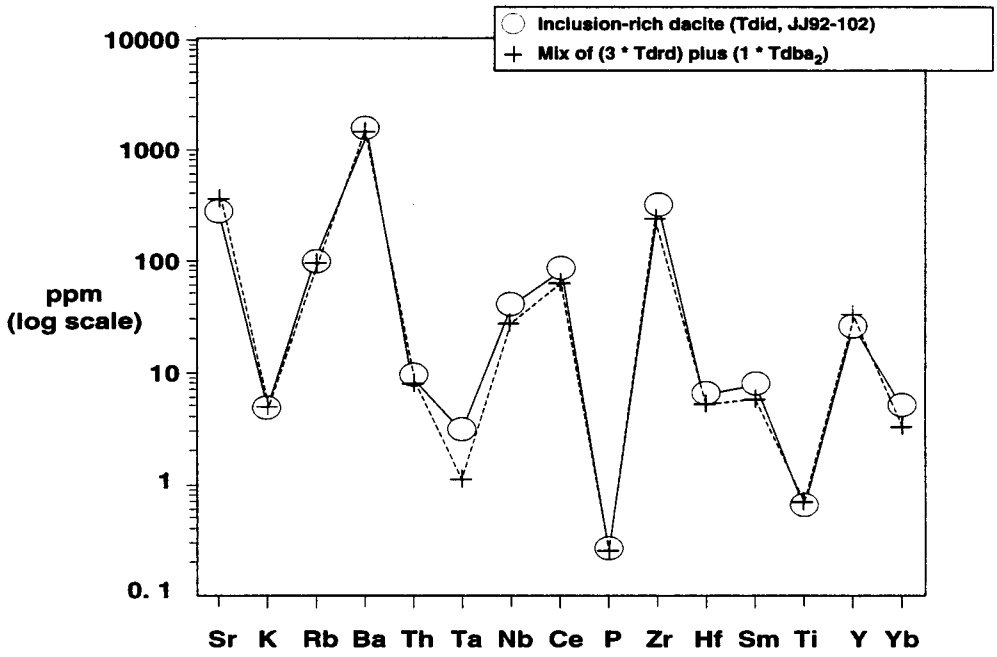


**Figure 5-7** : Trace element concentrations in Tdid (inclution-rich dacite) compared to a 3:1 mix of Tdrd (rhyodacite of Duck Creek Butte) and $Tdba_1$ (olivine-bearing basaltic andesite).

The dacite cannot be derived from the andesite by simple crystal fractionation. Dacite, the logical precursor of rhyodacite in crystal fractionation, can more easily be derived from Tdrd rather than the reverse on a mathematical basis. Figure 5-7 shows that a 3:1 mix of Tdrd with $Tdba_1$ produces a good fit for most trace elements. This is also supported by linear element-element variation diagrams (Figs. 4-4 and 4-5) and the trace-element-ratio mix model in Figure 56. Experimental work by Kouchi and Sunagawa (1983) indicates that, even under uniform high temperature, small quantities of basaltic magma form inclusions when incorporated into a silicic melt. Basalt, on the other hand dissolves the dacite to form hybrid andesites which can be incorporated more easily into a silicic melt. The inherent question then is: under what conditions can a larger volume of silicic magma mix with a smaller volume of mafic magma and not quench it?

Mixing of disparate melts can be accomplished in a "wet" system (Fig. 5-8). Physical impediments to hybridization of magmas with significantly different properties can be lessened by: (1) incorporation of $H_2O$ into mafic melt with coincident fractionation of magnetite which decreases the density; (2) assimilation of alkalis to decrease viscosity of silicic or hybrid melts; (3) step-wise mixing of a hybrid intermediate boundary layer; (4) maintaining a high temperature, and commensurably lower viscosity, of the silicic melt; (5) steady supply of high temperature basaltic liquids into the base of the chamber to promote robust convection (Huppert and Sparks, 1988). Under these conditions the mafic melt, which has both a higher convective velocity than the silicic (due to both lower viscosity and a higher coefficient of thermal expansion) as well as a higher chemical diffusion rate, can entrain the silicic magma in small increments and produce a homogenized layer at its upper boundary (Koyaguchi, 1986). With limited mafic injection, the hybrid can evolve to a significant volume with mechanical and thermal properties similar to those of the silicic melt. Under the boundary conditions, the chemically and thermally similar silicic and intermediate magmas are able to mix essentially in a liquid state in a wide range of mixing ratios.

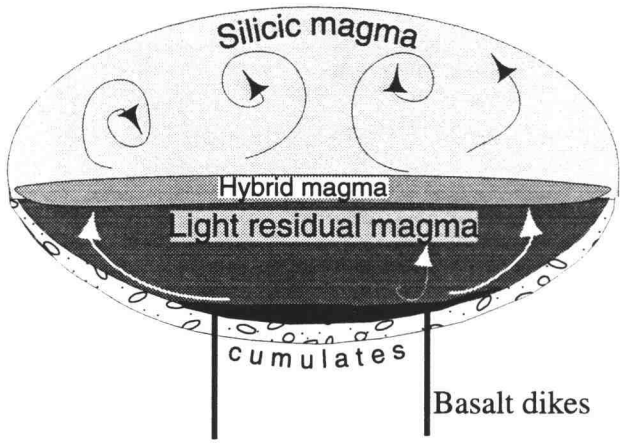


**Figure 5-8:** Cartoon illustrating a "wet" magma system. Differentiated basalt magmas (incipient hybrids) in a wet basalt are lower in density than parental basalts due to early fractionation of magnetite. At elevated temperatures, evolved convecting magmas form a hybrid interface and, through a step-wise evolution, can produce a variety of hybrid magmas. Injection of basalt into the base of the chamber provides heat necessary for homogenization. (R.M. Conrey, written commun., 1994).

## 5.5 Petrogenesis of rhyodacite and rhyolite

### 5.5.1 Introduction

Duck Creek Butte is dominated by the rhyodacite of Duck Creek Butte (Tdrd) and the rhyolite of Indian Creek Buttes, which represent about 90 percent of the erupted volume of DBEC. The rhyodacite of Duck Creek Butte is interpreted to be derived largely from open-system processes including partial crustal melt, magma mixing, and fractional crystallization. The rhyolite of Indian Creek Buttes ($Tdr_1$) is derived by partial crustal melt, similar to that of the rhyodacite of Duck Creek Butte with a much higher contribution from crystal fractionation in a relatively closed system.

Attempts to rigorously apply melt and fractionation models are limited by (1) unknown crustal lithology, (2) large variations in partition coefficients for individual minerals due to solid solution as well as evolving liquid composition, and (3) lack of phenocrysts in the rhyolite to determine phases removed.

### 5.5.2 Rhyodacite of Duck Creek Butte

The rhyodacite of Duck Creek Butte (Tdrd) covers most of the study area with laterally extensive flows that erupted from multiple vents located near, or parallel to, the Duck Pond Ridge fault scarp. Although the flows of rhyodacite are fairly homogeneous with respect to major elements, trace element concentrations vary widely. The variation is attributed to local concentrations of different minerals and mineral assemblages.

The rhyodacite did not evolve by crystal fractionation from the inclusion-rich dacite (Tdid) but by a more complex path derived by crustal melting, magma mixing, and fractionation of mineral phases. Although fractionation of 16 percent plagioclase, ilmenite, clinopyroxene, apatite, and orthopyroxene from inclusion-rich dacite (Tdid) can produce rhyolite (XLFRAC; Stormer and Nicholls, 1978), trace element concentrations, calculated using bulk partition coefficients consistent with the mineral assemblage, predict much

lower values of incompatible elements than observed. In addition, the concentration of chromium in the rhyodacite is too high to have resulted from crystal fractionation.

Petrographic evidence for a convecting, periodically recharged magma chamber includes complexly zoned plagioclase phenocrysts that may reflect attempts at equilibration during relatively brief contact with changing magmatic fluids (See Fig. 5-8 and Sec. 5.4.4 on "wet" system). The diverse phenocryst assemblage comprising plagioclase, biotite, clinopyroxene, orthopyroxene, hornblende, Fe-Ti oxides, quartz, and unidentified trace phases suggests mixed silicic melts. The wide range of plagioclase core and rim compositions ($An_{27}$ to $An_{62}$ and $An_{29}$ to $An_{65}$, respectively) argues for the periodic injection of mafic to silicic magmas, common in large silicic systems (Weibe, 1993a, b). Most plagioclase is subhedral to anhedral, resorbed and sieve textured. Sieve texture is common in rocks of hybrid origin.

Evidence for a mafic basal layer and possibly an intermediate hybrid layer in the magma chamber is found in small round very fine grained andesite inclusions that are compositionally similar to the DBEC andesites. These sparse inclusions, found in one of the upper flows, were probably entrained by convection during overturning following eruption of early flows of the rhyodacite.

The potential source rocks for partial melting in the DBEC area include metamorphosed volcanic and related sedimentary rocks. Dehydration melting of metamorphosed basalt and andesite under low pressure and moderate temperature provides a fairly good model for a derivation of the rhyodacite of Duck Creek Butte, with the exception of having lower potassium and higher sodium (Beard and Lofgren, 1991). Alkali concentrations, however, are sensitive to small variations in the melting protolith. The nearest exposures of basement rocks are Jurassic-Triassic volcanic and volcanically derived sedimentary rocks exposed 100 km north and south-southwest of the study area; Triassic-Paleozoic rocks of ophiolite suites are found 135 km north-northeast of the study area (Walker and MacLeod, 1991). Andesitic to basaltic metagraywacke is also found as xenoliths in the Rattlesnake Ash-flow

Tuff that erupted 90 km west of DBEC (Martin Streck, oral commun., 1995). Hence a mafic to intermediate-composition crustal protolith is reasonable.

Experimental results on fluid-absent partial melting of metagraywackes indicate that the residual feldspar is strongly enriched in orthoclase component, which would not explain the high-potassium suite at DBEC (Vielzeuf and Montel, 1994). High degrees of partial melting of a graywacke produce a sodium-rich melt. Therefore, presence of pelite, which would yield a more potassium-rich liquid on melting (for example, Beard and Lofgren, 1991), as sandwiched layers within the crust may be indicated (Hall, 1987).

Another potential source for the rhyodacite is vapor-absent melting of a biotite- and amphibole-bearing tonalitic gneiss (Skjerlie and Johnston, 1992). Elements that would be enriched during low degrees of partial melting include Rb, Cs, Mn, Sc, Hf, Nb, Ta, Th, and Yb.

To fabricate the trace element abundances in a hypothetical protolith, I used a batch melt equation as a crude approximation (Wood and Fraser, 1976). Partition coefficients are from Arth (1976) and Nash and Crecraft (1985). Proportions of solid phases that would be in equilibrium with the rhyodacite at 20 percent melting (at 975°C, 10 kbar) were taken from the experimental work of Skjerlie and Johnston (1992). I then manipulated the trace-element concentrations for a hypothetical crustal composition. The resulting values (Fig. 5-9) are consistent with those expected for an evolved mafic protolith. This model is a crude test because partition coefficients are poorly known and the model parameters will change during the evolution of the melt. In assuming a closed system, the batch-melt model ignores contributing processes such as mixing, recharge, and fractional crystallization.

The rhyodacite of Duck Creek Butte has $^{87}Sr/^{86}Sr$ of 0.70490 (Appendix 5), which may reflect contamination by small amounts of an isotopically more primitive Sr-rich mafic melt. The original silicic melt that evolved to the rhyodacite likely had an original $^{87}Sr/^{86}Sr$ value equal to, or slightly lower than, that of the rhyolite of Indian Creek Buttes ($Tdr_1$; $^{87}Sr/^{86}Sr$ of 0.70741). The assumption that the rhyodacite evolved from a crustal melt

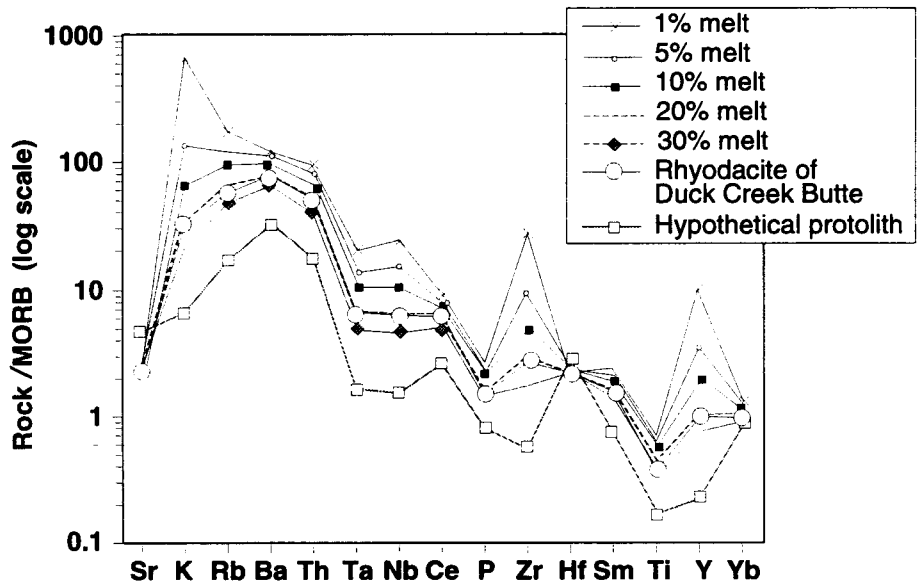


**Figure 5-9**: Trace-element spider diagram using hypothetical protolith to create the element concentrations in the rhyodacite of Duck Creek Butte. The batch melt equation is from Wood and Fraser (1976).

similar to the rhyolite implies that spatial proximity indicates similar protoliths. DePaolo's (1981) model for isotope ratios and trace element concentrations indicates that the incorporation of a small amount (~1 percent) of hypothetical primitive melt with an $^{87}Sr/^{86}Sr$ value of 0.704 into a Sr-depleted rhyolite with a 0.70741 ratio yields the 0.70496 value for Tdrd when coupled with 10 percent fractional crystallization. The ease of contaminating a Sr-poor magma during the magmatic stage makes the interpretation less straightforward than in more mafic rocks (Mahood and Halliday, 1988).

The rhyodacite resulted from complex interactions involving zone melting during extension and change in crustal thickness. As hot mantle-derived basalt is injected into the thinning crust as sills and dikes, initiation of partial melting is facilitated by progressive heating of the crust, release of volatiles, and decreased pressure. Continued heat input aids both greater degrees of melting and the bouyant rise of multiple pods of silicic melt. If a primitive basaltic magma with a liquidus temperature of 1,230°C (as calculated for $Qb_2$), intrudes an already heated (~500°C) $H_2O$-rich crust at a shallow depth (5-10 km), dehydration and decompression melting can produce a partial melt equal to the volume of the intruded mafic melt (Weibe, 1993b). The heat content of a large body of basaltic magma is sufficient to cause this volume of silicic melt to form if little heat is lost.

### 5.5.3 Rhyolite of Indian Creek Buttes

The rhyolite of Indian Creek Buttes ($Tdr_1$) erupted from multiple vents located west of vents and flows of the rhyodacite of Duck Creek Butte. The model I present is a high-level stratified magma body that evolved by crystal fractionation from a rhyodacite that was produced by crustal melting and hybridization of coalescing silicic magmas. Field relations indicate that a more-evolved upper part of the chamber erupted first as aphyric to very-sparsely porphyritic flows that were quenched to glass. Enrichment in phenocrysts on capping flows may reflect tapping of a magma chamber in which crystal settling or a volatile gradient have led to increasing phenocryst abundance downward (Hildreth, 1981).

Trace-element systematics, as well as phenocryst assemblages, are consistent with fractional crystallization of a melt similar in composition to the rhyodacite of Duck Pond Ridge as the dominant controlling process in producing the rhyolite of Indian Creek Buttes. Other processes are assumed to be minor because trends in element concentrations are closely matched by fractionation models. Extremely low concentrations of Sr and Ba rule out an origin by single-stage melting of any crustal lithology. Strong depletions in Eu, Sr, Ba, Zr, and Sc, in concert with moderate enrichments in Rb, Th, U, MREE, HREE, Nb, Y, and Ta, argue for derivation from a melt similar to the rhyodacite of Duck Creek Butte (Tdrd) by crystal fractionation (Fig. 4-5, Table 4-7). All models show that removal of observed phenocryst phases from the rhyodacite (Tdrd) can adequately account for most of the element variations. Trace phases, which were not observed but may be present, may account for other differences; for example, fractionation of monazite and allanite could account for lower LREE concentration (Miller and Mittlefehldt, 1982).

Least-squares method for modeling of major elements to determine approximate proportions of fractionating phases was performed using XLFRAC (Stormer and Nichols, 1978). Variations in trace elements were calculated by a Rayleigh fractionation equation (Cox and others, 1979). Bulk partition coefficients were determined using mineral distribution coefficients of Mahood and Hildreth (1983), Nash and Crecraft (1985), and Arth (1976).

An adequate fractionating assemblage as indicated by low residuals ($\Sigma r^2 = 0.11$) can produce the trends between Tdrd and $Tdr_1$ (JJ92-5). This assemblage comprises 13.6 percent plagioclase, 5.4 percent biotite, 2.7 percent amphibole, 0.6 percent apatite, and 0.4 percent ilmenite. Although the model uses no more than five minerals, the addition of approximately 1 percent each of clinopyroxene and orthopyroxene in place of a portion of that assigned to amphibole would match the observed modal assemblage. Potassium feldspar, though absent in Tdrd, likely became a fractionating phase as the melt evolved.

Additional fractionation produced the more evolved $Tdr_1$ (JJ92-4), but lack of phenocrysts and changes in partition coefficients make determination less tenable.

Trace element ratios also indicate that plagioclase and biotite played major roles in the fractionating assemblage. Strong increase in K/Ba indicates fractionation of biotite and potassium feldspar; increase in Rb/Sr by plagioclase removal is slightly tempered by removal of biotite; K/Rb depletion reflects potassium feldspar removal; no change in Sr/Ba indicates that plagioclase fractionation is balanced by biotite and potassium feldspar fractionation.

Previously discussed AFC models for the origin of the suite of rocks erupted at DBEC indicate a Ba-enriched biotite-bearing mafic protolith. Small degrees of partial melting of such a rock would produce large concentrations of K, Ba, Nb, and Y. To produce the large volume of low-Sr, low-Ba magma seen at Indian Creek Buttes by low degrees of partial melting requires simultaneous fractionation of large volumes of feldspar-, clinopyroxene-, and biotite-rich cumulates larger than the erupted volume.

The interpretation of Sr-isotopic compositions of rhyolites is less straight forward than in more mafic rocks, owing to the ease of contamination of Sr-poor magmas during magmatic and post-magmatic processes. $^{87}Sr/^{86}Sr$ value of 0.70741 for the rhyolite (Appendix 5) suggests origin by anatexis of isotopically evolved crust rather than fractionation of a mafic melt. High Rb/Sr values in a magma chamber can bring about measurable variations in the $^{87}Sr/^{86}Sr$ ratio by *in situ* decay of $^{87}Rb$ resulting in increased $^{87}Sr/^{86}Sr$ (Christensen and DePaolo, 1987; Mahood and Halliday, 1988). Subsequent closed-system fractionation accounts for the trace-element concentrations. Although the Sr-isotopic ratio of Tdrd is too low to be directly parental to $Tdr_1$, it provides an adequate major- and trace-element model parent based on the assumption that the original crustal melt parental to Tdrd was probably higher in initial $^{87}Sr/^{86}Sr$, and open-system contamination by mafic melts served to lower the ratio.

# CHAPTER 6: DISCUSSION AND CONCLUSIONS

The discussion of the Duck Creek Butte eruptive center focuses on two aspects: (1) the relationship between compositional and textural trends and the tectonomagmatic evolution of DBEC, and (2) the northwest-younging trend of silicic vents and late-stage primitive basalt erupted along the High Lava Plains.

## 6.1 Tectonomagmatic summary of DBEC

The abundance of rhyodacite and dacite and the preponderance of mixed textures in lavas of DBEC is in contrast to the high-silica rhyolite typical of other silicic eruptive centers of the High Lava Plains and indicates that it had a different history. DBEC also differs in that it lies astride a long-lived fault. The following scenario accounts for the regional and local tectonic setting of DBEC and places the petrologic constraints in a physical context.

Early magmatism prior to the development of DBEC consisted of basalt and basaltic andesite derived by fractional crystallization and mixing of small proportions of crustal melt. Following a brief lull in magmatic activity, DBEC produced a suite of magmas that varies in composition from rhyodacite to basaltic andesite. Each compositional type is characterized by abundant evidence for mixing. This suite records the eruptive decay of a magmatic system disrupted by faulting. Following a period of tectonic quiescence the rhyolite of Indian Creek Buttes, derived by fractional crystallization of a crustal melt, erupted from vents west of the rhyodacite of Duck Creek Butte. The principal petrologic sequence of events is depicted in Figure 6-1 and 6-2 and includes the following points.

(1) Crustal thinning and faulting by Basin-and-Range extension facilitated the ascent of relatively unfractionated basalt (Tb) in the vicinity of DBEC between 12 and 11 Ma.

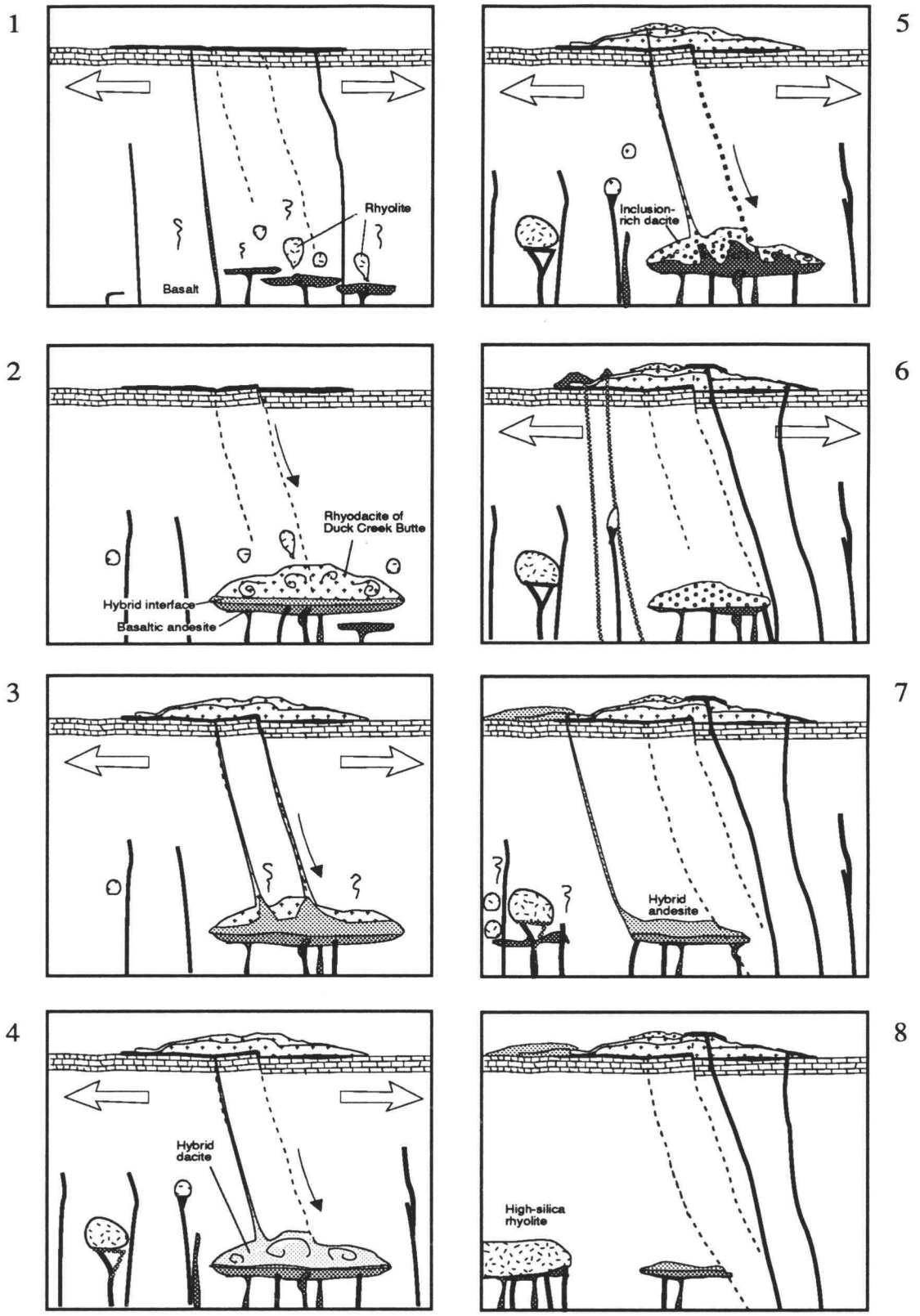


**Figure 6-1**: Cartoon of the tectonomagmatic evolution of the Duck Creek Butte eruptive center. Numbers refer to descriptions in the text.

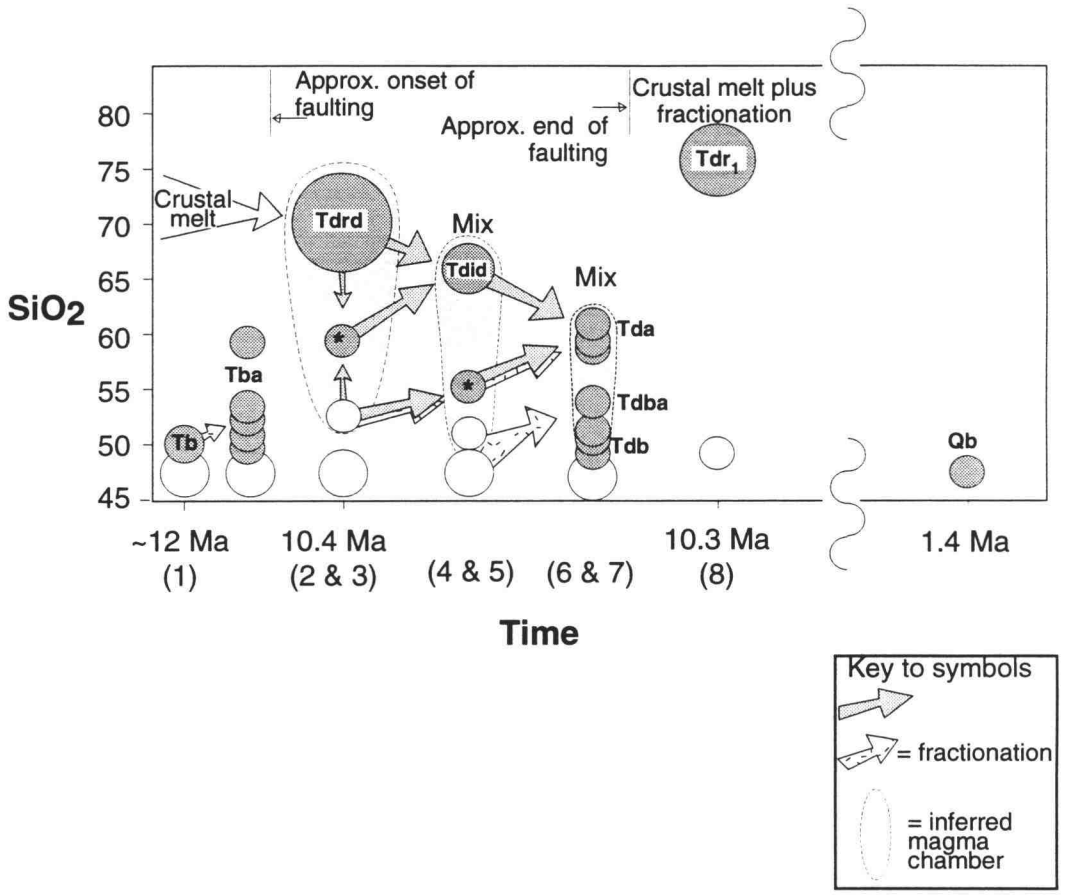


**Figure 6-2**: Graph of time versus $SiO_2$. Shaded circles indicate compositions of rock types observed at DBEC; open circles indicate compositions inferred to have been present; asterisk indicates presence as quenched inclusions. Numbers in parentheses refer to panel numbers in Fig. 6-1.

Injection of basaltic sills and dikes into crustal rocks resulted in small degrees of crustal melting and the formation of pods of silicic melt (Fig. 6.1, panel 1).

(2) With continued thermal input, silicic magma pods coalesced to form a large, well-mixed magma chamber that evolved to a doubly convecting layered chamber capped by the rhyodacite of Duck Creek Butte (Tdrd) (panel 2). Most of the lava is chemically homogeneous plagioclase-biotite-clinopyroxene rhyodacite. Minor phenocrysts of orthopyroxene and amphibole indicate some variations in water content or temperature differences in the chamber. Generation of a well-mixed upper silicic chamber implies coalescencing pods of crustal melts during tectonic quiescence. A layered chamber with mafic underpinnings is inferred because hybrid andesite was entrained as inclusions; the inclusions probably represent an intermediate layer that was a mixture of rhyodacite and basaltic andesite. A basaltic andesite derived from assimilation and fractional crystallization likely formed the hotter convecting basal layer (panel 2). Continued basal injection of mafic magmas supplied heat to the convecting chamber.

(3) Eruption of the rhyodacite of Duck Creek Butte (Tdrd) was initiated by an explosive phase and resulted in the emplacement of block-and-ash deposits to the east, and finer, well-sorted deposits to the west. More than 6 $km^3$ of rhyodacite lava flows followed (panel 3). Distribution of vents imply the chamber was at least 5 by 3 km across. Weakness along faults provided a conduit for eruption, allowing the magma to escape without freezing. Rapid drawdown entrained sparse blobs of andesite, which occur mainly in late-erupted lavas inferred to originate from deeper in the chamber. Although syneruptive faulting cannot be proven, I infer that tectonic activity facilitated rapid drawdown and near-complete evacuation of the chamber because subsequent volumes of silicic magma are very small. In addition, field evidence indicates that movement along the Duck Pond Ridge fault both predated and postdated eruption of the rhyodacite.

(4) Eruption was followed by convective mixing of much of the residual rhyodacite melt with the hybrid andesite intermediate layer to form the inclusion-rich dacite (Tdid), which erupted as lavas (panel 4). Mixing may have been facilitated by movement along the Duck Pond Ridge fault following evacuation of the rhyodacite.

(5) The initial small volume of dacite lava has few mafic magmatic inclusions, but as many as 30 percent quenched basaltic andesite inclusions are evenly distributed in later dacite lavas. The size and distribution of the entrained inclusions indicate strong convection that was driven by increased mafic input. Alternatively, faulting may have driven rapid eruption which then caused entrainment. The inclusions represent basalt that was filter pressed during quenching (see Sec. 5.4.2.4). The mingled magma was evacuated from the chamber before equilibration overgrowths formed on minerals in the dacite. Following the evacuation of the dacite, only a small amount of silicic magma remained, as indicated by the change in composition of erupted magma.

(6) Reduced size of the silicic magma chamber is indicated by the eruption of basalts near the previous silicic vents. The basalt of Duck Pond Ridge ($Tdb_1$) erupted near the central vent of the rhyodacite of Duck Creek Butte. Lack of mineralogic evidence for contamination by the rhyodacite indicates that the basalt dike bypassed the diminished magma chamber. To the east $3^1/_4$ km, a virtually aphyric basaltic andesite mixed with a small proportion of biotite-bearing rhyodacite and formed the basaltic andesite dike ($Tdba_2$). Although the dike cuts flows of the rhyodacite of Duck Creek Butte, it likely erupted near the shadow zone of the silicic magma chamber, assimilating only a small amount of rhyodacite. Near the northeastern vent of the rhyodacite of Duck Pond Ridge, a chemically distinct high-potash low-titania fine-grained basalt ($Tdb_2$) was the last eruptive unit in the northern part of DBEC. Movement along the Duck Pond Ridge fault truncates both $Tdb_1$ and $Tdb_2$.

(7) Mixing of the residual dacite with basaltic andesite yielded andesites of Duck Creek Spring ($Tda_1$) and Duck Creek ($Tda_2$). The andesites can be obtained by a 3:1 mix of

olivine-bearing basaltic andesite ($Tdba_1$) and the rhyodacite of Duck Creek Butte (Tdrd) (Fig. 5-7). Although the two andesites are compositionally identical, they are mineralogically distinct in that the andesite of Duck Creek has very coarse (up to 3 cm in length) blocky plagioclase, suggesting the andesites were possibly sequentially tapped from a cooling mixed chamber representing the final stage of magmatism at DBEC.

(8) The locus of magmatism then migrated northwestward to Indian Creek Buttes. The basaltic andesite of Brokendown Waterhole ($Tdba_3$), which is compositionally similar to the other basaltic andesites, erupted from a vent west of Duck Butte. The eruption locale indicates that it is not related to the plumbing of Duck Creek Butte, but may be a precursor to the development of Indian Creek Buttes proper. This is inferred by lack of evidence for contamination of the mafic magma with high-silica rhyolite. The emplacement of the rhyolite of Indian Creek Buttes may have followed quickly or lagged by as much as 0.2 m.y. on the basis of a 10.38±0.04-Ma biotite age from the rhyodacite of Duck Creek Butte and a sanidine age of 10.32±0.04 Ma from the rhyolite of Indian Creek Buttes (Table 2-1). The shift in the predominance of partial melting of the crust to crystal fractionation in developing the high-silica rhyolite chamber suggests tectonic quiescence. Continued basaltic underplating maintained a high temperature, which served to prevent the system from freezing during crystallization. The rhyolite of Indian Creek Buttes erupted through centrally located vents in two stages that represent the eruption of a weakly stratified rhyolitic chamber composed of an aphyric highly evolved layer overlying a sparsely porphyritic layer. Any injections of hot basaltic magma presumably remained ponded beneath the silicic chamber, owing to compositional and thermal contrasts.

In summary, Duck Creek Butte eruptive center initially produced abundant intermediate and mixed magmas, presumably as a consequence of synmagmatic faulting. Structural

disruption and frequent eruption prevented development of a high-silica rhyolite. Indian Creek Buttes, in contrast, is extremely differentiated suggesting quiescent conditions.

Following a 9-m.y. hiatus in extrusive magmatic activity, primitive Quaternary basalt erupted in Duck Creek Flat and Duck Creek. Compositionally similar basalt erupted across the High Lava Plains with no obvious temporal pattern. Although the basalt of Duck Creek Flat has an isotopic signature distinct from DBEC rocks (Appendix 5), it possesses trace-element enrichment similar to, but more depleted than, the DBEC series rocks (Fig. 4-10).

## 6.2 Age Progression

The High Lava Plains and Brothers fault zone have a complex tectonic and magmatic history. On the basis of my work at Duck Creek Butte eruptive center, Frederick Butte, and the Malheur Cave area (Fig. 1-2), and on structural and magmatic patterns of the region (Walker and others, 1967; Walker, 1969; Greene and others, 1972; MacLeod and others, 1976; MacLeod and Sherrod, 1988; Walker and MacLeod, 1991; MacLeod and Sherrod, 1992; MacLean, 1994; Streck, 1994), I here develop the argument that the High Lava Plains represents a propagating transform boundary that developed in the past 12 million years, and that silicic volcanism is related to migration at the tip of this system. On the basis of observations at DBEC and across the High Lava Plains, the following aspects are noted:

(1) Largely unfractionated basalt (Tb) erupted between 12 and 11 Ma, prior to the development of DBEC. Compositional changes in basalt at this time (Carlson and Hart, 1985) may mark the transition from Basin-Range extension to an incipient extension-related transform system.

(2) Unit Tb gives way to evolved basaltic andesites and andesites (Tba) not later than 10.5 Ma.

(3) About 10.4 Ma the rhyodacite of Duck Pond Ridge erupts explosively, followed by the emplacement of over 6 $km^3$ of lava flows. Subsequent eruptions discharge subordinate mixed dacites, andesites and fractionated basalts. Less than 0.1 m.y. later, silicic magmatism propagates a short distance westward resulting in the deposition of the rhyolite of Indian Creek Buttes.

(4) Following a 9-m.y. lull, the primitive high-Mg, low-Ti Quaternary basalt of Duck Creek Flat erupts.

(5) Along the High Lava Plains, a linear series of silicic vents shows a systematic age progression westward from 10.4 Ma at DBEC to 0.6 Ma at Newberry volcano (MacLeod and others, 1976). The High Lava Plains silicic trend began its migration away from the inferred location of the Snake River Plain-Yellowstone hot spot at about 11 Ma.

(6) And, steep northwest-striking faults, parallel to the younging direction, are broadly distributed similar to that of a propagating continental rift (Benes and others, 1994). Inflation during thermal uplift during an extended period of magmatic input, and subsidence related to cooling and deflation during waning stages of magmatism may have contributed to the widely dispersed northwest-striking small-offset faults.

Between 17 and 15 Ma widespread basaltic volcanism in southeastern Washington, eastern Oregon, western Idaho, and north-central Nevada resulted from approximately east-west directed extensional tectonics (Fig. 6-3) (Stewart, 1978; Zoback, 1989; Li and others, 1990). This volcanism in southeastern Oregon deposited 12,000-15,000 $km^3$ of Steens Basalt over a surface of little topographic expression (Mankinen and others, 1985; Carlson and Hart, 1983b). To the north on the Columbia Plateau, a major magmatic event is preserved in the voluminous Columbia River Basalt Group (Fig. 6-3), which includes over 174,000 $km^3$ of basalt erupted from multiple vent locations during less than 2 m.y. (Tolan and others, 1989).

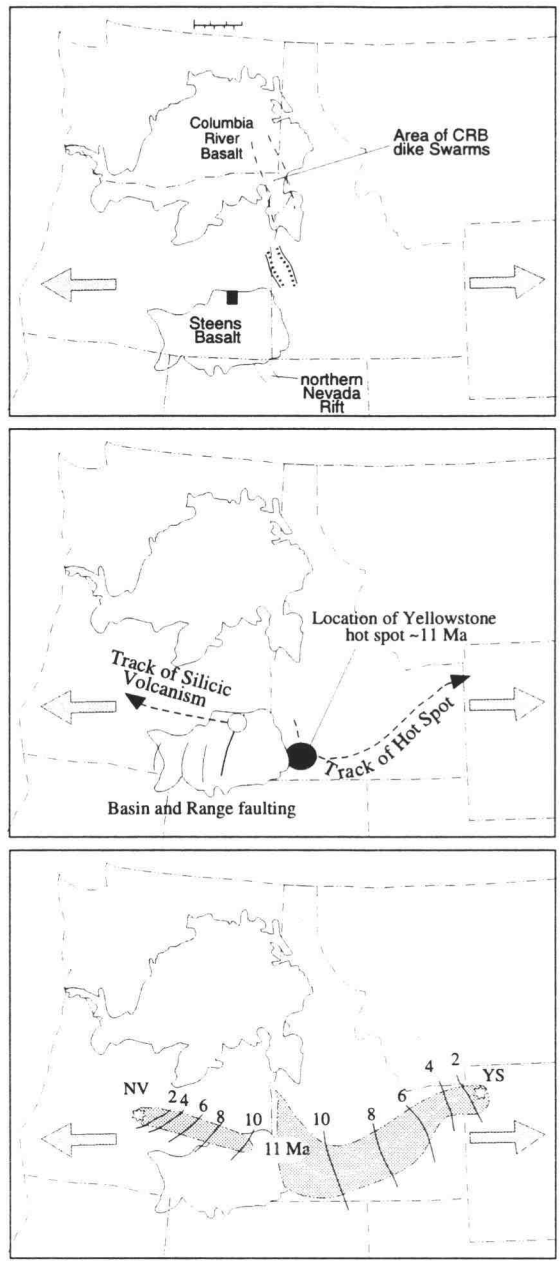


**Figure 6-3**: Evolution of the age progression.
(A) ~17 Ma extension direction (Zoback and Thompson, 1978), Steens Basalt and Columbia River Basalt group.
(B) Basin and Range faulting in southeastern Oregon and direction of the track of younging silicic volcanism. (C) Dark shaded areas show High Lava Plains in southeastern Oregon and Snake River Plain in Idaho and Wyoming with isochrons superimposed.
NV = Newberry volcano; YS = Yellowstone.

The theory that a mantle plume resided near the tri-state region of Oregon, Idaho and Nevada at ~17 Ma is generally accepted. Interpretations on the origin of the plume include the emergence of a hot spot at that location or the re-emergence of an Eocene fore-arc hot spot that was prevented from ascending by the subducting Farallon plate (Duncan, 1982; Brandon and Goles, 1988; Humphries and others, 1992; Geist and Richards, 1993). By one theory, the mantle plume may have been diverted 200 km to the north, producing the main sequence of Columbia River Basalt flows before its traverse beneath the Snake River Plain (Hooper and Hawkesworth, 1993; and Camp, 1995) . Simultaneously, propagating Basin-and-Range extension northward into Oregon may have been facilitated by softening of the lithosphere by the plume. By ≈11 Ma the eruption of voluminous basalt was replaced by isolated, fault-related fissures that produced less-fractionated high-alumina olivine tholeiites (McKee and others, 1983; Carlson and Hart, 1987).

About 11 Ma a transition to predominantly silicic volcanism began at the eastern end of the High Lava Plains. MacLeod and others (1976) noted two subparallel, 250-km-long, age-progressive belts of rhyolitic domes, flows, and ash-flow tuffs in southeastern Oregon. These belts, which trend roughly N 75° W, form a mirror image to the Snake River Plain-Yellowstone eastward-younging age trend (Figs. 1-2 and 6-3). A little-noted feature is that domes discrepant to the age progression crop out along the isochrons that represent the trend of age progression. Specifically, older (pre-11 Ma) domes crop out locally as far west as 119° 45' (Horsehead Mountain, A.L. Grunder, unpub. data), but domes younger than the age progression are uncommon. The belts of westward-younging domes are roughly perpendicular to the Steens Mountain escarpment and subparallel to faults of the Brothers fault zone.

Theories regarding the age trend along the High Lava Plains remain in dispute. Walker (1969) introduced the anomalous trend by noting that many of the northeast-trending graben-forming structures in southeastern Oregon terminate at the Brothers fault zone and suggested that the normal faults of the zone and the volcanic vents along it "represent the

surface manifestations of deformation on a large, deeply buried structure, the exact nature of which is not known." Christiansen and McKee (1978) attributed the younging age trend in southeastern Oregon to progressive heating and ductile deformation of the lithosphere due to mantle upwelling in the central part of the Great Basin, with brittle deformation, maximum extension, and volcanism migrating toward the edges of the province. The northern-boundary transverse structures of the Brothers fault zone are interpreted to compensate for Basin-Range extension along the High Lava Plains where it abuts the nonextending terrane of the Blue Mountains province to the north (Lawrence, 1976; Walker and Nolf, 1981). Hart and Carlson (1987a) attributed the distribution of volcanism to crustal rifting in a back-arc environment related to the subduction of the Juan de Fuca plate beneath the North American plate. In order to address both the rhyolitic age progression and the absence of a similar mafic progression, Draper (1991) proposed that a trailing edge of the Snake River Plain hot mantle "blob" migrated westward, progressively melting the crust producing rhyolitic material. He suggested that as extension in the region increased along the Brothers fault zone, smaller volumes of primitive basalt saw shorter crustal residence, and the volume of rhyolitic material erupted decreased.

These theories do not, however, address (1) the lack of evidence for strike-slip displacement on the Brothers fault zone, or (2) the copious Quaternary mafic volcanism with no temporal trend scattered throughout the area.

I tentatively suggest that the High Lava Plains northwest-younging age trend can be accommodated in a magmatic/tectonic model that employs a "leaky" transform system that emanates from the major north-south-trending Steens Mountain escarpment. The age progression is consistent with the time-dependent evolution of a propagating transform. Propagation is an essentially passive response to plate driving forces whose origins may be remote from the axis (Christie and Sinton, 1986). In southeastern Oregon the kinematics of plate movement and adjustment with respect to the Basin and Range, Cascade Range, Blue Mountains, Idaho Batholith, and Snake River Plain is poorly understood. It is

possible that the High Lava Plains region represents a transition from "passive" lithospheric stretching of an oblique transform related to east-west extension to an "active", magmatically driven extensional propagating continental rift. The younging trend appears to have begun near the Duck Creek Butte eruptive center, which straddles the Steens Mountain escarpment at its northern end. Duck Creek Butte lies 100-150 km from the inferred position of the Yellowstone hot-spot plume at ~11 Ma. The thermal/magmatic energy of the spreading plume head (Draper, 1991) may have facilitated melting and elevation of the crust along a tectonically weakened boundary beneath the High Lava Plains away from the hot spot at Duck Creek Butte.

Benes and others (1994) note that continental rifting proceeds as distributed deformation whereby extension is being proportioned among all faults by means of a "book shelf" mechanism, versus the concentration of faulting adjacent to the central axis region of oceanic rifts. The broadly distributed faults of the Brothers fault zone may reflect a similar process.

To support evidence for a propagating transform at DBEC, the following compositional and temporal variations can be found in a petrogenetic model based on a propagating rift (Christie and Sinton, 1986). The points are numbered to match the descriptions of DBEC listed in the first part of this section and depicted in Figure 6-4:

(1) Largely unfractionated lava is erupted near the active tip because the heat budget does not allow adequate residence time for magma at shallow depths to evolve.

(2) A diverse population of mixed magma compositions erupts 5 and 20 km from the tip.

(3) About 20 to 30 km behind the tip both maximum degree of fractionation and maximum compositional diversity yields highly differentiated silicic magma.

(4) Basalt decreases toward normal MORB range (MgO >9 percent, FeO ~9 percent, $TiO_2$ ~0.9 percent) approximately 100 km behind the propagating rift tip.

(5) Discrete, widely separated pods of rhyolite show a younging age progression toward the tip of the propagating rift, and may migrate away from a hot spot.

(6) Normal faulting parallel to the rift is ubiquitous, with a more widely dispersed pattern of faulting in continental rifts (Benes and others, 1994).

The relationship between northwest-striking normal faults, regional tectonic regimes, and Quaternary basaltic volcanism is unclear. The rapid rise to the surface of fairly primitive "depleted mantle"-derived basalt, such as the basalt of Duck Creek Flat, was tied to short residence times (Draper, 1991) in response to extension-related crustal thinning and presence of shallow asthenospheric mantle beneath the High Lava Plains following propagation of the Duck Creek Butte-Newberry volcano silicic trend. I propose that the normal faults may result in part from buckling during cooling of the inflated crust.

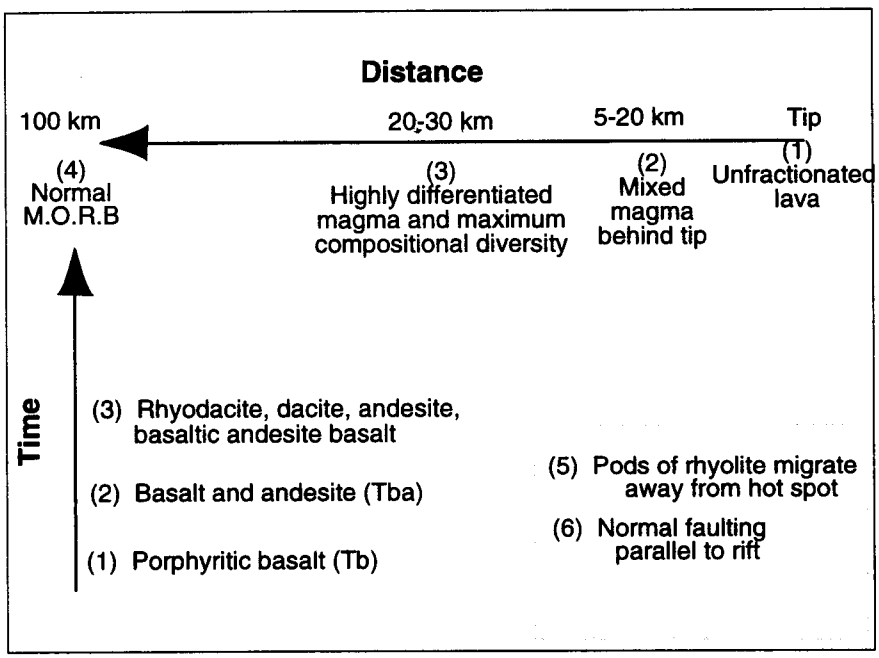


**Figure 6-4**: Compositional characteristics of a propagating oceanic rift over distance (Christie & Sinton, 1986) compared to compositional changes through time at DBEC.

## 6.3 Conclusion

In conclusion, I propose two dominant mechanisms contribute to the character of the Duck Creek Butte eruptive center:

The formation of magmas at Duck Creek Butte eruptive center is attributed to a combination of processes including partial crustal melting during injection of mantle-derived magmas into the crust, active faulting, convection, mixing, mingling, and fractional crystallization. Active tectonic processes during extension may have facilitated the mixing and eruption of the hybrid magmas, whereas periods of tectonic quiescence may have allowed homogenization and fractionation to occur. The basis for this model is chemical and isotopic evidence that reflects crustal contamination, mixing, and fractional crystallization and textural evidence which strongly indicates mixing and convective circulation. Compositional changes found in the DBEC series suggest the evolution of a mutually convecting layered magma chamber that is periodically disrupted. Field evidence for coeval faulting and magmatism supports this hypothesis.

Existing models that attempt to explain the westward-younging trend of silicic vents across the High Lava Plains are incomplete because they do not fully account for the following: (1) the age progression is not a broad swath but represents two discrete parallel belts; (2) individual silicic centers range in composition from basalt to high-silica rhyolite; (3) late-stage primitive Quaternary high-alumina olivine tholeiites have no age progression. A model that includes a propagating transform fault, produced by intricately linked tectonic forces including Basin-Range extension, hot spots, and distant back-arc effects, can explain many features found within the study area and across the High Lava Plains. Although much yet remains unanswered, classical geological investigations using additional field work and geochemistry will be valuable in testing the model.

## References cited

Anders, E., and Ebihara, M., 1982, Solar system abundances of the elements: Geochimica et Cosmochimica Acta, v. 46, p. 2,363-2,380.

Anderson, R.L., Leeman, W.P., and Malde, H.E., 1975, K-Ar dating, Quaternary and Neogene volcanic rocks of the Snake River Plain, Idaho: American Journal of Science, v. 275, p. 225-251.

Arth, J.G., 1976, Behavior of trace elements during magmatic processes: a summary of theoretical models and their applications: Journal of Research of the U.S. Geological Survey, v.4, p. 41-47.

Avent, J.C., 1965, Cenozoic stratigraphy and structure of Pueblo Mountains region, Oregon-Nevada: Seattle,Univeristy of Washington, Ph.D. dissertation, 119 p.

Bacon, C.R., 1986, Magmatic inclusions in silicic and intermediate volcanic rocks: Journal of Geophysical Research, v. 91, p. 6,091-6,112.

Bacon, C.R., and Metz, J., 1984, Magmatic inclusions in rhyolites, contaminated basalts, and compositional zonation beneath the Coso volcanic field, California: Contributions to Mineralogy and Petrology, v. 85, p. 346-365.

Bailey, D.G., and Conrey, R.M., 1992, Common parent magma for Miocene to Holocene mafic volcanism in the northwestern United States: Geology, v. 20, p. 1,131-1,134.

Basaltic Volcanism Study Project, 1981, Basaltic Volcanism on Terrestrial Planets, Permagon Press, 1,286 p.

Beard, J.S., and Lofgren, G.E., 1991, Dehydration melting and water-saturated melting of basaltic and andesitic greenstones and amphibolites at 1, 3, and 6.9 kb: Journal of Petrology, v. 32, . p. 365-401.

Benes, V., and Scott, S.D., and Binns, R.A., 1994, Tectonics of rift propagation into a continental margin, western Woodlark Basin, Papua New Guinea: Journal of Geophysical Research, v. 99, p. 4,439-4,455.

Blackwell, D.D., 1978, Heat flow and energy loss in the western United States, *in* Smith, R.B., and Eaton, G.P., eds., Cenozoic tectonics and regional geophysics of the western Cordillera: Geological Society of America Memoir 152, p. 175-208.

Brandon, A.D., and Goles, G.G., 1988, A Miocene subcontinental plume in the Pacific Northwest: geochemical evidence: Earth and Planetary Science Letters, v. 88, p. 273-283.

Camp, V.E., 1995, Mid-Miocene propagation of the Yellowstone mantle plume head beneath the Columbia River Basalt source region: Geology, v. 23, p. 435-438.

Carlson, R.W., 1984, Tectonic influence on magma composition of Cenozoic basalts from the Columbia Plateau and northwestern Great Basin, U.S.A., *in* Explosive volcanism: inception, evolution, and hazards: Washington, D.C., National Academy Press, p. 23-33.

Carlson, R.W., and Hart, W.K., 1983a, Areal extent and isotope geochemistry of the Steens Mountain flood basalt, southeastern Oregon [abs.]: Eos (American Geophysical Union, Transactions), v. 64, no. 18, p. 338.

———1983b, Geochemical study of the Steens Mountain flood basalt: Carnegie Institution of Washington Yearbook 82, p. 475-481.

———1985, Regional extent and significance of Steens Mountain-type basalts in the northern Great Basin [abs]: Geological Society of America Abstracts with Programs, v. 17, no. 4, p. 212.

———1987, Crustal genesis on the Oregon Plateau: Journal of Geophysical Research, v. 92, p. 6,191-6,206.

Carmichael, I.S.E., Turner, F.J., and Verhoogen, J., 1974, Igneous Petrology: New York, McGraw-Hill Book Co., 739 p.

Christensen, J.N., and DePaolo, D.J., 1987, Isotopic study in a silicic magma chamber: the Bishop Tuff, Long Valley, California [abs.]: Eos (American Geophysical Union, Transactions), v. 68, p. 434.

Christiansen, R.L., and McKee, E.H., 1978, Late Cenozoic volcanic and tectonic evolution of the Great Basin and Columbia Intermontane regions, *in* Smith, R.B., and Eaton, G.P., eds., Cenozoic tectonics and regional geophysics of the western Cordillera: Geological Society of America Memoir 152, p. 283-311.

Christie, D.M., and Sinton, J.M., 1986, Evolution of abyssal lavas along propagating segments of the Galapagos spreading center: Earth and Planetary Science Letters, v. 56, p. 321-335.

Clayton, R.W., 1989, Kinematics of the northern margin of the Basin and Range, Oregon [abs.]: Geological Society of America Abstracts with Programs, v. 21, no. 5 , p. 66.

Cox, K.G., Bell, J.D., and Pankhurst, R.J., 1979, Interpretation of Igneous Rocks: London, George Allen and Unwin, 450 p.

DePaolo, D.J., 1981, Trace element and isotopic effects of combined wallrock assimilation and fractional crystallization: Earth and Planetary Science Letters, v. 53, p. 189-202.

Draper, D.S., 1991, Late Cenozoic bimodal magmatism in the northern Basin and Range Province of southeastern Oregon: Journal of Volcanology and Geothermal Research, v. 47, p. 299-328.

Duncan, R.A., 1982, A captured island chain in the Coast Range of Oregon and Washington: Journal of Geophysical Research, v. 87, p. 193-198.

Eggler, E.H., and Burnham, C.W., 1973, Crystallization and fractionation trends in the system andesite-$H_2O$-$CO_2$-$O_2$ at preasures to 10 kb: Geological Society of America Bulletin, v. 84, p. 2,517-2,532.

Feeley, T.C., and Grunder, A.L., 1991, Mantle contribution to the evolution of middle Tertiary silicic magmatism during early stages of extension: the Egan Range volcanic complex, east-central Nevada: Contributions to Mineralogy and Petrology, v. 106, p. 154-169.

Ferns, M.L., Evans, J.G., and Cummings, M.L., 1993, Geologic map of the Mahogany Mountain 30- by 60-minute quadrangle, Malheur County, Oregon, and Owyhee County, Idaho: Oregon Department of Geology and Mineral Industries Geological Map Series GMS-78, scale 1:100,000.

Fiebelkorn, R.B., Walker, G.W., MacLeod, N.S., McKee, E.H., and Smith, J.G., 1982, Index to K-Ar age determinations for the state of Oregon: U.S. Geological Survey Open-File Report 82-596. [Also available in revised form, Isochron/West, 1983, no. 37, p. 3-60.]

Freidel, D.E., and McDowell, P.F., Late-Quaternary paleolakes in the Fort Rock, Alkali, and Chewaucan basins: Guidebook to Active Faulting in south-central Oregon, Geological Society of America Fieldtrip Guide, no. 5, sec. 2, p. 1-10.

Fuller, R.E., 1931, The geomorphology and volcanic sequence of Steens Mountain in southeastern Oregon: University of Washington Publications in Geology, v. 3, no. 1, 130 p.

Geist, D., and Richards, M.A., 1993, Origin of the Columbia Plateau and Snake River Plain: deflection of the Yellowstone plume: Geology, v. 21, p. 789-792.

Gill, James, 1981, Orogenic andesites and plate tectonics: Berlin, Springer-Verlag, 390 p.

Greene, R.C., 1973, Petrology of the welded tuff of Devine Canyon, southeastern Oregon: U.S. Geological Survey Professional Paper 797, 26 p.

Greene, R.C., Walker, G.W., and Corcoran, R.E., 1972, Geologic map of the Burns quadrangle, Oregon: U.S. Geological Survey Miscellaneous Geologic Investigations Map I-680, scale 1:250,000.

Grove, T.L., and Bence, 1979, Crystallization kinetics in a multiply saturated basalt magma, an experimental study of Luna 24 ferrobasalt: Proceedings of the Lunar and Planetary Science Conference, v. 1, p. 439-478.

Grove, T.L., Gerlach, D.C., and Sando, T.W., 1982, Origin of calc-alkaline series lavas at Medicine Lake volcano by fractionation, assimilation and mixing: Contributions to Mineralogy and Petrology, v. 80, p. 160-182.

Grunder, A.L., Streck, M.J., and MacLean, J.W., 1994, Interaction of basalt and rhyolite in a bimodal suite [abs.]: Geological Society of America Abstracts with Programs, v. 26, no. 7, p. 476-477.

Grunder, A.L., Johnson, J.A., and Streck, M.J., 1995, Basalt-rhyolite volcanism of the High Lava Plains, mirror of the Snake River Plain [abs.]: Proceedings of the IUGS/IAVCEI Conference on Volcanism, Denver, Colo.

Gunn, B.M., and Watkins, N.D., 1970, Geochemistry of the Steens Mountain Basalts, Oregon: Geological Society of America Bulletin, v. 81, no. 5, p. 1,497-1,516.

Hall, Anthony, 1987, Igneous Petrology: Essex, England, Longman Scientific and Technical, 573 p.

Hart, W.K., Aronson, J.L., and Mertzman, S.A., 1984, Areal distribution and age of low-K, high-alumina olivine tholeiite magmatism in the northwestern Great Basin, U.S.A.: Geological Society of America Bulletin, v. 95, no. 2, p. 186-195.

Hart, W.K., and Carlson, R.W., 1985, Distribution and geochronology of Steens Mountain-type basalts from the northwestern Great Basin: Isochron/West, no. 43, p. 5-10.

———1987a, Tectonic controls on magma genesis and evolution in the northwestern United States: Journal of Volcanology and Geothermal Research, v. 32, p. 119-135.

———1987b, Crustal genesis on the Oregon Plateau: Journal of Geophysical Research, v. 92, no. B7, p. 6,191-6,206.

Hart, W.K., Carlson, R. W., and Mosher, S.A., 1989, Petrogenesis of the Pueblo Mountains basalt, southeastern Oregon and northern Nevada, *in* Reidel, S.R., and Hooper, P.R., eds., Volcanism and tectonism in the Columbia River flood-basalt province: Geological Society of America Special Paper 239, p. 367-378.

Hart, W.K., and Mertzman, S.A., 1982, K-Ar ages of basalts from south-central and southeastern Oregon: Isochron/West, no. 33, p. 23-26.

Hemphill-Haley, M.A., and Carver, G.A., 1988, Late Holocene displacement along the Alvord fault, Steens Mountain, southeastern Oregon [abs.]: Geological Society of America Abstracts with Programs, v. 20, no. 3, p. 168.

Hildreth, Wes, 1979, The Bishop Tuff: Evidence for the origin of compositional zonation in silicic magma chambers, *in* Chapin, C.E., and Elston, W.E., eds, Ash-flow tuffs: Geological Society of America Special Paper 180, p. 29-42.

———1981, Gradients in silicic magma chambers: Implications for lithospheric magmatism: Journal of Geophysical Research, v. 86, p. 10,153-10,192.

Hildreth, Wes, Halliday, A.N., and Christiansen, R.L., 1991, Isotopic and chemical evidence concerning the genesis and contamination of basaltic and rhyolitic magma beneath the Yellowstone Plateau volcanic field: Journal of Petrology, v. 32, p. 63-138.

Hooper, P.H., and Hawkesworth, C.J., 1993, Isotopic and geochemical constraints on the origin and evolution of the Columbia River Basalt: Journal of Petrology, v. 34, p. 1,203-1,246.

Humphries, E.D., Dueker, K.G., and Biasi, G.P., 1992, Western U.S. tectonic and volcanic activity: the role of the mantle [abs.]: Geological Society of America Abstracts with Programs, v. 24, no. 5, p. 34.

Huppert, H.E., and Sparks, R.S.J., 1988, The generation of granitic magmas by intrusion of basalt into continental crust: Journal of Petrology, v. 29, p. 599-624.

Irvine, T.N., and Baragar, W.R.A., 1971, A guide to the chemical classification of the common volcanic rocks: Canadian Journal of Earth Science, v. 8, p. 523-48.

Johnson, J.A., 1994, Geologic map of the Krumbo Reservoir quadrangle, Harney County, southeastern Oregon: U.S. Geological Survey Miscellaneous Field Studies Map MF-2267, scale 1:24,000.

Johnson, J.A., and Deino, A.L., 1994, Timing of volcanism and extension, Duck Creek Butte eruptive center, northern Basin and Range Province, S.E. Oregon [abs.]: Geological Society of America Abstracts with Programs, v. 26, no. 7, p. 192.

Johnson, J.A., Nielsen, R.A., and Fisk, M., 1995, Plagioclase-hosted melt inclusions in the Steens Basalt, southeastern Oregon: Petrologica, in press.

Kouchi, A., and Sunagawa, I., 1983, Mixing basaltic and dacitic magmas by forced convection: Nature, v. 304, p. 527-528.

Koyaguchi, T., 1986, Evidence for two-stage mixing in magmatic inclusions and rhyolitic lava domes on Niijima Island, Japan: Journal of Volcanology and Geothermal Research, v. 29, p. 71-98.

Langer, V. 1992, Geology and petrologic evolution of the silicic to intermediate volcanic rocks underneath Steens Mountain basalt, southeastern Oregon: Corvallis, Oregon State University, M.S. thesis, 109 p.

Langmuir, C.H., Vocke, R.D., Jr., and Hanson, G.N., 1978, A general mixing equation with applications to Icelandic basalts: Earth and Planetary Science Letters, v. 37, p. 380-392.

Laul, J.C., 1979, Neutron activation analysis of geological materials: Atomic Energy Review, v. 17-3, p. 603-695.

Lawrence, R.D., 1976, Strike-slip faulting terminates the Basin and Range province in Oregon: Geological Society of America Bulletin, v. 87, no. 6, p. 846-850.

Leeman, W.P., 1982, Tectonic and magmatic significance of strontium isotope variations in Cenozoic rocks from the western United States: Geological Society of America Bulletin, v. 93, p. 487-503

Le Bas, M.J., Le Maitre, R.W., Streckeisen, A., and Zenettin, B., 1986, A chemical classification of volcanic rocks based on the total alkali-silica diagram: Journal of Petrology, v. 27, p. 745-750.

LeMaitre, R.W., 1980, A generalised petrological mixing model program: Computers in Geoscience, v. 7, p. 229-247.

Li, Y., Geissman, J.W., Nur, A., Ron, H., and Huang, Q., 1990, Paleomagnetic evidence for counterclockwise block rotation in the north Nevada rift region: Geology, v. 18, p. 79-82.

Lindsley, D.H., 1983, Pyroxene thermometry: American Mineralogist, v. 68, p. 477-493.

Linneman, S.K., 1990, The petrologic evolution of the Holocene magmatic system of Newberry volcano, central Oregon: Laramie, University of Wyoming, Ph.D. dissertation, 293 p.

Linneman, S.K., and Myers, J.D., 1990, Magmatic inclusions in the Holocene rhyolites of Newberry volcano, central Oregon: Journal of Geophysical Research, v. 95, p. 17,677-17,691.

MacDonald G.A., and Katsura, T., 1964, Chemical composition of Hawaiian lavas: Journal of Petrology, v. 5, p. 82-133.

MacLean, J.W., 1994, Geology and geochemistry of Juniper Ridge, Horsehead Mountain, and Burns Butte: Implications for the petrogenesis of silicic magma on the High Lava Plains, southeastern Oregon: Corvallis, Oregon State University, M.S. thesis, 141 p.

MacLeod, N.S., and Sherrod, D.R., 1988, Geologic evidence for a magma chamber beneath Newberry volcano, Oregon: Journal of Geophysical Research, v. 93, no. B9, p. 10,067-10,079.

———1992, Reconnaissance geologic map of the west half of the Crescent 1° by 2° quadrangle, central Oregon: U.S. Geological Survey Miscellaneous Investigations Map I-2215, scale 1:250,000.

MacLeod, N.S., Sherrod, D.R., Chitwood, L.A., and Jensen, R.A., 1995, Geologic map of Newberry volcano, Deschutes, Klamath, and Lake Counties, Oregon: U.S. Geological Survey Miscellaneous Investigations Map I-2455, scales 1:62,500 and 1:24,000.

MacLeod, N.S., Walker, G.W., and McKee, E.H., 1976, Geothermal significance of eastward increase in age of Upper Cenozoic rhyolitic domes in southeastern Oregon, *in* Second United Nations Symposium on the Development and Use of Geothermal Resources, San Francisco, Calif., U.S.A., Proceedings, v. 1, Government Printing Office, p. 465-474.

Mahood, G.A., and Halliday, A.N., 1988, Generation of high-silica rhyolite: A Nd, Sr, and O isotopic study of Sierra La Primavera, Mexican neovolcanic belt: Contributions to Mineralogy and Petrology, v. 100, p. 183-191.

Mahood, G.A., and Hildreth, Wes, 1983, Large partition coefficients for trace elements in high-silica rhyolites: Geochimica et Cosmochimica Acta, v. 47, p. 11-30.

Mankinen, E.A., Prevot, Michel, Gromme, C.S., and Coe, R.S., 1985, The Steens Mountain (Oregon) geomagnetic polarity transition, 1. Directional history, duration of episodes, and rock magnetism; Journal of Geophysical Research, v. 90, no. B12, p. 10,393-10,416.

Marsh, J.S., 1989, Geochemical constraints on coupled assimilation and fractional crystallization involving upper crustal compositions and continental tholeiitic magma: Earth and Planetary Science Letters, v. 92, p. 70-80.

McKee, E.H., Duffield, W.A., and Stern, R.J., 1983, Late Miocene and early Pliocene basaltic rocks and their implications for crustal structure, northeastern California and south-central Oregon: Geological Society of America Bulletin, v. 94, p. 292-304.

Metz, J.M., and Mahood, G.A., 1991, Development of the Long Valley, California, magma chamber recorded in precaldera rhyolites of Glass Mountain: Contributions to Mineralogy and Petrology, v. 106, p. 379-397.

Miller, C.F., and Mittlefehldt, D.W., 1982, Depletion of light rare-earth elements in felsic magmas: Geology, v.10, p. 129-133.

Minor, S.A., 1986, Stratigraphy and structure of the western Trout Creek and northern Bilk Creek Mountains, Harney County, Oregon, and Humboldt County, Nevada: Boulder, University of Colorado, M.S. thesis, 177 p.

Minor, S.A., Plouff, D., Esparza, L.E., and Peters, T.J., 1987a, Geologic map of the High Steens and Little Blitzen Gorge wilderness study areas, Harney County, Oregon: U.S. Geological Survey Miscellaneous Field Studies Map MF-1876, scale 1:24,000.

Minor, S.A., Rytuba, J.J., Goeldner, C.A., and Tegtmeyer, K.J., 1987b, Geologic map of the Alvord Hot Springs quadrangle, Harney County, Oregon: U.S. Geological Survey Miscellaneous Field Studies Map MF-1916, scale 1:24,000.

Minor, S.A., Plouff, Donald, Esparza, L.E., and Peters, T.J., 1987c, Mineral resources of the High Steens and Little Blitzen Gorge Wilderness Study Areas, Harney County, Oregon: U.S. Geological Survey Bulletin 1740-A, 21 p.

Minor, S.A., Rytuba, J.J., Meulen, D.B., Grubensky, M.J., and Tegtmeyer, K.J., 1987b, Geologic map of the Wildhorse Lake quadrangle, Harney County, Oregon: U.S. Geological Survey Miscellaneous Field Studies Map MF-1915, scale 1:24,000.

Mullen, E.D., 1983, $MnO/TiO_2/P_2O_5$: a minor element discriminant for basaltic rocks of oceanic environments and its implications for petrogenesis: Earth and Planetary Science Letters, v. 62, p. 53-62.

Nash, W.P., and Crecraft, H.R., 1985, Partition coefficients for trace elements in silicic magmas: Geochemica et Cosmochimica Acta, v. 49, p. 2,309-2,322.

Nielsen, R.L., 1989, Phase equilibria constraints on liquid lines of descent generated by paired assimilation and fractional crystallization: trace elements and Sr and Nd isotopes: Journal of Geophysical Research, v. 94, p. 787-794.

———1990, A numerical approach to *in situ* fractionation: application to differentiation in open magma systems [abs.]: Eos (American Geophysical Union, Transactions), v. 71, p. 1,665.

Nielsen, R.L., and DeLong, S.E., 1992, A numerical approach to boundary layer fractionation: application to differentiation in natural magma systems: Contributions to Mineralogy and Petrology, v. 110, p. 355-369.

Pearce, J.A., 1983, The role of sub-continental lithosphere in magma genesis at destructive plate margins, *in* Hawkesworth, C.J., and Norry, M.J., eds, Continental basalts and mantle xenoliths: Nantwich, Shiva Press, p. 230-249.

Philpotts, A.R., 1990, Principles of Igneous and Metamorphic Petrology: Englewood Cliffs, New Jersey, Prentice Hall, 498 p.

Piper, A.M., Robinson, T.W., Jr., and Park, C.F., Jr., 1939, Geology and ground-water resources of the Harney basin, Oregon: U.S. Geological Survey Water-Supply Paper 841, 189 p.

Rytuba, J.J., and McKee, E.H., 1984, Peralkaline ash-flow tuffs and calderas of the McDermitt volcanic field, southeast Oregon and north central Nevada: Journal of Geophysical Research, v. 89, no. B10, p. 8,616-8,628.

Sack, R.O., Carmichael, I.S.E., Rivers, M., and Ghiorso, M.S., 1980, Ferric-ferrous equilibria in natural silicate liquids at 1 bar: Contributions to Mineralogy and Petrology, v. 75, p. 369-376.

Samson, S.D., and Alexander, Jr., E.C., 1987, Calibration of the interlaboratory $^{40}Ar/^{39}Ar$ dating standard: Chemical Geology, v. 66, n. 1-2, p. 27-34.

Shand, S.J., 1951, The study of rocks: London, Thomas Murby and Co., 236 p.

Sherrod, D.R., Minor, S.A., and Vercoutere, T.L., 1989, Geologic map of the Sheepshead Mountains, Harney and Malheur Counties, Oregon: U.S. Geological Survey Miscellaneous Field Studies Map MF-2079, scale 1:50,000.

Sherrod, D.R., and Johnson, J.A., 1994, Geologic map of the Irish Lake quadrangle, U.S. Geological Survey Miscellaneous Field Studies Map MF-2256, scale 1:24,000.

Sisson, T.W., and Bacon, C.R., 1994, Differentiation of silicic magmas by gas-driven filter pressing [abs.]: Geological Society of America Abstracts with Programs, v. 26, p. 452

Skjerlie, K.P., and Johnston, A.D., 1992, Vapor-absent melting at 10 kbar of a biotite- and amphibole-bearing tonalitic gneiss: Implications for the generation of A-type granites: Geology, v. 20, p. 263-266.

Snyder, C.T., Hardman, G., and Zdenek, F.F., 1964, Pleistocene lakes in the Great Basin: U.S. Geological Survey Miscellaneous Investigations Map I-416, scale 1:1,000,000.

Sparks, R.S.J., and Marshall, L., 1985, Thermal and mechanical constraints on mixing between mafic and silicic magmas: Journal of Volcanology and Geothermal Research, v. 29, p. 99-124.

Stewart, J.H., 1978, Basin and range structure in western North America, *in* Smith, R.B., and Eaton, G.P., eds., Cenozoic tectonics and regional geophysics of the western Cordillera: Geological Society of America Memoir 152, p. 1-31.

Streck, M.J., 1994, Volcanology and petrology of the Rattlesnake Ash-flow Tuff, eastern Oregon: Corvallis, Oregon State University, Ph.D. dissertation, 185 p.

Stormer, J.C., and Nicholls, J., 1978, XLFRAC: a program for the interactive testing of magmatic differentiation models: Computers and Geosciences, v. 4, p. 143-159.

Swisher, C.C., Ach, J.A., and Hart, W.K., 1990, Laser fusion $^{40}Ar/^{39}Ar$ dating of the type Steens Mountain Basalt, southeastern Oregon, and the age of the Steens geomagnetic polarity transition [abs.]: Eos (American Geophysical Union Transactions), v. 71, no. 43, p. 1296.

Taylor, J.R., 1982, An introduction to error analysis: Mill Valley, Calif., University Science Books, 270 p.

Tolan, T.L., Reidel, S.P., Beeson, M.H., Anderson, J.L., Fecht, K.R., and Swanson, D.A., 1989, Revisions to the estimates of the areal extent and volume of the Columbia River Basalt Group, *in* Reidel, S.P., and Hooper, P.R., eds., Volcanism and tectonism in the Columbia River flood-basalt province: Geological Society of America Special Paper 239, p. 1-20.

Turrin, B.D., Griscom, Andrew, Turner, R.L., Lawson, W.A., Buehler, A.R., and Graham, D.E., 1989, Mineral resources of the Alvord Desert and East Alvord Wilderness Study Areas, Harney and Malheur Counties, Oregon: U.S. Geological Survey Bulletin 1739-B, 16 p.

Vielzeuf, D., and Montel, J.M., 1994, Partial melting of metagreywackes. Part 1. Fluid-absent experiments and phase relationships: Contributions to Mineralogy and Petrology, v. 117, p. 375-393.

Walker, G.W., 1960, Age and correlation of some unnamed volcanic rocks in south-central Oregon: U.S. Geological Survey Professional Paper 400B, p. B298-B300.

———1969, Geology of the High Lava Plains province, *in* Weissenborn, A.E., ed., Mineral and Water Resources of Oregon, State of Oregon Department of Geology and Mineral Industries Bulletin 64, p. 77-79.

———1974, Some implications of late Cenozoic volcanism to geothermal potential in the High Lava Plains of south-central Oregon: Ore Bin, v. 36, no. 7, p. 109-119.

———1977, Geologic map of Oregon east of the 121st meridian: U.S. Geological Survey, scale 1:500,000.

———1979, Revisions to the Cenozoic stratigraphy of Harney Basin, southeastern Oregon: U.S. Geological Survey Bulletin 1475, 35 p.

———1981, Uranium, thorium, and other metal associations in silicic volcanic complexes of the northern Basin and Range, a preliminary report: U.S. Geological Survey Open-File Report 81-1290, 45 p.

Walker, G.W., and MacLeod, N.S., 1991, Geologic map.of Oregon: U.S. Geological Survey, scale 1;500,000.

Walker, G.W., MacLeod, N.S., and McKee, E.H., 1974, Transgressive age of late Cenozoic silicic volcanic rocks across southeastern Oregon—implications for geothermal potential [abs.]: Geologic Society of America Abstracts with Programs, v. 6, no. 3, p. 272.

Walker, G.W., and Nolf, Bruce, 1981, High Lava Plains, Brothers fault zone to Harney Basin, Oregon, *in* Johnston, D.A., and Donnelly-Nolan, J.M., eds., Guides to some

volcanic terranes in Washington, Idaho, Oregon, and northern California: U.S. Geological Survey Circular 838, p. 105-118.

Walker, G.W., Peterson, N.V., and Greene, R.C., 1967, Reconnaissance geological map of the east half of the Crescent quadrangle, Lake, Deschutes, and Crook Counties, Oregon: U.S. Geological Survey Miscellaneous Investigations Map I-493, scale 1:250,000.

Walker, G.W., and Repenning, C.A., 1965, Reconnaissance geologic map of the Adel quadrangle, Lake, Harney, and Malheur Counties, Oregon: U.S. Geological Survey Miscellaneous Investigations Map I-446, scale 1:250,000.

Walker, G.W., and Robinson, 1990, Paleocene(?), Eocene, and Oligocene(?) rocks of the Blue Mountains region, *in* Walker, G.W., ed, Geology of the Blue Mountains Region of Oregon, Idaho, and Washington: U.S. Geological Survey Professional Paper 1437, p.13-17.

Watson, E.B., 1982, Basalt contamination by continental crust: some experiments and models: Contributions to Mineralogy and Petrology, v. 80, p. 73-87.

Wiebe, R.A., 1993a, Basaltic injections into floored silicic magma chambers [abs.]: Eos (American Geophysical Union, Transactions), v. 74, p. 1-3.

———1993b, The Pleasant Bay layered gabbro-diorite, coastal Maine: ponding and crystallization of basaltic injections into a silicic magma chamber: Journal of Petrology, v. 34, p. 461-489.

Wood, B.J., and Fraser, D.G., 1976, Elementary thermodynamics for geologists: London, Oxford University Press, 303 p.

Zoback, M.L., 1989, State of stress and modern deformation of the northern Basin and Range province: Journal of Geophysical Research, v. 94, p. 7,105-7,128.

# APPENDICES

**APPENDIX 1:** Map locations and additional procedures performed on rocks that were analyzed by XRF. See also Figure A1-1 on next page for sample locations.
Does not include locations for additional thin section analysis. XRF = X-ray fluorescence, INAA = Instrumental neutron activation analysis, TS = petrographic thin section.

| Sample | Map Unit | XRF | INAA | Micro probe | Age | Isotopes Sr | Nd | TS | Longitude degr. | min | sec | Latitude degr | min | sec |
|---|---|---|---|---|---|---|---|---|---|---|---|---|---|---|
| JJ92-1 | Tdrd | * | * | * | * | * | * | * | 118° | 9' | 5" | 43° | 10' | 16" |
| JJ92-4 | Tdr1 | * | * | | | * | | * | 118° | 11' | 35" | 43° | 10' | 41" |
| JJ92-5 | Tdr1 | * | * | * | * | | | * | 118° | 10' | 54" | 43° | 10' | 38" |
| JJ92-6 | $Tdba_1$ | * | * | | | | | * | 118° | 9' | 35" | 43° | 9' | 59" |
| JJ92-7 | Tdrd | * | | | | | | * | 118° | 9' | 10" | 43° | 9' | 44" |
| JJ92-19 | Tba | * | * | | | | | * | 118° | 8' | 47" | 43° | 8' | 45" |
| JJ92-20 | Qb2 | * | * | | * | * | * | * | 118° | 8' | 52" | 43° | 8' | 41" |
| JJ92-27 | Tdb1 | * | * | | | | | * | 118° | 10' | 5" | 43° | 10' | 11" |
| JJ92-38 | $Tdba_2$ | * | * | | | | | * | 118° | 8' | 27" | 43° | 10' | 44" |
| JJ92-41 | $Tda_1$ | * | * | | | | | * | 118° | 8' | 55" | 43° | 11' | 44" |
| JJ92-51 | Tdid | * | * | * | | * | * | * | 118° | 8' | 14" | 43° | 10' | 9" |
| JJ92-59 | Ts? | * | * | | | | | * | 118° | 12' | 1" | 43° | 12' | 41" |
| JJ92-62 | $Tdba_3$ | * | * | | | | | * | 118° | 12' | 13" | 43° | 12' | 5" |
| JJ92-88 | Tdrd | * | | | | | | * | 118° | 7' | 12" | 43° | 9' | 0" |
| JJ92-90 | Tr | * | * | | | | | * | 118° | 0' | 58" | 43° | 11' | 6" |
| JJ92-99 | $Tdb_2$ | * | * | * | | | | * | 118° | 3' | 31" | 43° | 13' | 25" |
| JJ92-101 | Tdrd | * | | | | | | * | 118° | 7' | 17" | 43° | 14' | 11" |
| JJ92-102 | Tdid | * | * | | | * | * | * | 118° | 7' | 14" | 43° | 12' | 12" |
| JJ93-123 | Ttd | * | | | | | | * | 118° | 7' | 49" | 43° | 7' | 2" |
| JJ93-124 | Tots | * | * | | | | | * | 118° | 7' | 57" | 43° | 7' | 2" |
| JJ93-126 | $Tda_2$ | * | * | | | | | * | 118° | 8' | 5" | 43° | 7' | 3" |
| JJ93-130 | $Tdb_1$ | * | * | * | | * | | * | 118° | 6' | 6" | 43° | 10' | 35" |
| JJ93-134 | Tas | * | * | | | | | * | 118° | 3' | 37" | 43° | 12' | 47" |
| JJ93-140 | $Tda_2$ | * | * | | | | | * | 118° | 9' | 11" | 43° | 7' | 22" |
| JJ93-147 | Tad | * | | | | | | * | 118° | 3' | 41" | 43° | 12' | 9" |
| JJ94-151 | Qb3 | * | | | | | | * | 118° | 7' | 36" | 43° | 7' | 3" |
| JJ93-158 | Tdr2 | * | | | | | | * | 118° | 14' | 31" | 43° | 9' | 35" |
| JJ93-161 | Tas | * | | | | | | * | 118° | 2' | 6" | 43° | 12' | 59" |
| JJ93-163 | Tbs | * | | | | | | * | 118° | 2' | 1" | 43° | 14' | 4" |
| | | | | | | | | | | | | | | |
| FF94-23 | Tb | * | | | | | | | 118° | 10' | 37" | 43° | 5' | 21" |
| FF94-36 | Tba | * | | | | | | | 118° | 13' | 24" | 43° | 6' | 50" |
| FF94-39 | Tba | * | | | | | | | 118° | 12' | 2" | 43° | 8' | 24" |
| FF94-49 | Ts | * | | | | | | | 118° | 14' | 40" | 43° | 4' | 53" |
| | | | | | | | | | | | | | | |
| JN94-16 | $Tdr_2$ | * | | | | | | | 118° | | | 43° | | |

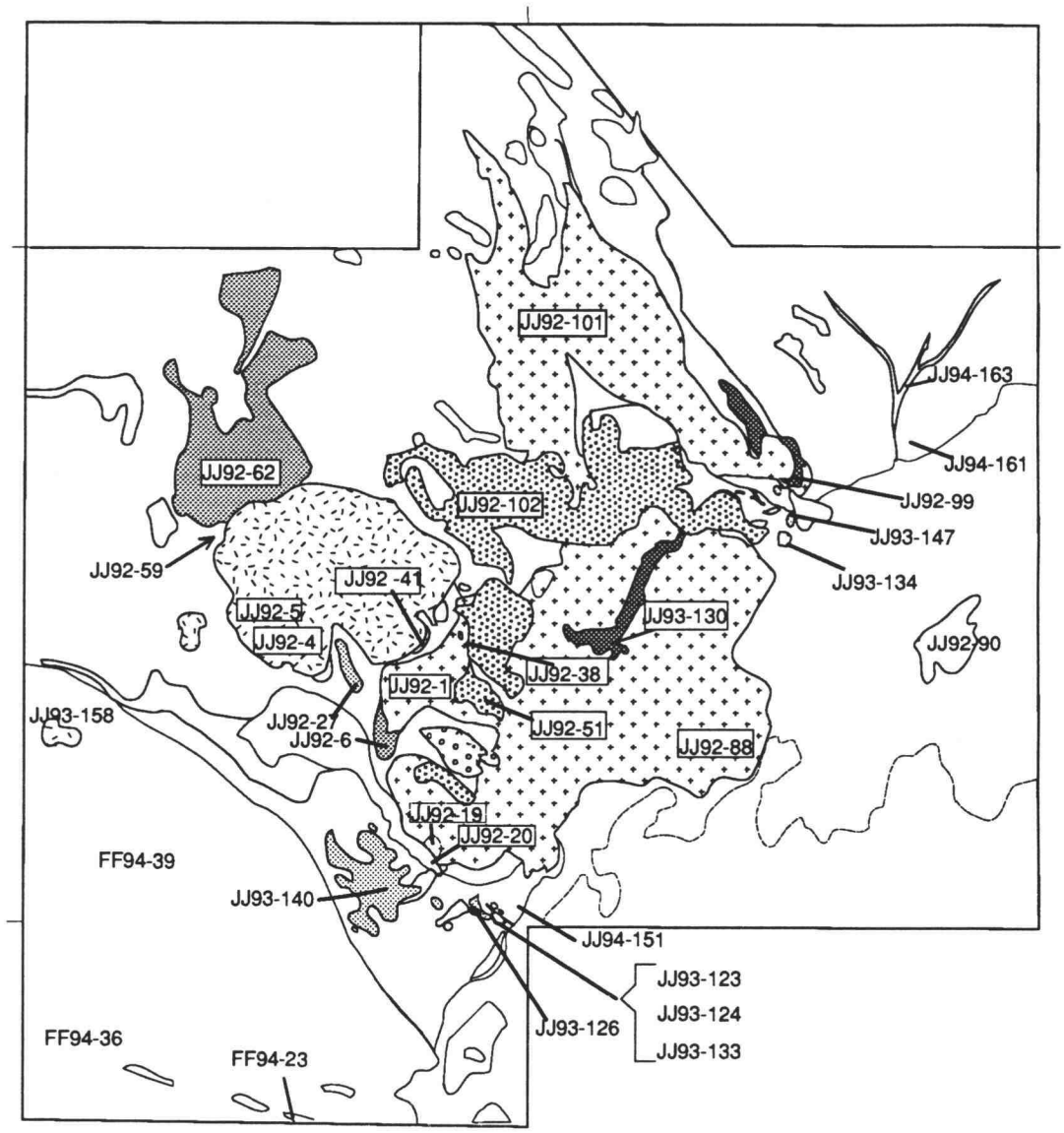


**Figure A1-1:** Sample locations for chemical analyses listed in Tables 4-7 through 4-9.

# Appendix 2: Petrography and mineralogy

Samples are first separated into two broad groups: older units and locally erupted units, which include DBEC series and Quaternary basalt. The locally erupted units then are separated on the basis of silica content into basalt-to-rhyolite categories and are arranged within those categories in stratigraphic order from oldest to youngest. Sample number in parentheses refers to chemical analyses (Tables 4-7 through 4-9). All sample locations are listed in Appendix 1; chemical analyses are noted on the sample location map (Fig. A-1) and on Plate 1. Sample numbers for petrographic analyses that have no accompanying chemistry are not listed.

## 4.1 OLDER UNITS

**Steens Basalt (Ts, JJ92-59):** Steens basalt in the study area is a medium- to medium-dark gray, diktytaxitic olivine-bearing basalt that varies from aphanitic to coarsely porphyritic. A key marker unit has 25 to 30 percent crudely aligned plagioclase to 2 cm in length. In general, the modal assemblage consists of **plagioclase** (35 to 70 percent), ophitic to subophitic **clinopyroxene** (15 to 30 percent), **olivine** (10 percent), **FeTi oxides** (4 to 6 percent), and cryptocrystalline **groundmass** (0 to 15 percent). Textures include porphyritic, diktytaxitic, ophitic, subophitic, intergranular, and seriate. Rare small glomerocrysts of plagioclase and olivine are present. Plagioclase is tabular, euhedral to subhedral, displays both albite and Carlsbad twinning, and ranges from 1-20 mm in length. Olivine varies from subhedral to anhedral, shows incipient to complete alteration to iddingsite, and ranges from 0.25 to 2 mm across. Clinopyroxene is present chiefly as intergranular or subophitic to ophitic late-stage crystallization, though some phenocrysts as large as 0.5 mm are present. Fe-Ti oxides are anhedral to subhedral and range from 0.25 to 0.5 mm across.

**Older tuff and tuffaceous sedimentary rocks (Tots, JJ93-124)** A 3-4 m thick exposure of moderately indurated white ash was collected in a road cut. It is composed chiefly cryptocrystalline glass-dust matrix with approximately 5 percent incipiently devitrified **glass** shards to 0.25 mm in length. It also contains 0.5 percent crystals of anhedral **alkali feldspar** (0.25 mm), anhedral **quartz** (0.15 mm), and green **clinopyroxene** (0.05 mm).

**Basalt of Stockade Creek (Tbs, JJ94-163)** The basalt of Stockade Creek is very fine-grained, holocrystalline, intersertal to intergranular to subophitic to ophitic, with random arrangement of groundmass. **Plagioclase** megacrysts, as long as 9 cm, are locally abundant, but are chiefly less than 1.5 cm in length. The megacrysts are subhedral and normally zoned. The **groundmass** comprises plagioclase (60-70 percent), clinopyroxene (15-20 percent) FeTi oxides (4-8 percent) and glass (5-20 percent). No olivine was found.

**Porphyritic basalt (Tb, FF94-23)** The holocrystalline fine-grained porphyritic basalt has 2 to 5 percent phenocrysts of subhedral **plagioclase** (1-3 mm; anhedral olivine inclusions present in larger crystals) and anhedral

**olivine** (0.5-0.7 mm with >50 percent iddingsite alteration). The intergranular **groundmass** is comprises 55-65 percent plagioclase, 20-30 percent olivine, 10-20 percent clinopyroxene, and 2 percent FeTi oxides (late stage dendritic).

**Lithic Tuff (Tlt)** The moderately welded rock contains 3-20 percent cryptocrystalline to fine-grained andesitic lithic fragments, in glassy to cryptocrystalline groundmass. Sparse spherulites are found in the center of glassy areas. Subangular lithics fragments as large as 0.5 cm include the following assemblages: (1) very fine grained pilotaxitic plagioclase-rich andesite (?) with FeTi oxides as the only mafic phase, (2) fine grained intersertal plagioclase with FeTi oxides, (3) fine-grained intergranular plagioclase, clinopyroxene, FeTi oxides, with ~2 percent spongy plagioclase phenocrysts, (4) holocrystalline medium grained plagioclase plus olivine. A rare 7-cm across lithic fragment has a glassy to cryptocrystalline matrix with >5 percent crystal fragments of mottled euhedral to subhedral plagioclase to 2 mm in length, euhedral to anhedral zoned clinopyroxene to 1.5 mm in length, FeTi oxides, and sparse orthopyroxene.

**Basaltic andesites (Tba, JJ93-19, JJ93-133)** The basaltic andesites are all intergranular and fine- to very-fine grained and have "fuzzy" indistinct grain boundaries and/or abundant clay alteration. **Groundmass** phases include **plagioclase** (35 to 70 percent), **clinopyroxene** (20 to 40 percent), **FeTi oxides** (5 to 12 percent), **olivine** (0 to 2 percent), **glass** (0 to 3 percent), and unidentifiable **clays** (5 to 25 percent). The basaltic andesites are generally aphanitic, but can also be sparsely porphyritic with about 1 percent plagioclase phenocrysts to 3 mm and rare glomerocrysts of plagioclase and olivine. In Dick Creek (JJ93-134) the flows are very-fine-grained (all crystals are smaller than 0.1 mm); groundmass varies from pilotaxitic to randomly oriented crystals, and comprises 70-80 percent plagioclase, 3-5 percent FeTi oxides, 5-10 percent intergranular clinopyroxene, and 3 percent sideromelane. The phenocrysts make up 3-5 percent of the volume and include euhedral to subhedral plagioclase (0.25-2 mm) that shows normal, oscillatory, and reverse zoning, less than 0.5 percent anhedral FeTi oxides (0.3 mm), and few small glomerocrysts of plagioclase and clinopyroxene.

**Andesite dikes of Dick Creek (Tad, JJ93-147)** Petrographic analysis of a clast shows a cryptocrystalline groundmass with 4 percent FeTi oxides, 1 percent subhedral to euhedral plagioclase (0.5-2 mm, probably andesine), less than 1 percent anhedral clinopyroxene (0.1-0.2 mm), and trace anhedral quartz (0.25 mm). The matrix is similar to the clast in mineralogy, but has about 50 percent green and brown glass.

**Rhyolite of Dowell Butte ($Tr_1$, JJ92-90)** The rhyolite is very light gray to pinkish gray, and is finely porphyritic with 8-10 percent phenocrysts in a clear vitric matrix. Phenocrysts comprise 6-8 percent bent, strained, and fractured euhedral to subhedral **alkali feldspar** (0.1- 0.75 mm) with ubiquitous undulatory extinction. Feathery **sericite** (1 percent) preferentially follows flow lines. There are fewer than 0.5 percent anhedral, embayed, strained **quartz**, and less than 0.25 percent hornblende.

## 4.2 DUCK BUTTE ERUPTIVE CENTER UNITS

### Basalt

**Basalt of Duck Pond Ridge ($Tdb_1$, JJ93-130)** is a medium-dark gray, porphyritic, holocrystalline, intergranular basalt with 25-30 percent phenocrysts of plagioclase, olivine, and FeTi oxides. Coarse-grained, angular, subhedral to euhedral, blocky anhedral seriate **plagioclase** phenocrysts (20-25 percent) occur as 2 dominant populations: 2 to 20 mm (rarely to 3 cm), and 1 mm. Plagioclase composition ranges from $An_{51}$ to $An_{61}$. A few plagioclase crystals poikilitically enclose olivine and FeTi oxides. Anhedral to subhedral equant **olivine** (7 to 10 percent), ranges from 0.1 to 0.6 mm, has Mg content ranging from $Fo_{53}$ to $Fo_{65}$, and shows 40 to 90 percent alteration to iddingsite. The fine-grained intergranular **groundmass** comprises 65-70 percent plagioclase ($An_{42-45}$), 20-25 percent mafics which are chiefly olivine with 5-20 percent alteration to iddingsite, sparse clinopyroxene (identified in thin section but not found during microprobe analysis), and 10 to 12 percent FeTi oxides. Two percent round to oval **vesicles**, 0.5 to 5 mm in diameter, are widely separated.

**Fine-grained basalt ($Tdb_2$, JJ92-99)** is a medium dark gray, intergranular and ophitic to subophitic, porphyritic, sparsely vesicular basalt with approximately 10 percent phenocrysts of plagioclase and olivine in a fine-grained groundmass. Anhedral to subhedral **plagioclase** crystals (8-9 percent) to 0.5 cm in length, exhibit Carlsbad, albite, and pericline twins all with varying degrees of oscillatory zoning between $An_{45}$ and $An_{72}$; a few crystals poikilitically enclose olivine. Clots of sector-zoned plagioclase are common. Anhedral iddingsitized (3 to 5 percent altered) **olivine** ($Fo_{53-65}$) to 3 mm in diameter form 1-2 percent of the volume. The **groundmass** is composed of an interlocking matrix of approximately 70 percent euhedral to subhedral tabular plagioclase ($An_{35-55}$ by Michel-Levy method; 0.1-0.4 mm in length), 15 percent ophitic to subophitic clinopyroxene (0.5-1 mm), 10 percent anhedral, equant, intergranular iddingsitized (0 to 90 percent altered) olivine (0.1-0.2 mm), and 5 percent euhedral to subhedral FeTi oxides (0.1-0.2 mm).

**Glomerophyric basalt ($Qb_1$)** $Qb_1$ is vesicular, very fine grained, porphyritic, diktytaxitic, and ophitic to subophitic. Grayish red oxidation surrounds the vesicles. It has 2-3 percent glomerocrysts, to 1 cm, composed of olivine and subordinate plagioclase, as well as ~2 percent each of **plagioclase** laths (to 3 mm) and **olivine** (to 2 mm) as phenocryst phases. Modal analysis of the **groundmass** includes approximately 55-60 percent plagioclase laths to 3 mm, 20-25 percent ophitic clinopyroxene, 8-12 percent olivine (includes 2 percent phenocrysts and 6-10 percent intersertal grains), 5-8 percent FeTi oxides, and 10-15 percent vesicles. Several 1 mm diameter quartz xenocrysts were found in hand sample (JJ93-146), but none were found in thin section.

**Basalt of Duck Creek Flat ($Qb_2$, JJ93-20)** $Qb_2$ is a diktytaxitic, ophitic, porphyritic basalt with 2 to 3 percent phenocrysts of olivine. **Olivine**, to 2 mm, is subhedral to euhedral with iddingsite alteration around the edges. **Plagioclase** is not a phenocryst phase in $Qb_2$. The very fine-grained **groundmass** is comprised of subhedral to euhedral plagioclase laths

(50-55 percent; compositions, determined by the Michel-Lévy method, range from An52-58); ophitic clinopyroxene (25-30 percent) enclosing both plagioclase and olivine; intergranular olivine (8-11 percent) to 2 mm in diameter which is almost completely altered to iddingsite; subhedral FeTi oxides (3-9 percent) occur as equant grains to ___ mm, and are found partially enclosing (ophitic) plagioclase implying late-stage mineralization. Vesicles (10-15 percent) are round, to ___ mm in diameter, with plagioclase laths intruding the voids (diktytaxitic). A rarely exposed basal flow has __ times more FeTi oxides than the upper flow, otherwise they are texturally and mineralogically similar.

**Basalt of Cord ($Qb_3$, JJ94-151)** $Qb_3$ is similar in modal composition to $Qb_1$. Phenocrysts include 1 percent each of **plagioclase** to 2 mm in length and **olivine** to 0.6 mm in diameter. It differs from $Qb_1$ by lack of glomerocrysts and coarser groundmass.glomerocrysts.

## Basaltic Andesite

**Olivine-bearing basaltic andesite ($Tdba_1$, JJ92-6)** has an incipiently-altered, brownish-black glassy groundmass with clear microlites, and 15 percent phenocrysts. Phenocrysts include 10 percent euhedral to subhedral **plagioclase** (0.1-4 mm; many with abundant black cryptocrystalline inclusions), 3 percent euhedral **olivine** (0.1-1.0 mm), and 2 percent **FeTi oxides** (0.1-0.2 mm).

**Basaltic andesite dike ($Tdba_2$ JJ92-38)** Petrographic analysis of the dike of basaltic andesite that cuts the low-silica rhyolite reveals a dark brown glass with incipient devitrification confined to flow lines. The rock has ~5 percent subhedral to euhedral plagioclase (~$An_{20}$) 0.1 to 1 mm in length (many have either sieve texture or clinopyroxene inclusions), 3-4 percent anhedral clinopyroxene, 2 percent FeTi oxides, and less than 0.5 percent orthopyroxene. A single glomerocryst of olivine and plagioclase was seen in thin section, and a single xenocryst of biotite.

**Basaltic andesite of Brokendown Waterhole ($Tdba_3$, JJ92-62)** The upper basaltic-andesite flow that caps a thick package of andesite flows (-62) is composed of approximately 50-55 percent plagioclase laths (to 0.5 mm in length), 12-15 percent intersertal clinopyroxene (± orthopyroxene?) (to 0.15 mm across), 4-6 percent olivine (to 0.25 mm in diameter), 4 percent FeTi oxides, plus a 20-25 percent grainy cryptocrystalline material (clay-altered glass?). Sparse, small glomerocrysts of plagioclase and olivine are found in thin section.

## Andesite

**Andesite of Duck Creek Spring ($Tda_1$, JJ92-27, JJ92-41)** The basal andesite that forms the flow lobe to the southwest of Indian Creek Buttes (JJ92-27) has a very fine-grained groundmass with approximately 2-3 percent phenocrysts of plagioclase and olivine. The plagioclase and olivine phenocrysts appear chiefly as sparse glomerocrysts. The subhedral to euhedral **plagioclase** is 0.5 to 2 mm in length, has both albite and Carlsbad/pericline twins, and exhibits some overgrowths and/or sieve textures indicative of disequilibrium conditions. The anhedral **olivine** (0.5 mm) has

approximately 5 percent iddingsite alteration. The **groundmass** is composed of 65-70 percent plagioclase, 20 percent clinopyroxene (± opx?), 7 percent FeTi oxides, and 3-8 percent clay alteration. Sparse, small olivine-rich glomerocrysts are evident only in thin section. The basal flow of this southeastern lobe has 3-7 percent phenocrysts of plagioclase (to 1 cm) and clinopyroxene (to 1 mm) in a groundmass of plagioclase, clinopyroxene, and intersertal glass.
The eastern flow (-41) has a microcrystalline pilotaxitic groundmass that appears to be chiefly plagioclase and clay-altered glass. Phenocrysts (4-5 modal percent) include euhedral to subhedral oscillatory plagioclase (1-7 mm with abundant sieve textures, ~1% anhedral olivine (0.1-0.3 mm), and sparse clinopyroxene. Glomerocrysts of plagioclase and iddingsitized olivine are common.

**Andesite of Duck Creek ($Tda_2$, JJ93-126, -140):** These include porphyritic and glomeroporphyritic trachyandesite flows and dikes with 5 to 10 percent phenocrysts of plagioclase and olivine. **Plagioclase** (5-9 percent) occurs as subhedral to euhedral albitic laths as long as 1 cm in length , and as blocky, equant anhedral to subhedral crystals to 2.5 mm across. The blocky grains display Carlsbad, albite, or no twinning, and are commonly zoned (both normal and reverse) or have sieve textures in the cores. **Olivine** ($\leq$ 1 percent; 0.1-0.5 mm) is subhedral to euhedral. Individual phenocrysts are almost completely altered to iddingsite and/or sideromelane, whereas the olivine that occurs with plagioclase as sparse glomerocrysts is 20 to 50 percent altered to iddingsite. The **groundmass** varies from cryptocrystalline to very fine grained, and is comprises randomly oriented interlocking euhedral plagioclase (60 to 80 percent), intergranular anhedral clinopyroxene (10 to 35 percent), FeTi oxides (2 to 4 percent), brown glass (0-3 percent), and up to 15 percent miscellaneous non identifiable cryptocrystalline "dust".
**Magmatic inclusions** were found in thin-section analysis from both sample locations. The inclusions are 2.5 mm in diameter and are composed of 40 percent brown glass, 40 percent euhedral plagioclase laths (0.1 to 0.3 mm), 5 percent equant euhedral FeTi oxides (0.025 to 0.05 mm)with rare dendritic needles (0.1 mm), and 5 percent anhedral to subhedral clinopyroxene (0.05 to 0.1 mm).

## Dacite

**Inclusion-rich dacite (Tdid: JJ92-102; basaltic andesite inclusion is JJ92-51):** The dacite is medium-dark to dark gray and is characterized by 3-30 percent magmatic inclusions which range from 0.2 to 5 cm in diameter. It is sparsely porphyritic, with 3-5 percent phenocrysts of feldspar > FeTi oxides > orthopyroxene > clinopyroxene > quartz, and has an aphanitic groundmass. Rare hornblende and olivine were seen in only one thin section. (Phenocrysts >0.1 mm may be xenoliths from the basaltic andesite melt) **Feldspar** (1-3 percent) phenocrysts to 1 mm anhedral with some resorption. Sieve-textured reaction rim or core common. Exhibits normal, oscillatory, and reversed zoning. **FeTi oxides** (0.2 to 1 percent) to 0.2 mm (mostly 0.03 mm) are finely disseminated. **Orthopyroxene and clinopyroxene** (0.5-1 percent, OPX>CPX; <0.5 mm) are anhedral. **Quartz** crystals (<1 percent; to 1 mm in diameter) are anhedral and resorbed. Overgrowth fabric on some of the feldspar and pyroxene indicates

disequilibrium conditions. **Groundmass** is cryptocrystalline with random orientation of abundant feldspar (?) crystallites in a brown matrix.

The **basaltic andesite inclusions** are fine grained, intersertal, vesicular, sparsely porphyritic (2 percent), and commonly have glassy rims indicative of rapid quenching. Phenocrysts (in decreasing abundance) include anhedral plagioclase ($An_{48-51}$) to 0.8 mm in length, subhedral clinopyroxene laths to 0.5 mm in length, and rare fine-grained anhedral olivine (not found in microprobe analysis). The **groundmass** comprises 40-50 percent subhedral to euhedral plagioclase to 0.4 mm, 20-40 percent partially devitrified glass, 10-20 percent orthopyroxene > clinopyroxene to 0.3 mm, 5 percent dendritic>blocky FeTi oxides (blocky to 0.02 mm, dendritic to 0.6 mm indicative of quenching), and 3 percent clear euhedral apatite to 0.01 mm. Vesicles in a 3 cm inclusion varied from 20 percent of mode in the glassy rim to less than 5 percent in core.

## Rhyodacite

**Rhyodacite of Duck Creek Butte (Tdrd, JJ92-1, JJ92-7, JJ92-88, JJ92-101)** varies from incipiently hydrated (grayish black to dark reddish brown), to perlitic (light to medium gray), to stony, slightly phase-altered devitrified (light-gray sugary to brownish-gray stony), to a light-gray to grayish-orange pink pumiceous carapace. It is porphyritic with 7 to 12 percent phenocrysts of plagioclase > biotite > orthopyroxene > clinopyroxene > FeTi oxides > amphibole. **Plagioclase** (5-8 percent), to 4 mm in length, occurs as anhedral to subhedral simple to complicated phenocrysts. It occurs as zoned (normal and reversed), sieve textured, occasionally resorbed, and rarely as glomerocrysts. Chemical composition is oligoclase to andesine (Table 4-2). **Orthopyroxene** (0-1 percent), is 0.25 to 0.5 mm in length and is chiefly subhedral. **Biotite** (1-2 percent), is subhedral to euhedral, to 2 mm across. Green **clinopyroxene** (0.5 to 1 percent) is anhedral to euhedral, 0.05 to 0.7 mm, and exhibits simple twinning. **Fe-Ti oxides** (0.5 to 1 percent) are anhedral to euhedral, 0.1 to 0.25 mm equant grains. **Amphibole** (< 0.25 percent) is subhedral to euhedral to 0.8 mm. The **groundmass** ranges from almost completely glassy with abundant flow aligned microlites (acicular to 0.025 mm, blocky to 0.005 mm), to incipiently devitrified. Spherulitic alteration was found in only one location, where it was pervasive. Sparse **glomerocrysts** vary from microcrystalline to very fine grained (probably plagioclase & clinopyroxene). Cryptocrystalline to very fine-grained plagioclase-rich melt inclusions were also found A 20-cm clast of rhyolite from the **surge deposit** found beneath the rhyolite flows had 5-10 percent vesicles, and 7 percent phenocrysts comprises of 4 percent anhedral to subhedral plagioclase to 2 mm, 1-1.5 percent subhedral biotite to 0.5 mm, 1 percent anhedral orthopyroxene to 0.25 mm, 1 percent anhedral to euhedral FeTi oxides to 0.25 mm, <0.5 percent anhedral clinopyroxene to 0.25 mm. No amphibole was found, The clast had a glassy groundmass with incipient devitrification of the flow lines. An altered fine-grained inclusion in the rhyolite clast had 40-50 percent clear glass, 40-50 percent plagioclase, 8 percent FeTi oxides, 3 percent orthopyroxene, and 3 percent clay.

## Rhyolite

**Rhyolite of Indian Creek Buttes ($Tdr_1$, JJ92-5, JJ92-4):** Sparsely phyric to aphyric rhyolite occurs chiefly as light gray to very-light gray partly devitrified. Textures that vary from perlitic to sugary to stony, with 0 to 90 percent spherulitic alteration; it also occurs as cobbles of black to black/reddish brown streaked obsidian. **Groundmass** is glassy to cryptocrystalline with parallel alignment of microlites along flow lines. Phenocrysts include $\leq$ 1 percent subhedral and embayed **sanidine** to 3 mm. Most are unzoned but they also show undulatory, or checkerboard (microcline) extinction, $\leq$ 1 percent 0.25 mm euhedral blocky **plagioclase** aligned parallel to flow lines, 0.5 percent anhedral and embayed **quartz** to 1 mm, and rare elongate subhedral **hornblende** to 3 mm. One sample from low in the section had >90 percent spherulitic alteration with coarser quartz filling the vugs (?) between the radial aggregates, plus approximately 2 percent speckling of very-fine-grained FeTi oxides, and 2 percent brown glass. The only xenolith found was a 15 cm diameter rounded xenolith comprises of 85 percent plagioclase, 8 percent FeTi oxides, 7 percent mafics. Alteration obscures precise identification, but the xenolith was probably plucked from the older basaltic andesite that overlies the Steens Basalt.

## Appendix 3: Microprobe analyses performed for this study.

| FELDSPAR | | Mineral | $SiO_2$ | $Al_2O_3$ | CaO | $Na_2O$ | $K_2O$ | MgO | FeO | BaO | Total |
|---|---|---|---|---|---|---|---|---|---|---|---|
| JJ92-1 | Tdrd | Plagiocl. | 61.26 | 24.17 | 5.42 | 7.45 | 1.18 | 0.01 | 0.10 | 0.02 | 99.61 |
| JJ92-1 | Tdrd | Plagiocl. | 60.66 | 24.53 | 5.83 | 7.41 | 1.08 | 0.00 | 0.21 | 0.02 | 99.74 |
| JJ92-1 | Tdrd | Plagiocl. | 60.26 | 24.80 | 6.38 | 7.16 | 1.04 | 0.01 | 0.20 | 0.08 | 99.93 |
| JJ92-1 | Tdrd | Plagiocl. | 60.52 | 24.73 | 5.97 | 7.24 | 1.23 | 0.02 | 0.20 | 0.03 | 99.94 |
| JJ92-1 | Tdrd | Plagiocl. | 58.49 | 26.37 | 7.82 | 6.34 | 0.85 | 0.03 | 0.15 | 0.01 | 100.06 |
| JJ92-1 | Tdrd | Plagiocl. | 59.19 | 25.56 | 7.10 | 6.88 | 0.95 | 0.02 | 0.23 | 0.04 | 99.97 |
| JJ92-1 | Tdrd | Plagiocl. | 59.75 | 25.17 | 6.71 | 6.94 | 1.11 | 0.00 | 0.20 | 0.12 | 100.00 |
| JJ92-1 | Tdrd | Plagiocl. | 59.37 | 25.09 | 6.87 | 6.64 | 0.88 | 0.04 | 0.41 | 0.04 | 99.34 |
| JJ92-1 | Tdrd | Plagiocl. | 58.39 | 26.00 | 7.60 | 6.52 | 0.73 | 0.01 | 0.17 | 0.03 | 99.45 |
| JJ92-1 | Tdrd | Plagiocl. | 59.67 | 25.74 | 7.18 | 6.76 | 0.92 | 0.00 | 0.23 | 0.00 | 100.50 |
| JJ92-1 | Tdrd | Plagiocl. | 60.75 | 24.53 | 5.92 | 7.27 | 1.09 | 0.00 | 0.17 | 0.05 | 99.78 |
| JJ92-1 | Tdrd | Plagiocl. | 60.74 | 24.62 | 5.95 | 7.26 | 1.14 | 0.00 | 0.16 | 0.04 | 99.91 |
| JJ92-1 | Tdrd | Plagiocl. | 58.96 | 25.52 | 7.09 | 6.69 | 0.99 | 0.01 | 0.28 | 0.14 | 99.68 |
| JJ92-1 | Tdrd | Plagiocl. | 57.52 | 26.08 | 7.96 | 6.43 | 0.81 | 0.00 | 0.31 | 0.15 | 99.26 |
| JJ92-1 | Tdrd | Plagiocl. | 60.25 | 24.92 | 6.28 | 7.01 | 1.25 | 0.01 | 0.23 | 0.18 | 100.13 |
| JJ92-1 | Tdrd | Plagiocl. | 60.03 | 24.77 | 6.01 | 7.07 | 1.33 | 0.01 | 0.22 | 0.28 | 99.72 |
| JJ92-1 | Tdrd | Plagiocl. | 60.65 | 25.07 | 6.40 | 7.10 | 0.99 | 0.02 | 0.25 | 0.02 | 100.50 |
| JJ92-1 | Tdrd | Plagiocl. | 59.80 | 25.27 | 6.59 | 6.99 | 1.02 | 0.00 | 0.18 | 0.04 | 99.89 |
| JJ92-1 | Tdrd | Plagiocl. | 63.36 | 22.85 | 6.42 | 5.98 | 1.01 | 0.06 | 0.56 | 0.12 | 100.36 |
| JJ92-1 | Tdrd | Plagiocl. | 57.03 | 26.78 | 9.18 | 5.51 | 0.58 | 0.02 | 0.42 | 0.09 | 99.61 |
| JJ92-1 | Tdrd | Plagiocl. | 56.33 | 27.92 | 9.82 | 5.50 | 0.47 | 0.04 | 0.32 | 0.08 | 100.48 |
| JJ92-1 | Tdrd | Plagiocl. | 57.27 | 26.63 | 8.51 | 6.09 | 0.69 | 0.03 | 0.33 | 0.12 | 99.67 |
| JJ92-1 | Tdrd | Plagiocl. | 57.57 | 26.39 | 8.84 | 5.92 | 0.61 | 0.02 | 0.44 | 0.09 | 99.88 |
| JJ92-1 | Tdrd | Plagiocl. | 59.26 | 25.08 | 6.41 | 7.06 | 1.00 | 0.00 | 0.21 | 0.02 | 99.04 |
| JJ92-1 | Tdrd | Plagiocl. | 58.65 | 25.15 | 6.74 | 6.77 | 0.86 | 0.02 | 0.14 | 0.02 | 98.35 |
| JJ92-1 | Tdrd | Plagiocl. | 59.49 | 24.99 | 6.18 | 7.25 | 1.06 | 0.01 | 0.19 | 0.05 | 99.22 |
| JJ92-1 | Tdrd | Plagiocl. | 59.72 | 24.83 | 6.23 | 6.98 | 1.12 | 0.00 | 0.15 | 0.06 | 99.09 |
| JJ92-1 | Tdrd | Plagiocl. | 59.94 | 24.42 | 5.99 | 7.21 | 1.19 | 0.01 | 0.17 | 0.07 | 99.00 |
| JJ92-1 | Tdrd | Plagiocl. | 60.58 | 24.35 | 5.94 | 7.21 | 0.96 | 0.01 | 0.17 | 0.08 | 99.30 |
| JJ92-1 | Tdrd | Plagiocl. | 65.03 | 20.66 | 5.60 | 5.54 | 1.31 | 0.05 | 0.64 | 0.08 | 98.91 |
| JJ92-1 | Tdrd | Plagiocl. | 65.57 | 19.83 | 5.58 | 4.69 | 1.54 | 0.08 | 0.79 | 0.13 | 98.21 |
| JJ92-1 | Tdrd | Plagiocl. | 59.15 | 25.13 | 6.63 | 6.92 | 1.07 | 0.01 | 0.28 | 0.10 | 99.29 |
| JJ92-1 | Tdrd | Plagiocl. | 56.14 | 27.07 | 8.52 | 5.98 | 0.75 | 0.02 | 0.28 | 0.22 | 98.98 |
| JJ92-1 | Tdrd | Plagiocl. | 60.79 | 23.90 | 5.26 | 7.38 | 1.44 | 0.02 | 0.24 | 0.10 | 99.13 |
| JJ92-1 | Tdrd | Plagiocl. | 59.09 | 24.91 | 6.42 | 7.15 | 1.01 | 0.01 | 0.20 | 0.04 | 98.83 |
| JJ92-1 | Tdrd | Plagiocl. | 59.24 | 24.52 | 6.03 | 7.22 | 1.16 | 0.00 | 0.23 | 0.05 | 98.45 |
| JJ92-1 | Tdrd | Plagiocl. | 59.38 | 24.49 | 6.18 | 7.11 | 1.26 | 0.01 | 0.21 | 0.09 | 98.73 |
| JJ92-1 | Tdrd | Plagiocl. | 60.95 | 24.04 | 6.35 | 6.30 | 1.14 | 0.02 | 0.34 | 0.16 | 99.30 |
| JJ92-5 | Tdr1 | Sanidine | 62.67 | 19.45 | 0.79 | 5.77 | 7.11 | 0.02 | 0.17 | 0.40 | 96.38 |
| JJ92-5 | Tdr1 | Sanidine | 65.10 | 19.17 | 0.17 | 3.58 | 11.35 | 0.01 | 0.06 | 0.24 | 99.68 |
| JJ92-5 | Tdr1 | Sanidine | 65.12 | 19.26 | 0.22 | 3.63 | 11.29 | 0.01 | 0.12 | 0.27 | 99.92 |
| JJ92-5 | Tdr1 | Sanidine | 65.19 | 19.13 | 0.22 | 3.75 | 11.09 | 0.00 | 0.07 | 0.22 | 99.67 |
| JJ92-5 | Tdr1 | Sanidine | 65.79 | 19.19 | 0.20 | 4.81 | 9.42 | 0.01 | 0.09 | 0.23 | 99.74 |
| JJ92-5 | Tdr1 | Sanidine | 64.25 | 19.18 | 0.19 | 3.57 | 11.36 | 0.00 | 0.05 | 0.22 | 98.82 |
| JJ92-5 | Tdr1 | Sanidine | 65.51 | 19.53 | 0.29 | 7.21 | 5.65 | 0.01 | 0.09 | 0.16 | 98.45 |

**Appendix 3** (cont.):

| | | Mineral | $SiO_2$ | $Al_2O3$ | CaO | $Na_2O$ | $K_2O$ | MgO | FeO | BaO | Total |
|---|---|---|---|---|---|---|---|---|---|---|---|
| JJ92-5 | **Tdr1** | Sanidine | 65.85 | 19.47 | 0.32 | 6.91 | 6.18 | 0.00 | 0.13 | 0.42 | 99.28 |
| JJ92-99 | **Tdb2** | Plagiocl. | 51.35 | 30.22 | 13.30 | 3.82 | 0.25 | 0.12 | 0.55 | 0.03 | 99.64 |
| JJ92-99 | **Tdb2** | Plagiocl. | 50.37 | 30.89 | 14.29 | 3.17 | 0.27 | 0.11 | 0.73 | 0.04 | 99.87 |
| JJ92-99 | **Tdb2** | Plagiocl. | 53.21 | 28.91 | 11.74 | 4.58 | 0.38 | 0.10 | 0.77 | 0.00 | 99.69 |
| JJ92-99 | **Tdb2** | Plagiocl. | 53.23 | 28.99 | 11.89 | 4.43 | 0.37 | 0.09 | 0.84 | 0.04 | 99.88 |
| JJ92-99 | **Tdb2** | Plagiocl. | 56.47 | 26.69 | 9.21 | 5.39 | 1.26 | 0.06 | 0.79 | 0.09 | 99.96 |
| JJ92-99 | **Tdb2** | Plagiocl. | 53.01 | 27.49 | 11.91 | 4.30 | 0.44 | 0.51 | 1.13 | 0.02 | 98.81 |
| JJ92-99 | **Tdb2** | Plagiocl. | 49.96 | 31.50 | 14.60 | 3.14 | 0.21 | 0.12 | 0.48 | 0.01 | 100.02 |
| JJ92-99 | **Tdb2** | Plagiocl. | 50.99 | 30.77 | 13.72 | 3.52 | 0.23 | 0.09 | 0.49 | 0.05 | 99.86 |
| JJ92-99 | **Tdb2** | Plagiocl. | 49.74 | 31.50 | 14.59 | 3.02 | 0.20 | 0.11 | 0.49 | 0.00 | 99.65 |
| JJ92-99 | **Tdb2** | Plagiocl. | 51.46 | 30.63 | 13.47 | 3.63 | 0.24 | 0.12 | 0.51 | 0.00 | 100.06 |
| JJ92-99 | **Tdb2** | Plagiocl. | 53.43 | 28.60 | 11.57 | 4.65 | 0.40 | 0.10 | 0.88 | 0.01 | 99.64 |
| JJ92-99 | **Tdb2** | Plagiocl. | 49.60 | 31.43 | 14.79 | 2.92 | 0.27 | 0.20 | 0.76 | 0.00 | 99.97 |
| JJ92-99 | **Tdb2** | Plagiocl. | 51.07 | 30.83 | 13.72 | 3.34 | 0.26 | 0.08 | 0.73 | 0.01 | 100.04 |
| JJ92-99 | **Tdb2** | Plagiocl. | 52.10 | 29.65 | 12.97 | 3.92 | 0.31 | 0.08 | 0.80 | 0.02 | 99.85 |
| JJ92-99 | **Tdb2** | Plagiocl. | 50.86 | 30.37 | 13.73 | 3.43 | 0.29 | 0.12 | 0.52 | 0.01 | 99.33 |
| JJ92-99 | **Tdb2** | Plagiocl. | 49.49 | 31.47 | 14.91 | 2.99 | 0.15 | 0.11 | 0.49 | 0.03 | 99.64 |
| JJ92-99 | **Tdb2** | Plagiocl. | 51.85 | 29.82 | 13.16 | 3.93 | 0.30 | 0.11 | 0.76 | 0.01 | 99.94 |
| JJ92-99 | **Tdb2** | Plagiocl. | 52.11 | 29.06 | 12.22 | 3.99 | 0.38 | 0.17 | 0.86 | 0.01 | 98.80 |
| JJ92-99 | **Tdb2** | Plagiocl. | 51.85 | 29.69 | 12.90 | 3.80 | 0.31 | 0.12 | 1.08 | 0.03 | 99.78 |
| JJ92-99 | **Tdb2** | Plagiocl. | 53.53 | 28.71 | 11.63 | 4.50 | 0.43 | 0.19 | 1.04 | 0.04 | 100.07 |
| JJ93-130 | **Tdb1** | Plagiocl. | 53.09 | 28.62 | 11.70 | 4.53 | 0.42 | 0.19 | 1.05 | 0.01 | 99.61 |
| JJ93-130 | **Tdb1** | Plagiocl. | 53.41 | 28.56 | 11.58 | 4.65 | 0.42 | 0.11 | 0.82 | 0.01 | 99.56 |
| JJ93-130 | **Tdb1** | Plagiocl. | 52.57 | 28.43 | 11.51 | 4.62 | 0.43 | 0.09 | 0.88 | 0.02 | 98.55 |
| JJ93-130 | **Tdb1** | Plagiocl. | 51.56 | 27.77 | 11.51 | 4.45 | 0.37 | 0.08 | 0.88 | 0.02 | 96.64 |
| JJ93-130 | **Tdb1** | Plagiocl. | 50.21 | 27.18 | 11.14 | 4.43 | 0.41 | 0.09 | 0.87 | 0.07 | 94.40 |
| JJ93-130 | **Tdb1** | Plagiocl. | 51.88 | 29.98 | 12.85 | 4.10 | 0.26 | 0.09 | 0.80 | 0.00 | 99.96 |
| JJ93-130 | **Tdb1** | Plagiocl. | 51.51 | 30.13 | 13.29 | 3.87 | 0.19 | 0.07 | 0.56 | 0.04 | 99.66 |
| JJ93-130 | **Tdb1** | Plagiocl. | 52.88 | 28.84 | 11.99 | 4.62 | 0.28 | 0.07 | 0.81 | 0.01 | 99.50 |
| JJ93-130 | **Tdb1** | Plagiocl. | 51.01 | 30.14 | 13.46 | 3.73 | 0.22 | 0.06 | 0.77 | 0.00 | 99.39 |
| JJ93-130 | **Tdb1** | Plagiocl. | 56.33 | 26.56 | 9.38 | 5.81 | 0.50 | 0.05 | 1.19 | 0.03 | 99.85 |
| JJ93-130 | **Tdb1** | Plagiocl. | 51.67 | 30.07 | 13.17 | 3.87 | 0.20 | 0.09 | 0.65 | 0.01 | 99.73 |
| JJ93-130 | **Tdb1** | Plagiocl. | 55.02 | 27.97 | 10.84 | 5.26 | 0.47 | 0.08 | 0.71 | 0.09 | 100.44 |
| JJ93-130 | **Tdb1** | Plagiocl. | 51.66 | 30.08 | 13.10 | 4.03 | 0.14 | 0.09 | 0.59 | 0.02 | 99.71 |
| JJ93-130 | **Tdb1** | Plagiocl. | 53.37 | 29.12 | 12.18 | 4.55 | 0.29 | 0.07 | 0.81 | 0.05 | 100.44 |
| JJ93-130 | **Tdb1** | Plagiocl. | 52.15 | 29.77 | 12.95 | 4.13 | 0.18 | 0.10 | 0.54 | 0.01 | 99.83 |
| JJ93-130 | **Tdb1** | Plagiocl. | 54.62 | 27.80 | 10.83 | 5.20 | 0.35 | 0.06 | 0.81 | 0.08 | 99.75 |
| JJ93-130 | **Tdb1** | Plagiocl. | 56.77 | 26.90 | 9.02 | 5.99 | 0.78 | 0.04 | 1.06 | 0.07 | 100.63 |
| Dacite | **Tdid** | Plagiocl. | 55.66 | 27.36 | 10.35 | 5.28 | 0.61 | 0.07 | 0.65 | 0.04 | 100.02 |
| Dacite | **Tdid** | Plagiocl. | 56.01 | 27.34 | 10.04 | 5.23 | 0.73 | 0.08 | 0.70 | 0.08 | 100.21 |
| Dacite | **Tdid** | Plagiocl. | 55.71 | 27.67 | 10.02 | 5.22 | 0.68 | 0.03 | 0.55 | 0.06 | 99.94 |
| Dacite | **Tdid** | Plagiocl. | 60.38 | 21.91 | 7.00 | 4.34 | 2.52 | 0.51 | 2.07 | 0.04 | 98.77 |
| inclusion | **Tdid** | Plagiocl. | 54.76 | 28.11 | 10.68 | 5.23 | 0.61 | 0.06 | 0.77 | 0.03 | 100.25 |
| inclusion | **Tdid** | Plagiocl. | 58.58 | 25.22 | 7.42 | 6.25 | 1.19 | 0.01 | 0.59 | 0.21 | 99.47 |

**Appendix 3** (cont.):

| | | Mineral | $SiO_2$ | $Al_2O_3$ | CaO | $Na_2O$ | $K_2O$ | MgO | FeO | BaO | Total |
|---|---|---|---|---|---|---|---|---|---|---|---|
| inclusion | **Tdid** | Plagiocl. | 56.28 | 26.93 | 9.43 | 5.46 | 0.71 | 0.08 | 0.98 | 0.05 | 99.92 |
| inclusion | **Tdid** | Plagiocl. | 55.85 | 26.54 | 9.30 | 5.71 | 0.63 | 0.10 | 1.21 | 0.06 | 99.40 |
| inclusion | **Tdid** | Plagiocl. | 53.42 | 24.74 | 12.37 | 5.16 | 0.83 | 0.07 | 0.71 | 0.10 | 97.40 |
| inclusion | **Tdid** | Plagiocl. | 57.14 | 26.55 | 9.01 | 5.79 | 0.91 | 0.03 | 0.57 | 0.11 | 100.11 |
| inclusion | **Tdid** | Plagiocl. | 57.41 | 26.06 | 8.50 | 5.89 | 0.93 | 0.07 | 0.76 | 0.04 | 99.66 |
| Dacite | **Tdid** | Plagiocl. | 57.70 | 23.55 | 8.18 | 4.32 | 1.84 | 0.10 | 1.15 | 0.08 | 96.92 |
| Dacite | **Tdid** | Plagiocl. | 56.93 | 26.97 | 9.03 | 5.68 | 0.76 | 0.05 | 0.50 | 0.09 | 100.01 |
| Dacite | **Tdid** | Plagiocl. | 59.10 | 24.24 | 7.67 | 5.21 | 1.48 | 0.07 | 0.99 | 0.06 | 98.82 |
| Dacite | **Tdid** | Plagiocl. | 56.00 | 26.89 | 9.60 | 5.16 | 0.78 | 0.10 | 0.78 | 0.10 | 99.41 |

| **PYROXENE** | | **Mineral:** | $SiO_2$ | $TiO_2$ | $Al_2O_3$ | FeO | MnO | MgO | CaO | $Na_2O$ |
|---|---|---|---|---|---|---|---|---|---|---|
| JJ92-99 | **Tdb2** | ClinoPyx | 50.23 | 1.49 | 3.45 | 9.78 | 0.19 | 14.26 | 20.40 | 0.37 |
| JJ92-99 | **Tdb2** | Orthopyx. | 51.39 | 0.96 | 1.85 | 9.82 | 0.24 | 15.82 | 19.51 | 0.32 |
| JJ92-99 | **Tdb2** | ClinoPyx | 50.16 | 1.27 | 2.86 | 9.38 | 0.19 | 13.63 | 20.06 | 0.37 |
| JJ92-99 | **Tdb2** | ClinoPyx | 50.63 | 1.58 | 2.78 | 10.84 | 0.27 | 13.92 | 19.36 | 0.39 |
| JJ92-99 | **Tdb2** | ClinoPyx | 52.36 | 1.04 | 1.45 | 11.77 | 0.38 | 14.99 | 18.55 | 0.36 |
| JJ92-99 | **Tdb2** | ClinoPyx | 51.17 | 1.28 | 2.04 | 11.61 | 0.36 | 13.74 | 19.39 | 0.37 |
| JJ92-99 | **Tdb2** | ClinoPyx | 57.98 | 0.61 | 11.64 | 7.59 | 0.21 | 7.82 | 12.53 | 3.10 |
| JJ92-99 | **Tdb2** | ClinoPyx | 59.86 | 0.41 | 14.83 | 4.77 | 0.12 | 5.19 | 9.77 | 3.24 |
| JJ92-1 | **Tdrd** | Orthopyx. | 50.97 | 0.15 | 0.64 | 29.78 | 0.95 | 15.11 | 1.51 | 0.01 |
| JJ92-1 | **Tdrd** | ClinoPyx | 51.38 | 0.13 | 0.99 | 14.93 | 0.84 | 9.91 | 18.50 | 0.32 |
| JJ92-1 | **Tdrd** | ClinoPyx | 52.09 | 0.11 | 0.74 | 14.91 | 0.85 | 11.13 | 20.00 | 0.26 |
| JJ92-1 | **Tdrd** | ClinoPyx | 51.78 | 0.18 | 0.92 | 14.51 | 0.74 | 11.13 | 20.15 | 0.31 |
| JJ92-1 | **Tdrd** | Orthopyx. | 49.93 | 0.15 | 0.58 | 29.07 | 1.41 | 16.84 | 1.41 | 0.06 |
| JJ92-1 | **Tdrd** | Orthopyx. | 51.28 | 0.19 | 0.59 | 29.23 | 1.42 | 15.89 | 1.43 | 0.01 |
| JJ92-1 | **Tdrd** | Orthopyx. | 50.68 | 0.12 | 0.58 | 30.63 | 1.55 | 14.34 | 1.35 | 0.03 |
| JJ92-1 | **Tdrd** | Orthopyx. | 50.65 | 0.13 | 0.57 | 30.06 | 1.40 | 14.88 | 1.45 | 0.01 |
| JJ92-1 | **Tdrd** | Orthopyx. | 51.41 | 0.11 | 0.72 | 27.42 | 0.97 | 16.91 | 1.37 | 0.05 |
| JJ92-1 | **Tdrd** | Orthopyx. | 50.41 | 0.10 | 0.81 | 28.68 | 1.40 | 13.28 | 1.30 | 0.06 |
| JJ92-1 | **Tdrd** | Orthopyx. | 50.97 | 0.09 | 0.38 | 29.35 | 1.25 | 15.71 | 1.24 | 0.02 |
| JJ92-1 | **Tdrd** | Orthopyx. | 51.46 | 0.14 | 0.37 | 28.94 | 1.15 | 16.45 | 1.23 | 0.03 |
| JJ92-1 | **Tdrd** | Orthopyx. | 51.42 | 0.10 | 0.43 | 28.03 | 0.96 | 16.29 | 1.20 | 0.05 |
| JJ92-1 | **Tdrd** | ClinoPyx | 51.42 | 0.43 | 1.69 | 11.99 | 0.42 | 13.20 | 19.30 | 0.37 |
| JJ92-1 | **Tdrd** | ClinoPyx | 51.44 | 0.36 | 1.55 | 13.11 | 0.47 | 12.71 | 18.78 | 0.33 |
| JJ92-1 | **Tdrd** | ClinoPyx | 51.43 | 0.12 | 0.89 | 15.30 | 0.92 | 10.56 | 20.12 | 0.36 |
| JJ92-1 | **Tdrd** | ClinoPyx | 66.18 | 0.24 | 11.14 | 6.88 | 0.24 | 4.10 | 8.65 | 0.86 |
| JJ92-1 | **Tdrd** | ClinoPyx | 51.54 | 0.12 | 0.82 | 14.95 | 0.92 | 10.30 | 20.42 | 0.32 |
| JJ92-1 | **Tdrd** | ClinoPyx | 52.27 | 0.12 | 0.85 | 15.05 | 0.87 | 10.19 | 19.84 | 0.30 |
| JJ92-1 | **Tdrd** | Orthopyx. | 51.37 | 0.06 | 0.36 | 30.70 | 1.35 | 15.20 | 1.16 | 0.00 |
| JJ92-1 | **Tdrd** | Orthopyx. | 51.44 | 0.09 | 0.40 | 30.61 | 1.53 | 14.99 | 1.19 | 0.02 |
| JJ92-1 | **Tdrd** | Orthopyx. | 51.60 | 0.12 | 0.56 | 29.08 | 1.21 | 16.02 | 1.22 | 0.02 |
| JJ92-1 | **Tdrd** | Orthopyx. | 51.28 | 0.16 | 0.52 | 29.01 | 1.12 | 15.75 | 1.23 | 0.01 |

## Appendix 3 (cont.)

| PYROXENE | | Mineral: | $SiO_2$ | $TiO_2$ | $Al_2O_3$ | FeO | MnO | MgO | CaO | $Na_2O$ |
|---|---|---|---|---|---|---|---|---|---|---|
| inclusion | **Tdid** | ClinoPyx | 51.98 | 0.75 | 2.04 | 12.94 | 0.53 | 14.13 | 18.38 | 0.31 |
| inclusion | **Tdid** | ClinoPyx | 48.77 | 2.07 | 5.80 | 12.87 | 0.36 | 13.07 | 16.89 | 0.45 |
| inclusion | **Tdid** | ClinoPyx | 50.59 | 1.41 | 4.08 | 12.89 | 0.34 | 15.71 | 15.90 | 0.41 |
| inclusion | **Tdid** | ClinoPyx | 50.69 | 1.47 | 4.13 | 11.75 | 0.29 | 14.59 | 17.92 | 0.43 |
| inclusion | **Tdid** | ClinoPyx | 50.22 | 1.47 | 4.05 | 11.34 | 0.31 | 14.76 | 17.97 | 0.37 |
| inclusion | **Tdid** | Orthopyx. | 50.74 | 0.66 | 2.68 | 20.26 | 0.49 | 22.50 | 2.20 | 0.06 |
| dacite | **Tdid** | Orthopyx. | 53.59 | 0.57 | 2.13 | 17.82 | 0.45 | 24.93 | 2.00 | 0.05 |
| dacite | **Tdid** | ClinoPyx | 49.71 | 1.12 | 3.16 | 12.43 | 0.41 | 14.81 | 17.34 | 0.34 |
| dacite | **Tdid** | ClinoPyx | 50.36 | 1.05 | 3.09 | 10.96 | 0.34 | 14.83 | 18.73 | 0.39 |
| dacite | **Tdid** | ClinoPyx | 52.09 | 0.51 | 1.55 | 19.06 | 0.51 | 23.90 | 1.98 | 0.04 |
| dacite | **Tdid** | ClinoPyx | 50.11 | 0.94 | 2.92 | 13.23 | 0.46 | 14.35 | 17.07 | 0.29 |
| dacite | **Tdid** | Orthopyx. | 51.79 | 0.46 | 1.42 | 22.03 | 0.56 | 21.67 | 2.04 | 0.02 |
| dacite | **Tdid** | Orthopyx. | 53.29 | 0.43 | 1.29 | 18.79 | 0.49 | 24.29 | 1.87 | 0.05 |
| dacite | **Tdid** | ClinoPyx | 51.76 | 1.28 | 2.05 | 10.95 | 0.33 | 14.36 | 20.38 | 0.38 |
| JJ93-130 | **Tdb1** | ClinoPyx | 50.37 | 1.13 | 1.57 | 11.38 | 0.33 | 14.35 | 19.43 | 0.35 |
| JJ93-130 | **Tdb1** | ClinoPyx | 49.95 | 1.07 | 1.72 | 10.59 | 0.35 | 14.24 | 19.62 | 0.61 |
| JJ93-130 | **Tdb1** | Ilmenite | 0.12 | 20.84 | 1.62 | 70.94 | 0.61 | 1.88 | 0.1 | 0.03 |

| OLIVINE | | Mineral | $SiO_2$ | $TiO_2$ | $Al2O_3$ | FeO | MnO | MgO | CaO | NiO | ZnO | Total |
|---|---|---|---|---|---|---|---|---|---|---|---|---|
| JJ93-130 | **Tdb1** | Olivine | 35.36 | 0.02 | 0.01 | 36.62 | 0.71 | 27.80 | 0.27 | 0.01 | 0.10 | 100.90 |
| JJ93-130 | **Tdb1** | Olivine | 36.17 | 0.03 | 0.00 | 30.90 | 0.37 | 32.63 | 0.18 | 0.07 | 0.01 | 100.36 |
| JJ93-130 | **Tdb1** | Olivine | 35.95 | 0.00 | 0.00 | 32.66 | 0.52 | 30.90 | 0.16 | 0.07 | 0.03 | 100.29 |
| JJ93-130 | **Tdb1** | Olivine | 35.55 | 0.04 | 0.00 | 35.00 | 0.56 | 29.09 | 0.16 | 0.03 | 0.10 | 100.53 |
| JJ93-130 | **Tdb1** | Olivine | 34.83 | 0.07 | 0.00 | 37.89 | 0.64 | 26.21 | 0.11 | 0.03 | 0.03 | 99.81 |
| JJ93-130 | **Tdb1** | Olivine | 35.20 | 0.07 | 0.00 | 36.02 | 0.55 | 27.87 | 0.16 | 0.01 | 0.00 | 99.88 |
| JJ93-130 | **Tdb1** | Olivine | 35.10 | 0.06 | 0.00 | 36.33 | 0.54 | 27.87 | 0.15 | 0.06 | 0.00 | 100.11 |
| JJ93-130 | **Tdb1** | Olivine | 36.01 | 0.03 | 0.00 | 32.89 | 0.47 | 30.56 | 0.18 | 0.05 | 0.10 | 100.29 |
| JJ93-130 | **Tdb1** | Olivine | 35.76 | 0.03 | 0.00 | 32.65 | 0.53 | 30.53 | 0.17 | 0.08 | 0.00 | 99.75 |
| JJ93-130 | **Tdb1** | Olivine | 35.55 | 0.05 | 0.00 | 34.35 | 0.48 | 29.04 | 0.14 | 0.03 | 0.00 | 99.64 |
| JJ93-130 | **Tdb1** | Olivine | 35.55 | 0.02 | 0.00 | 33.31 | 0.55 | 30.18 | 0.19 | 0.05 | 0.03 | 99.88 |
| JJ93-130 | **Tdb1** | Olivine | 35.34 | 0.03 | 0.00 | 34.39 | 0.57 | 28.97 | 0.17 | 0.07 | 0.10 | 99.64 |
| JJ93-130 | **Tdb1** | Olivine | 35.02 | 0.04 | 0.00 | 35.83 | 0.63 | 27.81 | 0.16 | 0.02 | 0.00 | 99.51 |
| JJ93-130 | **Tdb1** | Olivine | 34.79 | 0.06 | 0.00 | 37.58 | 0.65 | 26.24 | 0.09 | 0.00 | 0.05 | 99.46 |
| JJ93-130 | **Tdb1** | Olivine | 34.95 | 0.06 | 0.00 | 37.52 | 0.71 | 26.45 | 0.10 | 0.04 | 0.01 | 99.84 |
| JJ93-130 | **Tdb1** | Olivine | 34.74 | 0.06 | 0.00 | 37.86 | 0.71 | 26.02 | 0.15 | 0.03 | 0.10 | 99.67 |
| JJ93-130 | **Tdb1** | Olivine | 34.41 | 0.07 | 0.00 | 38.08 | 0.66 | 25.44 | 0.07 | 0.02 | 0.03 | 98.78 |
| JJ92-99 | **Tdb2** | Olivine | 36.24 | 0.03 | 0.00 | 30.93 | 0.33 | 32.20 | 0.18 | 0.08 | 0.01 | 100.00 |
| JJ92-99 | **Tdb2** | Olivine | 36.20 | 0.03 | 0.00 | 31.87 | 0.43 | 30.87 | 0.15 | 0.07 | 0.11 | 99.73 |
| JJ92-99 | **Tdb2** | Olivine | 35.32 | 0.05 | 0.00 | 34.77 | 0.49 | 28.86 | 0.18 | 0.10 | 0.02 | 99.79 |
| JJ92-99 | **Tdb2** | Olivine | 34.53 | 0.12 | 0.00 | 39.04 | 0.53 | 23.26 | 0.12 | 0.01 | 0.08 | 97.69 |
| JJ92-99 | **Tdb2** | Olivine | 36.05 | 0.01 | 0.00 | 31.32 | 0.40 | 31.45 | 0.15 | 0.05 | 0.05 | 99.48 |
| JJ92-99 | **Tdb2** | Olivine | 35.69 | 0.04 | 0.00 | 32.69 | 0.40 | 30.35 | 0.17 | 0.06 | 0.01 | 99.41 |
| JJ92-99 | **Tdb2** | Olivine | 35.43 | 0.05 | 0.00 | 34.87 | 0.44 | 28.85 | 0.18 | 0.07 | 0.03 | 99.92 |

## Appendix 3 (cont)

| OLIVINE | | Mineral | $SiO_2$ | $TiO_2$ | $Al2O_3$ | FeO | MnO | MgO | CaO | NiO | ZnO | Total |
|---|---|---|---|---|---|---|---|---|---|---|---|---|
| JJ92-99 | **Tdb2** | Olivine | 35.35 | 0.08 | 0.00 | 36.21 | 0.46 | 26.36 | 0.14 | 0.05 | 0.06 | 98.71 |
| JJ92-99 | **Tdb2** | Olivine | 34.47 | 0.09 | 0.00 | 39.69 | 0.56 | 24.62 | 0.07 | 0.06 | 0.03 | 99.59 |
| JJ92-99 | **Tdb2** | Olivine | 34.32 | 0.05 | 0.00 | 38.56 | 0.58 | 25.58 | 0.16 | 0.05 | 0.03 | 99.33 |
| JJ92-99 | **Tdb2** | Olivine | 36.16 | 0.02 | 0.00 | 31.22 | 0.41 | 31.69 | 0.15 | 0.11 | 0.09 | 99.85 |
| JJ92-99 | **Tdb2** | Olivine | 35.58 | 0.01 | 0.00 | 32.99 | 0.48 | 30.04 | 0.15 | 0.04 | 0.06 | 99.35 |
| JJ92-99 | **Tdb2** | Olivine | 34.99 | 0.09 | 0.00 | 34.54 | 0.42 | 28.88 | 0.06 | 0.06 | 0.00 | 99.04 |
| JJ92-99 | **Tdb2** | Olivine | 35.54 | 0.04 | 0.00 | 34.32 | 0.46 | 29.40 | 0.23 | 0.04 | 0.02 | 100.05 |
| JJ92-99 | **Tdb2** | Olivine | 35.46 | 0.02 | 0.00 | 35.12 | 0.48 | 28.98 | 0.19 | 0.08 | 0.08 | 100.41 |
| JJ92-99 | **Tdb2** | Olivine | 34.81 | 0.05 | 0.00 | 37.64 | 0.48 | 26.22 | 0.15 | 0.00 | 0.00 | 99.35 |
| JJ92-99 | **Tdb2** | Olivine | 34.51 | 0.11 | 0.00 | 38.85 | 0.59 | 24.85 | 0.14 | 0.03 | 0.10 | 99.18 |

| AMPHIBOLE | | | $SiO_2$ | $TiO_2$ | $Al_2O_3$ | FeO | MnO | MgO | CaO | $Na_2O$ | $K_2O$ | $Cr_2O_3$ | F | Cl |
|---|---|---|---|---|---|---|---|---|---|---|---|---|---|---|
| JJ92-5 | **Tdr1** | Amph. | 42.00 | 2.15 | 8.61 | 28.22 | 0.52 | 4.55 | 9.97 | 1.90 | 1.04 | 0.01 | 0.53 | 0.22 |
| JJ92-5 | **Tdr1** | Amph. | 41.76 | 2.18 | 8.65 | 28.04 | 0.54 | 4.31 | 10.01 | 1.88 | 1.05 | 0.04 | 0.38 | 0.21 |
| JJ92-5 | **Tdr1** | Amph. | 41.76 | 2.17 | 8.80 | 27.93 | 0.51 | 4.59 | 9.94 | 1.89 | 1.05 | 0.00 | 0.34 | 0.22 |
| JJ92-5 | **Tdr1** | Amph. | 42.05 | 2.17 | 8.71 | 27.77 | 0.53 | 4.41 | 10.07 | 1.78 | 1.08 | 0.02 | 0.45 | 0.23 |
| JJ92-5 | **Tdr1** | Amph. | 41.91 | 2.15 | 8.58 | 27.76 | 0.55 | 4.64 | 9.92 | 1.82 | 1.09 | 0.02 | 0.42 | 0.20 |
| JJ92-5 | **Tdr1** | Amph. | 41.83 | 2.16 | 8.73 | 27.47 | 0.51 | 4.48 | 9.95 | 1.83 | 1.09 | 0.05 | 0.33 | 0.22 |
| JJ92-5 | **Tdr1** | Amph. | 43.68 | 1.80 | 8.47 | 23.90 | 0.51 | 7.49 | 10.37 | 1.76 | 0.95 | 0.00 | 0.60 | 0.14 |
| JJ92-5 | **Tdr1** | Amph. | 44.24 | 1.59 | 8.25 | 23.55 | 0.50 | 7.63 | 10.19 | 1.80 | 0.91 | 0.02 | 0.51 | 0.14 |
| JJ92-5 | **Tdr1** | Amph. | 43.97 | 1.35 | 8.12 | 24.10 | 0.51 | 7.43 | 10.14 | 1.81 | 0.92 | 0.00 | 0.63 | 0.15 |
| JJ92-5 | **Tdr1** | Amph. | 43.81 | 1.73 | 8.21 | 24.42 | 0.52 | 7.11 | 10.32 | 1.81 | 0.94 | 0.00 | 0.49 | 0.16 |
| JJ92-5 | **Tdr1** | Amph. | 43.28 | 1.78 | 8.45 | 24.46 | 0.50 | 6.86 | 10.28 | 1.80 | 1.01 | 0.00 | 0.38 | 0.18 |
| JJ92-5 | **Tdr1** | Amph. | 43.98 | 1.67 | 7.83 | 23.69 | 0.53 | 7.81 | 10.21 | 1.73 | 0.91 | 0.02 | 0.50 | 0.13 |
| JJ92-5 | **Tdr1** | Amph. | 44.05 | 1.62 | 8.15 | 24.00 | 0.54 | 7.71 | 10.36 | 1.79 | 0.89 | 0.01 | 0.36 | 0.13 |

| BIOTITE | | | $SiO_2$ | $TiO_2$ | $Al2O_3$ | FeO | MnO | MgO | CaO | $Na_2O$ | $K_2O$ | $Cr_2O_3$ | F | Cl |
|---|---|---|---|---|---|---|---|---|---|---|---|---|---|---|
| JJ92-1 | **Tdrd** | Biot. | 37.63 | 5.84 | 13.63 | 20.39 | 0.08 | 11.82 | 0.00 | 0.58 | 9.08 | 0.05 | 0.78 | 0.08 |
| JJ92-1 | **Tdrd** | Biot. | 37.26 | 5.81 | 13.78 | 20.56 | 0.16 | 11.89 | 0.00 | 0.58 | 9.19 | 0.00 | 0.66 | 0.08 |
| JJ92-1 | **Tdrd** | Biot. | 39.10 | 5.46 | 12.96 | 21.02 | 0.16 | 11.28 | 0.04 | 0.58 | 8.68 | 0.00 | 0.62 | 0.07 |

**APPENDIX 4:** XRF analyses of Steens Basalt collected near type section at Steens Mountain. Lower, middle, and upper denote relative outcrop location for 3 groups of flows in the >900-m-thick section. Collected by P.R. Hooper, C.J. Hawkesworth, and me. Analyst: Diane Johnson, GeoAnalytical Lab, WSU, Pullman, WA.

| Sample No. | $SiO_2$ | $Al2O_3$ | $TiO_2$ | FeO* | MnO | CaO | MgO | $K_2O$ | $Na_2O$ | $P_2O_5$ | Cr | Ba | Rb | Zr | Y | Nb |
|---|---|---|---|---|---|---|---|---|---|---|---|---|---|---|---|---|
| MF63 | 49.71 | 16.27 | 2.23 | 11.19 | 0.17 | 9.26 | 6.96 | 0.88 | 3.02 | 0.32 | 160 | 243 | 12 | 161 | 30 | 14 |
| MF64 | 49.85 | 18.39 | 2.09 | 9.84 | 0.16 | 10.62 | 5.03 | 0.60 | 3.14 | 0.29 | 189 | 238 | 8 | 150 | 27 | 13 |
| MF65 | 49.45 | 14.71 | 2.03 | 11.49 | 0.18 | 9.18 | 8.89 | 0.89 | 2.85 | 0.33 | 500 | 263 | 15 | 151 | 28 | 14 |
| MF66 | 49.34 | 14.32 | 1.81 | 11.06 | 0.18 | 9.88 | 10.09 | 0.64 | 2.45 | 0.23 | 650 | 203 | 11 | 132 | 26 | 10 |
| MF67 | 50.24 | 14.77 | 2.32 | 11.81 | 0.18 | 10.23 | 6.51 | 0.79 | 2.87 | 0.28 | 296 | 205 | 12 | 165 | 31 | 13 |
| MF68 | 50.90 | 16.09 | 1.96 | 9.76 | 0.17 | 10.32 | 7.01 | 0.69 | 2.87 | 0.23 | 274 | 175 | 15 | 138 | 29 | 11 |
| MF69 | 49.43 | 14.77 | 1.81 | 10.37 | 0.17 | 10.28 | 9.82 | 0.56 | 2.58 | 0.21 | 463 | 148 | 12 | 127 | 26 | 11 |
| MF70 | 49.88 | 18.11 | 1.97 | 9.53 | 0.16 | 10.42 | 6.01 | 0.59 | 3.04 | 0.29 | 153 | 196 | 11 | 140 | 25 | 12 |
| MF71A | 49.01 | 15.51 | 2.24 | 11.66 | 0.19 | 10.16 | 7.31 | 0.69 | 2.94 | 0.30 | 238 | 238 | 10 | 148 | 30 | 11 |
| MF71B | 48.91 | 16.55 | 2.22 | 11.24 | 0.18 | 10.13 | 6.64 | 0.69 | 3.14 | 0.31 | 183 | 242 | 7 | 159 | 30 | 12 |
| JS 1 | 50.26 | 17.75 | 2.00 | 9.73 | 0.12 | 9.99 | 6.11 | 0.77 | 2.99 | 0.28 | 146 | 211 | 13 | 143 | 26 | 11 |
| JS 2 | 50.15 | 14.66 | 1.94 | 10.63 | 0.18 | 10.60 | 8.57 | 0.66 | 2.39 | 0.23 | 489 | 187 | 12 | 138 | 26 | 10 |
| JS 3 | 50.78 | 16.16 | 1.98 | 9.94 | 0.17 | 10.33 | 6.93 | 0.68 | 2.78 | 0.24 | 278 | 189 | 12 | 140 | 28 | 11 |
| JS 4 | 49.06 | 14.35 | 1.79 | 10.89 | 0.18 | 9.99 | 10.66 | 0.57 | 2.31 | 0.21 | 461 | 136 | 10 | 126 | 25 | 10 |
| JS 5 | 49.40 | 16.84 | 1.92 | 10.38 | 0.17 | 10.78 | 7.12 | 0.50 | 2.67 | 0.22 | 292 | 167 | 8 | 138 | 26 | 11 |
| JS 6 | 50.42 | 16.44 | 2.04 | 9.96 | 0.17 | 10.65 | 6.66 | 0.67 | 2.76 | 0.23 | 281 | 178 | 12 | 140 | 28 | 11 |
| JS 8 | 49.97 | 14.76 | 2.24 | 11.20 | 0.18 | 10.83 | 7.43 | 0.61 | 2.52 | 0.27 | 330 | 148 | 11 | 154 | 30 | 12 |
| JS 9 | 50.16 | 14.92 | 2.20 | 11.15 | 0.17 | 10.63 | 7.31 | 0.70 | 2.52 | 0.25 | 329 | 143 | 16 | 154 | 31 | 12 |
| JS10 | 48.93 | 14.71 | 2.49 | 11.99 | 0.19 | 11.08 | 7.33 | 0.54 | 2.48 | 0.26 | 276 | 106 | 8 | 165 | 32 | 15 |
| JS11 | 48.03 | 15.79 | 1.80 | 10.96 | 0.17 | 10.74 | 9.79 | 0.28 | 2.26 | 0.18 | 424 | 66 | 3 | 122 | 25 | 10 |
| **MIDDLE FLOWS** | | | | | | | | | | | | | | | | |
| JS31 | 49.25 | 16.56 | 1.90 | 11.09 | 0.19 | 9.69 | 7.46 | 0.70 | 3.14 | 0.23 | 137 | 262 | 13 | 130 | 31 | 7 |
| JS32 | 53.67 | 16.30 | 1.80 | 9.52 | 0.16 | 7.85 | 4.68 | 1.96 | 2.74 | 0.48 | 84 | 584 | 47 | 181 | 32 | 14 |
| JS33 | 52.39 | 15.98 | 2.10 | 10.55 | 0.19 | 8.10 | 4.89 | 1.75 | 3.61 | 0.49 | 66 | 593 | 35 | 183 | 33 | 14 |
| JS34 | 51.05 | 16.19 | 2.02 | 10.59 | 0.19 | 8.76 | 6.20 | 1.22 | 3.59 | 0.40 | 76 | 444 | 20 | 157 | 34 | 12 |
| JS36 | 50.19 | 15.54 | 2.10 | 11.45 | 0.19 | 9.15 | 6.09 | 1.11 | 3.43 | 0.37 | 107 | 386 | 19 | 156 | 36 | 10 |
| JS37 | 51.26 | 16.08 | 2.65 | 11.71 | 0.19 | 8.13 | 5.46 | 1.50 | 3.29 | 0.52 | 84 | 473 | 31 | 211 | 37 | 15 |
| JS38 | 50.00 | 15.10 | 2.51 | 12.22 | 0.20 | 8.99 | 5.55 | 1.26 | 3.52 | 0.46 | 95 | 415 | 22 | 190 | 38 | 13 |
| JS39 | 50.13 | 15.41 | 3.63 | 12.94 | 0.22 | 8.27 | 5.24 | 1.47 | 3.39 | 0.60 | 58 | 497 | 26 | 223 | 39 | 17 |
| JS40 | 49.01 | 14.26 | 2.96 | 13.35 | 0.21 | 8.62 | 5.69 | 1.23 | 3.65 | 0.55 | 85 | 430 | 18 | 205 | 40 | 16 |
| **UPPER FLOWS** | | | | | | | | | | | | | | | | |
| JS50 | 49.76 | 14.89 | 2.85 | 13.02 | 0.21 | 8.79 | 5.31 | 3.60 | 3.57 | 0.49 | 64 | 456 | 14 | 191 | 50 | 14 |
| JS51 | 49.12 | 16.10 | 2.32 | 12.73 | 0.19 | 8.89 | 5.82 | 3.59 | 3.56 | 0.40 | 45 | 369 | 16 | 191 | 51 | 10 |
| JS52 | 49.96 | 14.37 | 3.20 | 13.95 | 0.22 | 7.80 | 4.31 | 3.83 | 3.82 | 0.68 | 13 | 619 | 28 | 251 | 52 | 19 |
| JS53 | 50.19 | 17.15 | 2.56 | 11.22 | 0.19 | 8.61 | 4.62 | 1.23 | 3.82 | 0.49 | 48 | 447 | 18 | 187 | 53 | 13 |
| JS54 | 48.75 | 16.37 | 2.40 | 12.03 | 0.20 | 9.12 | 6.40 | 0.96 | 3.47 | 0.42 | 135 | 366 | 11 | 166 | 54 | 12 |
| JS55 | 50.03 | 18.25 | 2.20 | 10.38 | 0.16 | 9.26 | 4.76 | 0.96 | 3.66 | 0.40 | 69 | 369 | 11 | 158 | 55 | 10 |
| JS56 | 53.14 | 15.62 | 2.60 | 10.91 | 0.18 | 7.10 | 3.86 | 2.12 | 3.85 | 0.66 | 9 | 745 | 38 | 245 | 56 | 19 |
| JS57 | 53.62 | 15.12 | 2.37 | 11.27 | 0.18 | 6.94 | 4.21 | 2.18 | 3.71 | 0.49 | 13 | 600 | 43 | 231 | 57 | 16 |
| JS58 | 49.86 | 16.82 | 2.07 | 12.09 | 0.18 | 8.27 | 5.78 | 1.13 | 3.53 | 0.38 | 76 | 409 | 18 | 158 | 58 | 11 |

## APPENDIX 5: Strontium and neodymium isotope data

The following isotope data are part of a reconnaissance study and are discussed only briefly in the text: Additional analyses are being received as this thesis is being completed; therefore critical analysis of the data will be included in later publications. Variation diagrams are presented in Figure A5-1 (next page).

| Map Unit | Sample Number | $^{87}Sr/^{86}Sr$ | $^{143}Nd/^{144}Nd$ |
|---|---|---|---|
| Tdrd | JJ92-1 | 0.70490 | 0.512553 |
| $Tdr_1$ | JJ92-4 | 0.70741 | n.d. |
| $Qb_2$ | JJ93-20 | 0.70508 | 0.512717 |
| Tdid (incl.) | JJ92-51 | 0.70494 | 0.512534 |
| Tdid | JJ92-102 | 0.70483 | 0.512552 |
| $Tdb_1$ | JJ93-130 | 0.70481 | n.d. |

Analytical data were obtained on a Finigan 261 mass spectrometer using standard chemical preparation techniques. The Sr-isotope data are normalized to a value of 0.71022 for the international standard NBS 987. Two standard deviations on the mean of repeated analyses of the standard are 0.000036. The Nd isotopes represent initial values and have not been renormalized to a particular standard. n.d. indicates isotope not determined. Analyses were performed at The Open University, Milton Keynes, United Kingdom, under the supervision of C.J. Hawkesworth.

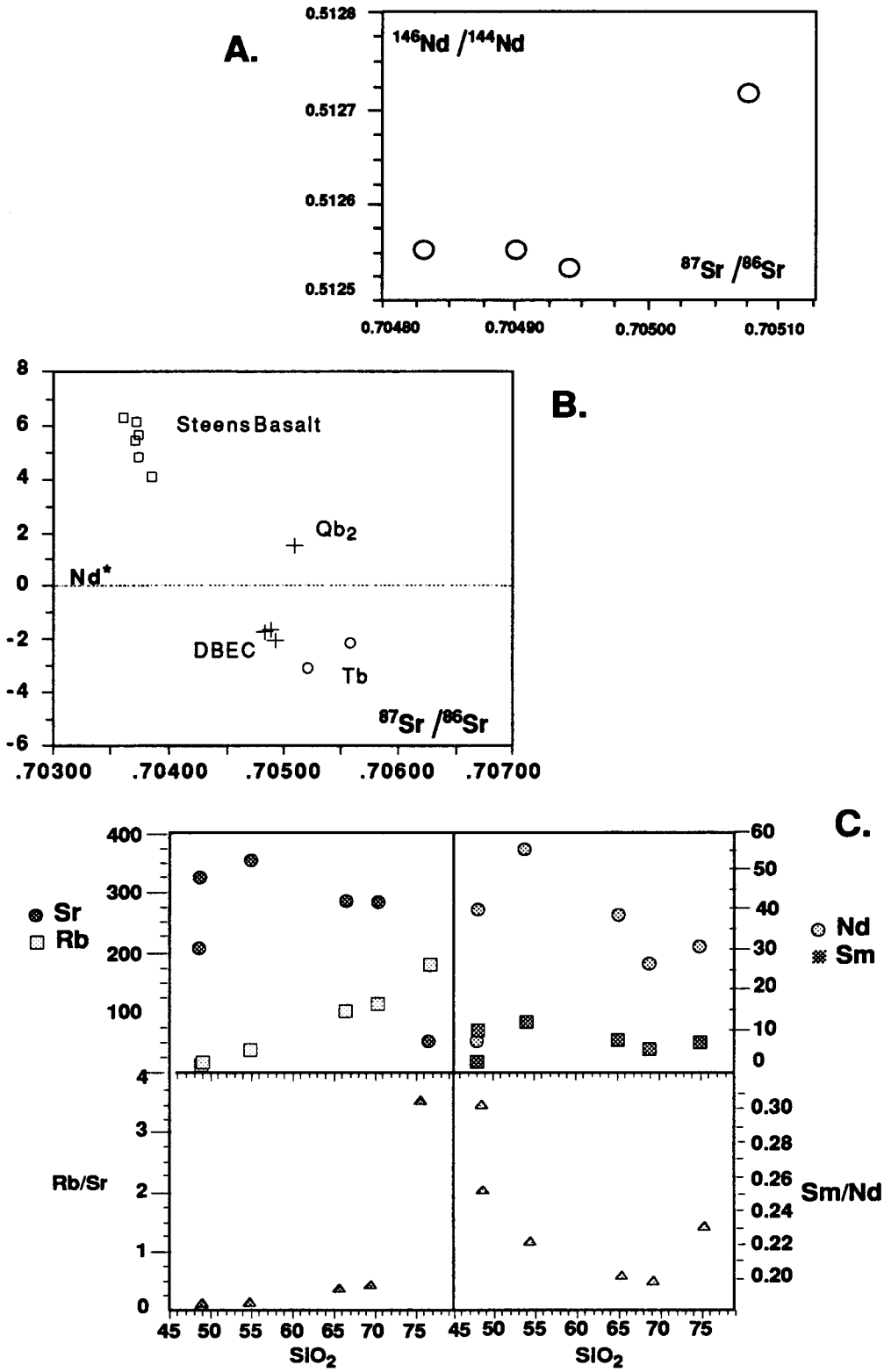


**Figure A5-1**: (A) Strontium and neodymium isotopes for DBEC samples listed in Appendix 5; (B) Steens basalt, "Steens-type" basalt (Tb), and DBEC samples plotted on $^{87}Sr/^{86}St$ vs $\Sigma_{Nd}$ diagram; (C) Abundance of Sr, Rb, Sm, and Nd for DBEC samples. Values from Table 4-7.

**APPENDIX 6:** Unnormalized XRF data for samples in Tables 4-7-4-9.

| Sample No. | XRF Lab | Map Unit | Litho Type | $SiO_2$ | $TiO_2$ | $Al_2O_3$ | FeO* | MnO | MgO | CaO | $Na_2O$ | $K_2O$ | $P_2O_5$ | Total |
|---|---|---|---|---|---|---|---|---|---|---|---|---|---|---|
| JJ92-1 | XRAL | **Tdrd** | L | 67.70 | 0.53 | 14.00 | 3.04 | 0.07 | 0.77 | 2.10 | 3.46 | 4.62 | 0.17 | 96.46 |
| JJ95-1iA | WSU | **Tdrd** | Qi | 59.28 | 1.51 | 15.52 | 8.78 | 0.13 | 1.20 | 4.51 | 3.90 | 2.72 | 0.79 | 98.33 |
| JJ95-1iB | WSU | **Tdrd** | Qi | 58.79 | 1.40 | 15.30 | 8.26 | 0.17 | 1.37 | 4.62 | 4.26 | 2.90 | 0.87 | 97.44 |
| JJ92-4 | XRAL | **$Tdr_1$** | O | 75.80 | 0.11 | 12.70 | 1.17 | 0.04 | 0.04 | 0.66 | 3.71 | 5.03 | 0.02 | 99.27 |
| JJ92-6 | XRAL | **$Tdba_1$** | L | 51.20 | 2.05 | 15.60 | 10.62 | 0.18 | 4.14 | 7.03 | 3.59 | 2.10 | 0.72 | 97.22 |
| JJ92-5 | XRAL | **Tdr1** | L | 73.50 | 0.11 | 12.60 | 1.25 | 0.04 | 0.10 | 0.64 | 3.45 | 4.98 | 0.04 | 96.71 |
| JJ92-7 | XRAL | **Tdrd** | L | 67.80 | 0.51 | 14.10 | 2.92 | 0.07 | 0.65 | 1.91 | 3.63 | 4.78 | 0.14 | 96.50 |
| JJ92-19 | WSU | **Tba** | L | 56.11 | 2.00 | 13.84 | 11.05 | 0.17 | 3.95 | 7.45 | 3.25 | 1.78 | 0.31 | 99.91 |
| JJ92-20 | WSU | **Qb2** | L | 47.68 | 0.90 | 15.88 | 9.76 | 0.18 | 9.82 | 10.82 | 2.48 | 0.25 | 0.10 | 97.86 |
| JJ92-27 | XRAL | **Tdba1** | L | 58.50 | 1.41 | 14.80 | 7.76 | 0.14 | 2.97 | 5.42 | 3.64 | 3.08 | 0.43 | 98.14 |
| JJ92-38 | XRAL | **$Tdba_2$** | D | 52.50 | 2.05 | 15.60 | 10.62 | 0.18 | 4.15 | 6.99 | 3.36 | 2.10 | 0.72 | 98.26 |
| JJ92-41 | WSU | **Tda1** | L | 61.25 | 1.31 | 15.77 | 6.11 | 0.13 | 2.52 | 5.26 | 3.82 | 3.23 | 0.32 | 99.72 |
| JJ92-51 | XRAL | **Tdid** | Qi | 53.40 | 2.43 | 13.90 | 10.62 | 0.21 | 3.24 | 6.82 | 3.09 | 2.37 | 1.35 | 97.43 |
| JJ92-59 | XRAL | **Ts?** | L | 50.10 | 2.51 | 14.90 | 11.88 | 0.18 | 4.85 | 8.55 | 3.14 | 1.21 | 0.39 | 97.70 |
| JJ92-62 | XRAL | **$Tdba_3$** | L | 54.60 | 2.10 | 14.50 | 10.53 | 0.18 | 4.02 | 6.42 | 4.08 | 2.40 | 0.50 | 99.32 |
| JJ92-88 | XRAL | **Tdrd** | L | 68.00 | 0.53 | 14.10 | 2.92 | 0.07 | 0.65 | 2.00 | 3.64 | 4.98 | 0.15 | 97.04 |
| JJ92-90 | XRAL | **Tr** | L | 73.60 | 0.06 | 12.50 | 0.78 | 0.05 | 0.03 | 0.69 | 4.08 | 4.39 | 0.02 | 96.19 |
| JJ92-99 | XRAL | **$Tdb_2$** | L | 50.10 | 1.71 | 16.70 | 10.17 | 0.17 | 5.47 | 8.71 | 3.53 | 1.26 | 0.69 | 98.50 |
| JJ92-101 | XRAL | **Tdrd** | L | 67.20 | 0.54 | 14.50 | 2.86 | 0.08 | 0.64 | 1.86 | 3.93 | 4.96 | 0.17 | 96.74 |
| JJ92-102 | XRAL | **Tdid** | L | 65.00 | 0.85 | 14.50 | 5.20 | 0.12 | 1.04 | 3.06 | 3.98 | 4.01 | 0.32 | 98.08 |
| JJ93-123 | WSU | **Ttd** | UT | 75.51 | 0.20 | 11.05 | 2.65 | 0.05 | 0.00 | 0.30 | 4.03 | 5.27 | 0.02 | 99.08 |
| JJ93-124 | WSU | **Tots** | WT | 75.79 | 0.23 | 10.20 | 4.47 | 0.07 | 0.00 | 0.21 | 4.90 | 4.63 | 0.01 | 100.51 |
| JJ93-126 | WSU | **$Tda_2$** | L | 60.36 | 1.16 | 15.64 | 6.88 | 0.14 | 2.62 | 5.42 | 3.88 | 2.92 | 0.32 | 99.34 |
| JJ93-140 | WSU | **$Tda_2$** | L | 59.54 | 1.12 | 15.64 | 7.09 | 0.13 | 3.02 | 5.63 | 3.72 | 2.82 | 0.30 | 99.01 |
| JJ93-130 | WSU | **$Tdb_1$** | L | 48.76 | 2.56 | 15.86 | 13.02 | 0.21 | 5.44 | 9.04 | 3.41 | 0.87 | 0.69 | 99.86 |
| JJ93-133 | WSU | **Tba** | L | 56.53 | 2.01 | 14.58 | 9.48 | 0.16 | 4.11 | 7.99 | 3.41 | 1.45 | 0.30 | 100.01 |
| JJ93-134 | WSU | **Tba** | L | 61.93 | 1.06 | 16.58 | 5.57 | 0.11 | 2.24 | 5.29 | 4.00 | 2.97 | 0.37 | 100.12 |
| JJ93-147 | WSU | **Tad** | L | 58.85 | 2.32 | 14.01 | 10.07 | 0.15 | 1.92 | 5.30 | 3.88 | 2.23 | 0.56 | 99.28 |
| JJ94-151 | WSU | **$Qb_3$** | L | 50.14 | 1.15 | 17.21 | 9.62 | 0.18 | 8.48 | 11.32 | 2.86 | 0.35 | 0.15 | 101.45 |
| JJ94-158 | WSU | **$Tdr_2$** | L | 77.24 | 0.08 | 13.21 | 1.16 | 0.04 | 0.00 | 0.77 | 4.06 | 5.01 | 0.01 | 101.58 |
| JJ94-161 | WSU | **Tbas** | L | 55.20 | 2.13 | 15.53 | 10.60 | 0.19 | 3.19 | 6.35 | 3.82 | 2.53 | 0.74 | 100.28 |
| JJ94-163 | WSU | **Tbs** | L | 49.84 | 2.49 | 15.50 | 12.22 | 0.17 | 5.62 | 8.78 | 3.21 | 1.23 | 0.76 | 99.81 |
| FF94-23 | WSU | **Tb** | L | 50.69 | 2.06 | 16.58 | 11.08 | 0.17 | 5.67 | 10.43 | 3.09 | 0.61 | 0.25 | 100.63 |
| FF94-36 | WSU | **Tba** | L | 51.00 | 1.95 | 15.80 | 12.09 | 0.17 | 6.11 | 9.45 | 3.26 | 0.58 | 0.26 | 100.68 |
| FF94-39 | WSU | **Tba** | L | 60.07 | 2.03 | 13.84 | 10.38 | 0.16 | 2.35 | 5.69 | 3.82 | 2.38 | 0.32 | 101.03 |
| FF94-49 | WSU | **Ts** | L | 49.53 | 1.96 | 17.25 | 12.11 | 0.18 | 5.83 | 9.03 | 3.48 | 0.84 | 0.30 | 100.51 |
| JN94-16 | WSU | **$Tdr_2$** | L | 76.15 | ### | 0.07 | 0.86 | 0.07 | 1.12 | 0.00 | 4.62 | 4.40 | 0.02 | 101.49 |

L = lava; Qi = quenched inclusion; O = obsidian; D = dike; UT = unwelded tuff; WT = welded tuff

XRAL = XRAL Laboratories, British Columbia; WSU = GeoAnalytical Lab, Washington State University, Pullman Washington.

Appendix 7: CIPW normative minerals for select rocks of study area

| Sample # | Map Unit | Q | C | Or | Ab | An | Di | Hy | Ol | Mt | Il | Ap |
|---|---|---|---|---|---|---|---|---|---|---|---|---|
| JJ92-1 | Tdrd | 23.4 | 0.0 | 27.3 | 29.3 | 9.0 | 0.2 | 5.0 | 0.0 | 1.0 | 1.0 | 0.4 |
| JJ92-4 | Tdrl | 32.9 | 0.0 | 29.7 | 31.4 | 3.1 | 0.0 | 1.5 | 0.0 | 0.4 | 0.2 | 0.1 |
| JJ92-5 | Tdrl | 32.3 | 0.5 | 29.4 | 29.2 | 2.9 | 0.0 | 1.7 | 0.0 | 0.4 | 0.2 | 0.1 |
| JJ92-7 | Tdrd | 22.5 | 0.0 | 28.3 | 30.7 | 8.1 | 0.4 | 4.4 | 0.0 | 0.9 | 1.0 | 0.3 |
| JJ92-6 | Tdbal | 0.4 | 0.0 | 12.4 | 30.4 | 20.3 | 8.2 | 16.8 | 0.0 | 3.4 | 3.9 | 1.7 |
| JJ93-19 | Tba | 8.0 | 0.0 | 10.5 | 27.5 | 17.9 | 14.1 | 14.0 | 0.0 | 3.6 | 3.8 | 0.7 |
| JJ93-20 | Qb2 | 0.0 | 0.0 | 1.5 | 21.0 | 31.5 | 17.4 | 6.6 | 15.1 | 3.2 | 1.7 | 0.2 |
| JJ92-27 | Tdal | 9.1 | 0.0 | 18.2 | 30.8 | 15.0 | 7.6 | 11.5 | 0.0 | 2.5 | 2.7 | 1.0 |
| JJ92-38 | Tdba2 | 2.8 | 0.0 | 12.4 | 28.4 | 21.3 | 7.2 | 17.4 | 0.0 | 3.4 | 3.9 | 1.7 |
| JJ92-41 | Tdal | 11.5 | 0.0 | 19.1 | 32.3 | 16.4 | 6.3 | 9.1 | 0.0 | 2.0 | 2.5 | 0.8 |
| JJ92-51 | Tdid-incl | 7.9 | 0.0 | 14.0 | 26.1 | 17.1 | 6.6 | 14.8 | 0.0 | 3.4 | 4.6 | 3.2 |
| JJ92-59 | Ts? | 1.2 | 0.0 | 7.2 | 26.6 | 23.0 | 13.9 | 16.6 | 0.0 | 3.8 | 4.8 | 0.9 |
| JJ92-62 | Tdba3 | 1.7 | 0.0 | 14.2 | 34.5 | 14.2 | 11.9 | 14.5 | 0.0 | 3.4 | 4.0 | 1.2 |
| JJ92-88 | Tdrd | 21.9 | 0.0 | 29.4 | 30.8 | 7.4 | 1.3 | 4.0 | 0.0 | 0.9 | 1.0 | 0.4 |
| JJ92-90 | Tr | 31.2 | 0.0 | 26.0 | 34.5 | 2.8 | 0.4 | 0.9 | 0.0 | 0.3 | 0.1 | 0.1 |
| JJ92-99 | Tdb2 | 0.0 | 0.0 | 7.5 | 29.9 | 26.0 | 10.4 | 10.9 | 6.0 | 3.3 | 3.3 | 1.6 |
| JJ92-101 | Tdrd | 19.7 | 0.0 | 29.3 | 33.3 | 7.3 | 0.7 | 4.2 | 0.0 | 0.9 | 1.0 | 0.4 |
| JJ92-102 | Tdid | 17.5 | 0.0 | 23.7 | 33.7 | 9.9 | 2.7 | 6.7 | 0.0 | 1.7 | 1.6 | 0.8 |
| JJ93-126 | Tda2 | 10.5 | 0.0 | 17.3 | 32.8 | 16.6 | 6.8 | 10.4 | 0.0 | 2.2 | 2.2 | 0.8 |
| JJ93-130 | Tdb1 | 0.0 | 0.0 | 5.1 | 28.9 | 25.4 | 12.3 | 10.6 | 7.2 | 4.2 | 4.9 | 1.6 |
| JJ93-133 | Tba | 8.3 | 0.0 | 8.6 | 28.9 | 20.2 | 14.4 | 12.3 | 0.0 | 3.1 | 3.8 | 0.7 |
| JJ93-134 | Tas | 12.3 | 0.0 | 17.6 | 33.8 | 18.5 | 4.4 | 9.0 | 0.0 | 1.8 | 2.0 | 0.9 |
| JJ93-140 | Tda2 | 9.8 | 0.0 | 16.7 | 31.5 | 17.7 | 6.9 | 11.6 | 0.0 | 2.3 | 2.1 | 0.7 |
| JJ93-147 | Tad | 12.6 | 0.0 | 13.2 | 32.8 | 14.2 | 7.1 | 10.6 | 0.0 | 3.3 | 4.4 | 1.3 |

Q = quartz; C = corundum; Or = Orthoclase; Ab = albite; An = anorthite; Di = diopside;
Hy = hypersthene; Ol = olivine; Mt = magnetite; Il = ilmenite; Ap = apatite

## Appendix 8: Complete $^{40}Ar/^{39}Ar$ analytical data.

The following tables were received after the thesis was prepared. Weighted mean ages may differ slightly from those in the thesis. The plagioclase age for the rhyodacite of Duck Creek Butte, JJ92-1, is presented here for the first time.

| Lab ID# | Temp. °C or Watts | Ca/K | $^{36}Ar/^{39}Ar$ | $\%(^{36}Ar/^{39}Ar)_{Ca}$ | $^{40}Ar^*/^{39}Ar$ | $\%^{40}Ar^*$ | Age (Ma) ±1σ |
|---|---|---|---|---|---|---|---|
| Sample JJ93-20 (whole-rock bulk incremental heating, furnace) | | | | | | | |
| 8238-01A | 600 | 25.5 | 17.9 | 0.0 | 34.23 | 0.6 | 86 ± 226 |
| 8238-01B | 700 | 24.8 | 0.102 | 3.4 | 0.714 | 2.4 | 1.84 ± 0.52 |
| 8238-01C | 800 | 21.7 | 0.0104 | 29.2 | 0.444 | 16.8 | 1.15 ± 0.07 |
| 8238-01D | 875 | 13.3 | 0.0074 | 25.2 | 0.536 | 24.6 | 1.39 ± 0.07 |
| 8238-01E | 1000 | 13.3 | 0.0093 | 20.0 | 0.614 | 21.7 | 1.58 ± 0.08 |
| 8238-01F | 1100 | 17.8 | 0.0159 | 15.7 | 0.598 | 13.0 | 1.54 ± 0.15 |
| 8238-01G | 1200 | 21.6 | 0.0239 | 12.6 | 0.558 | 8.2 | 1.44 ± 0.22 |
| 8238-01H | 1400 | 221 | 0.0723 | 42.8 | 0.740 | 5.3 | 1.91 ± 0.45 |
| 8238-01I | 1650 | 228 | 0.238 | 13.4 | 0.606 | 0.9 | 1.56 ± 3.77 |
| Sample JJ92-5 (sanidine single-crystal laser-fusion) | | | | | | | |
| 7494-01 | t.f. | 0.017 | 0.00005 | 4.5 | 1.734 | 99.2 | 10.37 ± 0.04 |
| 7494-02 | t.f. | 0.017 | 0.00009 | 2.5 | 1.719 | 98.5 | 10.28 ± 0.04 |
| 7494-03 | t.f. | 0.019 | 0.00030 | 0.8 | 1.733 | 95.2 | 10.37 ± 0.05 |
| 7494-04 | t.f. | 0.016 | 0.00006 | 3.7 | 1.732 | 99.0 | 10.36 ± 0.04 |
| 7494-05 | t.f. | 0.017 | 0.00008 | 3.0 | 1.722 | 98.7 | 10.30 ± 0.04 |
| 7494-06 | t.f. | 0.016 | 0.00009 | 2.5 | 1.718 | 98.6 | 10.28 ± 0.04 |
| 7494-07 | t.f. | 0.017 | 0.00006 | 3.9 | 1.726 | 99.1 | 10.33 ± 0.04 |
| 7494-08 | t.f. | 0.015 | 0.00008 | 2.6 | 1.711 | 98.7 | 10.24 ± 0.05 |
| 7494-09 | t.f. | 0.016 | 0.00008 | 2.8 | 1.715 | 98.7 | 10.26 ± 0.04 |
| 7494-10 | t.f. | 0.018 | 0.00004 | 6.2 | 1.736 | 99.4 | 10.39 ± 0.04 |
| Sample JJ92-1 aliquot #1 (biotite bulk laser incremental heating) | | | | | | | |
| 8159-01A | 0.6 | 0.157 | 0.01136 | 0.2 | 0.826 | 19.8 | 7.50 ± 0.43 |
| 8159-01B | 0.8 | 0.126 | 0.00341 | 0.5 | 1.099 | 52.3 | 9.97 ± 0.21 |
| 8159-01C | 1.3 | 0.074 | 0.00202 | 0.5 | 1.153 | 66.0 | 10.45 ± 0.10 |
| 8159-01D | 1.9 | 0.033 | 0.00083 | 0.5 | 1.147 | 82.5 | 10.40 ± 0.05 |
| 8159-01E | 2.3 | 0.048 | 0.00068 | 0.9 | 1.142 | 85.2 | 10.36 ± 0.05 |
| 8159-01F | 2.6 | 0.072 | 0.00063 | 1.5 | 1.141 | 86.1 | 10.35 ± 0.06 |
| 8159-01G | 3.0 | 0.063 | 0.00047 | 1.8 | 1.148 | 89.5 | 10.41 ± 0.05 |
| 8159-01H | 3.5 | 0.037 | 0.00031 | 1.6 | 1.144 | 92.7 | 10.38 ± 0.04 |
| 8159-01I | 6.0 | 0.033 | 0.00024 | 1.9 | 1.152 | 94.4 | 10.45 ± 0.04 |
| 8159-01J | 8.6 | 0.069 | 0.01090 | 0.1 | 0.574 | 15.1 | 5.21 ± 0.27 |
| Sample JJ92-1 aliquot #2 | | | | | | | |
| 8159-02A | 0.6 | 0.055 | 0.00987 | 0.1 | 1.224 | 29.6 | 11.10 ± 0.40 |
| 8159-02B | 0.8 | 0.081 | 0.00259 | 0.4 | 1.212 | 61.4 | 10.99 ± 0.30 |
| 8159-02C | 1.3 | 0.034 | 0.00155 | 0.3 | 1.165 | 71.8 | 10.57 ± 0.12 |
| 8159-02D | 1.9 | 0.016 | 0.00084 | 0.3 | 1.151 | 82.3 | 10.44 ± 0.05 |
| 8159-02E | 2.3 | 0.020 | 0.00063 | 0.4 | 1.146 | 86.1 | 10.39 ± 0.05 |
| 8159-02F | 2.6 | 0.048 | 0.00058 | 1.1 | 1.138 | 86.9 | 10.32 ± 0.05 |
| 8159-02G | 3.0 | 0.055 | 0.00047 | 1.6 | 1.149 | 89.3 | 10.42 ± 0.06 |
| 8159-02H | 3.5 | 0.033 | 0.00031 | 1.4 | 1.153 | 92.8 | 10.45 ± 0.05 |
| 8159-02I | 6.0 | 0.034 | 0.00028 | 1.7 | 1.153 | 93.5 | 10.45 ± 0.04 |
| 8159-02J | 8.6 | 0.040 | 0.00042 | 1.3 | 1.142 | 90.3 | 10.36 ± 0.13 |

(cont'd.)

Appendix 8 (continued)

| Lab ID# | Temp. °C or Watts | Ca/K | $^{36}Ar/^{39}Ar$ $\%(^{36}Ar/^{39}Ar)_{Ca}$ | | $^{40}Ar^*/^{39}Ar$ | $\%^{40}Ar^*$ | Age (Ma) ±1σ |
|---|---|---|---|---|---|---|---|
| Sample JJ92-1 aliquot #1 (plagioclase bulk laser incremental heating) | | | | | | | |
| 7443-01A | 1.0 | 3.71 | 0.0501 | 1.0 | 13.97 | 48.8 | 9.84 ± 0.25 |
| 7443-01B | 3.0 | 5.98 | 0.0075 | 11.2 | 14.70 | 88.2 | 10.35 ± 0.08 |
| 7443-01C | 6.0 | 6.16 | 0.0124 | 7.0 | 15.86 | 82.3 | 11.16 ± 0.08 |
| 7443-01D | 7.6 | 5.90 | 0.0062 | 13.3 | 15.16 | 90.5 | 10.67 ± 0.07 |
| 7443-02A | 1.0 | 3.52 | 0.0365 | 1.3 | 15.81 | 59.8 | 11.13 ± 0.38 |
| 7443-02B | 3.0 | 4.87 | 0.0048 | 14.2 | 15.30 | 92.6 | 10.77 ± 0.05 |
| 7443-02C | 6.0 | 5.01 | 0.0288 | 2.4 | 15.63 | 65.2 | 11.00 ± 0.09 |
| 7443-02D | 7.6 | 5.39 | 0.0017 | 45.4 | 15.43 | 98.3 | 10.86 ± 0.10 |
| 7443-03A | 1.0 | 2.66 | 0.0437 | 0.9 | 14.39 | 52.9 | 10.13 ± 0.16 |
| 7443-03B | 3.0 | 6.00 | 0.0069 | 12.2 | 15.77 | 89.8 | 11.10 ± 0.08 |
| 7443-03C | 6.0 | 6.12 | 0.0153 | 5.6 | 18.89 | 81.5 | 13.28 ± 0.08 |
| 7443-03D | 7.6 | 6.17 | 0.0044 | 19.7 | 16.01 | 93.9 | 11.26 ± 0.17 |
| 7443-04A | 1.0 | 3.23 | 0.0387 | 1.2 | 15.24 | 57.4 | 10.73 ± 0.20 |
| 7443-04B | 3.0 | 5.40 | 0.0046 | 16.3 | 14.85 | 92.8 | 10.45 ± 0.06 |
| 7443-04C | 5.0 | 5.66 | 0.0017 | 45.6 | 15.34 | 98.2 | 10.79 ± 0.07 |
| 7443-04D | 7.6 | 5.15 | 0.0030 | 23.6 | 15.16 | 95.7 | 10.66 ± 0.10 |

Notes: Errors in age quoted for individual runs are 1σ analytical uncertainty. 't.f.' indicates total fusion. Weighted averages are calculated using the inverse variance as the weighting factor (Taylor, 1982), while errors in the weighted averages are 1σ standard error of the mean (Samson and Alexander, 1987). Ca/K is calculated from $^{37}Ar/^{39}Ar$ using a multiplier of 1.96. $^{40}Ar^*$ refers to radiogenic argon. $\lambda = 5.543 \times 10^{-10}$ $y^{-1}$. Isotopic interference corrections: $(^{36}Ar/^{37}Ar)_{Ca} = 2.74 \times 10^{-4} \pm 1 \times 10^{-6}$, $(^{39}Ar/^{37}Ar)_{Ca} = 7.02 \times 10^{-4} \pm 2 \times 10^{-6}$, $(^{40}Ar/^{39}Ar)_K = 7 \times 10^{-4} \pm 3 \times 10^{-4}$. For sample JJ93-20, $J$=0.001432 ± .000005; for sample JJ92-5, $J = 0.003326 \pm 0.000001$; for sample JJ92-1 biotite, $J = 0.005042 \pm 0.000015$; for sample JJ92-1 plagioclase, $J = 0.0003912 \pm 0.000001$. Data for sample JJ93-20 were acquired at the New Mexico Bureau of Mines and Mineral Resources (Socorro); all other data were acquired at the Berkeley Geochronology Center (Berkeley). Irradiations were performed in the CLICIT facility of the Oregon State University TRIGA reactor.